Advances in Clinical and Experimental Medicine

MONTHLY ISSN 1899-5276 (PRINT) ISSN 2451-2680 (ONLINE) www.advances.umed.wroc.pl

2018, Vol. 27, No. 7 (July)

Impact Factor (IF) – 1.262
Ministry of Science and Higher Education – 15 pts.
Index Copernicus (ICV) – 155.19 pts.

Wroclaw Medical University

Advances
in Clinical and Experimental Medicine

ISSN 1899-5276 (PRINT) ISSN 2451-2680 (ONLINE) www.advances.umed.wroc.pl

MONTHLY 2018
Vol. 27, No. 7
(July)

Advances in Clinical and Experimental Medicine is a peer-reviewed open access journal published by Wroclaw Medical University. Its abbreviated title is Adv Clin Exp Med. Journal publishes original papers and reviews encompassing all aspects of medicine, including molecular biology, biochemistry, genetics, biotechnology, and other areas. It is published monthly, one volume per year.

Editorial Office
ul. Marcinkowskiego 2–6
50-368 Wrocław, Poland
Tel.: +48 71 784 12 05
E-mail: redakcja@umed.wroc.pl

Publisher
Wroclaw Medical University
Wybrzeże L. Pasteura 1
50-367 Wrocław, Poland

Online edition is the original version of the journal

Editorial Policy

Advances in Clinical and Experimental Medicine (Adv Clin Exp Med) is an independent multidisciplinary forum for exchange of scientific and clinical information, publishing original research and news encompassing all aspects of medicine, including molecular biology, biochemistry, genetics, biotechnology and other areas. During the review process, the Editorial Board conforms to the "Uniform Requirements for Manuscripts Submitted to Biomedical Journals: Writing and Editing for Biomedical Publication" approved by the International Committee of Medical Journal Editors (www.ICMJE.org/). The journal publishes (in English only) original papers and reviews. Short works considered original, novel and significant are given priority. Experimental studies must include a statement that the experimental protocol and informed consent procedure were in compliance with the Helsinki Convention and were approved by an ethics committee.

For all subscription related queries please contact our Editorial Office:

redakcja@umed.wroc.pl

For more information visit the journal's website:

www.advances.umed.wroc.pl

Pursuant to the ordinance no. 134/XV R/2017 of the Rector of Wroclaw Medical University (as of December 28, 2017) from January 1, 2018 authors are required to pay a fee amounting to 700 euros for each manuscript accepted for publication in the journal "Advances in Clinical and Experimental Medicine."

Indexed in: MEDLINE, Science Citation Index Expanded, Journal Citation Reports/Science Edition,

Scopus, EMBASE/Excerpta Medica, Ulrich's™ International Periodicals Directory, Index Copernicus

Typographic design: Monika Kolęda, Piotr Gil
DTP: Wydawnictwo UMW, TYPOGRAF
Cover: Monika Kolęda
Printing and binding: EXDRUK

Advances
in Clinical and Experimental Medicine

MONTHLY 2018, Vol. 27, No. 7 (July)

ISSN 1899-5276 (PRINT)
ISSN 2451-2680 (ONLINE)
www.advances.umed.wroc.pl

Contents

Original papers

867 Ewa Szczerba, Agnieszka Zajkowska, Anna Bochowicz, Katarzyna Pankiewicz, Grzegorz Szewczyk, Katarzyna Markiewicz, Grzegorz Opolski, Tomasz Maciejewski, Maciej Małecki, Anna Fijałkowska
Rise in antifibrotic and decrease in profibrotic microRNA protect the heart against fibrosis during pregnancy: A preliminary study

873 Hanan Abdelmawgoud, Asmaa Saleh
Anti-inflammatory and antioxidant effects of mesenchymal and hematopoietic stem cells in a rheumatoid arthritis rat model

881 Maria W. Kondrat-Wróbel, Jarogniew J. Łuszczki
Isobolographic additivity among lacosamide, lamotrigine and phenobarbital in a mouse tonic-clonic seizure model

887 Xiaoying Fan, Yuan Yao, Yao Zhang
Calreticulin promotes proliferation and extracellular matrix expression through Notch pathway in cardiac fibroblasts

893 Hasan Riza Aydin, Hasan Turgut, Ayşegül Kurt, Ramazan Sahan, Ömer Faruk Kalkan, Huseyin Eren, Ahmet Ayar
Ivabradine inhibits carbachol-induced contractions of isolated rat urinary bladder

899 Yuwen Wang, Jianshu Yuan, Liangyan Yang, Pengyun Wang, Xiajun Wang, Yue Wu, Kan Chen, Rong Ma, Yike Zhong, Xiaohong Guo, Yan Gong, Mengfang Gui, Yaming Jin
Inhibition of migration and invasion by berberine via inactivation of PI3K/Akt and p38 in human retinoblastoma cell line

907 Esra Saygılı Yılmaz, Tansel Sapmaz, Halil Kazgan, Şule Menziletoglu Yildiz, Derya Kocamaz, Nusret Akpolat, Ekrem Sapmaz
Examination of the antioxidant effects of pre-HSG melatonin use on ovarian surface epithelium in rats: An experimental study

913 Hejia Hu, Yan Li, Zengfeng Xin, Xiangfeng Zhang
Ginkgolide B exerts anti-inflammatory and chondroprotective activity in LPS-induced chondrocytes

921 Abdullah Hakan Karadoğan, Hilal Arikoglu, Fatma Göktürk, Funda İşçioğlu, Süleyman Hilmi İpekçi
***PIK3R1* gene polymorphisms are associated with type 2 diabetes and related features in the Turkish population**

929 Arzu Yay, Özge Göktepe, Anzel Bahadir, Saim Özdamar, Ibrahim Suat Öktem, Atilla Çoruh, Münevver Baran
Assessment of markers expressed in human hair follicles according to different skin regions

941 Faezeh Asghari, Navideh Haghnavaz, Darioush Shanehbandi, Vahid Khaze, Behzad Baradaran, Tohid Kazemi
Differential altered expression of let-7a and miR-205 tumor-suppressor miRNAs in different subtypes of breast cancer under treatment with Taxol

947 Xiaodong Guan, Zhiyu Liu, Jianhua Zhang, Xunbo Jin
Myeloid-derived suppressor cell accumulation in renal cell carcinoma is correlated with CCL2, IL-17 and IL-18 expression in blood and tumors

955 Katarzyna Lipiec, Piotr Adamczyk, Elżbieta Świętochowska, Katarzyna Ziora, Maria Szczepańska
L-FABP and IL-6 as markers of chronic kidney damage in children after hemolytic uremic syndrome

963 Karol Polom, Daniele Marrelli, Giandomenico Roviello, Valeria Pascale, Costantino Voglino, Carla Vindigni, Daniele Generali, Franco Roviello
***PIK3CA* mutation in gastric cancer and the role of microsatellite instability status in mutations of exons 9 and 20 of the *PIK3CA* gene**

971 Hyunjin Lee, Sung-Il Lee, Youngkyung Ko, Jun-Beom Park
Evaluation of the secretion and release of vascular endothelial growth factor from two-dimensional culture and three-dimensional cell spheroids formed with stem cells and osteoprecursor cells

979 Witold Zgodziński, Ewelina Grywalska, Dorota Siwicka-Gieroba, Agata Surdacka, Krzysztof Zinkiewicz, Dariusz Szczepanek, Grzegorz Wallner, Jacek Roliński
The clinical importance of changes in Treg and Th17 lymphocyte subsets in splenectomized patients after spleen injury

987 Ewelina Grywalska, Małgorzata Bartkowiak-Emeryk, Marcin Pasiarski, Karolina Olszewska-Bożek, Michał Mielnik, Martyna Podgajna, Monika Pieczykolan, Anna Hymos, Elżbieta Fitas, Agata Surdacka, Stanisław Góźdź, Jacek Roliński
Relationship between the expression of CD25 and CD69 on the surface of lymphocytes T and B from peripheral blood and bone marrow of patients with chronic lymphocytic leukemia and established prognostic factors of this disease

1001 Babak Rastegar, Brice Thumilaire, Guillaume A. Odri, Sergio Siciliano, Jan Zapała, Pierre Mahy, Raphael Olszewski
Validation of a windowing protocol for accurate in vivo tooth segmentation using i-CAT cone beam computed tomography

Reviews

1009 Rodrigo A. Giacaman, Cecilia Muñoz-Sandoval, Klaus W. Neuhaus, Margherita Fontana, Renata Chałas
Evidence-based strategies for the minimally invasive treatment of carious lesions: Review of the literature

1017 Anna Markowska, Stefan Sajdak, Adam Huczyński, Sandra Rehlis, Janina Markowska
Ovarian cancer stem cells: A target for oncological therapy

Rise in antifibrotic and decrease in profibrotic microRNA protect the heart against fibrosis during pregnancy: A preliminary study

Ewa Szczerba[1,2,A–D,F], Agnieszka Zajkowska[3,A–D,F], Anna Bochowicz[1,A,B,E,F], Katarzyna Pankiewicz[4,B–D,F], Grzegorz Szewczyk[4,5,B,C,E,F], Katarzyna Markiewicz[6,B,C,E,F], Grzegorz Opolski[2,A,C,E,F], Tomasz Maciejewski[4,A–C,E,F], Maciej Małecki[3,A,C,E,F], Anna Fijałkowska[1,A –F]

[1] Department of Cardiology, Institute of Mother and Child, Warszawa, Poland
[2] 1st Department of Cardiology, Medical University of Warsaw, Poland
[3] Department of Applied Pharmacy and Bioengineering, Medical University of Warsaw, Poland
[4] Department of Obstetrics and Gynecology, Institute of Mother and Child, Warszawa, Poland
[5] Department of General and Experimental Pathology, Medical University of Warsaw, Poland
[6] Department of Clinical Immunology, Institute of Mother and Child, Warszawa, Poland

A – research concept and design; B – collection and/or assembly of data; C – data analysis and interpretation;
D – writing the article; E – critical revision of the article; F – final approval of the article

Advances in Clinical and Experimental Medicine, ISSN 1899-5276 (print), ISSN 2451-2680 (online) *Adv Clin Exp Med*. 2018;27(7):867–872

Address for correspondence
Ewa Szczerba
E-mail: ewa_szczerba@poczta.onet.pl

Funding sources
This work was supported by the Institute of Mother and Child (grant number 510-36-02).

Conflict of interest
None declared

Received on November 15, 2016
Reviewed on December 5, 2016
Accepted on February 13, 2017

Abstract

Background. Physiological pregnancy is associated with volume overload. Unlike cardiac pathologies linked with volume overload, such as mitral or aortic regurgitation, pregnancy is thought to be unrelated to fibrosis of the heart. However, changes in the cardiac extracellular matrix during pregnancy remain poorly understood.

Objectives. The aim of the study was to examine the expression of 11 microRNAs associated with cardiac fibrosis (miR-21, miR-26a, miR-26b-5p, miR-29b-3p, miR-29c-3p, miR-101a, miR-146a, miR-208a, miR-223 and miR-328) during pregnancy and to compare them with a healthy control group.

Material and methods. Six women in singleton pregnancy (30–36 weeks) and 6 non-pregnant women as a control group were included in the study. Each woman underwent an echocardiographic examination, and had blood pressure on both arms measured and a blood sample taken. MicroRNAs expression was analyzed using Custom TaqMan® Array MicroRNA Cards (Applied Biosystems, Foster City, USA).

Results. Median age of the pregnant women was 34 years (range 25–39 years) and of the control group 32 years (range 29-43 years). Median week of pregnancy was 34 years (range 31–36 years). Most of the examined microRNAs had a lower expression in the pregnancy group (fold change 1.0).

Conclusions. In the 3rd trimester of physiological pregnancy, there is a 244% increase in expression of miR-101a and a decrease by 73% in expression of miR-328. Both of these changes can protect against fibrosis during volume overload occurring in physiological pregnancy.

Key words: pregnancy, microRNA, cardiac remodeling, cardiac fibrosis, volume overload

DOI
10.17219/acem/68945

Introduction

Extracellular matrix (ECM) plays a pivotal role in the proper systolic and diastolic function of the heart as well as in transduction of electrical and chemical signals. It provides structural support for the cardiomyocytes, allowing them to perform their mechanical function. It also ensures communication between cardiomyocytes and fibroblasts. Collagen types I and III are the main types of fibrillar collagens in the cardiac muscle. They are produced by cardiac fibroblasts. The secretion profile of cardiac fibroblasts is influenced by several factors, such as neurohormonal activation, inflammation, age, injury and overload.[1,2] In reaction to different stress stimuli, the action of cardiac fibroblasts changes in order to maintain ECM homeostasis.

Volume overload results in chamber dilation, eccentric cardiac myocyte hypertrophy and changes in ECM remodeling. Increased preload causes augmentation in mechanical stress and rise in neurohormonal activation. Mitral and aortic valve regurgitation are the primary pathological causes of volume overload.[3] This remodeling is different from the reaction to pressure overload. Volume overload is characterized by thinning of the wall and chamber dilatation, which changes the ratio of left ventricle end-diastolic diameter to wall thickness and increases mechanical stress on the wall of the heart. This may be due to expression of anti-fibrotic factors by cardiac myocytes in response to acute volume overload, leading to changes in the proportion between cardiac-specific metalloproteinases and tissue inhibitors of metalloproteinase. As a result, degradation of ECM appears and a structure of changed geometry and shifted proportions between collagen I and III is produced. During end-stage heart failure, which develops as a consequence of prolonged volume overload, an increase of collagen is noted.[3]

Pregnancy is a state which results in progressive continuous volume overload of the heart due to a rise in blood volume with a decrease of peripheral vascular resistance.[4] In this situation, volume overload causes mild eccentric hypertrophy to develop, thought to be physiological. Crucially, the increase in chamber dimension coexists with a proportional increase in wall thickness as well as a proportional increase in myocyte length and width. The mass of the left and right ventricle enlarges.[5] The hemodynamic changes develop throughout the pregnancy and reach their peak in the 3rd trimester, around 30–34 weeks of the pregnancy. It is thought that pregnancy-related cardiac remodeling is not related to fibrosis, but changes in the ECM remain poorly understood.

The aim of this study was to examine the expression of microRNAs associated with fibrosis in pregnant women in the 3rd trimester of pregnancy in order to identify the potential mechanism of ECM remodeling during pregnancy. The hypothesis was that, in pregnant women, an increase in activity of antifibrotic microRNAs or a decrease in profibrotic microRNAs will be observed. This could be a protective mechanism to prevent fibrosis in a state of cardiac overload.

Material and methods

Study population

Six women in singleton pregnancy and 6 non-pregnant women as a control group were included in the study. The recruitment took place in the Cardiology Department of the Institute of Mother and Child in Warszawa, Poland, from October 2013 to October 2014. The study was approved by the Bioethics Committee of the Institute, in accordance with the principles of Good Clinical Practice and the Declaration of Helsinki. All patients gave written informed consent. Inclusion criteria were age >18 years old and singleton pregnancy between 30 and 36 weeks of gestation. Exclusion criteria included known prior cardiovascular disease such as congenital heart disease, myocardial infarction, heart failure, prior myocarditis, clinically relevant arrhythmia, hypertension, and hypertension associated with pregnancy. Each woman underwent an echocardiographic examination, and had blood pressure on both arms measured and a blood sample taken.

Sample preparation and RNA isolation

Blood was collected and subjected to centrifugation. Obtained serum samples were stored in –80°C until the extraction of RNA. Total RNA containing a fraction of miRNA was isolated from 350 µL of each serum sample with a mirVana PARIS Kit (Ambion: Thermo Fisher Scientific, Waltham, USA), according to the manufacturer's protocol.

MicroRNA measurement

Expression of microRNA was analyzed using Custom TaqMan® Array MicroRNA Cards (Applied Biosystems, Foster City, USA). The selected miRNAs were reverse-transcribed using a TaqMan® MicroRNA Reverse Transcription Kit (Applied Biosystems Foster City, USA), according to the manufacturer's instruction. Briefly, 3 µL of sample containing 18 ng of total RNA was added to a prepared reverse-transcription (RT) reaction mix consisting of 6 µL of custom RT primer pool, 0.3 µL of deoxynucleotides (dNTPs) with deoxythymidine triphosphate (dTTP) (100 mM), 3 µL of MultiScribe Reverse Transcriptase (50 U/µL), 1.5 µL of 10 × RT buffer, 0.19 µL of RNase inhibitor (20 U/µL)and 1.01 µL of nuclease-free water (Ambion; Thermo Fisher Scientific, Waltham, USA). A reverse transcription reaction was carried out under the following thermal conditions: 16°C for 30 min, 42°C for 30 min, 85°C for 5 min and then the RT mixture was held at 4°C. Next, the preamplification reaction was

performed using TaqMan® PreAmp Master Mix, ×2 and Custom PreAmp Primer pool (Applied Biosystems, Foster City, USA), according to the protocol of the manufacturer. In brief, 22.5 µL of the preamplification reaction mix was combined with 2.5 µL of each RT product and the reaction was run with thermal-cycling conditions specified by the manufacturer. The preamplification reaction products were diluted 8-fold with ×0.1 TE buffer, pH 8.0 (Ambion; Thermo Fisher Scientific, Waltham, USA) to a final volume of 200 µL. To prepare the quantitative polymerase chain reaction (qPCR), 1.13 µL of diluted PreAmp product was combined with 56.25 µL of TaqMan® Universal Master Mix II, No AmpErase UNG (×2) (Applied Biosystems, Foster City, USA) and 55.12 µL of nuclease-free water (Ambion; Thermo Fisher Scientific, Waltham, USA), and then mixed. Finally, 100 µL of the qPCR reaction mix was dispensed into each port of the TaqMan® MicroRNA Array Card (Applied Biosystems, Foster City, USA), subjected to centrifugation (2 × 1 min, 1200 rpm) and mechanically sealed. Quantitative reverse-transcription polymerase chain reactions (qRT-PCRs) were performed in triplicate for each sample and carried out on ViiA7 Real-Time PCR System (Applied Biosystems, Foster City, USA) with thermal cycling conditions recommended by the manufacturer. Automatic baseline and manual cycle threshold (Ct) were set to 0.2 for all samples. The relative expression level of each miRNA was calculated using the delta delta cycle threshold (ΔΔCt) method. For analysis, we selected 11 microRNAs associated with fibrosis: miR-21 (Assay ID 000397), miR-26a (Assay ID 000405), miR-26b-5p(Assay ID 000407), miR-29a-3p (Assay ID 002112), miR-29b-3p (Assay ID 000413), miR-29c-3p (Assay ID 000587), miR-101a (Assay ID 002253), miR-146a (Assay ID 000468), miR-208a (Assay ID 000511), miR-223 (Assay ID 002295) and miR-328 (Assay ID 000543). Five small RNAs (HY3 (Assay ID 001214), U6 (Assay ID 001973), RNU44 (Assay ID 001094), RNU48 (Assay ID 001006) and miR-103 (Assay ID 000439) were chosen and tested as candidates for endogenous controls. Finally, miRNAs levels were normalized to a U6 snRNA molecule.

Statistical analysis

Due to the small number of participants, variables were not tested for a normal distribution and in all statistical analyses nonparametric tests were used. Continuous variables are represented as median and range of collected values. Categorical variables are presented as number (percentage). In comparisons of nonparametric variables between 2 studied groups, the Mann-Whitney U test was used. To compare nominal variables, a χ^2 test was performed. ΔCt and ΔΔCt were calculated. Descriptions regarding microRNA findings were presented in 2 forms – as frequency of expression, defined as the number of subjects in whom microRNA expression was found/sample size, and as fold change in microRNA expression between the pregnancy group and the control group. Fold change was defined as the amount of times microRNA expression was changed between the control group and pregnancy. A difference in fold change between the groups larger than 2 or less than 0.5 was considered relevant; p-value <0.05 was regarded as statistically significant. SPSS Statistics v. 21 (IBM Corp., Armonk, USA) was used for statistical analysis.

Results

Study group characteristics

The median age of the pregnant women was 34 years (range 25–39 years) and of the control group was 32 years (29–43 years). The median week of pregnancy was 34 (range 31–36 weeks). Upon echocardiographic examination, we did not find any abnormalities to exclude any participant from further analysis. The median left ventricle ejection fraction in the pregnancy group was 60.5% (range 57–62%) and in the control group was 64.5% (range 59–72%) (Mann-Whitney U test = 23.5; p = 0.394). The walls of the heart were thicker in the pregnancy group: for the intraventricular septum the median thickness was 9.5 mm in the pregnancy group (8–11 mm) and 8 mm for the control group (6–11 mm) in diastole (Mann-Whitney U test = 6.5; p = 0.065). For the posterior wall, the median thickness was 8 mm in the pregnancy group (7–10 mm) and 7.5 mm for the control group (7–8 mm) in diastole (Mann-Whitney U test = 9; p = 0.18). The median systolic left ventricle diameter was 32 mm (25–40 mm) in the pregnancy group and 30 mm in the control group (28–37 mm) (Mann-Whitney U test = 16; p = 0.818) and for diastolic the left ventricle diameter was 44.5 mm (39–50 mm) in the pregnancy group and 49 in the control group (40–51 mm) (Mann-Whitney U test = 25; p = 0.310). Upon examination of mitral inflow, the E/A ratio was lower in the pregnancy group (1.19 vs 1.35; Mann-Whitney U test = 25; p = 0.310). A higher dimension of the left atrium (34.5 vs 30.5 mm; Mann-Whitney U test = 8; p = 0.132) and right ventricle (23.5 vs 20.5 mm; Mann-Whitney U test = 7.5; p = 0.093) were observed in the pregnancy group.

Frequency of expression of selected microRNAs

Firstly, we assessed whether the selected microRNAs were expressed in participants from both study groups by calculating expression frequency. Full results are shown in Table 1. In brief, most of the selected microRNAs (miR-21, miR-26a, miR-29a-3p, miR-146a and miR-223) were found in all of the participants, regardless of the study group. There was no presence

Table 1. Frequency of expression of selected microRNAs – number of subjects in whom microRNA expression was found/sample size

Group	miR-21	miR-26a	miR-26b-5p	miR-29a-3p	miR-29b-3p	miR-29c-3p	miR-101a	miR-146a	miR-208a	miR-223	miR-328
Control	6/6	6/6	6/6	6/6	0/6	5/6	3/6	6/6	0/6	6/6	6/6
Pregnancy	6/6	6/6	5/6	6/6	0/6	6/6	4/6	6/6	0/6	6/6	5/6

Table 2. Fold change and interquartile range (IQR) for selected microRNAs in pregnant women in comparison to healthy controls. Difference in fold change between the group larger than 2 or less than 0.5 is considered relevant

Pregnancy	miR-21	miR-26a	miR-26b-5p	miR-29a-3p	miR-29c-3p	miR-101a	miR-146a	miR-223	miR-328
Fold change	0.57	0.60	0.66	1.30	0.95	2.44	0.72	0.91	0.27
IQR (25–75%)	0.23–2.64	0.40–1.25	0.43–2.22	0.72–1.86	0.61–1.96	0–6.42	0.56–1.41	0.72–1.65	0.11–1.29

of miR-29b-3p or miR-208a detected in any of the serum samples. Both miR-26b-5p and miR-328 were found in all of the participants from the control group and 5 in the pregnancy group (83.3%). Expression of miR-29c-3p was detected in 5 samples from the control group and 6 samples from the pregnancy group. As for expression of miR-101a, it was identified in 3 subjects from the control group and 4 from the pregnancy group.

Fold change for selected microRNAs

Further analysis to establish fold change for selected microRNAs in pregnant women in comparison to healthy controls was performed (Table 2). Most of the examined microRNAs had a lower expression in the pregnancy group expressed by a fold change <1.0. The lowest fold change was observed for miR-328, miR-21 and miR-26a. Fold change for miR-29a-3p and miR-101a was >1.0. For miR-101a, fold change between pregnant participants and control group was 2.44 and for miR-29a-3p it was 1.30.

Discussion

Our results show that expression of miR-101a and miR-328 are changed in pregnancy compared to non-pregnant women. Expression of miR-101a increases and miR-328 decreases.

MicroRNA-101a

The data regarding the role of miR-101a indicates that it might play a pivotal role in protecting against fibrosis modulated by transforming growth factor beta signaling (TGFβ). In an animal model of myocardial infarction, it was observed that administration of miR-101a significantly suppressed the expression of TGFβ receptor type 1 (*TGFβRI*), cardiac fibroblast differentiation and collagen content of cardiac ECM. Moreover, overexpression of miR-101a lowered the migration and proliferation of cardiac fibroblasts in response to hypoxia.[6] It was also observed that miR-101a inhibited the hypoxia-induced up-regulation of *TGFβRI* but not TGFβ itself in cardiac fibroblasts. Additionally, it reversed the hypoxia-induced proapoptotic intracellular changes and reduced calcium overload.[6] These indicate the possible role of miR-101a in protecting against hypoxia-induced apoptosis.

MicroRNA-328

Among many others, microRNA miR-328 was tested as a marker of myocardial infarction. He et al. proved that miR-328 and miR-134 are elevated in patients with myocardial infarction.[7] It was also proved that miR-328 was a predictor of mortality and development of heart failure in a 6-month observation. This remained significant after including values of troponin, NT-proBNP, age, gender and smoking status into the multivariable analysis model. It was also proven to be a good biomarker for differentiation of heart failure with reduced or preserved ejection fraction.[8] Interestingly, an up-regulation of miR-328 suppresses matrix metalloproteinase-2 in human osteosarcoma, influencing negatively the metastatic ability of the cancerous cells.[9] This shows its role on the extracellular matrix in different organs and pathological states. High levels of miR-328 seem to have a profibrotic influence on cardiac tissue, resulting in worse prognosis in patients after myocardial infarction. A possible mechanism might be connected to the suppression of metalloproteinases, as in osteosarcoma cells.

Other microRNAs

In our study, there were no differences between the groups in fold change of miR-21, miR-26a, miR-26b-5p, miR-29a-3p, miR-29c-3p, miR-146a and miR-223.

Both miR-146a and miR-21 were assessed in ischemic heart disease. The data suggests that those miRs are related to left ventricle remodeling after myocardial infarction.[10] It is suggested that miR-21 is an important factor of cardiac fibrosis mediated by angiotensin II, through the osteopontin pathway and by increasing fibroblast survival.[11] Other studies suggest, however, that angiotensin II does not influence the level of miR-21 in cardiac fibroblasts.[12]

On the other hand, miR-26a seems to be an antifibrotic agent whose expression level depends on the activity of NF-κB. A rise in the level of miR-26a attenuates collagen I and connective tissue growth factor gene expression in the presence of angiotensin II.[13] Moreover, miR-26 has been linked with stopping cardiac hypertrophy through attenuating glycogen synthase kinase 3β expression.[14]

Other highly examined microRNAs in the context of fibrosis are those of the miR-29 family. They seem to be involved in fibrosis processes in many different organs.[15] The miR-29 family suppresses the expression of several collagens and ECM proteins. Also, miR-29b is downregulated after myocardial infarction, probably influencing scar formation.[16] In in vitro studies, pre-miR-29b reduced collagen and matrix metalloproteinase-2 secretion by cardiac fibroblasts. MiR-29b seems to reduce the profibrotic influence of transforming growth factor beta.[17] Others point to its involvement in apoptosis and angiogenesis after myocardial infarction.[18]

Most mechanisms of action of the miRs described above, in which we did not notice any differences between the 2 examined groups, are related to angiotensin II and its negative influence on cardiac muscle. Very little data is available on the renin–angiotensin–aldosterone system in physiological pregnancy. The data on its comparison between pregnant and non-pregnant women is also scarce. However, this problem has been studied in the context of pregnancy-induced hypertension and preeclampsia. Most available data compares the activity of angiotensin II and angiotensin-converting enzyme between normal pregnancy and the preeclampsia state. Some observations show that, from the renin–angiotensin–aldosterone system, only plasma levels of angiotensin II are elevated in preeclampsia compared to healthy pregnant women. Serum levels of angiotensin 1–7, known for its hypotensive role, were reduced in preeclampsia when compared to normal pregnancy.[19,20] According to other researchers, the levels of angiotensin II is comparable between normal pregnancy and severe preeclampsia in the last weeks of pregnancy.[21] It is suggested that although angiotensin II levels are comparable between normal pregnancy and preeclampsia, there is a lower response to the vasoconstrictive action of angiotensin II. There seems to a be an increase of angiotensin II inactivation by angiotensinase in the serum and placenta with advancing gestation in normal pregnancy.[19,20,22] Therefore, the data on the function and role of the angiotensin–aldosterone system is conflicting and is based on a small amount of data. These observations should be a topic for further studies in order to establish whether the heart of a pregnant woman in a normal pregnancy remains immune to the negative influence of the angiotensin–aldosterone system and what are the possible underlying mechanisms.

It is worthy of note that the data regarding microRNA associated with fibrosis mainly concentrates on patients with myocardial infarction. Data concerning microRNA expression in volume overload is available mostly for animal models and on a small number of subjects.[23,24]

One study compares microRNA expression in patients with bicuspid aortic valve with either stenosis or insufficiency requiring surgical treatment. In this study, microarrays containing 1421 miRNAs were used. The authors describe a 65% reduction in miR-26a, 59% reduction in miR-195 and a 62% reduction in miR-30b in patients with aortic stenosis in comparison with aortic insufficiency. The authors comment that, additionally in in vitro testing, these miRNAs may modulate the genes responsible for the calcification process.[25]

Conclusions

The results of our study show that in physiological pregnancy in the 3rd trimester, there is a 244% increase in the level of miR-101a and a decrease by 73% in the levels of miR-328. Both of these changes can be protective of fibrosis during the volume overload occurring in physiological pregnancy.

References

1. Goldsmith EC, Bradshaw AD, Zile MR, Spinale F. Myocardial fibroblast-matrix interactions and potential therapeutic targets. *J Mol Cell Cardiol*. 2014;70:92–99.
2. Bowers SLK, Banerjee I, Baudino TA. The extracellular matrix: At the center of it all. *J Mol Cell Cardiol*. 2010;48:474–482.
3. Hutchinson KR, Stewart JA, Lucchesi PA. Extracellular matrix remodeling during the progression of volume overload-induced heart failure. *J Mol Cell Cardiol*. 2010;48:564–569.
4. Chung E, Leinwand LA. Pregnancy as a cardiac stress model. *Cardiovasc Res*. 2014;101:561–570.
5. Sanghavi M, Rutherford JD. Cardiovascular physiology of pregnancy. *Circulation*. 2014;130:1003–1008.
6. Zhao X, Wang K, Liao Y, et al. MicroRNA-101a inhibits cardiac fibrosis induced by hypoxia via targeting TGFβRI on cardiac fibroblasts. *Cell Physiol Biochem*. 2015;35:213–226.
7. He F, Lv P, Zhao X, et al. Predictive value of circulating miR-328 and miR-134 for acute myocardial infarction. *Mol Cell Biochem*. 2014;394:137–144.
8. Watson CJ, Gupta SK, O'Connell E, et al. MicroRNA signatures differentiate preserved from reduced ejection fraction heart failure. *Eur J Heart Fail*. 2015;17:405–415.
9. Yang SF, Lee WJ, Tan P, et al. Upregulation of miR-328 and inhibition of CREB-DNA-binding activity are critical for resveratrol-mediated suppression of matrix metalloproteinase-2 and subsequent metastatic ability in human osteosarcomas. *Oncotarget*. 2015;6:2736–2753.
10. Liu X, Dong Y, Chen S, et al. Circulating microRNA-146a and microRNA-21 predict left ventricular remodeling after ST-elevation myocardial infarction. *Cardiology*. 2015;132:233–241.
11. Lorenzen JM, Schauerte C, Hübner A, et al. Osteopontin is indispensable for AP1-mediated angiotensin II-related miR-21 transcription during cardiac fibrosis. *Eur Heart J*. 2015;36:2184–2196.
12. Ning Q, Jiang X. Angiotensin II upregulated the expression of microRNA-224 but not microRNA-21 in adult rat cardiac fibroblasts. *Biomed Rep*. 2013;5:776–780.
13. Wei C, Kim IK, Kumar S, et al. NF-κB mediated *miR-26a* regulation in cardiac fibrosis. *J Cell Physiol*. 2013;228:1433–1442.
14. Zhang ZH, Li J, Liu BR, et al. MicroRNA-26 was decreased in rat cardiac hypertrophy model and may be a promising therapeutic target. *J Cardiovasc Pharmacol*. 2013;62:312–319.
15. He Y, Huang C, Lin X, Li J. MicroRNA-29 family, a crucial therapeutic target for fibrosis diseases. *Biochimie*. 2013;95:1355–1359.
16. van Rooij E, Sutherland LB, Thatcher JE, et al. Dysregulation of microRNAs after myocardial infarction reveals a role of miR-29 in cardiac fibrosis. *Proc Natl Acad Sci U S A*. 2008;105:13027–13032.

17. Abonnenc M, Nabeebaccus AA, Mayr U, et al. Extracellular matrix secretion by cardiac fibroblasts: Role of microRNA-29b and microRNA-30c. *Circ Res*. 2013;113:1138–1147.
18. Zhang G, Shi H, Wang L, et al. MicroRNA and transcription factor mediated regulatory network analysis reveals critical regulators and regulatory modules in myocardial infarction. *PLoS One*. 2015;10(8):e0135339. https://doi.org/10.1371/journal.pone.0135339
19. Tanbe AF, Khali RA. Circulating and vascular bioactive factors during hypertension in pregnancy. *Curr Bioact Compd*. 2010;6:60–75.
20. Mizutani S, Tomoda Y. Effects of placental proteases on maternal and fetal blood pressure in normal pregnancy and preeclampsia. *Am J Hypertens*. 1996;9:591–597.
21. Furuhashi N, Tsujiei M, Kimura H, Yajima A, Nahae H, Kimur C. Maternal and fetal atrial natriuretic peptide levels, maternal plasma renin activity, angiotensin II, prostacyclin and thromboxane A2 levels in normal and preeclamptic pregnancies. *Tohoku J Exp Med*. 1991;165:79–86.
22. Mizutani S, Tamodo Y. Effects of placental proteases on maternal and fetal blood pressure in normal pregnancy and preeclampsia. *Am J Hypertens*. 1996;9:591–597.
23. Cirera S, Moesgaard SG, Zois NE, et al. Plasma proANP and SDMA and microRNAs are associated with chronic mitral regurgitation in a pig model. *Endocr Connect*. 2013;2:161–171.
24. Li Q, Freeman LM, Rush JE, Laflamme DP. Expression profiling of circulating microRNAs in canine myxomatous mitral valve disease. *Int J Mol Sci*. 2015;16:14098–14108.
25. Nigam V, Sievers HH, Jensen BC, et al. Altered microRNAs in bicuspid aortic valve: A comparison between stenotic and insufficient valves. *J Heart Valve Dis*. 2010;19:459–465.

Anti-inflammatory and antioxidant effects of mesenchymal and hematopoietic stem cells in a rheumatoid arthritis rat model

Hanan Abdelmawgoud[A–F], Asmaa Saleh[A–F]

Department of Biochemistry, Faculty of Pharmacy, Al-Azhar University, Cairo, Egypt

A – research concept and design; B – collection and/or assembly of data; C – data analysis and interpretation;
D – writing the article; E – critical revision of the article; F – final approval of the article

Advances in Clinical and Experimental Medicine, ISSN 1899-5276 (print), ISSN 2451-2680 (online) *Adv Clin Exp Med*. 2018;27(7):873–880

Address for correspondence
Hannan Abdelmawgoud
E-mail: hananmoawad@gmail.com

Funding sources
None declared

Conflict of interest
None declared

Received on March 15, 2017
Reviewed on April 25, 2017
Accepted on May 14, 2017

Abstract

Background. Mesenchymal stem cells (MSCs) are of increased importance because of their capacity to counteract inflammation and suppress host immune responses.

Objectives. The aim of the study was to compare the effectiveness of MSCs and hematopoietic stem cells (HSCs) in the treatment of rheumatoid arthritis (RA).

Material and methods. Paw swelling was assessed by measuring the thickness of the hind paws using a caliper. Cytokines – interleukin (IL)-6, tumor necrosis factor-alpha (TNF-α), transforming growth factor-beta (TGF-β), and IL-10 – and rheumatoid factor (RF) were measured using enzyme-linked immunosorbent assay (ELISA) kits. Oxidative stress biomarkers – malondialdehyde (MDA) and reduced glutathione (GSH) were assessed. Nuclear factor-kappaB (*NF-κB*) was detected by the western blot technique. Toll-like receptor-2 (*TLR-2*), matrix metalloproteinase-3 (*MMP-3*) and cartilage oligomeric matrix protein-1 (*COMP-1*) gene expression were assessed by the real-time quantitative analysis. Mesenchymal stem cells were isolated from the bone marrow (BM) of rats and HSCs were isolated from human umbilical cord blood (UCB).

Results. Paw edema, RA score, RF, cytokine assay, antioxidant state, *NF-κB*, *TLR-2*, *MMP3*, and *COMP-1* showed improvement in the group that received MSCs compared to the group that received HSCs and the group that received methotrexate.

Conclusions. Mesenchymal stem cells are very effective in reducing RA inflammation; they are superior to HSC and methotrexate treatment. Mesenchymal stem cells could become a better therapeutic opportunity for the treatment of RA.

Key words: methotrexate, rheumatoid arthritis, mesenchymal stem cells, hematopoietic stem cells

DOI
10.17219/acem/73720

Introduction

Rheumatoid arthritis (RA) is a systemic autoimmune disease that basically affects the joints and is influenced by hereditary and environmental factors.[1] Patients with RA have short lifespans due to comorbidities. Inflammation plays a vital role in the development of cardiovascular disease; however, little is known about its association with other comorbidities.[2] In the pathophysiology of RA, there is interaction between T cells, B cells and some cytokines. Pro-inflammatory cytokines have not only articular effects, but also systemic effects, like acute-phase protein production, cardiovascular disease, osteoporosis, and anemia.[3]

Tumor necrosis factor-alpha (TNF-α) plays an important role in the regulation of the production of other pro-inflammatory cytokines in rheumatic synovial tissue.[4] Interleukin (IL)-4, IL-10 and IL-13 are anti-inflammatory cytokines that compensate for the action of pro-inflammatory cytokines in the synovial membrane in RA. Transforming growth factor-beta (TGF-β) is a pleiotropic cytokine that has different functions in angiogenesis, hematopoiesis, cell proliferation, differentiation, migration, and apoptosis. As Gonzalo-Gil and Galindo-Izquierdo wrote: „Although its role in rheumatoid arthritis is not well defined, the TGF-β activation leads to functional immunomodulatory effects according to environmental conditions."[5]

In the synovial cells of RA patients, the stimulation of the nuclear factor-kappaB (*NF-κB*) pathway leads to the transactivation of a lot of responsive genes that result in the inflammatory phenotype, including matrix metalloproteinases (MMPs) from synovial fibroblasts, TNF-α from macrophages and chemokines that deliver immune cells to the inflamed pannus.[6]

Toll-like receptors (TLRs) are expressed by the cells inside the RA joint, and there is a group of endogenous TLR ligands in the inflamed joints of RA patients. The activation by these ligands may result in the continuous expression of pro-inflammatory cytokines by macrophages and the joint damage that takes place in RA. This supports a possible role for the TLR signalling suppression as a new curative line in RA.[7]

Measurement of biological markers for cartilage degradation and repair would be a useful approach in RA monitoring. Cartilage oligomeric matrix protein (COMP) is one of the arthritis markers that is released into the synovial fluid and other body fluids, like blood. In several studies, COMP has been used as a diagnostic and prognostic marker of disease severity and the effect of treatment.[8] Cartilage oligomeric matrix protein binds to many extracellular matrix proteins, and other proteins, like MMPs, are known to regulate the levels of COMP under different conditions.[9]

Methotrexate is the most frequently used treatment in RA. For most RA patients, it is suggested as the first disease-modifying anti-rheumatic drug (DMARD), and its co-prescription is recommended with biologic DMARDs.[10,11] Due to the side effects and high cost of these medications, it is important to develop a new and more effective therapy for RA.

Mesenchymal stem cells (MSCs) exist in all tissues as multipotent adult stem cells that can differentiate into various tissues, arising from mesoderm-like cartilage, bone and cardiac muscle. Mesenchymal stem cells are very effective in cell therapy because of their easy access, straightforward isolation and their bio-preservation with minimal loss of potency. Therefore, MSCs are being examined to regenerate injured tissue and cure inflammation.[12]

Mesenchymal stem cells can be used to adjust autoimmune responses and in autoimmune disease treatment, because they cause immunosuppression by modulating T and B cell proliferation and differentiation, dendritic cell growth and the activity of natural killer cells.[13] Mesenchymal stem cells can differentiate to several cell lineages, such as osteoblasts and chondrocytes.[14] Furthermore, MSCs show high migration and motility, and can secrete cytokines to enhance the repair of damaged tissues; accordingly, MSCs have been used to treat many diseases in clinical trials.[15] Mesenchymal stem cells are thought to be able to treat several congenital and acquired bone degenerative diseases, and to fix and regenerate injured bone tissues, contributing to better clinical results in skeletal tissue repair and regeneration. Mesenchymal stem cells can be transplanted by blending with autogenous plasma/serum or by packing onto repair/induction supportive resorbable structures.[16]

This study aimed to compare the effectiveness of MSCs and hematopoietic stem cells (HSCs) in the treatment of RA.

Material and methods

Preparation of the animal model

The study was carried out on 40 male Wistar rats (average weight: 150–200 g). All the ethical protocols for animal treatment were followed and supervised by the animal facilities at the Faculty of Medicine of Cairo University (Egypt). The rats were divided into 5 groups of 8 animals each. Group 1 was the negative control (NC) group, and received 1 mL saline by intravenous injection. Group 2 was the positive control (PC), in which arthritis was induced by injecting each rat with 0.1 mL of complete Freund's adjuvant (CFA) (Sigma-Aldrich, St. Louis, USA), producing definite edema within 24 h, with progressive arthritis by day 9 after inoculation.[17] Treatments were initiated from day 10 and continued through day 37. Group 3 (MTX) comprised arthritis rats that received 2 mg/kg of methotrexate (MTX) once a week for 4 weeks.[18] Group 4 (MSC) comprised arthritis rats that received MSCs in a single intravenous dose in the form of a cell suspension containing 10^6 allogeneic MSCs derived from the bone marrow (BM)

of rats. Group 5 (HSC) was composed of arthritis rats that received HSCs in a single intravenous dose in the form of a cell suspension containing 10^6 allogeneic HSCs derived from human umbilical cord blood (UCB).[19]

Isolation and culture of bone marrow mesenchymal stem cells

Bone marrow was harvested by flushing the tibiae and femurs of rats with Dulbecco's modified Eagle's medium (DMEM) (Lonza Bioscience, Verviers, Belgium) supplemented with 10% fetal bovine serum. Nucleated cells were isolated with a density gradient (Ficoll-Paque; Gibco-Invitrogen, Grand Island, USA). This mononuclear layer was aspirated, washed twice in phosphate-buffered saline (PBS) containing 2 mM of ethylenediaminetetraacetic acid (EDTA) and centrifuged for 10 min at 200 × g at 10°C, and re-suspended in complete culture medium supplemented with 1% penicillin-streptomycin. The cells were incubated at 37°C in 5% CO_2 for 14 days. When large colonies developed (80–90% confluence), the cultures were washed twice with PBS and the cells were trypsinized with 0.25% trypsin in 1 mM EDTA for 5 min at 37°C. After centrifugation, the cells were re-suspended in serum-supplemented medium and incubated in Falcon® tissue culture flasks. The cultured MSCs were confirmed by morphology and fluorescent analysis cell sorting (FACS), by detecting CD29+ve and CD34–ve specific to MSCs (Fig. 1).[20]

Collection of human umbilical cord blood and isolation of hematopoietic stem cells

Human umbilical cord blood was withdrawn immediately after normal vaginal delivery within 24 h of the rupture of the membranes and before the separation of the placenta. Written informed consent was obtained from each woman after a full explanation of the study. The umbilical cord was sterilized with 70% alcohol followed by betadine at the needle insertion site. As much bloodflow as possible was collected. Anti-coagulated UCB was diluted 1:4 with PBS containing 2 mM EDTA. Cord blood mononuclear cells (MNCs) were separated by centrifugation over Ficoll-Paque (Gibco-Invitrogen) at 400 × g for 35 min at 10°C. The MNC fraction was washed first in PBS, then with magnetic cell sorting buffer (MACS: PBS supplemented with 0.5% bovine serum albumin and 2 mM EDTA, pH 7.2). CD34+ cells were isolated from MNCs using a CD34+ positive cell selection kit (Mini-Macs; Miltenyi Biotec, Bergisch Gladbach, Germany) according to the manufacturer's instructions. The percentage of isolated CD34+ cells was characterized by flow cytometry (Fig. 1).[21]

Clinical scoring of paw edema

Paw swelling was assessed by measuring the thickness of the hind paws using a caliper. Joint swelling was scored using an arthritis index. Briefly, a score of 0–4 was assigned, where 0 means there was no evidence of hyperemia and/or inflammation; 1 indicates hyperemia with little or no paw swelling; 2 represents swelling confined predominantly to the ankle region, with modest hyperemia; 3 indicates increased paw swelling and hyperemia of the ankle and metatarsal regions; and 4 indicates maximal paw swelling and hyperemia involving the ankle, metatarsal and tarsal regions.

Biochemical measurement of rheumatoid factor, IL-6, IL-10, TNF- α, and TGF-β

Serum rheumatoid factor (RF) was determined using a QUANTA Lite enzyme-linked immunosorbent assay (ELISA) kit (Inova Diagnostics, San Diego, USA) according to the manufacturer's instructions. Serum IL-6, IL-10, TNF-α, and TGF-β were measured using Quantikine ELISA kits (R&D Systems Inc., Minneapolis, USA) according to the manufacturer's instructions.

Measurement of malondialdehyde

Joint tissue was homogenized in 1 mL PBS, pH 7.0, with a micropestle in a microtube. Then 20% trichloroacetic acid (TCA) was added to the tissue homogenate to precipitate the protein, and the mixture was centrifuged. Supernatants were collected and the thiobarbituric acid (TBA) solution was added to them. After boiling for 10 min in a water bath, the absorbance of the clear supernatant was determined at 535 nm. The concentration of malondialdehyde (MDA) was calculated using a series of standard solutions (0, 0.625, 1.25, 2.5, 5.0, and 10 nmol/mL).[22]

Measurement of reduced glutathione

Joint tissue was homogenized in PBS, pH 8.0, and then 5% TCA was added to the homogenate to precipitate the protein. After centrifugation, the dithiobisnitrobenzoate (DTNB) solution was added to the supernatants of the tissue homogenate, and they were incubated for 1 h.

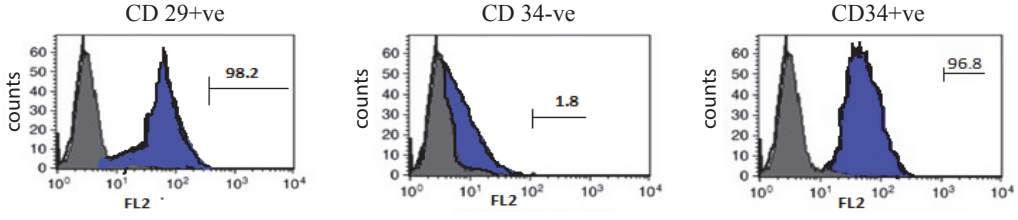

Fig. 1. Characterization of BM-MSCs by CD 29+ve and CD 34–ve and characterization of HSCs by CD 34+ve

BM-MSCs – bone marrow mesenchymal stem cells; HSCs – hematopoietic stem cells.

The absorbance was measured at 412 nm. The concentration of reduced glutathione (GSH) was calculated using the standard curve with the following concentrations: 0, 10, 20, 40, 50, and 100 mmol/mL.[23]

Real-time quantitative analysis for *MMP-3*, *COMP-1* and *TLR2* gene expression

Total RNA was extracted from the joint tissue homogenate using the SV Total RNA Isolation System (Promega, Madison, USA) according to the manufacturer's instructions. Complementary DNA (cDNA) was synthesized from 1 µg RNA using the SuperScript III First-Strand Synthesis System as described in the manufacturer's protocol (No. K1621, Fermentas, Waltham, USA). The real-time quantitative polymerase chain reaction (PCR) amplification and analysis were performed using a StepOne™ real-time quantitative PCR system with software v. 3.1 (Applied Biosystems, Thermo-Fisher Scientific Inc., Waltham, USA). The reaction contained a SYBR Green Master Mix (Applied Biosystems), gene-specific primer pairs designed with Gene Runner Software (Hasting Software Inc., Hasting, USA) from RNA sequences from GenBank. The data from the real-time assays were calculated using Sequence Detection Software v. 1.7 (PE Biosystems, Foster City, USA). The relative quantification (RQ) of the studied gene mRNA was calculated using the comparative Ct method. All values were normalized to *β-actin*, which was used as the control housekeeping gene, and were reported as fold changes over background levels detected in the disease groups.

Detection of *NF-κB* by western blot technique

Nuclear factor-kappaB was detected using a V3 Western Workflow™ Complete System (Bio-Rad Laboratories Inc., Hercules, USA). The protein was extracted from the tissue homogenates using the ice-cold radioimmunoprecipitation assay (RIPA). The lysis buffer PL005 (Bio BASIC Inc., Markham, Canada) consisting of 50 mM Tris hydrochloride (Tris HCL), 150 mM sodium chloride (NaCl), 1% Triton X-100, 1% sodium deoxycholate, and 0.1% sodium dodecyl sulfate (SDS) was supplemented with phosphatase and protease inhibitors, and then centrifuged at 12,000 rpm for 20 min at 4°C. The protein concentration for each sample was determined using the Bradford assay. Equal amounts of protein (20–30 µg of total protein) and the 2X Laemmli buffer were heated at 70°C for 5–10 min and separated by SDS/polyacrylamide gel electrophoresis (SDS-PAGE) using a Mini-Protein II system (Bio-Rad Laboratories Inc.). The protein was transferred to polyvinylidene difluoride (PVDF) membranes (Pierce Biotechnology Inc., Rockford, USA) with a TGX Stain-Free™ FastCast™ Acrylamide Kit (Bio-Rad Laboratories Inc.). After the transfer, the membranes were washed with Tris-buffered saline (TBS) and blocked for 1 h at room temperature with 5% (w/v) skimmed milk powder in TBS. The manufacturer's instructions were followed for the primary antibody reactions. Following the blocking, the blots were developed using antibodies for *NF-κB* and *β-actin* (Thermo Fisher Scientific, Rockford, USA), incubated overnight at pH 7.6 at 4°C with gentle shaking. After washing, peroxidase-labeled secondary antibodies were added, and the membranes were incubated at 37°C for 1 h, then washed with TBS 5 times for 5 min. Clarity Western ECL chemiluminescent substrate (Bio-Rad Laboratories Inc.) was applied to the blot according to the manufacturer's recommendations. Band intensity was analyzed using a ChemiDoc™ imaging system with Image Lab™ software v. 5.1 (Bio-Rad Laboratories Inc.). The results were expressed as arbitrary units after normalization for *β-actin* protein expression.

Statistical analysis

The normality of data distribution was tested using the Shapiro-Wilk normality test. The analysis of normally distributed data was done by one-way analysis of variance (ANOVA), followed by Tukey's multiple comparison test (the data is expressed as mean with standard deviation – SD). For non-normally distributed data, the Kruskal-Wallis test was used to compare the median of each group, followed by Dunn's multiple comparison test using Prism v. 5.03 software (GraphPad Software, La Jolla, USA). Statistical significance was set at $p < 0.05$.

Results

Paw edema was lower in the MTX group (3.37 ±0.65 mm), the MSC group (2.73 ±0.52 mm) and the HSC group (3.32 ±0.57 mm) than in the PC group (4.88 ±1.17 mm), with p-values <0.001, <0.0001 and <0.001, respectively (Fig. 2A). The evaluation of the RA score indicated that the PC group showed the top score (median: 4, range: 3–4), which was significantly higher than that observed in the MTX group (median: 2, range: 1–2) with p-value <0.05 and in the MSC group (median: 1, range: 1–2) with p-value <0.0001 (Fig. 2B). There was no significant difference between the PC group and the HSC group (median: 2, range: 1–3). There was also no significant difference between the MTX group and both the MSC and HSC groups, nor between the MSC and HSC groups. Serum RF was lower in the MTX (29.1 ±8.3 IU/mL), MSC (18.36 ±2.72 IU/mL) and HSC (33.3 ±4.13 IU/mL) groups compared to the PC group (45.49 ±8.95 IU/mL) with p-values <0.0001, <0.0001 and <0.001, respectively. The decrease in RF in the MSC group was significantly greater than in the MTX or HSC groups ($p < 0.001$ and $p < 0.0001$, respectively) (Fig. 2C).

Serum levels of IL-6, TNF-α and TGF-β were decreased in the MTX group (88.36 ±13.04, 99.43 ±16.01

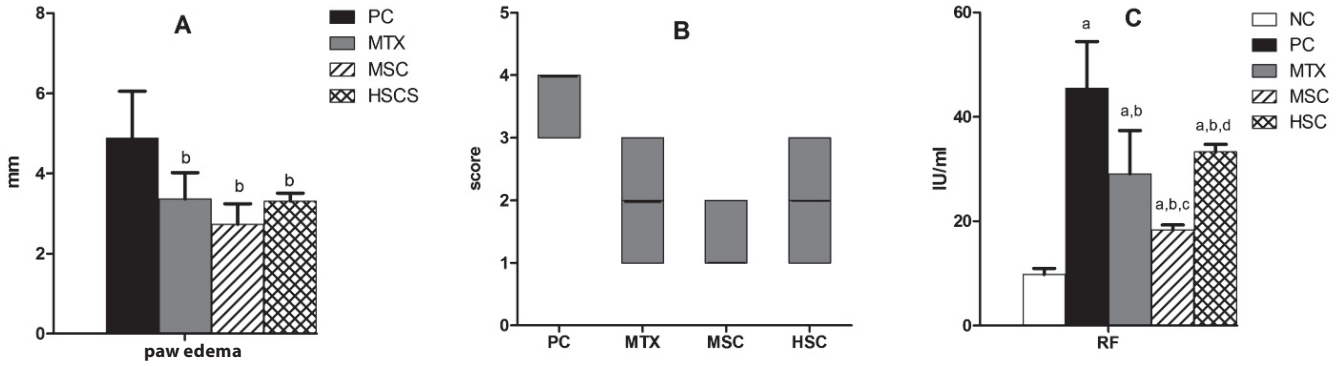

Fig. 2. The effects of different treatments on paw edema (A), RA score (B) and RF (C)

Parameters are presented on the charts as means ±SD (A, C) and as median and range (B); NC – negative control group; PC – positive control group; MTX – methotrexate group; MSC – mesenchymal stem cells group; HSC – hematopoietic stem cells group; a – significantly different from NC; b – significantly different from PC; c – significantly different from MTX; d – significantly different from MSC.

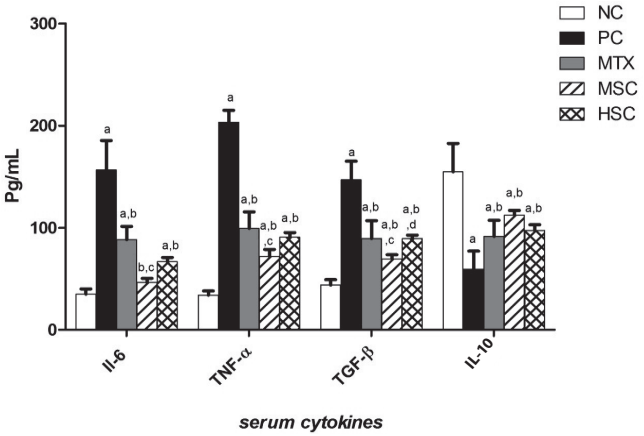

Fig. 3. The effects of different treatments on IL-6, TNF-α, TGF-β and IL-10

Parameters are presented on the charts as means ±SD; NC – negative control group; PC – positive control group; MTX – methotrexate group; MSC – mesenchymal stem cells group; HSC – hematopoietic stem cells group; IL-6 – interleukin-6; TNF-α – tumor necrosis factor-alpha; TGF-β – transforming growth factor-beta; IL-10 – interleukin-10; a – significantly different from NC; b – significantly different from PC; c – significantly different from MTX; d – significantly different from MSC.

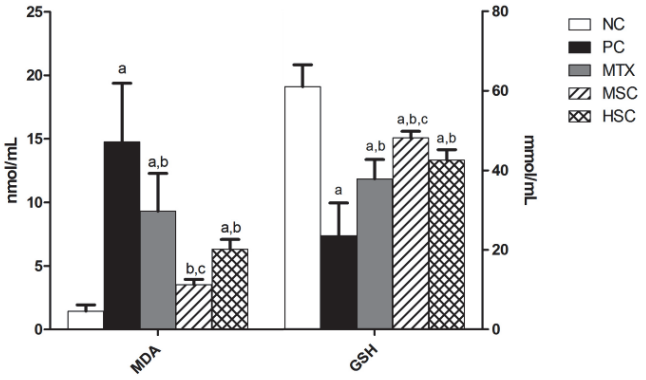

Fig. 4. The effects of different treatments on MDA and GSH

Parameters are presented on the charts as means ±SD; NC – negative control group; PC – positive control group; MTX – methotrexate group; MSC – mesenchymal stem cells group; HSC – hematopoietic stem cells group; MDA – malondialdehyde; GSH – reduced glutathione; a – significantly different from NC; b – significantly different from PC; c – significantly different from MTX; d – significantly different from MSC.

and 89.53 ±17.34 Pg/mL, respectively), the MSC group (46.38 ±11.63, 72 ±19.19 and 69.19 ±12.38 Pg/mL, respectively) and the HSC group (66.83 ±11.24, 90.75 ±12.73 and 89.4 ±9.2 Pg/mL, respectively) compared to the PC group (156.6 ±28.74, 203.3 ±11.73 and 146.8 ±18.38 Pg/mL, respectively) ($p < 0.0001$). In the MSC group, IL-6 and TNF-α were significantly lower than in the MTX group ($p < 0.0001$ and $p < 0.001$, respectively); there was no significant difference in IL-6 compared to the NC group (34.93 ±5.1 Pg/mL) ($p > 0.05$). Furthermore, TGF-β was lower in the MSC group than in the MTX and HSC groups ($p < 0.05$). The 3 treated groups (MTX, MSC and HSC) showed elevated IL-10 levels in comparison to the PC group (59.49 ±17.67 Pg/mL) ($p < 0.05$, $p < 0.0001$ and $p < 0.001$, respectively). Interleukin-10 was also elevated in the MSC group (112.3 ±13.33 Pg/mL) compared with the MTX (91.44 ±15.83 Pg/mL) and HSC (97.23 ±16.36 Pg/mL) groups, but this elevation was not significant (Fig. 3).

Malondialdehyde was significantly lower in the MTX (9.33 ±2.96 nmol/mL), MSC (3.53 ±1.17 nmol/mL) and HSC (6.33 ±2.16 nmol/mL) groups than in the PC group (14.76 ±4.62 nmol/mL) ($p < 0.001$, $p < 0.0001$ and $p < 0.0001$, respectively); it was also significantly lower in the MSC group than in the MTX group ($p < 0.001$). Glutathione was significantly higher in the MTX (37.83 ±4.86 nmol/mL), MSC (48.13 ±4.76 nmol/mL) and HSC (42.51 ±7.45 nmol/mL) groups than in the PC group (23.54 ±8.24 nmol/mL) ($p < 0.0001$), and in the MSC group than in the MTX group ($p < 0.05$). There was no significant difference between the MSC group and the NC group (1.45 ±0.49 nmol/mL) with respect to MDA (Fig. 4).

The MSC group showed lower *TLR-2*, *MMP-3* and *COMP-1* (relative quantification) (2.47 ±0.39, 2.72 ±1.04 and 2.73 ±0.64, respectively) than the PC (13.35 ±1.65, 13.34 ±3.7 and 13.25 ±1.94, respectively) and MTX

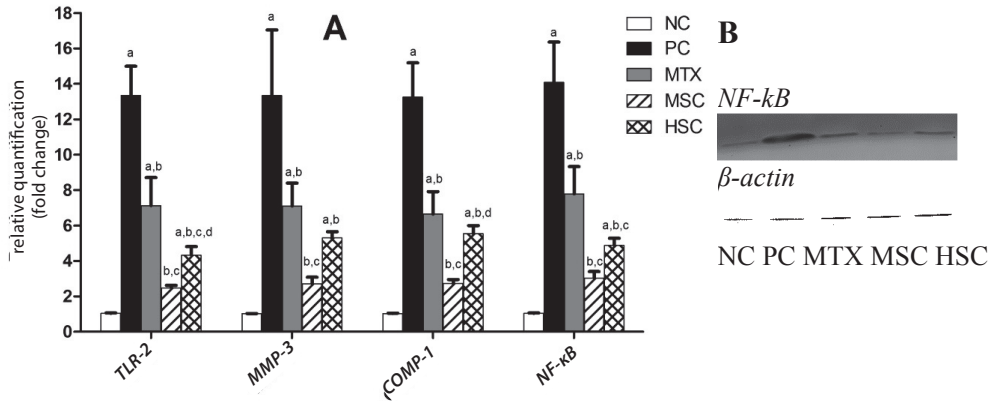

Fig. 5. The effects of different treatments on *TLR-2*, *MMP-3*, *COMP-1* and *NF-κB* (A) and *NF-κB* protein blotting (B)

Parameters are presented on the charts as means ±SD; NC – negative control group; PC – positive control group; MTX – methotrexate group; MSC – mesenchymal stem cells group; HSC – hematopoietic stem cells group; *TLR-2* – toll-like receptor-2; *MMP-3* – matrix metalloproteinase-3; *COMP-1* – cartilage oligomeric matrix protein-1; *NF-κB* – nuclear factor-kappaB; b – significantly different from PC; c – significantly different from MTX; d – significantly different from MSC.

(7.13 ±1.6, 7.11 ±1.28 and 6.65 ±1.26, respectively) groups ($p < 0.0001$). Toll-like receptor-2 and *COMP-1* were also significantly lower in the MSC group than in the HSC group (4.33 ±1.35 and 5.55 ±1.26, respectively), with p-values <0.05 and <0.0001, respectively. Toll-like receptor-2 was significantly decreased in the HSC group in comparison to both the PC and MTX groups ($p < 0.0001$), while *MMP-3* and *COMP-1* were only lower in the HSC group (5.3 ±0.99 and 5.55 ±1.26, respectively) compared to the PC group ($p < 0.0001$) (Fig. 5A). Nuclear factor-kappaB was significantly decreased in the 3 treated groups (MTX: 7.78 ±1.55, MSC: 3.02 ±1.06 and HSC: 4.88 ±1.15), with the lowest value in the MSC group compared to the PC group (1.04 ±0.07) ($p < 0.0001$). Nuclear factor-kappaB was lower in the MSC and HSC groups than in the MTX group, with p-values <0.0001 and <0.001, respectively (Fig. 5A, 5B).

Discussion

In the last 10 years, MSCs have drawn attention in the field of regenerative medicine because of their capacity to differentiate into specific cell types, their substantial production of soluble growth factors and cytokines and their hematopoiesis-supporting properties. Moreover, MSCs can move to areas of inflammation and exert potent immunomodulatory and anti-inflammatory actions by cell-to-cell interactions between MSCs and lymphocytes or by soluble factor production. Thus, it should be possible to use MSCs for future clinical treatment of several diseases.[24]

Mesenchymal stem cells are suggested by many studies to be highly immunosuppressive both in vivo and in vitro. They intensely inhibit the proliferation of many immune cells, such as T cells, B cells, dendritic cells and natural killer cells. Furthermore, some soluble factors such as TGF-β and human growth factor (HGF) have been shown to play a role in the immunosuppressive actions of MSCs. This suggests that MSCs have the ability to treat immune disorders, prevent organ transplantation rejection and heal injured tissue.[25]

Various studies have been performed on MSCs originating from BM. Their transplantation from BM is assumed to be safe, and the results of their effects on neurological, cardiovascular and immunological diseases are hopeful. Mesenchymal stem cells have been found to enhance angiogenesis and have been used in the treatment of kidney, lung and muscle injuries as well as of chronic skin wounds.[12]

In RA, joint inflammation is caused by the infiltration of immune cells, synovial hyperproliferation, and the overproduction of proinflammatory cytokines, such as TNFα, IL-1β, IL-6, IL-17 and IFNγ, finally causing cartilage and bone damage.[26] The therapeutic effect of MSCs in collagen-induced arthritis (CIA) might be related to the induction of regulatory T cells (Treg) by MSCs.[27]

In the current study, BM-derived MSCs were isolated, grown and characterized by CD29+ve, one of the surface markers of MSCs, and were used to investigate the role of MSCs, compared to HSCs (CD34+ve) and methotrexate, in the amelioration of arthritis in an experimental rat model, and to assess whether MSCs and HSCs could improve arthritis. We found that injecting MSCs into RA rats resulted in a rapid reversal of tissue inflammation. This drastic effect was accompanied by a diminished tissue level of IL-6, TNF-α, TGF-β, *NF-κB*, *TLR-2*, *MMP-3*, *COMP-1*, and RF, a better antioxidant state and an elevated production of anti-inflammatory cytokine IL-10 in RA/MSC rats.

This concurs with the results published by Ganesan et al., who showed the ability of MSCs to suppress the immune system.[28] A study by Augello et al. demonstrated that MSC injection stopped bone and cartilage damage and induced T cell hyporesponsiveness in the form of reduced proliferation and modified inflammatory cytokine

expression; serum TNF-α levels in particular were significantly lowered.[29]

The ability of MSCs to inhibit the proliferation of stimulated T cells as well as TNF-α secretion was observed by Liu et al.[30] The valuable effect of MSCs was proven by their attenuation of systemic inflammation, the reduction of proinflammatory cytokines (IL-6 and TNF-α) and an increased production of the anti-inflammatory cytokine IL-10 in CIA mice. After injecting CIA mice with MSCs, the severity of arthritis was significantly reduced. Moreover, MSC injection caused complete disappearance of paw swelling.[31]

Little is known about the mechanisms of the immunoregulatory activities of MSCs, but both direct and indirect effects have been proposed, through either cell-to-cell interaction or soluble factors. The immunosuppression of MSCs needs the MSCs to be activated first by immune cells via the secretion of some proinflammatory cytokines, such as IFN-γ, TNF-α, IL-1α or IL-1β.[32] Various studies done on BM MSCs have revealed that the immunomodulation effect mediated by MSCs depends on IFN-γ, and is primarily mediated by soluble factors, like indolamine 2,3-dioxygenase or prostaglandin E2 (PGE2), which inhibit the proliferation and function of both T and B cells. Prostaglandin E2 potentially suppresses the immune system through the inhibition of T cell mitogenesis and IL-2 production, and helps stimulate the activity of Th type 2 lymphocytes. The stimulation of TNF-α or IFN-γ enhances the production of PGE2 by MSCs, which stimulates IL-10 production from the macrophages and blocks the differentiation of monocytes to dendritic cells.[33]

It has been reported that IL-6, another factor derived from MSCs, could inhibit monocyte differentiation to dendritic cells, decreasing their ability to stimulate T cells. Activated MSCs have been found to produce hepatocyte growth factor, heme oxygenase-1, leukemia inhibitory factor, and TGF-β1. The cell-to-cell contact between MSCs and activated T cells prompts the production of IL-10, which participates in human leukocyte antigen (HLA)-G5 release. The immunoregulation mediated by MSCs is therefore considered a sum of the collective activities of various molecules.[34]

Greish et al. reported that injecting stem cells (MSCs and HSCs) obtained from human UCB into CFA rats significantly decreased arthritis severity.[35] They found that paw swelling had totally disappeared 21–34 days after stem cell administration. Moreover, they found a significant downregulation of TNF-α, IL-1 and IFN-γ, and the upregulation of IL-10 after the injection of HSCs and MSCs.[35] Park et al. also found that MSCs significantly increased the levels of IL-10 and TGF-β, and decreased serum IL-1β, TNF-α, IL-6, and IFN-γ.[27]

Mesenchymal stem cell licensing is related to the activation of TLRs expressed on the MSC surface. Mesenchymal stem cells are polarized toward either an inflammatory or an anti-inflammatory direction, depending on the TLR type. Toll-like receptor-4 (TLR-4) stimulation produces pro-inflammatory cytokines, such as IL-6, IL-8 and TGF-β, developing the MSC1 phenotype. Conversely, when certain ligands bind to TLR-3, immunosuppressive MSC2 cells are stimulated to release indolamine 2,3-dioxygenase.[36, 37]

El-denshary et al. reported that the expression of *MMP-3*, *COMP* and *TNF-α* genes was significantly reduced, while *IL-10* gene expression was significantly increased in the MSC group compared to the CIA group.[38] Their results indicated that MSCs were better than betamethasone in treating CIA, probably by modifying cytokine expression. Mesenchymal stem cells caused complete improvement in the oxidative stress environment in the form of lowered MDA and increased GSH.

In conclusion, MSCs are very effective in reducing RA inflammation and could become a better therapeutic opportunity for the treatment of RA.

References

1. Ikari K. Genetic risk factors for rheumatoid arthritis. *Nihon Rinsho*. 2016;74(6):897–901.
2. Innala L, Sjöberg C, Möller B, et al. Co-morbidity in patients with early rheumatoid arthritis – inflammation matters. *Arthritis Res Ther*. 2016;18:33. doi: 10.1186/s13075-016-0928-y
3. Choy E. Understanding the dynamics: Pathways involved in the pathogenesis of rheumatoid arthritis. *Rheumatology (Oxford)*. 2012; 51(5):3–11.
4. Monaco C, Nanchahal J, Taylor P, et al. Anti-TNF therapy: Past, present and future. *Int Immunol*. 2015;27(1):55–62.
5. Gonzalo-Gil E, Galindo-Izquierdo M. Role of transforming growth factor-beta (TGF) beta in the physiopathology of rheumatoid arthritis. *Reumatol Clin*. 2014;10(3):174–179.
6. Simmonds RE, Foxwell BM. Signalling, inflammation and arthritis: NF-kappaB and its relevance to arthritis and inflammation. *Rheumatology (Oxford)*. 2008;47(5):584–590.
7. Huang QQ, Pope RM. Role of toll like receptors in rheumatoid arthritis. *Curr Rheumatol Rep*. 2009;11(5):357–364.
8. Aref MI, Ahmed H. Cartilage oligomeric matrix protein as new marker in diagnosis of rheumatoid arthritis. *Mod Chem Appl*. 2015;3(2): 1000151. doi:10.4172/2329-6798.1000151
9. Acharya C, Yik JH, Kishore A, et al. Cartilage oligomeric matrix protein and its binding partners in the cartilage extracellular matrix: Interaction, regulation and role in chondrogenesis. *Matrix Biol*. 2014;37:102–111.
10. Smolen JS, Landewé R, Breedveld FC, et al. EULAR recommendations for the management of rheumatoid arthritis with synthetic and biological disease-modifying antirheumatic drugs: 2013 update. *Ann Rheum Dis*. 2014;73(3):492–509.
11. Singh JA, Saag KG, Bridges SL, et al. 2015 American College of Rheumatology Guideline for the Treatment of Rheumatoid Arthritis. *Arthritis Care Res (Hoboken)*. 2016;68(1):1–25.
12. Malgieri A, Kantzari E, Patrizi MP, et al. Bone marrow and umbilical cord blood human mesenchymal stem cells: State of the art [published online ahead of print September 7, 2010]. *Int J Clin Exp Med*. 2010;3(4):248–269.
13. Sun L, Akiyama K, Zhang H, et al. Mesenchymal stem cell transplantation reverses multiorgan dysfunction in systemic lupus erythematosus mice and humans. *Stem Cells*. 2009;27:1421–1432.
14. Zippel N, Limbach CA, Ratajski N, et al. Purinergic receptors influence the differentiation of human mesenchymal stem cells. *Stem Cells Dev*. 2012;21(6):884–900.
15. Salem HK, Thiemermann C. Mesenchymal stromal cells: Current understanding and clinical status. *Stem Cells*. 2010;28(3):585–596.
16. Saeed H, Ahsan M, Saleem Z, et al. Mesenchymal stem cells (MSCs) as skeletal therapeutics – an update [published online ahead of print April 16, 2016]. *J Biomed Sci*. 2016;23:41. doi: 10.1186/s12929-016-0254-3

17. Borashan FA, Ilkhanipoor M, Hashemi M, et al. Investigation the effects of curcumin on serum hepatic enzymes activity in a rheumatoid arthritis model. *eJBio*. 2008;4(4):129–133.
18. Banji D, Pinnapureddy J, Banji OJ, et al. Synergistic activity of curcumin with methotrexate in ameliorating Freund's complete adjuvant-induced arthritis with reduced hepatotoxicity in experimental animals. *Eur J Pharmacol.* 2011;668(1–2):293–298.
19. Djouad F, Bony C, Haupl T, et al. Transcriptional profiles discriminate bone marrow-derived and synovium-derived mesenchymal stem cells. *Arthritis Res Ther.* 2005;7:1304–1315. doi: org/10.1186/ar1827
20. Zhao DC, Lei JX, Chen R, et al. Bone marrow derived mesenchymal stem cells protect against experimental liver fibrosis in rats. *World J Gastroentrol*. 2005;11(22):3431–3440.
21. Mohamed AO, Idriss NK, Sabry D, et al. Comparative study between the effects of human CD34 and rat bone marrow mesenchymal stem cells on amelioration of CCl4 induced liver fibrosis. *EJB*. 2015;33(1–2): 34–51.
22. Wills ED. Evaluation of lipid peroxidation in lipids and biological membranes. In: Snell K, Mullock B, eds. *Biochemical Toxicology: A practical approach*. Oxford & Washington, DC: IRL Press; 1987:127–152.
23. Ellman GL. Tissue sulfhydryl groups. *Arch of Bioch & Biophys*. 1959;82: 70–77.
24. Zhao Q, Ren H, Han Z. Mesenchymal stem cells: Immunomodulatory capability and clinical potential in immune diseases. *Journal of Cellular Immunotherapy.* 2016;2(1):3–20.
25. Han Z, Jing Y, Zhang S, et al. The role of immunosuppression of mesenchymal stem cells in tissue repair and tumor growth. *Cell Biosci*. 2012;2(1):8. doi: 10.1186/2045-3701-2-8
26. Roberts CA, Dickinson AK, Taams LS. The interplay between monocytes/macrophages and CD4+ T cell subsets in rheumatoid arthritis. *Front Immunol*. 2015;6:571. doi: 10.3389/fimmu.2015.00571
27. Park KH, Mun CH, Kang MI, et al. Treatment of collagen-induced arthritis using immune modulatory properties of human mesenchymal stem cells. *Cell Transplant*. 2016;25(6):1057–1072.
28. Ganesan K, Tiwari M, Balachandran C, et al. Estrogen and testosterone attenuate extracellular matrix loss in collagen-induced arthritis in rats. *Calcif Tissue Int*. 2008;83(5):354–364.
29. Augello A, Tasso R, Negrini SM, et al. Cell therapy using allogeneic bone marrow mesenchymal stem cells prevents tissue damage in collagen-induced arthritis. *Arthritis Rheum.* 2007;56(4):1175–1186.
30. Liu Y, Mu R, Wang S, et al. Therapeutic potential of human umbilical cord mesenchymal stem cells in the treatment of rheumatoid arthritis. *Arthritis Res Ther.* 2010;12(6):210. doi: 10.1186/ar3187
31. Mao F, Xu WR, Qian H, et al. Immunosuppressive effects of mesenchymal stem cells in collagen-induced mouse arthritis. *Inflamm Res*. 2010;59(3):219–225.
32. Ren G, Zhang L, Zhao X, et al. Mesenchymal stem cell-mediated immunosuppression occurs via concerted action of chemokines and nitric oxide. *Cell Stem Cell.* 2008;2:141–150.
33. Dazzi F, Krampera M. Mesenchymal stem cells and autoimmune diseases. *Best Pract Res Clin Haematol.* 2011;24(1):49–57.
34. Kang MI, Park Y. Immunomodulatory function of mesenchymal stem cells for rheumatoid arthritis. *J Rheum Dis*. 2016;23(5):279–287.
35. Greish S, Abogresha N, Abdel-Hady Z, et al. Human umbilical cord mesenchymal stem cells as treatment of adjuvant rheumatoid arthritis in a rat model. *World J Stem Cells*. 2012;4(10):101–109. doi: 10.4252/wjsc.v4.i10.101
36. Romieu-Mourez R, Francois M, Boivin MN, et al. Cytokine modulation of TLR expression and activation in mesenchymal stromal cells leads to a proinflammatory phenotype. *J Immunol.* 2009;182: 7963–7973.
37. Waterman RS, Tomchuck SL, Henkle SL, et al. A new mesenchymal stem cell (MSC) paradigm: Polarization into a pro-inflammatory MSC1 or an immunosuppressive MSC2 phenotype. *PLoS One.* 2010;5(4): 10088. doi: 10.1371/journal.pone.0010088
38. El-denshary ESM, Rashed LA, Elhussiny M. Mesenchymal stromal cells versus betamethasone can dampen disease activity in the collagen arthritis mouse model. *Clin Exp Med*. 2014;14(3):285–295.

Isobolographic additivity among lacosamide, lamotrigine and phenobarbital in a mouse tonic-clonic seizure model

Maria W. Kondrat-Wróbel[1,B–D], Jarogniew J. Łuszczki[1,2,A,C–F]

[1] Department of Pathophysiology, Medical University of Lublin, Poland
[2] Isobolographic Analysis Laboratory, Institute of Rural Health, Lublin, Poland

A – research concept and design; B – collection and/or assembly of data; C – data analysis and interpretation; D – writing the article; E – critical revision of the article; F – final approval of the article

Advances in Clinical and Experimental Medicine, ISSN 1899-5276 (print), ISSN 2451-2680 (online) *Adv Clin Exp Med*. 2018;27(7):881–886

Address for correspondence
Jarogniew J. Łuszczki
E-mail: jarogniew.luszczki@umlub.pl

Funding sources
None declared

Conflict of interest
Prof. J.J. Łuszczki has been involved in the design and development of new antiepileptics and CNS drugs. He has received, within the last 5 years, an unrestricted research grant from GlaxoSmith-Kline (Brentford, UK). Dr. M.W. Kondrat-Wróbel has no conflict of interest to disclose.

Acknowledgements
This study was supported by grants (DS474/2012-2014 and DS474/2015-2016) from the Medical University of Lublin (Poland).

Received on July 14, 2016
Reviewed on December 28, 2016
Accepted on February 23, 2017

Abstract

Background. Epilepsy is a serious neurological disease affecting about 1% of people worldwide (65 million). Seizures are controllable with antiepileptic drugs (AEDs) in about 70% of epilepsy patients, however, there remains about 30% of patients inadequately medicated with these AEDs, who need a satisfactory control of their seizure attacks. For these patients, one of the treatment options is administration of 2 or 3 AEDs in combination.

Objectives. To determine the anticonvulsant effects of a combination of 3 selected AEDs (i.e., lacosamide – LCM, lamotrigine – LTG and phenobarbital – PB) at the fixed-ratio of 1:1:1 in a mouse maximal electroshock-induced (tonic-clonic) seizure model by using isobolographic analysis.

Material and methods. Seizure activity was evoked in adult male albino Swiss mice by a current (sine-wave, 25 mA, 500 V, 50 Hz, 0.2 s stimulus duration) delivered via auricular electrodes. Type I isobolographic analysis was used to detect interaction for the 3-drug combination.

Results. With type I isobolographic analysis, the combination of LCM, LTG and PB (at the fixed-ratio of 1:1:1) exerted additive interaction in the mouse maximal electroshock-induced (tonic-clonic) seizure model.

Conclusions. The combination of LCM with LTG and PB produced additive interaction in the mouse tonic-clonic seizure model, despite various molecular mechanisms of action of the tested AEDs.

Key words: antiepileptic drugs, isobolographic analysis, maximal electroshock, 3-drug combination

DOI
10.17219/acem/69132

Introduction

Pharmacotherapy in epilepsy is still a challenge for clinicians and epileptologists because about one third of patients with epilepsy are not sufficiently treated with licensed antiepileptic drugs (AEDs) in monotherapy.[1] To reduce both seizure frequency and seizure activity in patients with refractory epilepsy, some combinations of 2 or 3 various AEDs should be considered as the most appropriate treatment regimen.[2–5] Nowadays, some combinations of AEDs are recommended to refractory patients in 3 consecutive monotherapies with the established first-line AEDs.[2,3] Generally, the combined application of AEDs possessing different anticonvulsant modes of action is clinically recommended to potentiate the anticonvulsive properties of AEDs.[5,6]

Direct clinical assessment of the interactions among 3 drugs in epilepsy patients is extremely difficult due to ethical restrictions and methodological limitations. However, preclinical studies in animal in vivo models of epilepsy provide us with plausible proof on the accurate type of interactions occurring among the selected 3 AEDs. There is no doubt that in preclinical in vivo experiments based on isobolographic analysis of interaction, it is easily to confirm whether the theoretically selected AED combinations are beneficial or not.[7] This is the reason to conduct experiments on animals with isobolography and subsequently translate the most favorable combinations into clinical settings.

Lacosamide (LCM) belongs to the 3rd generation of AEDs. Its unique molecular mechanisms of anticonvulsant action rely mainly on the enhancement of slow inactivation in voltage-gated sodium channels, preventing the sodium channels from opening and terminating the action potentials in hyperactive (epileptically changed) neurons for an extended time.[8,9] Thus, LCM inhibits repetitive neuronal firing and stabilizes hyperexcitable neuronal membranes without affecting the physiological functions of the neurons.[8,9] At present, LCM is licensed as an added drug prescribed to adult patients with partial-onset seizures that undergo generalization.[10,11]

The combined administration of LCM with lamotrigine (LTG) and phenobarbital (PB), 2 commonly prescribed AEDs for patients suffering from tonic-clonic and partial onset seizures,[12] should produce a favorable 3-drug combination, offering protection from tonic-clonic seizures in patients with epilepsy who are resistant to monotherapeutic use of these AEDs.[13] Furthermore, the combined treatment with LCM, LTG and PB theoretically fulfils the general principles of a perfect AED combination, giving a maximum of therapeutic effect and a minimum of side effects, due to diverse molecular mechanisms of action.[6] However, this hypothetically ideal combination requires experimental confirmation in a maximal electroshock-induced seizure (MES) test in mice. Of note, the MES test is considered an animal test reflecting generalized tonic-clonic seizures and partial convulsions in humans.[14]

This study was aimed at characterizing the interactions among LCM, LTG and PB in the MES test in mice. We used type I isobolographic analysis to evaluate the interaction among the fully effective drugs (i.e., LCM, LTG and PB) because this method is designed to investigate interaction in preclinical experiments.[15]

Material and methods

In all experimental tests, we used 4-month-old male albino Swiss mice. The local Ethics Committee (University of Life Sciences, Lublin, Poland) approved all of the described protocols and procedures (License No. 45/2014).

LCM (UCB Pharmaceuticals, Brussels, Belgium), LTG (GlaxoSmithKline, Brentford, UK) and PB (Polfa, Warszawa, Poland) were dispersed in an aqueous solution of Tween 80 (Sigma-Aldrich, St. Louis, USA). The AEDs were injected intraperitoneally (i.p.) to animals at the pretreatment times as follows: LCM – 30 min, LTG and PB – 60 min, respectively.

Alternating current (25 mA, 0.2 s stimulus duration) generated by rodent shocker (Hugo Sachs Elektronik, March, Germany) was used to evoke maximal electroconvulsions (seizure activity) in mice, as described earlier.[16,17] The animals, after receiving different drug doses, were subjected to the MES test and protection from maximal electroconvulsions was noted so as to construct dose-effect functions for the investigated AEDs (LCM, LTG and PB) when injected separately, as described earlier.[16,18] The anticonvulsant properties of LCM, LTG and PB, when injected alone and combined at a fixed-ratio of 1:1:1, were presented in the form of median effective doses (i.e., ED_{50} and $ED_{50\,exp}$ values).

Type I isobolographic analysis assessed the nature of the interactions among the 3 AEDs in combination.[15,19] Of note, isobolography is a mathematical method that makes it possible to precisely determine the kind of interactions occurring when drugs are combined together. Isobolographic analysis distinguishes 5 classes of drug interactions: synergy (supra-additivity), additivity, indifference, relative antagonism (sub-additivity), and absolute antagonism (infra-additivity).[20,21] Subsequently, a linear regression analysis based on logarithms and probits made it possible to construct dose-effect functions for the studied AEDs (LCM, LTG and PB).[22] To establish the proper class of interactions, the investigated AEDs are usually administered together in fixed drug dose ratio combinations. However, to properly select the fixed-ratio combinations, one should verify whether the dose-effect functions of the studied AEDs if used alone are collateral. If the drugs have their dose-response effect curves parallel to each other, at least 3 fixed-ratios (i.e., 3:1, 1:1 and 1:3) are experimentally investigated with isobolography.[23] Of note, many more fixed-ratio combinations are sometimes required to establish the exact types of interactions for particular drug mixtures.[21] On the other hand, for drugs

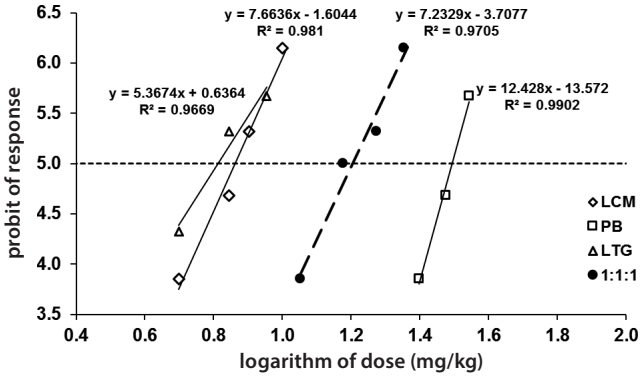

Fig. 1. Dose-effect functions of lacosamide, lamotrigine and phenobarbital injected separately and in combination (1:1:1) against maximal electroconvulsions in mice

Equations for the anticonvulsant effects of LCM, LTG, PB and their combination are presented graphically; R^2 – coefficient of determination.

having their dose-effect functions mutually nonparallel, only a fixed-ratio of 1:1 is analyzed with isobolography.[24] To the best of our knowledge, calculations of doses for particular drugs with their nonparallel dose-effect functions, applied in fixed-ratio combinations more diverse than 1:1 (i.e., 1:3 and 3:1), are not precise because the effects produced by the drug doses may be either over- or underestimated, ultimately providing improper information on the interaction among the drugs.[15,24] The isobolographic rule, concerning parallelism of dose-response effect curves for the tested AEDs when they are used alone, is obligatory not only for 2-drug combinations, but also for 3- and 4-drug combinations.[24] After verifying the parallelism of dose-effect functions of LCM, LTG and PB, the median additive dose of the mixture of these 3 AEDs ($ED_{50\ add}$) at a fixed-ratio combination of 1:1:1 was calculated according to the methods described earlier.[16,17] Admittedly, LCM displayed parallelism to PB and LTG. However, these latter 2 AEDs, when compared to each other, had their dose-effect functions nonparallel. Therefore, only 1 fixed-ratio (1:1:1) underwent investigation in this study because, as mentioned earlier, other tested fixed-ratios (i.e., 1:1:3, 1:3:1, 3:1:1, 3:3:1, 3:1:3 or 1:3:3) could provide false classification of interaction.[15,24–26] The anticonvulsant protection offered by the 3 AEDs in mixture 1:1:1 was presented in the form of $ED_{50\ exp}$ value, reflecting a dose of 3 drugs in mixture that protected 50% of the mice from MES-induced seizures.[16,17]

The unpaired Student's t-test was used to statistically compare the $ED_{50\ exp}$ and $ED_{50\ add}$ values.

Results

LCM, LTG and PB injected separately protected the mice from maximal electroconvulsions. From log-probit equations of dose-effect functions, the ED_{50} values for LCM, LTG and PB were calculated (Fig. 1), amounting to 7.27 ±0.77 mg/kg (LCM), 6.50 ±0.80 mg/kg (LTG) and 31.21 ±2.04 mg/kg (PB), respectively (Table 1).

Parallelism of dose-effect functions was observed between LCM and LTG, as well as between LCM and PB (Table 1, Fig. 1). In contrast, dose-effect functions between LTG and PB were non-collateral (Table 1).

LCM, PB and LTG combined together at a fixed-ratio of 1:1:1 produced an anti-electroshock effect and the $ED_{50\ exp}$ value was 15.99 ±1.80 mg/kg. With type I isobolographic analysis, the mixture of LCM, LTG and PB at a fixed-ratio of 1:1:1 produced additivity in mice subjected to the MES test (Fig. 2 A–C). The $ED_{50\ exp}$ value for the mixture of LCM, LTG and PB was 15.99 ±1.80 mg/kg and displayed no significant difference from the $ED_{50\ add}$ value, which amounted to 14.99 ±0.71 mg/kg.

Neither LCM, LTG and PB administered singly (in doses reflecting their ED_{50} values from the maximal electroconvulsions), nor the combination of LCM, LTG and PB (1:1:1) disturbed memory processes in mice challenged with the passive avoidance task, changed skeletal muscular strength in mice in the grip-strength test, and impaired motor coordination in mice subjected to the chimney test (Table 2).

Discussion

It was found experimentally that the combination of LCM, LTG and PB (1:1:1) produced additivity in the mouse MES-induced seizure test. The illustrated additivity for the combination of the 3 AEDs (LCM, LTG and PB) can be compared to the effects reported from experiments conducted for the combinations of 2 AEDs (i.e., PB + LTG, LCM + LTG, and LCM + PB) in the same seizure test. Previously, we have reported supra-additivity (synergy) for the combination of PB with LTG at a fixed-ratio of 1:1 against

Table 1. Anticonvulsant properties of lamotrigine, lacosamide and phenobarbital when administered separately in the MES-induced seizure test in mice

Drug	ED_{50}	n	Combination	#Parallelism
LTG	6.50 ±0.80	24	LCM vs LTG	parallel
LCM	7.27 ±0.77	16	LCM vs PB	parallel
PB	31.21 ±2.04	16	LTG vs PB	nonparallel

Results are median effective doses (ED_{50} values [mg/kg] ±SEM, where SEM is standard error of the mean) of LCM, LTG and PB administered separately in the MES-induced seizure test in mice. The drugs were administered systemically (i.p.), as follows: LCM – 30 min, LTG and PB – 60 min before the MES-induced seizures; n – total number of animals used at doses whose expected anticonvulsant effects ranged between the 4th and 6th probit; # test for parallelism was performed according to Litchfield and Wilcoxon.[22] For more details see Fig. 1.

Table 2. Effects of lamotrigine, lacosamide and phenobarbital, administered alone and in mixture at a fixed-ratio of 1:1:1 on long-term memory in the passive avoidance task, muscular strength in the grip-strength test and motor performance in the chimney test in mice

Treatment [mg/kg]	Retention time [s]	Muscular strength [N]	Motor coordination impairment [%]
Vehicle + vehicle	180 (180; 180)	0.987 ±0.067	0
LTG (6.50) + vehicle	180 (180; 180)	0.948 ±0.062	0
LCM (7.27) + vehicle	180 (180; 180)	0.949 ±0.065	0
PB (31.21) + vehicle	180 (180; 180)	0.962 ±0.072	0
LCM (2.58) + LTG (2.31) + PB (11.09)	180 (180; 180)	0.952 ±0.071	0

Results are median retention times (with 25th and 75th percentiles in parentheses) from the passive avoidance task, mean muscular strengths ±SEM from the grip-strength test and percentage of animals with impairment of motor coordination from the chimney test. Each experimental group consisted of 8 mice. Doses of particular drugs (in parentheses) correspond to their ED_{50} values from the MES test.

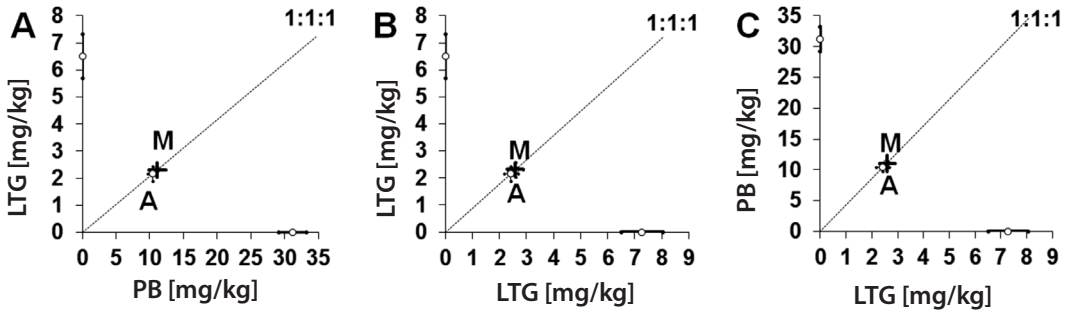

Fig. 2 A–C. Isobolograms illustrating additivity among lacosamide, lamotrigine and phenobarbital in mice subjected to maximal electroconvulsions

The $ED_{50\ exp}$ and $ED_{50\ add}$ values ±SEM for the mixture of LCM, LTG and PB (1:1:1) were plotted graphically as points M and A. A – additive interaction of PB with LTG; B – additive interaction of LCM with LTG; C – additive interaction of LCM with PB.

maximal electroconvulsions in mice.[27] Unfortunately, no information is available on the type of interactions for the combinations of LCM with PB and LTG against maximal electroconvulsions in mice. Nevertheless, in another experimental model of electrically-induced seizures, a 6 Hz psychomotor seizure test, the combination of LCM with LTG also produced supra-additivity (synergy) in mice.[28]

The interaction among the 3 AEDs (LCM, LTG and PB) from this study can also be compared to the interactions observed previously for the combinations of LCM, carbamazepine (CBZ) and PB,[16] or topiramate (TPM), CBZ and PB, against maximal electroconvulsions in mice.[17] More specifically, a supra-additivity (synergy) for the combination of TPM, CBZ and PB was found in the MES test in mice.[17] In contrast, the replacement of TPM with LCM in the mixture of LCM, CBZ and PB resulted in additivity with a trend to sub-additivity in the MES test in mice.[16] On the other hand, the replacement of CBZ with LTG produced additivity without any trend to sub-additivity (antagonism) in the MES test, as documented in this study for LCM, LTG and PB. Thus, it can be concluded that the mixture of LCM, LTG and PB is more favorable than that of LCM, CBZ and PB and, simultaneously, less beneficial than that of CBZ, PB and TPM in the MES-induced seizure test.

From a theoretical viewpoint, the mixture of LCM, LTG and PB should be favorable and of particular relevance for epileptic patients because of the diverse mechanisms of action of the component drugs.[6] Of note, the conjunction of LCM, LTG and PB complies with theoretical presumptions related to combining drugs with diverse mechanisms of anticonvulsant action. As is widely known, LTG attaches to inactive voltage-dependent sodium channels and thus, it reduces the sustained repetitive firing in neurons.[29] LTG also blocks voltage-activated N- and P/Q-type calcium channels.[30] LCM selectively enhances slow inactivation of sodium channels and makes hyperexcitable neurons stable.[8,31] Additionally, LCM allosterically blocks NMDA receptors containing the NR2B subunit.[8,31] As regards PB, the drug enhances the effects of $GABA_A$ receptors by attaching to an allosteric regulatory site within the complex of $GABA_A$-receptor and chloride ionophore.[32–34] Furthermore, PB inhibits AMPA receptors.[35] Thus, taking into account the mentioned mechanisms of action of LCM, LTG and PB, the mixture of these AEDs should supra-additively inhibit generalized tonic-clonic seizures in mice challenged with maximal electroconvulsions because their mechanisms of anticonvulsant action complement each other. Unfortunately, in this study we barely found additivity among LCM, LTG and PB against maximal electroconvulsions in mice.

Much more attention should be paid to the doses of particular AEDs used – we combined LCM, LTG and PB in doses 3 times lower than their respective ED_{50} values as denoted singly in the MES test in mice. This is the reason

we obtained results reflecting monotherapy with one effective AED, as regards the inhibition of maximal electroconvulsions in mice. Of note, any decrease in drug doses is beneficial due to the limitation of acute adverse effects exerted by AEDs used separately that would occur if the AEDs could be injected in higher doses into the mice.

Here we also determined the potential of acute adverse effects evoked by LCM, LTG and PB in a mixture with respect to their influence on motor performance, memory processes and skeletal muscular strength in the animals subjected to the chimney, passive avoidance and grip-strength tests, respectively. Generally, drugs or their mixtures that significantly affect motor performance in animals disturb coordination or make the animals unable to climb backward up the plastic Plexiglas tube within 60 s.[36,37] Similarly, in the passive avoidance test, drugs or their mixtures that significantly affect the animals' long-term memory may impair memory acquisition and/or remembering in experimental animals, which manifests by the entrance of the mice into the dark box of the passive avoidance apparatus without a period of staying in the light compartment for up to 180 s.[38,39] In the grip-strength test, drugs or their mixtures that significantly alleviate skeletal muscular strength induce flaccidity of the animal's bodies or reduce muscle tension in the mice that manifest in a low force in grasping and pulling the squared stainless steel wire mesh connected to the electronic dynamometer.[40,41] Of note, the mixture of LCM, LTG and PB was administered to animals in doses corresponding to the $ED_{50\ exp}$ value obtained in the MES-induced seizure test. In this study, the mixture of LCM, LTG and PB had no significant impact on motor performance in mice since all of the tested animals climbed backward up the tube within 1 min (Table 2). Similarly, the AEDs in combination had no significant effect on memory processes in the animals tested – the mice remained in the light compartment of the apparatus for up to 3 min (Table 2). The combination of LCM, LTG and PB had no significant impact on the animals' skeletal muscular strength because no significant changes in grasping and pulling the wire mesh connected to the dynamometer were observed in the mice (Table 2). Considering the results from these 3 behavioral tests, it can be concluded that LCM, LTG and PB in combination (1:1:1) exerted no acute side effects as compared to the animals from the control group, suggesting that the AEDs in mixture, at doses reflecting the $ED_{50\ exp}$ from the MES test, were safe enough to be recommended for application in further clinical settings, especially in epileptic patients treated with these AEDs in monotherapy.

Summing up, it can be concluded that the combined application of LCM, LTG and PB exerted additivity against maximal electroconvulsions in mice. Finally, LCM combined with LTG and PB can modify the interaction among drugs from synergistic to additive, despite their various anticonvulsant modes of action.

References

1. Kwan P, Schachter SC, Brodie MJ. Drug-resistant epilepsy. *N Engl J Med*. 2011;365:919–926.
2. Stephen LJ, Brodie MJ. Seizure freedom with more than one antiepileptic drug. *Seizure*. 2002;11:349–351.
3. Stephen LJ, Forsyth M, Kelly K, Brodie MJ. Antiepileptic drug combinations – Have newer agents altered clinical outcomes? *Epilepsy Res*. 2012;98:194–198.
4. Barker-Haliski M, Sills GJ, White HS. What are the arguments for and against rational therapy for epilepsy? *Adv Exp Med Biol*. 2014;813: 295–308.
5. Perucca E. Pharmacological principles as a basis for polytherapy. *Acta Neurol Scand Suppl*. 1995;162:31–34.
6. Deckers CL, Czuczwar SJ, Hekster YA, et al. Selection of antiepileptic drug polytherapy based on mechanisms of action: The evidence reviewed. *Epilepsia*. 2000;41:1364–1374.
7. Luszczki JJ, Czuczwar SJ. Preclinical profile of combinations of some second-generation antiepileptic drugs: An isobolographic analysis. *Epilepsia*. 2004;45:895–907.
8. Errington AC, Stohr T, Heers C, Lees G. The investigational anticonvulsant lacosamide selectively enhances slow inactivation of voltage-gated sodium channels. *Mol Pharmacol*. 2008;73:157–169.
9. Rogawski MA, Tofighy A, White HS, Matagne A, Wolff C. Current understanding of the mechanism of action of the antiepileptic drug lacosamide. *Epilepsy Res*. 2015;110:189–205.
10. Biton V, Gil-Nagel A, Isojarvi J, Doty P, Hebert D, Fountain NB. Safety and tolerability of lacosamide as adjunctive therapy for adults with partial-onset seizures: Analysis of data pooled from three randomized, double-blind, placebo-controlled clinical trials. *Epilepsy Behav*. 2015;52:119–127.
11. Zadeh WW, Escartin A, Byrnes W, et al. Efficacy and safety of lacosamide as first add-on or later adjunctive treatment for uncontrolled partial-onset seizures: A multicentre open-label trial. *Seizure*. 2015;31: 72–79.
12. Glauser T, Ben-Menachem E, Bourgeois B, et al. Updated ILAE evidence review of antiepileptic drug efficacy and effectiveness as initial monotherapy for epileptic seizures and syndromes. *Epilepsia*. 2013;54:551–563.
13. Loscher W. Single versus combinatorial therapies in status epilepticus: Novel data from preclinical models. *Epilepsy Behav*. 2015;49: 20–25.
14. Loscher W, Fassbender CP, Nolting B. The role of technical, biological and pharmacological factors in the laboratory evaluation of anticonvulsant drugs. II. Maximal electroshock seizure models. *Epilepsy Res*. 1991;8:79–94.
15. Tallarida RJ. Revisiting the isobole and related quantitative methods for assessing drug synergism. *J Pharmacol Exp Ther*. 2012;342:2–8.
16. Kondrat-Wróbel MW, Łuszczki JJ. Interaction of three-drug combination of lacosamide, carbamazepine and phenobarbital in the mouse maximal electroshock-induced seizure model – An isobolographic analysis. *Health Prob Civil*. 2016;10(1):55–61.
17. Luszczki JJ. Isobolographic analysis of interaction for three-drug combination of carbamazepine, phenobarbital and topiramate in the mouse maximal electroshock-induced seizure model. *Pharmacology*. 2016;97:259–264.
18. Żółkowska D, Zagaja M, Miziak B, et al. Isobolographic assessment of interactions between retigabine and phenytoin in the mouse maximal electroshock-induced seizure model and chimney test. *Health Prob Civil*. 2016;10(4):54–59.
19. Loewe S. The problem of synergism and antagonism of combined drugs. *Arzneimittelforschung*. 1953;3:285–290.
20. Luszczki JJ, Borowicz KK, Swiader M, Czuczwar SJ. Interactions between oxcarbazepine and conventional antiepileptic drugs in the maximal electroshock test in mice: An isobolographic analysis. *Epilepsia*. 2003;44:489–499.
21. Luszczki JJ, Czuczwar SJ. Isobolographic and subthreshold methods in the detection of interactions between oxcarbazepine and conventional antiepileptics – A comparative study. *Epilepsy Res*. 2003;56: 27–42.
22. Litchfield JT, Wilcoxon F. A simplified method of evaluating dose-effect experiments. *J Pharmacol Exp Ther*. 1949;96:99–113.
23. Luszczki JJ, Wu JZ, Raszewski G, Czuczwar SJ. Isobolographic characterization of interactions of retigabine with carbamazepine, lamotrigine, and valproate in the mouse maximal electroshock-induced seizure model. *Naunyn Schmiedebergs Arch Pharmacol*. 2009;379:163–179.

24. Luszczki JJ. Isobolographic analysis of interaction between drugs with nonparallel dose-response relationship curves: A practical application. *Naunyn Schmiedebergs Arch Pharmacol*. 2007;375:105–114.
25. Tallarida RJ. Quantitative methods for assessing drug synergism. *Genes Cancer*. 2011;2:1003–1008.
26. Luszczki JJ, Czuczwar SJ. Biphasic characteristic of interactions between stiripentol and carbamazepine in the mouse maximal electroshock-induced seizure model: A three-dimensional isobolographic analysis. *Naunyn Schmiedebergs Arch Pharmacol*. 2006;374:51–64.
27. Luszczki JJ, Czuczwar M, Kis J, et al. Interactions of lamotrigine with topiramate and first-generation antiepileptic drugs in the maximal electroshock test in mice: An isobolographic analysis. *Epilepsia*. 2003;44:1003–1013.
28. Shandra A, Shandra P, Kaschenko O, Matagne A, Stohr T. Synergism of lacosamide with established antiepileptic drugs in the 6-Hz seizure model in mice. *Epilepsia*. 2013;54:1167–1175.
29. Nakatani Y, Masuko H, Amano T. Effect of lamotrigine on Na(v)1.4 voltage-gated sodium channels. *J Pharmacol Sci*. 2013;123:203–206.
30. Pisani A, Bonsi P, Martella G, et al. Intracellular calcium increase in epileptiform activity: Modulation by levetiracetam and lamotrigine. *Epilepsia*. 2004;45:719–728.
31. Stohr T, Kupferberg HJ, Stables JP, et al. Lacosamide, a novel anticonvulsant drug, shows efficacy with a wide safety margin in rodent models for epilepsy. *Epilepsy Res*. 2007;74:147–154.
32. Mathers DA, Wan X, Puil E. Barbiturate activation and modulation of GABA(A) receptors in neocortex. *Neuropharmacology*. 2007;52: 1160–1168.
33. Twyman RE, Rogers CJ, Macdonald RL. Differential regulation of gamma-aminobutyric acid receptor channels by diazepam and phenobarbital. *Ann Neurol*. 1989;25:213–220.
34. Rho JM, Donevan SD, Rogawski MA. Direct activation of $GABA_A$ receptors by barbiturates in cultured rat hippocampal neurons. *J Physiol*. 1996;497(2):509–522.
35. Ko GY, Brown-Croyts LM, Teyler TJ. The effects of anticonvulsant drugs on NMDA-EPSP, AMPA-EPSP, and GABA-IPSP in the rat hippocampus. *Brain Res Bull*. 1997;42:297–302.
36. Boissier JR, Tardy J, Diverres JC. A new simple method to explore the "tranquillizing" action: The chimney test [in French]. Pharmacology. 1960;3:81–84.
37. Luszczki JJ, Czernecki R, Wojtal K, Borowicz KK, Czuczwar SJ. Agmatine enhances the anticonvulsant action of phenobarbital and valproate in the mouse maximal electroshock seizure model. *J Neural Transm*. 2008;115:1485–1494.
38. Venault P, Chapouthier G, de Carvalho LP, et al. Benzodiazepine impairs and beta-carboline enhances performance in learning and memory tasks. *Nature*. 1986;321:864–866.
39. Luszczki JJ, Wojcik-Cwikla J, Andres MM, Czuczwar SJ. Pharmacological and behavioral characteristics of interactions between vigabatrin and conventional antiepileptic drugs in pentylenetetrazole-induced seizures in mice: An isobolographic analysis. *Neuropsychopharmacology*. 2005;30:958–973.
40. Meyer OA, Tilson HA, Byrd WC, Riley MT. A method for the routine assessment of fore- and hindlimb grip strength of rats and mice. *Neurobehav Toxicol*. 1979;1;233–236.
41. Nieoczym D, Luszczki JJ, Czuczwar SJ, Wlaz P. Effect of sildenafil on the anticonvulsant action of classical and second-generation antiepileptic drugs in maximal electroshock-induced seizures in mice. *Epilepsia*. 2010;51:1552–1559.

Calreticulin promotes proliferation and extracellular matrix expression through Notch pathway in cardiac fibroblasts

Xiaoying Fan*[B,D,F], Yuan Yao*[C,D,F], Yao Zhang[A,D–F]

Department of Cardiovascular Medicine, 2nd Affiliated Hospital of Harbin Medical University, China

A – research concept and design; B – collection and/or assembly of data; C – data analysis and interpretation;
D – writing the article; E – critical revision of the article; F – final approval of the article

Advances in Clinical and Experimental Medicine, ISSN 1899-5276 (print), ISSN 2451-2680 (online) *Adv Clin Exp Med*. 2018;27(7):887–892

Address for correspondence
Yao Zhang
E-mail: zhangyao159@126.com

Funding sources
None declared

Conflict of interest
None declared

* The first 2 authors contributed equally to the work.

Received on April 20, 2017
Reviewed on May 17, 2017
Accepted on June 5, 2017

Abstract

Background. Cardiac fibrosis is one of the most important underlying causes of several cardiac diseases. The role of calreticulin (CRT) in cardiac diseases has already been established. The over- or under-expression of CRT can lead to cardiac diseases.

Objectives. This study was aimed to explore the effect of CRT on cardiac fibrosis and also to investigate the possible underlying molecular mechanism.

Material and methods. Human cardiac fibroblast cells (HCF) were used in the experiment. The cells were transfected with the CRT expression vector constructed by sub-cloning the full-length wild-type CRT coding sequence into pcDNA3.1 (pc-CRT group), empty construct pcDNA3.1 (pcDNA3.1 group), CRT-specific siRNA (si-CRT), and si-NC (negative control). The Cell Counting Kit-8 (CCK-8) assay, apoptosis assay and invasion assay were performed. Quantitative real time polymerase chain reaction (qRT PCR) and western blot analysis were performed to measure the expressions of different mRNAs and proteins.

Results. The CRT expression was significantly increased ($p < 0.01$) and decreased ($p < 0.01$) in the pc-CRT and si-CRT groups, respectively. The CRT over-expression led to increased cell viability and invasiveness ($p < 0.05$) and a decreased percentage of apoptotic cells. The over-expression of CRT led to a significant increase in the expressions of collagen (I and III) ($p < 0.01$) and matrix metalloproteinases (MMP-2 and 9) ($p < 0.05$). The Notch pathway was also significantly activated ($p < 0.05$) by the over-expression of CRT and vice versa when suppressed.

Conclusions. The results showed that the CRT over-expression was associated with increased cell viability and invasiveness and decreased apoptosis, and the activation of the Notch pathway in HCF, which suggests its possible implication in CRT-induced cardiac fibrosis.

Key words: calreticulin, Notch pathway, cardiac fibroblasts, extracellular matrix, proliferation

DOI
10.17219/acem/74430

Introduction

Cardiac fibrosis is a pathophysiological condition characterized by the accumulation of extracellular matrix in the myocardium and is considered one of the most important factors implicated in various cardiac diseases.[1,2] The regenerative capacity of the adult mammalian heart is negligible, and therefore fibrosis occurs in cardiac diseases associated with acute death of cardiomyocytes.[1–4] In acute myocardial infarction (AMI), sudden death of a large number of cardiomyocytes leads to the triggering of inflammatory pathways and dead cell replacement with collagen-based scar tissue formation.[5,6] Other than the acute onset of cardiac diseases like AMI, several other chronic cardiac diseases are associated with insidious accumulation of collagen in the interstitial and perivascular regions.[6] Aging is another factor that leads to the development of cardiac fibrosis and ultimately to diastolic failure.[1] Several long-standing cardiac diseases, like chronic hypertension and aortic stenosis, might also lead to widespread cardiac fibrosis, associated with loss of cardiac contractility and diastolic dysfunction, which ultimately leads to both systolic and diastolic heart failure because of persistent pressure overload.[4] Besides pressure overload, volume overload, as in the valvular regurgitant type of cardiac lesions, can also lead to cardiac fibrosis due to the deposit of a large amount of non-collagenous matrix.[4] Other common causes of cardiac fibrosis include alcoholism, anthracycline use, metabolic disturbances like diabetes, obesity, etc.[7–9]

Calreticulin (CRT) is a Ca2+ binding protein which acts as a chaperone in the storage of Ca2+ and the maintenance of Ca2+ homeostasis.[10] Calreticulin is widely expressed in the embryonic heart; however, its expression is downregulated following birth.[11] Kypreou et al. have explored the role of altered expression of CRT in the fibrosis of several organs, such as the lung, heart and renal epithelial cells. Although the over-expression of CRT could be implicated in lung and renal epithelial cell fibrosis, there were no changes in the expression of CRT in the cardiac model.[12] Only a few studies have been conducted to explore the implications of the CRT over-expression in certain cardiac conditions, namely diastolic dysfunction, ventricular dilation, cardiac arrhythmia, and sudden cardiac arrest.[10–14]

In this study, we have explored the effect of CRT on the proliferation and extracellular matrix expression in cardiac fibroblasts and also investigated the possible underlying mechanisms.

Material and methods

Cell culture

Human cardiac fibroblasts (HCF) were purchased from the Cell Bank of Tongpai Biotechnology Co., Ltd. (Shanghai, China). The base medium for the HCF cell line was formulated Dulbecco's Modified Eagle's Medium (DMEM; Gibco Inc., Thermo Fisher, Waltham, USA). To make the complete growth medium, we added the following components to the base medium: 4.5 g/L glucose and fetal bovine serum to a final concentration of 10%. Exponentially growing cultures were maintained in a humidified atmosphere of 5% carbon dioxide (CO_2) at 37°C.

Plasmids and siRNA transfection

The CRT expression vector (pcDNA3.1-CRT) was constructed by sub-cloning the full-length wild-type CRT coding sequence into pcDNA3.1, and was then confirmed by sequencing. The empty construct pcDNA3.1 was transfected as a control. The target sequence for CRT-specific siRNA was 5′-GGAGCAGUUUCUGGACGGA-3′, synthesized by GenePharma Co. (Shanghai, China). Cell transfections were conducted using Lipofectamine 3000 reagent (Invitrogen, Carlsbad, USA), following the manufacturer's protocol.

Cell Counting Kit-8 assay

Human cardiac fibroblasts were seeded in a 96-well plate with 5000 cells/well, and then transfected by the plasmids or siRNAs for 48 h. Cell proliferation was assessed by CCK-8 (Dojindo Molecular Technologies, Gaithersburg, USA). Briefly, after stimulation, the CCK-8 solution was added to the culture medium, and the cultures were incubated for 1 h at 37°C in humidified 95% air and 5% CO_2. The absorbance was measured at 450 nm, using a Microplate Reader (Bio-Rad, Hercules, USA).

Apoptosis assay

Cell apoptosis analysis was performed using propidium iodide (PI) and fluorescein isothiocynate (FITC)-conjugated Annexin V staining (Invitrogen, Grand Island, USA). Briefly, the cells were washed in phosphate buffered saline (PBS) and fixed in 70% ethanol. The fixed cells were then washed twice in PBS and stained in PI/FITC-Annexin V in the presence of 50 µg/mL RNase A (Sigma-Aldrich, St. Louis, USA), and then incubated for 1 h at room temperature in the dark. Flow cytometry analysis was done by using a FACScan (Beckman Coulter, Fullerton, USA). The data was analyzed using FlowJo software (Ashland, USA).

Invasion assay

The invasion behavior of HCF was determined using 24-well Millicell Hanging Cell Culture inserts with 8 mm PET membranes (Millipore, Bedford, USA). Briefly, after the cells were treated for the indicated condition, 5.0×10^4 HCF in 200 µL serum-free DMEM were plated onto BD BioCoat™ Matrigel™ invasion chambers (8 µM pore size polycarbonate filters; BD Biosciences, San Jose,

USA), while the complete medium, containing 10% FBS was added to the lower chamber. After processing the invasion chambers for 48 h (37°C, 5% CO_2) in accordance with the manufacturer's protocol, the non-invading cells were removed with a cotton swab; the invading cells were fixed in 100% methanol, and then stained with crystal violet solution and counted microscopically. The data is presented as the average number of cells attached to the bottom surface from 5 randomly chosen fields.

Quantitative real time polymerase chain reaction

Total RNA was isolated from transfected cells by using TRIzol reagent (Invitrogen) and treated with DNaseI (Promega, Madison, USA). Reverse transcription was performed by using the Multiscribe RT kit (Applied Biosystems, Foster City, USA) and random hexamers or oligo(dT). The reverse transcription conditions were 10 min at 25°C, 30 min at 48°C, and a final step of 5 min at 95°C. The sequences of the primers were as follows: CRT-forward, 5'-CGGGGTACCCGCCACCATGGCGATGCTGCTATCCGTGCCG-3'; reverse, 5'-CCGGAATTCCAGCTCGTCCTTGGCCTG-3', GAPDH-forward, 5'-GCACCGTCAAGGCTGAGAAC'-3; reverse, 5'-TGGTGAAGACGCCAGTGGA-3'.

Western blot

The protein used for western blotting was extracted using RIPA lysis buffer (Beyotime Biotechnology, Shanghai, China) supplemented with protease inhibitors (Roche, Guangzhou, China). The proteins were quantified using the BCA™ Protein Assay Kit (Pierce, Appleton, USA). The western blot system was established using the Bio-Rad Bis-Tris Gel system according to the manufacturer's instructions. Rabbit-anti-mouse CRT antibody was purchased from Biotechnology, Inc. (Santa Cruz, USA). Glyceraldehyde 3-phosphate dehydrogenase (GAPDH) antibody was purchased from Sigma-Aldrich. The primary antibodies were prepared in 5% blocking buffer at a dilution of 1:1,000. The primary antibody was incubated with the membrane at 4°C overnight, followed by washing and incubation with a secondary antibody marked by horseradish peroxidase for 1 h at room temperature. After rinsing, the polyvinylidene difluoride (PVDF) membrane carrying blots and antibodies was transferred into the Bio-Rad ChemiDoc™ XRS system, and then 200 µL Immobilon Western Chemiluminescent HRP Substrate (Millipore) was added to cover the membrane surface. The signals were captured and the intensity of the bands was quantified using Image Lab™ Software (Bio-Rad).

Statistical analysis

All experiments were repeated 3 times. The results of multiple experiments are presented as mean ± standard deviation (SD). Statistical analyses were performed using SPSS 19.0 statistical software (IBM, Armonk, USA). P-values were calculated using one-way analysis of variance (ANOVA). A p-value of <0.05 was considered to indicate a statistically significant result.

Results

Expression of calreticulin in different groups of human cardiac fibroblasts

The expression of CRT was measured in different groups of HCF cells by qRT-PCR. Human cardiac fibroblasts were transfected with a vector constructed by sub-cloning the full-length wild-type CRT coding sequence into pcDNA3.1. The pc-CRT cells showed a significant increase ($p < 0.01$) in the expression of CRT compared to the control group (pcDNA3.1 group) transfected with empty construct (Fig. 1A). Western blot analysis also revealed increased expression of CRT in the pc-CRT group (Fig. 1B). Similarly, mRNA expression of CRT in HCF transfected with CRT-specific siRNA, as in the si-CRT group, was significantly suppressed ($p < 0.01$) compared to the control group (si-NC group) (Fig. 1C). Western blot analysis also supported the above finding (Fig. 1D).

Effects of calreticulin expression on cell viability

The assessment of cell viability in different groups of HCF for 4 days revealed that the over-expression of CRT, as in the pc-CRT group, promoted cell viability, whereas the silencing of CRT expression in the si-CRT group of HCF suppressed it (Fig. 2).

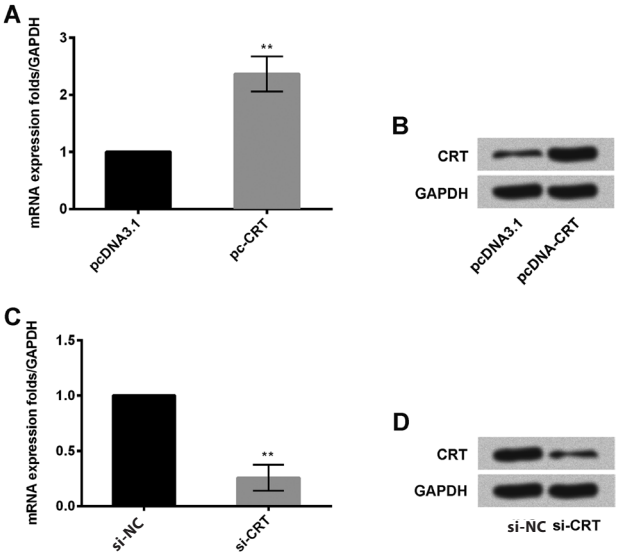

Fig. 1. Expression of CRT in different groups of HCF measured by qRT-PCR analysis (A,C) and western blot analysis (B,D)

CRT – calreticulin; GAPDH – glyceraldehyde 3-phosphate dehydrogenase; qRT-PCR – quantitative real time polymerase chain reaction; ** $p < 0.01$.

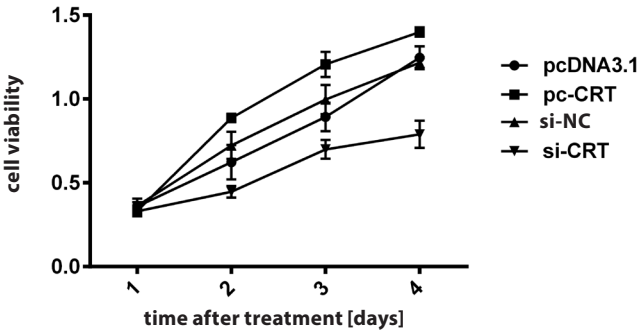

Fig. 2. Effects of CRT expression (both over- and under-expression) on cell viability

CRT – calreticulin.

Effect of calreticulin expression on apoptosis

The apoptosis assay revealed that although the over-expression of CRT, as in the pc-CRT group, showed no significant change in apoptotic cells as compared to the control group (pcDNA3.1 group), the down-regulation of CRT, as in the si-CRT group, revealed a significant increase in cell apoptosis compared to the si-NC group (Fig. 3).

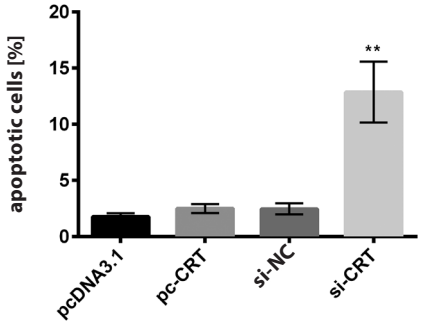

Fig. 3. Effects of CRT expression (both over- and under-expression) on the percentage of apoptotic cells

CRT – calreticulin; ** $p < 0.01$.

Effect of calreticulin expression on cellular invasiveness

The over-expression of CRT, as in the pc-CRT group, revealed a significant increase ($p < 0.05$) in cellular invasiveness compared to the control group (pcDNA3.1 group), whereas the suppression of the CRT expression, as in the si-CRT group, revealed a significant decrease ($p < 0.05$) in cellular invasiveness compared to the control group, si-NC (Fig. 4).

Effects of calreticulin expression on the expression of collagen and matrix metalloproteinases

Quantitative real time polymerase chain reaction revealed that collagen I, collagen III, metalloproteinases (MMPs) MMP-2 and MMP-9 mRNAs were significantly expressed ($p < 0.01$, $p < 0.01$, $p < 0.05$, and $p < 0.05$, respectively) in HCF overexpressing CRT, as in the pc-CRT group compared to the control group (Fig. 5A). Similarly, silencing of CRT expressions, as in the si-CRT group, led to decreased, although not significantly, expressions of collagen I, collagen III, MMP-2, and MMP-9 mRNAs compared to the control group (Fig. 5A). Western blot analysis also revealed that the expression levels of collagen I, collagen III, MMP-2, and MMP-9 proteins were decreased in the si-CRT group and increased in the pc-CRT group (Fig. 5B).

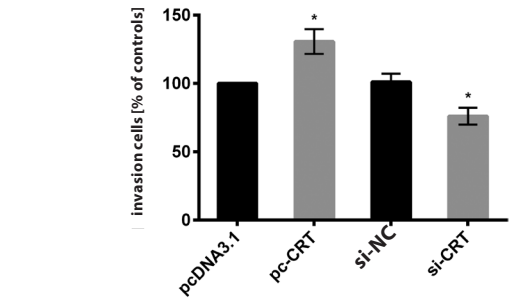

Fig. 4. Effects of CRT expression (both over- and under-expression) on cell invasiveness

CRT – calreticulin; * $p < 0.05$.

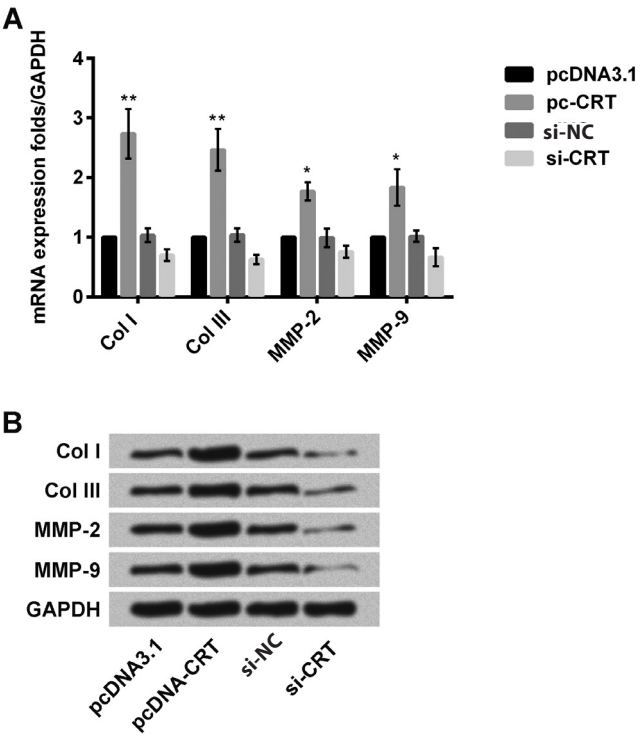

Fig. 5. Effects of CRT expression (both over- and under-expression) on the expression of collagen (I and III) and metalloproteinases (MMP-2 and MMP-9) measured by qRT-PCR analysis (A) and western blot analysis (B)

CRT – calreticulin; GAPDH – glyceraldehyde 3-phosphate dehydrogenase; qRT-PCR – quantitative real time polymerase chain reaction; * $p < 0.05$; ** $p < 0.01$.

Effect of calreticulin expression on the Notch pathway

The over-expression of CRT, as in the pc-CRT group, revealed a significant increase ($p < 0.05$) in the expression levels of Notch 1, 2 and 3 receptors (Fig. 6A). Again, HCF with the silencing of the CRT expression, as in the si-CRT group, revealed decreased expression levels of the 3 above-mentioned Notch receptors with a significant suppression ($p < 0.05$) of the expression of Notch 2 in the si-CRT group (Fig. 6A). Western blot analysis also revealed the same results; the expression levels of Notch 1, 2 and 3 receptors were increased and decreased in the pc-CRT and si-CRT groups, respectively (Fig. 6B).

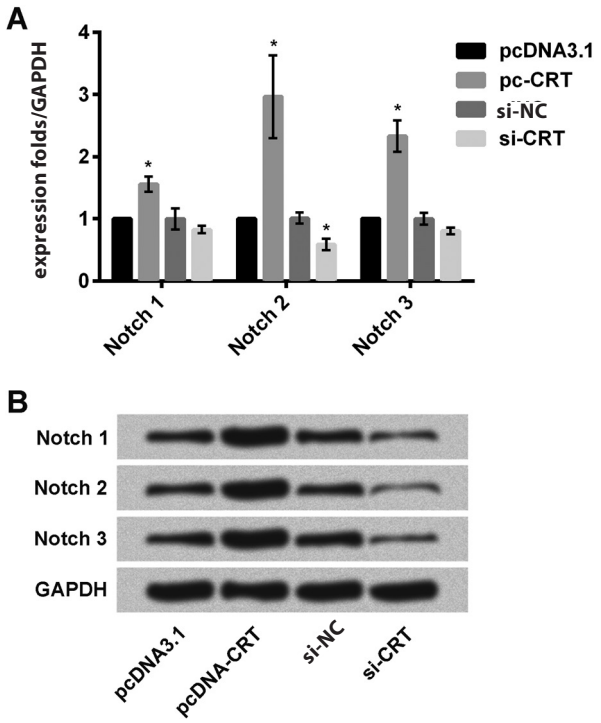

Fig. 6. Effect of CRT expression (both over- and under-expression) on the Notch pathway measured by qRT-PCR analysis (A) and western blot analysis (B)

CRT – calreticulin; GAPDH – glyceraldehyde 3-phosphate dehydrogenase; qRT-PCR – quantitative real time polymerase chain reaction; * $p < 0.05$.

Discussion

Cardiovascular diseases are one of the leading causes of mortality worldwide.[15] Like in the healing process of any other part of the body, cardiac injury is also healed by scar tissue formation. Scar tissue formation is mediated mainly by activating fibroblasts, which secrete collagen and ultimately produce myocardial fibrosis.[16] Fibrosis is very important in enhancing the mechanical stability of the cardiac wall to prevent its rupture following injury. However, it can, unfortunately, disrupt electrical coupling among the surrounding myocytes.[17]

In a healthy heart, fibroblasts play an important role in maintaining the integrity of the myocardial structure. These are one of the predominant cell types in the heart besides myocytes, which in turn exceed the myocytes in number but not in volume.[16] Fibroblasts act as the sentinel cells, which in turn maintain the balance between the synthesis and degradation of collagen and other components of the extracellular matrix. Myocardial injury triggers differentiation of these fibroblasts into myofibroblasts, thus facilitating the process of wound healing.[16]

Several studies have already established the role of CRT in the pathogenesis of different diseases, like cancer and cardiovascular disease.[18–20] Although it has already been established that CRT is critical for cardiac development, its role in cardiac disease remains elusive. In spite of demonstrating the deleterious effects on the heart, following the exposure to the over-expression of CRT, it has also been established that CRT is essential for the development of a normal heart.[19] Hence, it is said that balanced expression of CRT is essential for proper development and adequate functioning of the heart, and both the over- and under-expression of CRT can be deleterious to the heart.[19]

In this study, we have explored the effect of CRT on HCF and also its possible underlying mechanism.

Following the transfection of HCF, the expressions of CRT mRNA and protein were measured. The CRT expression was significantly increased ($p < 0.01$) both in terms of mRNA and protein expression in the pc-CRT group compared to controls (pcDNA3.1 group) (Fig. 1A,1B). Similarly, the CRT expression was significantly suppressed ($p < 0.01$) in the si-CRT group (Fig. 1C,1D).

Similar to our findings, several studies have established that the over-expression of CRT was associated with high prevalence of cardiac fibrosis.[19,20]

We also found out that the over-expression of CRT, as in the pc-CRT group, was associated with increased cell viability (Fig. 2) and invasiveness ($p < 0.05$) (Fig. 4), and the suppression of apoptosis (Fig. 3), whereas the knockdown of the CRT expression, as in the si-CRT group, showed just the opposite results (Fig. 2–4). Again, both qRT-PCR and western blot analysis demonstrated that the over-expression of CRT was associated with a significant increase in the expression levels of collagen and MMPs ($p < 0.01$ and $p < 0.05$), respectively (Fig. 5A,5B).

Similar to our findings, Groenendyk et al. also demonstrated that the over-expression of CRT was associated with increased cardiac fibrosis.[21]

Studies have already implicated the over-expression of the Notch pathway in cardiac fibrosis.[22] In this study, we demonstrated that the over-expression of CRT was associated with the activation of the Notch pathway (Fig. 6A, 6B).

It can be concluded that the over-expression of CRT is associated with increased expression of collagen and MMPs, and also the activation of the Notch pathway in HCF, which suggests its possible implication in cardiac fibrosis. Hence, CRT can be considered as a novel target for the treatment of cardiac fibrosis.

References

1. Kong P, Christia P, Frangogiannis NG. The pathogenesis of cardiac fibrosis. *Cell Mol Life Sci*. 2014;71:549–574.
2. Berk BC, Fujiwara K, Lehoux S. ECM remodeling in hypertensive heart disease. *J Clin Invest*. 2007;117:568–575.
3. Frangogiannis NG. Regulation of the inflammatory response in cardiac repair. *Circ Res*. 2012;110:159–173.
4. Borer JS, Truter S, Herrold EM, et al. Myocardial fibrosis in chronic aortic regurgitation molecular and cellular responses to volume overload. *Circulation*. 2002;105:1837.
5. Ashrafian H, Mckenna WJ, Watkins H. Disease pathways and novel therapeutic targets in hypertrophic cardiomyopathy. *Circ Res*. 2011; 109:86–96.
6. Kania G, Blyszczuk P, Eriksson U. Mechanisms of cardiac fibrosis in inflammatory heart disease. *Trends Cardiovasc Med*. 2009;19:247.
7. Bernaba BN, Chan JB, Lai CK, Fishbein MC. Pathology of late-onset anthracycline cardiomyopathy. *Cardiovasc Pathol*. 2010;19:308–311.
8. Asbun J, Villarreal FJ. The pathogenesis of myocardial fibrosis in the setting of diabetic cardiomyopathy. *J Am Coll Cardiol*. 2006;47:693–700.
9. Bharati S, Lev M. Cardiac conduction system involvement in sudden death of obese young people. *Am Heart J*. 1995;129:273–281.
10. Michalak M, Groenendyk J, Szabo E, Gold LI, Opas M. Calreticulin, a multi-process calcium-buffering chaperone of the endoplasmic reticulum. *Biochem J*. 2009;417:651.
11. Mesaeli N, Nakamura K, Zvaritch E, et al. Calreticulin is essential for cardiac development. *J Cell Biol*. 1999;144:857–868.
12. Kypreou KP, Kavvadas P, Karamessinis P, et al. Altered expression of calreticulin during the development of fibrosis. *Proteomics*. 2008;8: 2407–2419.
13. Hattori K, Nakamura K, Hisatomi Y, et al. Arrhythmia induced by spatiotemporal overexpression of calreticulin in the heart. *Mol Genet Metab*. 2007;91:285–293.
14. Nakamura K, Robertson M, Liu G, et al. Complete heart block and sudden death in mice overexpressing calreticulin. *J Clin Invest*. 2001;107: 1245–1253.
15. Miragoli M, Salvarani N, Rohr S. Myofibroblasts induce ectopic activity in cardiac tissue. *Circ Res*. 2007;101:755.
16. Nguyen TP, Qu Z, Weiss JN. Cardiac fibrosis and arrhythmogenesis: The road to repair is paved with perils. *J Mol Cell Cardiol*. 2014;70:83–91.
17. Vasquez C, Mohandas P, Louie KL, Benamer N, Bapat AC, Morley GE. Enhanced fibroblast–myocyte interactions in response to cardiac injury. *Circ Res*. 2010;107:1011.
18. Lu YC, Weng WC, Lee H. Functional roles of calreticulin in cancer biology. *Biomed Res Int*. 2015;2015:1–9.
19. Martinho-Dias D, Leite-Moreira A, Castro-Chaves P. Calreticulin in the heart: From embryological development to cardiac pathology. *Curr Mol Med*. 2015;16:112–119.
20. Lee D, Oka T, Hunter B, et al. Calreticulin induces dilated cardiomyopathy. *PLOS ONE*. 2013;8:e56387–e56387.
21. Groenendyk J, Lee D, Jung J, et al. Inhibition of the unfolded protein response mechanism prevents cardiac fibrosis. *PLOS ONE*. 2016;11: e0159682.
22. Collesi C, Zentilin L, Sinagra G, Giacca M. Notch1 signaling stimulates proliferation of immature cardiomyocytes. *J Cell Biol*. 2008;183:117–128.

Ivabradine inhibits carbachol-induced contractions of isolated rat urinary bladder

Hasan Riza Aydin[1,A,B], Hasan Turgut[2,B,C], Ayşegül Kurt[3,B,C], Ramazan Sahan[3,B,C], Ömer Faruk Kalkan[3,B,C], Huseyin Eren[4,A,F], Ahmet Ayar[3,A,C,D,F]

[1] Department of Urology, University of Health Sciences, Trabzon Kanuni Training and Research Hospital, Turkey
[2] Department of Urology, Akcaabat Hackali Baba State Hospital, Trabzon, Turkey
[3] Department of Physiology, Faculty of Medicine, Karadeniz Technical University, Trabzon, Turkey
[4] Department of Urology, Faculty of Medicine, Recep Tayyip Erdogan University, Rize, Turkey

A – research concept and design; B – collection and/or assembly of data; C – data analysis and interpretation; D – writing the article; E – critical revision of the article; F – final approval of the article

Advances in Clinical and Experimental Medicine, ISSN 1899-5276 (print), ISSN 2451-2680 (online) *Adv Clin Exp Med*. 2018;27(7):893–897

Address for correspondence
Ahmet Ayar
E-mail: aayar61@yahoo.com

Funding sources
None declared

Received on February 9, 2017
Reviewed on March 9, 2017
Accepted on May 9, 2017

Abstract

Background. Overactive bladder (OAB), a symptom syndrome defined as urgency, is a common clinical condition, which sometimes cannot be satisfactorily treated with current medications in every subject; therefore, alternatives are needed.

Objectives. The aim of this in vitro study was to investigate the effects of ivabradine, a selective pacemaker If current inhibitor, on agonist-induced isometric contractions of the bladder smooth muscles.

Material and methods. Urinary bladder strips were isolated from adult male Wistar rats and suspended in a tissue bath containing physiological solution. The strips were contracted by bath applications of carbachol (CCh, 1 μM). Ivabradine (30 μM, 60 μM or 90 μM) was added to the tissue bath either prior to or after the application of the agonist, and the resulting contractile activity was compared to the preceding contractile activity. The amplitude and area under force-time curves (AUFC) of the isometric contractions were evaluated.

Results. The addition of CCh caused a marked stimulation of contractile force in isolated urinary bladder strips, which was significantly inhibited by ivabradine, both in terms of peak amplitude (29% ±3%, 20% ±6% and 18% ±6% by 30 μM, 60 μM and 90 μM ivabradine, respectively) and AUFC (47% ±5.5%, 35% ±8% and 35% ±6% by 30 μM, 60 μM and 90 μM ivabradine, respectively; $n = 7$ for each). Pre-treatment with ivabradine (10 μM) significantly attenuated the contractile response to CCh (1 μM; mean peak amplitude from 1493 ±216 mg to 680 ±95 mg; $p < 0.003$; $n = 7$).

Conclusions. The results of this in vitro study demonstrated that ivabradine inhibits cholinergic agonist-induced bladder contractions, which means that in the future ivabradine may be used in OAB treatment.

Key words: urinary bladder, overactive bladder, ivabradine

DOI
10.17219/acem/71197

Introduction

The urinary bladder is a distensible, membranous, hollow organ, made of a thin layer of smooth muscle that provides its unique properties of relaxing to accommodate and contracting to empty out urine, one of the body's continuously produced fluid waste products. The smooth muscle wall of the bladder, also known as the detrusor, and the internal sphincter, the internal continuation of the detrusor, are under autonomic control, while the external urethral sphincter is under somatic control from higher centers.[1] The bladder temporarily stores urine until the person finds appropriate time and place to eliminate it from the body by coordinated actions of autonomic and somatic muscles that encircle the bladder neck.[2]

Thus, the process of physiological control of urination, notably the reflex contraction of the detrusor muscle, involves highly complex coordination between the central, autonomic and somatic nervous systems, and has been reviewed extensively elsewhere.[3,4] As the bladder fills up with urine and its volume reaches about 200 mL or more (bladder functional capacity is 300–600 mL), the stretch receptors in the bladder excite and send signals to higher centers, and the voluntary voiding is usually initiated. However, the detrusor can become too active and contract involuntarily, making the individual feel the urge to void inappropriately, even when the bladder has little urine. This clinical symptom is referred to as overactive bladder (OAB), typically caused by spasms of the bladder muscles with or without incontinence.[5] Overactive bladder is a very common chronic condition that affects the daily lives of a huge number of men, women and children worldwide.[5,6] Urinary urgency, frequent urination and nocturia are a common set of OAB symptoms that can be caused by a wide range of conditions, including detrusor hyperreflexia, urinary tract infections and obstructive prostatic hypertrophy.[5,6] Whatever the underlying cause, intense and involuntary bladder muscle contractions are present. Although symptoms can range in severity from mild to very severe, OAB is a condition that often requires treatment. And, despite a range of available treatment options, just as the etiology of OAB is often multifactorial, the treatment approaches and available tools are far from satisfactory.

Basic research studies of isolated bladder smooth muscle tissue have made important contributions to our current understanding of the physiology of the bladder, as well as the development of new and improved approaches for the control of clinically relevant detrusor contractility impairments, ranging from underactivity to overactivity, including OAB.

The "funny" (If) current (or funny channel or pacemaker current), originally described in the sinoatrial (SA) node and Purkinje fibers, is currently being investigated for its potential role(s) in smooth muscles with the capacity of generating spontaneous phasic activity.[7–10,11] Evidence is being accumulated that interstitial cells of Cajal (ICCs) and ICC-like cells possess the general and specific properties of pacemaker cells. Although less studied than those in cardiac tissue, they are ubiquitously expressed in smooth muscle tissues of many organs, including the gastrointestinal tract, uterine, lymph ducts, urinary bladder, and urethra.[8,9] The pacemaker structures have been suggested to contribute to spontaneous contractions of these smooth muscle tissues by funny currents (If currents) through hyperpolarization-activated cyclic nucleotide-gated (HCN) channels.[9,12] Indeed, the self-contractibility of the urinary bladder through myogenic excitation implicates a potential bladder pacemaker, possible through the signals from ICCs. Interstitial cells of Cajal, a group of cells present in the wall of the bladder, are suggested to play a role in OAB, although there is no clear evidence of signal transmission. Still, the results of a clinical study have implied that the use of ivabradine, a selective blocker of pacemaker If current, could possibly be used in the treatment of OAB.[13] However, studies involving the possible effects of ivabradine on smooth muscle contractility have never been carried out.

Hence, the aim of this in vitro study was to investigate the possible effects of ivabradine on agonist-stimulated contractions of isolated rat bladder smooth muscles.

Material and methods

Tissue preparation

The protocol of this study was reviewed and approved by the local Ethics Committee.

Adult male Wistar rats (250–300 g), obtained from the Karadeniz Technical University Surgical Research Center, Trabzon, Turkey, were sacrificed by cervical dislocation, and the urinary bladder was exposed by a midline incision of the abdomen. The urinary bladder was removed by cutting at the bladder neck and placed in a physiological saline solution (PSS) containing: 120 mM NaCl, 5.9 mM KCl, 2.5 mM $CaCl_2$, 1.1 mM $MgCl_2$, 15 mM $NaHCO_3$, 1.2 mM NaH_2PO_4, 11 mM $C_6H_{12}O_6$ (glucose), and 10 mM $C_8H_{18}N_2O_4S$ (HEPES). The bladder was cut open from the base to the dome and strips were prepared (~15 mm × 3 mm × 2 mm).

Recording of isometric tension

Bladder strips were mounted in 10 mL organ baths filled with PSS at 37°C and pH 7.4, constantly bubbled with 95% oxygen-5% carbon dioxide, and the isometric contractions were recorded. The lower end of the strip was fixed to a metal hook and the upper end was attached to an isometric force-displacement transducer (FTD 10A; Commat Ltd., Ankara, Turkey), and the signals were amplified and recorded through a data acquisition system (MP100 Data Acquisition System; Biopac Systems Inc., Goleta, USA).

The strips were allowed to equilibrate under a passive resting tension of 1 g for 45 min, and then the strips were contracted by bath applications of carbachol (CCh, 1 μM). Ivabradine (30 μM, 60 μM and 90 μM) was added to the tissue bath either prior to or after application of the agonist, and the resulting contractile activity was compared with the preceding contractile activity. The amplitude and area under force-time curves (AUFC) of the isometric contractions were evaluated and compared, averaged over 10-minute intervals.

Chemicals

Ivabradine, CCh and all constituents of the PSS were purchased from Sigma (Deisenhofen, Germany) and were of research grade. Ivabradine and CCh were dissolved in the PSS, and were added to the tissue bath at the indicated concentrations.

Statistical analysis

All statistical analyses and graphics were performed using the Microcal Origin v. 5.00 computer program (Microcal Software Inc., Northampton, USA). The data is expressed as the arithmetic mean of the „n" number of experiments and the standard error of mean (SEM). Statistical significance was analyzed by Student's t-test. The probability value of $p < 0.05$ was considered significant.

Results

In 3 out of the 22 strips studied, the bath application of CCh caused a marked stimulation of contractile force in isolated bladder strips. The remaining non-responding 3 strips were not further utilized for the study.

The application of ivabradine attenuated the peak amplitude of the CCh-induced contractions in a concentration-dependent manner. The peak amplitude of the contractions was reduced to 29% ±3% ($p < 0.001$), 20% ±6% ($p < 0.001$) and 18% ±6% ($p < 0.001$) of the CCh-induced period (100%) after the application of 30 μM, 60 μM and 90 μM ivabradine, respectively (Fig. 1–3). Ivabradine caused a similar attenuation in the AUFC values for CCh-evoked contractile responses. On the average, the normalized AUFC values of CCh-induced contractions was reduced to 47% ±5.5% ($p < 0.01$), 35% ±8% ($p < 0.01$) and 35% ±6% ($p < 0.01$) ($n = 7$ for each) of the CCh-induced period (100%) after the application of 30 μM, 60 μM and 90 μM ivabradine, respectively (Fig. 1–3).

In additional experiments, the strips of bladder were pre-treated with ivabradine. Pre-treatment with ivabradine significantly inhibited the contractile response to CCh without significantly effecting the resting tension (Fig. 4). Accordingly, ivabradine (10 μM) was applied before CCh-stimulation (1 μM), and the mean peak amplitude of these

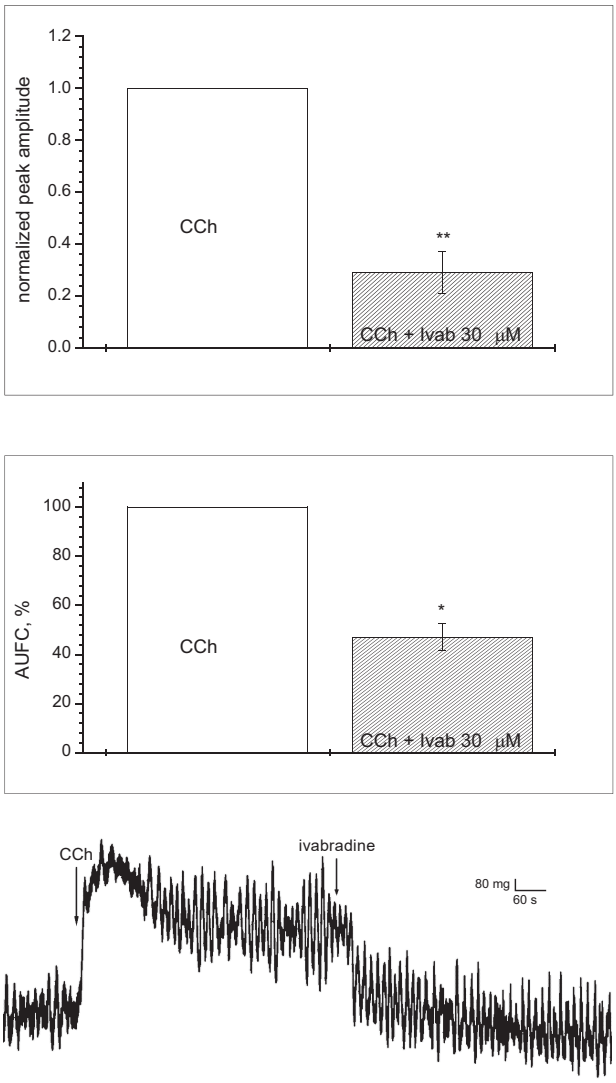

Fig. 1. Effect of 30 μM ivabradine on the carbachol (CCh, 1 μM)-induced contractions of rat bladder strips; normalized amplitude of CCh-evoked contractions and area under force-time curve (AUFC)

Results are expressed as mean ±SE; * $p < 0.01$ compared to the CCh-induced response period prior to ivabradine application ($n = 7$); ** $p < 0.001$ compared to the CCh-induced response period prior to ivabradine application ($n = 7$).

A representative tracing illustrating the contractile activity of bladder strip preparations in response to carbachol (CCh, 1 μM) and the inhibition of the contractile activity by ivabradine. Bladder strips developed a sustained tension in response to CCh, and ivabradine was applied at the indicated point and was continuously present afterwards.

contractions were significantly weaker when compared to the contractile response to CCh alone (680 ±95 mg, $n = 7$ vs 1493 ±216 mg; $n = 7$; $p < 0.003$) (Fig. 4).

Discussion

The results of the present in vitro study demonstrated, for the first time, that ivabradine inhibits cholinergic agonist-induced contraction of the rat bladder. This is the first evidence that the If channel inhibitor – ivabradine directly blocks bladder muscle contractility, implying that it might be useful in the treatment of OAB.

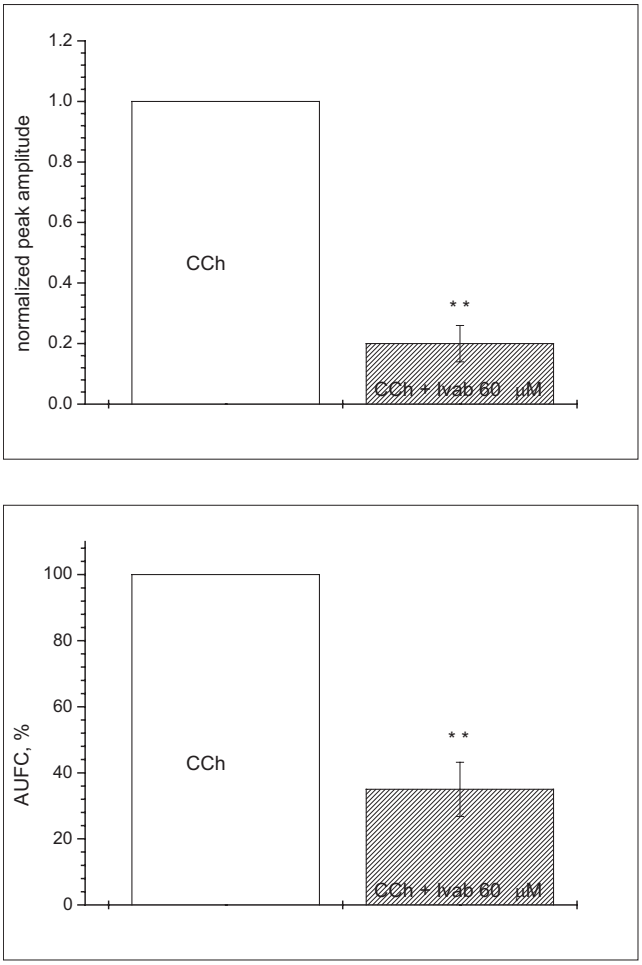

Fig. 2. Effect of 60 μM ivabradine on the carbachol (CCh, 1 μM)-induced contractions of rat bladder strips; normalized amplitude of CCh-evoked contractions and area under force-time curve (AUFC)

Results are expressed as mean ±SE; * $p < 0.01$ compared to the CCh-induced response period prior to ivabradine application (n = 7); ** $p < 0.001$ compared to the CCh-induced response period prior to ivabradine application (n = 7).

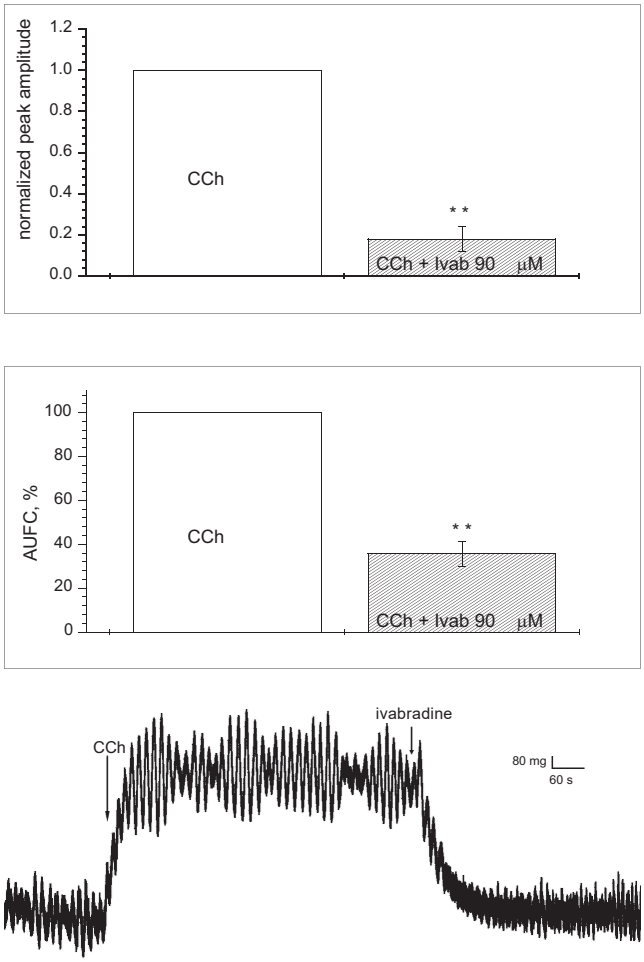

Fig. 3. Effect of 90 μM ivabradine on the carbachol (CCh, 1 μM)-induced contractions of rat bladder strips; normalized amplitude of CCh-evoked contractions and area under force-time curve (AUFC)

Results are expressed as mean ±SE; * $p < 0.01$ compared to the CCh-induced response period prior to ivabradine application (n = 7); ** $p < 0.001$ compared to the CCh-induced response period prior to ivabradine application (n = 7).

A representative tracing illustrating the contractile activity of bladder strip preparations in response to carbachol (CCh, 1 μM) and the inhibition of the contractile activity by ivabradine. Bladder strips developed a sustained tension in response to CCh, and ivabradine was applied at the indicated point and was continuously present afterwards.

Interstitial cells of Cajal play an important role in the regulation of the bladder excitation-contraction process, probably by providing the link between the neurogenic and myogenic mechanisms. The finding that normally single in nature ICCs predominantly appear as closely joined in unstable bladders, and the presence of a strong correlation between the density of ICCs and detrusor excitability further indicates this possibility.[14] Furthermore, following spinal cord injury, which typically leads to a neurogenic bladder exhibiting urinary retention, there is a significantly lower number of ICCs in the rat urinary bladder.[15,16] The HCN channels, which generate pacemaking currents, are present on the cell membranes of ICCs. Considering all these facts, it could be postulated that pacemaker current inhibitors might be useful in the treatment of OAB. In the present in vitro study, the amplitude of CCh-induced contractions of rat bladder strips was inhibited by ivabradine in a concentration-dependent manner.

Similar to previous the in vitro studies using detrusor smooth muscles, the application of muscarinic receptor agonist CCh (1 μM) evoked strong sustained tonic contractions.[17,18] In cultured ICCs, the in vitro application of CCh was shown to cause an increase in intracellular calcium, intracellular signaling essential for the generation of pacemaker potentials and contraction, suggesting that bladder ICCs might play a role in the regulation of cholinergic stimulation-mediated bladder contraction.[18–20] Although this information can help in the interpretation of the ivabradine effect on bladder contractility, we do not know whether the inhibitory effect of ivabradine obtained in the current study is mediated through ICCs. Although we have no direct evidence, the inhibitory actions of ivabradine on the rat detrusors might involve the modulation

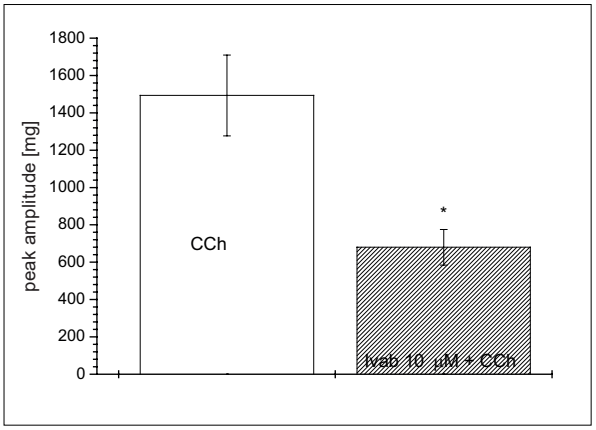

Fig. 4. Effect of 10 μM ivabradine pre-treatment on the carbachol (CCh, 1 μM)-induced contractions of rat bladder strips

* $p < 0.003$ compared to the CCh-induced response period prior to ivabradine application (n = 7).

of calcium release from the sarcoplasmic reticulum (SR). This is plausible, considering the role of Ca^{2+} released from the SR in regulating If in SA node preparations.[21]

In bladder overactivity, developed in a rat model following partial bladder outlet obstruction, it was shown that the physiological functioning of ICCs changes and the expression of the HCN channels in bladder ICCs significantly increases.[22–24] These findings suggest that the HCN channels and ICCs might play an important role in the pathogenesis of detrusor overactivity. Thus, the involvement of the HCN channels is another possible mechanism mediating the inhibition of cholinergic agonist-induced bladder contraction by ivabradine. Considering this structural evidence, our findings of the inhibitory effect of ivabradine on CCh-induced bladder contractility would be of importance in the management of OAB.

The concentrations of ivabradine tested in the present study are higher (about 100-fold) than its achieved max plasma concentration, following the recommended dose of 5 mg twice daily. This concentration is well-below the toxic dose reported in animal studies, although there is not enough clinical data revealing special hazards for humans.[25] In a case of a purposeful intoxication attempt with 280 mg of ivabradine, no serious complication, other than mild bradycardia, which was no more severe than the one observed with a therapeutic dosage, was reported.[26] In any case, lower doses of ivabradine could be used in combination with available drugs (i.e., anticholinergics) that would provide efficacy and minimize the risk of unwanted effects.

Conclusions

In conclusion, the results of this in vitro study demonstrate that ivabradine inhibits cholinergic agonist-induced bladder contractions. It shows that ivabradine could be potentially used in the future, alone or in combination with currently used agents (i.e., anticholinergic) in OAB treatment.

References

1. Fry CH, Meng E, Young JS. The physiological function of lower urinary tract smooth muscle. *Auton Neurosci*. 2010;154:3–13.
2. Andersson KE, Arner A. Urinary bladder contraction and relaxation: Physiology and pathophysiology. *Physiol Rev*. 2004;84:935–986.
3. Seth JH, Panicker JN, Fowler CJ. The neurological organization of micturition. *Handb Clin Neurol*. 2013;117:111–117.
4. Sugaya K, Nishijima S, Miyazato M, Ogawa Y. Central nervous control of micturition and urine storage. *J Smooth Muscle Res*. 2005;41:117–132.
5. Abrams P, Chapple CR, Jünemann KP, Sharpe S. Urinary urgency: A review of its assessment as the key symptom of the overactive bladder syndrome. *World J Urol*. 2012;30:385–392.
6. Apoznański W, Polok M, Rysiakiewicz J, et al. An evaluation of the effectiveness of external urethral meatus incision in girls with an anterior deflected urinary stream and symptoms of detrusor overactivity. *Adv Clin Exp Med*. 2014;23:283–287.
7. Verkerk AO, van Ginneken AC, Wilders R. Pacemaker activity of the human sinoatrial node: Role of the hyperpolarization-activated current, I(f). *Int J Cardiol*. 2009;132:318–336.
8. Kolęda P, Pilecki W. Nature of interstitial cells of Cajal of the upper urinary tract. *Adv Clin Exp Med*. 2014;23:627–632.
9. Siu CW, Lieu DK, Li RA. HCN-encoded pacemaker channels: From physiology and biophysics to bioengineering. *J Membr Biol*. 2006; 214:115–122.
10. Sanders KM, Ward SM, Koh SD. Interstitial cells: Regulators of smooth muscle function. *Physiol Rev*. 2014;94:859–907.
11. Takaki M, Suzuki H, Nakayama S. Recent advances in studies of spontaneous activity in smooth muscle: Ubiquitous pacemaker cells. *Prog Biophys Mol Biol*. 2012;102:129–135.
12. Postea O, Biel M. Exploring HCN channels as novel drug targets. *Nat Rev Drug Discov*. 2011;10:903–914.
13. Stamatiou K, Heretis I, Skoumbourdis E. Does ivabradine exhibit a role in the reduction of bladder overactivity? *Int Urol Nephrol*. 2008; 40:333–334.
14. Johnston L, Woolsey S, Cunningham RM, et al. Morphological expression of kit positive interstitial cells of Cajal in human bladder. *J Urol*. 2010;184:370–377.
15. Johnston L, Cunningham RM, Young JS, et al. Altered distribution of interstitial cells and innervation in the rat urinary bladder following spinal cord injury. *J Cell Mol Med*. 2012;16:1533–1543.
16. Akino H. Spontaneous contractile activity of the detrusor muscle and its role in the pathogenesis of overactive bladder syndrome. *Low Urin Tract Symptoms*. 2012;4:42–47.
17. Oh SJ, Ahn SC, Kim SJ, et al. Carbachol-induced sustained tonic contraction of rat detrusor muscle. *BJU Int*. 1999;84:343–349.
18. Hidayat Santoso AG, Liang W. Bladder contractility is mediated by different K+ channels in the urothelium and detrusor smooth muscle. *J Pharmacol Sci*. 2011;115:127–134.
19. Johnston L, Carson C, Lyons AD, Davidson RA, McCloskey KD. Cholinergic-induced Ca^{2+} signaling in interstitial cells of Cajal from the guinea pig bladder. *Am J Physiol Renal Physiol*. 2008;294:F645–655.
20. Kim SO, Jeong HS, Jang S, et al. Spontaneous electrical activity of cultured interstitial cells of Cajal from mouse urinary bladder. *Korean J Physiol Pharmacol*. 2013;17:531–536.
21. Nazarov IB, Schofield CJ, Terrar DA. Contributions of cardiac "funny" (f) channels and sarcoplasmic reticulum Ca2+ in regulating beating rate of mouse and guinea pig sinoatrial node. *Physiol Rep*. 2015;3(12): e12561. doi:10.14814/phy2.12561
22. Kim SO, Oh BS, Chang IY, et al. Distribution of interstitial cells of Cajal and expression of nitric oxide synthase after experimental bladder outlet obstruction in a rat model of bladder overactivity. *Neurourol Urodyn*. 2011;30:1639–1645.
23. Fry CH. Interstitial cells in the urinary tract, where are they and what do they do? *BJU Int*. 2014;114:434–435.
24. Deng T, Zhang Q, Wang Q, Zhong X, Li L. Changes in hyperpolarization-activated cyclic nucleotide-gated channel expression and activity in bladder interstitial cells of Cajal from rats with detrusor overactivity. *Int Urogynecol J*. 2015;26:1139–1145.
25. Colak MC, Parlakpinar H, Tasdemir S, et al. Therapeutic effects of ivabradine on hemodynamic parameters and cardiotoxicity induced by doxorubicin treatment in rat. *Hum Exp Toxicol*. 2012;31:945–954.
26. Mathiaux F, Dulaurent S, Julia F, Gaulier JM. Case report of ivabradine intoxication. *J Anal Toxicol*. 2014;38:231–232.

Inhibition of migration and invasion by berberine via inactivation of PI3K/Akt and p38 in human retinoblastoma cell line

Yuwen Wang[A,D,F], Jianshu Yuan[B,D,F], Liangyan Yang[B,D,F], Pengyun Wang[B,D,F], Xiajun Wang[B,D,F], Yue Wu[C,D,F], Kan Chen[C,D,F], Rong Ma[C,D,F], Yike Zhong[C,D,F], Xiaohong Guo[B,F], Yan Gong[B,F], Mengfang Gui[C,F], Yaming Jin[C,F]

Department of Ophthalmology, Ningbo Eye Hospital, China

A – research concept and design; B – collection and/or assembly of data; C – data analysis and interpretation; D – writing the article; E – critical revision of the article; F – final approval of the article

Advances in Clinical and Experimental Medicine, ISSN 1899-5276 (print), ISSN 2451-2680 (online) *Adv Clin Exp Med*. 2018;27(7):899–905

Address for correspondence
Yuwen Wang
E-mail: wangyuwen111@126.com

Funding sources
None declared

Conflict of interest
None declared

Received on January 16, 2017
Reviewed on February 26, 2017
Accepted on April 12, 2017

Abstract

Background. As a clinically important natural isoquinoline alkaloid, berberine has been reported to possess various pharmacological effects.

Objectives. This study was aimed to investigate the effect of berberine on cell migration and invasion in human retinoblastoma (Rb) cells.

Material and methods. The cytotoxicity of berberine was estimated by 3-(4,5-dimethylthiazol-2-yl)-2,5-diphenyltetrazolium bromide (MTT) assay. After being stimulated with berberine under various concentrations, the cell migration and invasion were evaluated by transwell assay. Then, the expression levels of epithelial-mesenchymal transition (EMT) markers were determined by quantitative reverse transcription PCR (qRT-PCR) and western blot analysis. Furthermore, the phosphorylation levels of protein kinase B (Akt) and p38 were detected by western blot analysis. Finally, the effect of phosphatidylinositol-3-kinase (PI3K) and p38 inhibitors on cell migration and invasion was estimated by transwell assay. Untreated cells acted as control for all the experiments.

Results. The concentrations of berberine for further studies were controlled in a range of 0 to 100 μM. The cell migration and invasion were both suppressed by berberine in a dose-dependent manner compared to the control ($p < 0.05$ or $p < 0.001$). Berberine remarkably down-regulated expression of E-cadherin and up-regulated expression of vimentin and α-SMA compared to the control ($p < 0.01$ or $p < 0.001$). Furthermore, the phosphorylation levels of Akt and p38 were both down-regulated by berberine in comparison to the control. Furthermore, the addition of berberine accompanied by LY294002 or SB203580 significantly suppressed cell migration and invasion compared to the addition of berberine alone ($p < 0.05$).

Conclusions. Berberine suppressed cell migration and invasion via inactivation of PI3K/Akt and p38.

Key words: berberine, invasion, epithelial-mesenchymal transition, phosphatidylinositol 3-kinase/protein kinase B/Akt, p38

DOI
10.17219/acem/70418

Introduction

Retinoblastoma (Rb) is the most common eye tumor which arises in the retina and represents 2.5–4% of pediatric cancers.[1] The etiology of Rb is the mutation of the Rb tumor-suppressor gene.[2] As a cancer that occurs most often in children before the age of 5 years, Rb affects 2–5 per million children in the USA and Europe.[3] The most frequent clinical manifestations of Rb are leukocoria (white reflection in the pupil) and strabismus (macular involvement).[4] Substantial therapies have been reported to control Rb, such as enucleation, focal therapy, gene therapy, cryotherapy, transpupillary thermotherapy, chemotherapy, and radiotherapy.[5–8] The therapies vary depending on the size of the tumor. Despite the good prognosis of Rb, mortality induced by development of a 2nd tumor remains high. Therefore, novel therapy should be further investigated.

Berberine is an isoquinoline alkaloid (Fig. 1A) isolated from the traditional Chinese medicine Coptis.[9] Extensive research within the past decade proposes that berberine possesses a wide range of pharmacological activities, including anti-diabetic, anti-inflammatory, and anti-tumoral activity.[10–13] Moreover, berberine has been reported to inhibit human colon cancer cell migration via down-regulation of integrin.[14] Chou et al. have implied that berberine could induce cytotoxicity in breast cancer cells.[15] Yip et al. illustrated that berberine induced apoptosis in liver cancer cells.[16] A recent study suggests that berberine is a promising safe anti-cancer agent through affecting the mitochondria.[17] To our knowledge, there is little study focus on the effect of berberine on Rb. Thus, we are interested to know whether berberine can play an efficient role against Rb.

The cell migration and invasion of cancer cells allow them to change position and make the neoplastic cells enter lymphatic and blood vessels for dissemination. After that, metastatic growth occurs in distant organs.[18] As a consequence, the control of cancer cell migration and invasion is a substantial focus of cancer treatment. The present study was designed to investigate the effects of berberine on cell migration, invasion and epithelial-mesenchymal transition (EMT) in human Rb Y-79 cells, which would make a contribution for the discovery of novel therapeutic methods. A previous study has demonstrated that phosphatidylinositol 3-kinase (PI3K)/Akt and p38 are involved in cell migration and invasion, thus we employed specific PI3K inhibitor 2-(4-morpholinyl)-8-phenyl-chromone (LY294002) and p38 inhibitor SB203580 to thoroughly investigate the underlying mechanism.[19]

Material and methods

Cell culture

The human Rb Y-79 cell line was purchased from American Type Culture Collection (ATCC, Manassas, USA). Cells were cultured in RPMI-1640 medium (Gbico, Grand Island, USA) supplemented with 10% fetal bovine serum (FBS), 2 mM L-glutamine, 1 mM sodium pyruvate, 100 U/mL penicillin, and 100 U/mL streptomycin (Gbico, Rockville, USA). Cell cultures were maintained in an incubator with a humidified atmosphere of 5% CO_2 at 37°C.

Berberine preparation

Berberine (purity ≥95%, Sigma, St. Louis, USA) was dissolved in dimethyl sulfoxide (DMSO) and filtrated by 0.2 μm disc filters (Millipore, Billerica, USA), resulting in appropriate amounts of stock solution (100 mM in DMSO). The stock solution of berberine was diluted with cultured medium to achieve the indicated concentrations. The final concentration of DMSO was less than 0.2%.

Cell viability assay

To estimate the cytotoxicity of berberine, the cell viability of Rb cells was performed using the 3-(4,5-dimethylthiazol-2-yl)-2,5-diphenyltetrazolium bromide (MTT) assay in line with the standard method described above.[20] Briefly, Rb cells were seeded onto a 96-well plate (Corning, Corning, USA) with a density of 4×10^3 cells/mL for 24 h. After that, the cells were treated with berberine under various concentrations (0, 5, 10, 20, 40, 80 and 160 μM) for 24 h or 48 h. Following removal of the medium and cell washing by phosphate buffer solution (PBS), 10 μL of MTT solution (5 mg/mL, Sigma, St. Louis, USA) was added to each well accompanied by incubation at 37°C for 4 h. Then, 200 μL of DMSO was added to solubilize the formazan. After measurement by a microplate reader (Bio-Rad, Hercules, USA) at 570 nm, the cell viability was calculated by comparison with untreated cells.

Migration and invasion assays

Cell migration and invasion assays were both performed with Hanging Cell Culture-inserts (BD Biosciences, San Jose, USA) with pores of 8.0 μm in 24-well plates (Corning, Corning, USA). Retinoblastoma cells were firstly stimulated with berberine under various concentrations and maintained for 24 h. After that, cells were treated with trypsin and resuspended with a density of 1×10^5/mL in serum-free medium. When the lower chamber was filled with medium containing 10% FBS, the cells were placed in the upper chamber. After culturing for 24 h, the non-migrated cells which stayed at the surface of the membrane were gently removed with a cotton-tipped swab. Cells that migrated across the filter as well as attached to the underside of the membrane were fixed with methanol and stained with 0.1% crystal violet. Finally, the stained cells were collected and counted under a light microscope (Olympus Optical Co. Ltd., Tokyo, Japan). Whether the inserted filter was pre-coated or not was the difference between the migration assay and invasion assay. In terms of the

invasion assay, the filter was pre-coated with 200 μg/mL Matrigel (BD Biosciences, San Jose, USA). As for the migration assay, the filter was not coated with Matrigel.

Quantitative reverse transcription of polymerase chain reaction

According to the corresponding manufacturer's instructions, isolation of total RNA, reverse transcription of RNA and PCR reactions were performed with TRIzol (Invitrogen, Carlsbad, USA), GoScript™ Reverse Transcription System (Promega, Madison, USA) and Power SYBR Green PCR master mix (Applied Biosystems, Foster City, USA), respectively. Primers were designed and synthetized as shown in Table 1 (Sangon Biotech, Shanghai, China). The results were estimated with $2^{-\Delta\Delta Ct}$ method and normalized to glyceraldehyde 3-phosphate dehydrogenase (GAPDH) for mRNAs.[21]

Table 1. Primers used in this study

Gene	Primer sequence
E-cadherin	forward 5′- TTCTGCTGCTCTTGCTGTTT -3′ reverse 5′- TGGCTCAAGTCAAAGTCCTG -3′
Vimentin	forward 5′- GCCCTTAAAGGAACCAATGA -3′ reverse 5′- AGCTTCAACGGCAAAGTTCT -3′
α-SMA	forward 5′- AGGTAACGAGTCAGAGCTTTGGC -3′ reverse 5′- CTCTCTGTCCACCTTCCAGCAG -3′
GAPDH	forward 5′- CATCAATGGAAATCCCATCA -3′ reverse 5′- TTCTCCATGGTGGTGAAGAC -3′

α-SMA - α-smooth muscle actin; GAPDH – glyceraldehyde 3-phosphate dehydrogenase.

Western blot analysis

After lysing by RIPA buffer (Beyotime, Shanghai, China) and centrifuged at 4°C, the protein in lysate was quantified using bicinchoninic acid (BCA) assay kit (Pierce, Rockford, USA). Fifty micrograms of protein was loaded and separated by sodium dodecyl sulfate polyacrylamide gel electrophoresis (SDS-PAGE). Then, the protein was transferred to polyvinylidene fluoride (PVDF) membranes (Millipore, Billerica, USA) and blocked with 5% skim milk (Nestlé, Shuangcheng, China) in Tris-buffered saline with Tween 20 (TBST). Subsequently, the membranes carrying blots were incubated with primary antibodies against E-cadherin (ab1416), vimentin (ab8978), α-smooth muscle actin (α-SMA, ab5694), β-actin (ab8226) (all from Abcam, Cambridge, UK), phosphorylated Akt (p-Akt, Ser473, 4060) and phosphorylated p38 (p-p38, 4511) (both from Cell Signaling, Beverly, USA) at 4°C overnight. After rinsing with TBST, the PVDF membranes were incubated with horseradish peroxidase (HRP)-conjugated secondary antibodies at 37°C for 1 h. Protein bands were visualized utilizing the EasyBlot enhanced chemiluminescence (ECL) kit (Sangon, Shanghai, China) and LAS-3000 (Fuji Photo Film, Tokyo, Japan). The housekeeping gene was β-actin.

Statistical analysis

All experiments were repeated 3 times. The results were presented as the mean ±standard deviation (SD) or the mean + SD. Statistical analysis was performed using GraphPad Prism 5 software (GraphPad, San Diego, USA). The p-values were calculated using the one-way analysis of variance (ANOVA) or Student's t-test. Significant differences were distinguished with $p < 0.05$.

Results

Cytotoxicity of berberine on retinoblastoma cells

Berberine is one kind of natural isoquinolyl-alkaloid which exist in a large number of medicinal materials. The molecular structure of berberine is shown in Fig. 1A. In order to examine the effect of berberine on cell viability of Rb cells, we employed MTT assay to analyze the cytotoxicity of berberine to Rb cells. In terms of berberine stimulation for 24 h or 48 h, concentrations ranging from 0 to 100 μM were suitable for further investigation (Fig. 1B). When the concentration of berberine was higher than 100 μM, the cell viability was too low to conduct other experiments. Thus, the concentrations of berberine for further studies were controlled in a range of 0 to 100 μM.

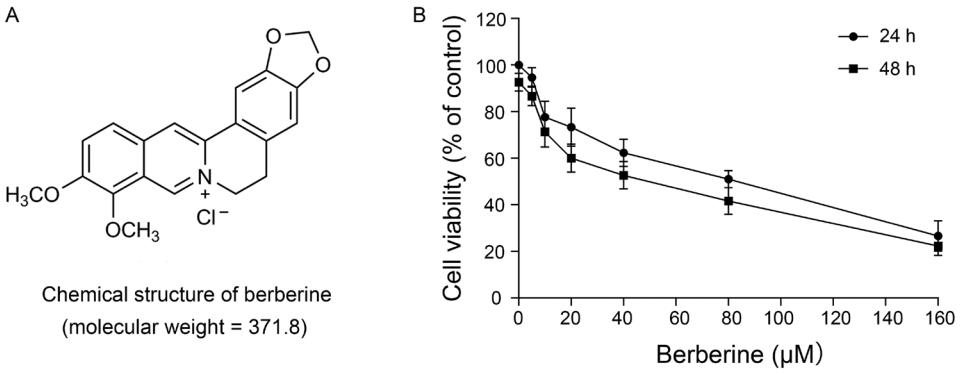

Fig. 1. The effect of berberine on the cell viability in human Rb cells

A – chemical structure of berberine; B – retinobladtoma cells were treated with berberine under various concentrations (0, 20, 40, 60, 80, 100, 120, 140 and 160 μM) for 24 h or 48 h. Thereafter, cell viability was determined by 3-(4,5-dimethylthiazol-2-yl)-2,5-diphenyltetrazolium bromide (MTT) assay. The data presented was the mean of 3 independent experiments. Error bars indicate standard deviation (SD).

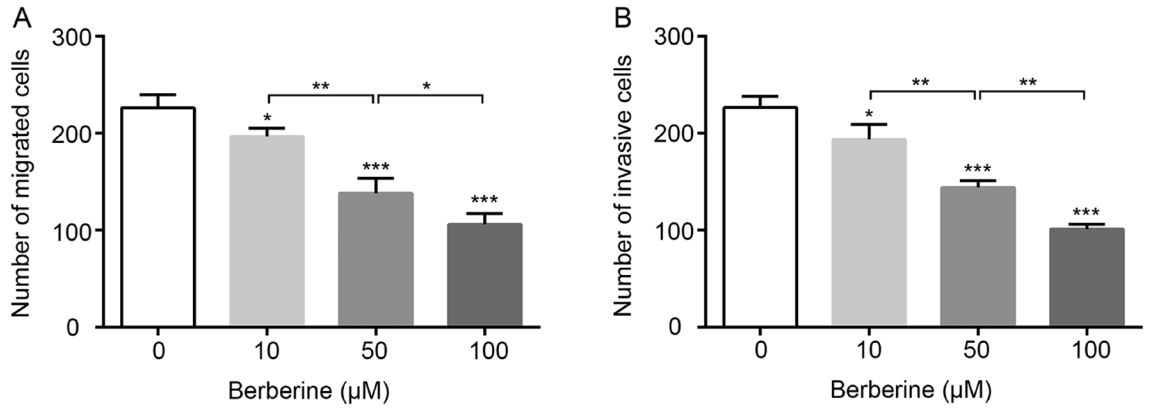

Fig. 2. The suppressive effect of berberine on cell migration and invasion in human Rb cells

Retinoblastoma cells were stimulated by berberine under 0, 10, 50 or 100 μM. After stimulation for 24 h, the cell migration (A) and invasion (B) were both measured by transwell analysis. The data presented was the mean of 3 independent experiments. Error bars indicate standard deviation (SD). * $p < 0.05$; ** $p < 0.01$; *** $p < 0.001$. The significance marked at the top of the columns refers to comparisons with the group treated with 0 μM berberine.

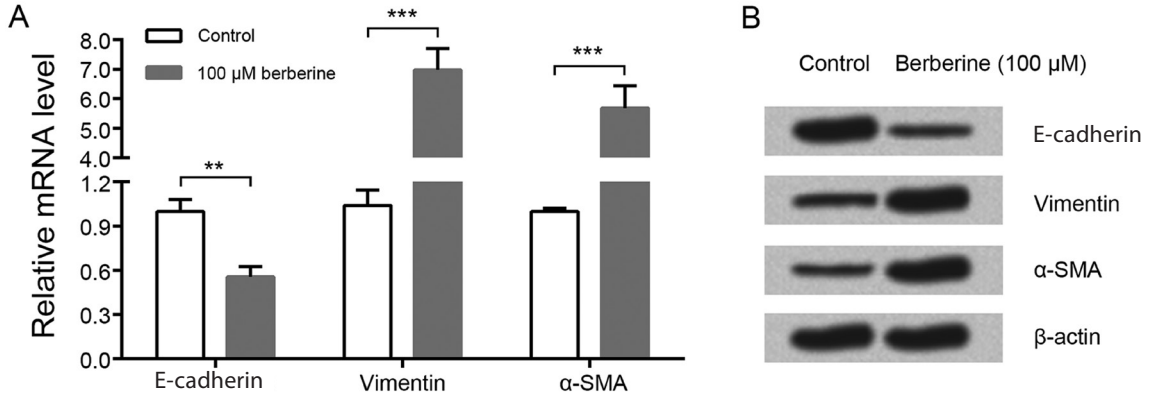

Fig. 3. The inhibitory effect of berberine on epithelial-mesenchymal transition (EMT) in human Rb cells

Retinoblastoma cells were stimulated with or without berberine (100 μM). Cells treated without berberine acted as the control. After stimulation for 24 h, the mRNA (A) and protein (B) levels of EMT markers were respectively estimated by quantitative reverse transcription PCR (qRT-PCR) and western blot analysis. The data presented was the mean of 3 independent experiments. Error bars indicate SD. ** $p < 0.01$; *** $p < 0.001$; α-SMA – α-smooth muscle actin.

Berberine suppressed cell migration and invasion of retinoblastoma cells in a dose-dependent manner

The cell migration and invasion assays were performed with berberine stimulation under various concentrations (0, 10, 50 and 100 μM). The cells without berberine treatment acted as a control group. In Fig. 2A, 2B, the cell migration and invasion of Rb cells were both suppressed by berberine under 10, 50 and 100 μM in comparison with controls ($p < 0.05$ or $p < 0.001$). Further comparison between the cells treated with 50 μM of berberine and 10 μM of berberine ($p < 0.01$) as well as 50 μM of berberine and 100 μM of berberine ($p < 0.05$ or $p < 0.01$) implied that berberine suppressed cell migration and invasion in a dose-dependent manner.

Berberine inhibited epithelial to mesenchymal transition in retinoblastoma cells

In view of the great importance of epithelial to mesenchymal transition (EMT) in the development of invasive cancer cells, we assessed the effect of berberine on EMT markers in Rb cells. The mRNA and protein levels of EMT markers were respectively estimated by qRT-PCR and western blot analysis. Retinoblastoma cells were treated with or without berberine (100 μM) and cells treated without berberine acted as the control. As shown in Fig. 3A, berberine treatment significantly decreased E-cadherin mRNA levels and increased vimentin and α-SMA mRNA levels compared to controls ($p < 0.01$ or $p < 0.001$). The effect of berberine on protein levels of E-cadherin, vimentin and α-SMA was in accordance with mRNA levels (Fig. 3B). Thus, we drew the conclusion that berberine inhibited EMT in Rb cells.

Berberine suppressed cell migration and invasion via inactivation of PI3K/Akt and p38 in retinoblastoma cells

The protein levels of p-Akt and p-p38 were evaluated by western blot analysis. Retinoblastoma cells were treated with or without berberine (100 μM) and the cells treated without berberine acted as the control. In Fig. 4A, the protein levels of p-Akt and p-p38 were both down-regulated by berberine stimulation. Furthermore, Rb cells were stimulated with berberine (100 μM) alone or accompanied with PI3K inhibitor LY294002 (10 μM, Sigma, San Francisco, USA) or p38 inhibitor SB203580 (10 μM, Sigma, St. Louis, USA). Cells treated without berberine acted as the control. In Fig. 4B, 4C, cell migration and invasion were remarkably inhibited by the addition of berberine compared to controls ($p < 0.01$ or $p < 0.001$). Reasonably, co-stimulation of berberine with LY294002 or SB203580 markedly suppressed cell migration and invasion in comparison with stimulation with berberine alone ($p < 0.05$). Taken together, we inferred that berberine suppressed cell migration and invasion through inactivation of PI3K/Akt and p38 in Rb cells.

Discussion

The prognosis of Rb alone is excellent in patients, with a cure rate of 95% in developed countries. Nonetheless, the existing therapies may enhance the risk of occurrence of secondary neoplasms. Hence, the development of novel non-mutagenic therapy is urgent for avoiding a 2nd tumor. In the present study, we found that berberine significantly suppressed cell migration, invasion and EMT. Additionally, the phosphorylation level of Akt and p38 were both down-regulated by stimulation of berberine. Further studies on co-stimulation of berberine with a specific inhibitor of PI3K or p38 implied that berberine suppressed cell migration and invasion via suppression of PI3K/Akt and p38 phosphorylation.

High cell migration and invasion are two substantial characteristics for cancer cells. Numerous reports have illustrated the suppressive effect of berberine on cancer cells. Berberine suppressed migration and invasion of human SCC-4 tongue squamous cancer cells via inhibition of focal adhesion kinase (FAK), nuclear factor-κB (NF-κB), IκB kinase (IKK), urokinase-type plasminogen activator (u-PA), matrix metalloproteinase 2 (MMP-2), and MMP-9.[22] Berberine has also been reported to inhibit the migration and invasion of T24 bladder cancer cells through reducing the expression of heparanase.[23] Moreover, berberine exerted suppressive effect on migration and invasion of hepatocellular carcinoma cells via altering the expression of plasminogen activator inhibitor-1 (PAI-1) and u-PA.[24] The effect of berberine on the cell migration and invasion of Rb cells was consistent with the studies described above.

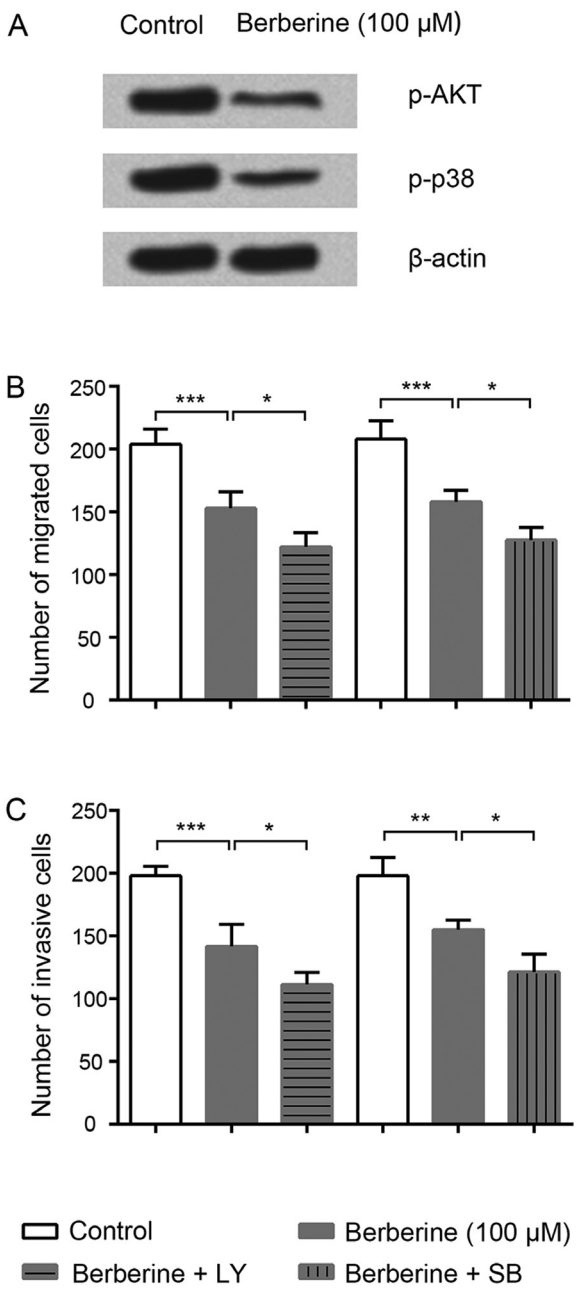

Fig. 4. The relationship between the suppressive effect of berberine on cell migration and invasion and inactivation of PI3K/Akt and p38

Cells were stimulated with or without berberine (100 μM). After stimulation for 24 h, the protein levels of p-Akt and p-p38 were estimated by western blot analysis (A). Furthermore, the cells were stimulated with berberine (100 μM) alone or respectively co-stimulated with 2-(4-morpholinyl)-8-phenyl-chromone (LY294002, 10 μM) or SB203580 (10 μM). After stimulation for 24 h, the cell migration (B) and invasion (C) were evaluated by transwell analysis. Cells treated without berberine acted as the control. The data presented was the mean of 3 independent experiments. Error bars indicate SD. * $p < 0.05$; ** $p < 0.01$; *** $p < 0.001$; LY – LY294002; SB – SB203580.

The complex metastasis of cancer consists of 5 continuous steps – proliferation, migration, invasion, adhesion, and angiogenesis.[25] Epithelial to mesenchymal transition is characterized by the loss of cell-cell adhesion, which makes cells gain mesenchymal features and stem-like

properties. The obvious effect of EMT on cells is improved migratory capacity and invasiveness, and reduced cell adhesion as well as resistance to cancer treatment.[26] A previous study claimed that inhibition of the mTOR pathway attenuated the migration and invasion of gallbladder cancer via EMT inhibition.[27] Recently, microRNA-133a was reported to suppress the migration and invasion of esophageal cancer cells by targeting the EMT regulator SOX4.[28] In the present study, the results relevant to EMT markers suggested that berberine markedly inhibited EMT, which might be one reason for the suppressive effect of berberine on cell migration and invasion of Rb cells.

Protein Kinase B is a kind of serine-threonine kinase which acts as the primary downstream mediator of PI3K and participates in a large numbers of bioprocesses.[29] P38 is one of the mitogen activated protein kinases (MAPKs), which also has been reported to be involved in various cell processes.[30] A previous study has claimed that a basic helix-loop-helix (bHLH) transcription factor (Twist), could increase migration and invasion of breast cancer cells via transcriptionally up-regulating Akt2.[31] Heparanase has been reported to promote human gastric cancer cells migration and invasion by increasing phosphorylation level of p38.[32] Specifically, Liu et al. have illustrated that inactivation of Akt or p38 induced down-regulation of both matrix metalloproteinase 2 (MMP-2) and MMP-9, leading to suppressive migration and invasion of human glioblastoma cells.[33] In the present study, berberine stimulation significantly decreased protein expression levels of p-Akt and p-p38, implying that the inactivation of Akt and p38 might be another reason for the suppressive migration and invasion of Rb cells. Additionally, the comparison between cells treated with berberine alone and cells treated with berberine accompanied by the extra addition of PI3K inhibitor LY294002 or p38 inhibitor SB203580 seems to verify the inference. Furthermore, extensive investigations have suggested that EMT was induced by Akt or p38 signaling pathway.[34–36] In a word, berberine suppressed cell migration and invasion through inactivation of PI3K/Akt and p38.

In summary, we are providing the first report for the suppressive effect of berberine on cell migration and invasion of human Rb cells in a dose-dependent manner. Furthermore, EMT was markedly inhibited by berberine. In addition, the suppressive effect of berberine on cell migration and invasion was due to the inactivation of PI3K/Akt and p38. Therefore, berberine may represent a new anticancer drug that can prevent metastasis of Rb and become a potential therapeutic agent.

References

1. Abramson DH, Schefler AC. Update on retinoblastoma. *Retina*. 2005;7:174–178.
2. Friend SH, Bernards R, Rogelj S, et al. A human DNA segment with properties of the gene that predisposes to retinoblastoma and osteosarcoma. *Nature*. 1986;323:187–206.
3. Parkin DM, Stiller CA, Draper GJ, Bieber CA. The international incidence of childhood cancer. *Int J Cancer*. 1988;42:511–520.
4. Phan IT, Stout T. Retinoblastoma presenting as strabismus and leukocoria. *J Pediatrics*. 2010;157:858–858.
5. Chawla B, Jain A, Azad R. Conservative treatment modalities in retinoblastoma. *Ind J Ophthalmol*. 2013;61:479–485.
6. Pandey AN. Retinoblastoma: An overview. *Saudi J Ophthalmol*. 2014; 28:310–315.
7. El Kettani A, Aderdour S, Daghouj G, et al. Retinoblastoma: Preliminary results of national treatment protocol at Casablanca university medical center. *J Fr Ophtalmol*. 2014;37:115–124.
8. Chang MW, Barr E, Seltzer J, et al. Cytostatic gene therapy for vascular proliferative disorders with a constitutively active form of the retinoblastoma gene product. *Science*. 1995;267:518–522.
9. Durairajan S, Liu LF, Lu JH, Chen LL. Berberine ameliorates β-amyloid pathology, gliosis, and cognitive impairment in an Alzheimer's disease transgenic mouse model. *Neurobiol Aging*. 2012;33:2903–2919.
10. Gulbahar O, Ozturk G, Erdem N, Kazandi AC, Kokuludag A. Antioxidant and anti-inflammatory activities of berberine in the treatment of diabetes mellitus: Evidence-based complementary and alternative medicine. *eCAM*. 2014;2014:71–80.
11. Chang W, Chen L, Hatch GM. Berberine as a therapy for type 2 diabetes and its complications: From mechanism of action to clinical studies. *Biochem Cell Biol*. 2014;1:1–8.
12. Cicero AF, Ertek S. Metabolic and cardiovascular effects of berberine: From preclinical evidences to clinical trial results. *Clin Lipidol*. 2015;4:553–563.
13. Xie J, Xu Y, Huang X, et al. Berberine-induced apoptosis in human breast cancer cells is mediated by reactive oxygen species generation and mitochondrial-related apoptotic pathway. *Tumour Biol*. 2015;36:1279–1288.
14. Park JJ, Seo SM, Kim EJ, et al. Berberine inhibits human colon cancer cell migration via AMP-activated protein kinase-mediated down-regulation of integrin β1 signaling. *Biochem Biophys Res Commun*. 2012;426:461–467.
15. Chou HC, Lu YC, Cheng CS, et al. Proteomic and redox-proteomic analysis of berberine-induced cytotoxicity in breast cancer cells. *J Proteomics*. 2012;75:3158–3176.
16. Yip NK, Ho WS. Berberine induces apoptosis via the mitochondrial pathway in liver cancer cells. *Oncol Rep*. 2013;30:1107–1112.
17. Diogo CV, Machado NG, Barbosa IA, Serafim TL, Burgeiro A, Oliveira PJ. Berberine as a promising safe anti-cancer agent – is there a role for mitochondria? *Curr Drug Targets*. 2011;12:850–859.
18. Chambers AF, Groom AC, Macdonald IC. Metastasis: Dissemination and growth of cancer cells in metastatic sites. *Nat Rev Cancer*. 2002;2: 563–572.
19. Chen PN, Hsieh YS, Chiou HL, Chu SC. Silibinin inhibits cell invasion through inactivation of both PI3K-Akt and MAPK signaling pathways. *Chem Biol Interact*. 2005;156:141–150.
20. Chen KS, Shi MD, Chien CS, Shih YW. Pinocembrin suppresses TGF-β1-induced epithelial-mesenchymal transition and metastasis of human Y-79 retinoblastoma cells through inactivating αvβ3 integrin/FAK/p38α signaling pathway. *Cell Biosci*. 2014;4:1–13.
21. Schefe JH, Lehmann KE, Buschmann IR, et al. Quantitative real-time RT-PCR data analysis: Current concepts and the novel 'gene expression's CT difference' formula. *J Mol Med*. 2006;84:901–910.
22. Ho YT, Yang JS, Li TC, et al. Berberine suppresses in vitro migration and invasion of human SCC-4 tongue squamous cancer cells through the inhibitions of FAK, IKK, NF-κB, u-PA and MMP-2 and -9. *Cancer Lett*. 2009;279:155–162.
23. Yan L, Yan K, Kun W, et al. Berberine inhibits the migration and invasion of T24 bladder cancer cells via reducing the expression of heparanase. *Tumour Biol*. 2013;34:215–221.
24. Liu X, Ji Q, Ye N, et al. Berberine inhibits invasion and metastasis of colorectal cancer cells via COX-2/PGE2 mediated JAK2/STAT3 signaling pathway. *PLOS One*. 2015;10:e0123478.
25. Qi H, Xin L, Xu X, Ji X, Fan L. Epithelial-to-mesenchymal transition markers to predict response of berberine in suppressing lung cancer invasion and metastasis. *J Transl Med*. 2014;12:116–122.
26. Medici D, Muñoz-Cánoves P, Yang PC, Brunelli S. Mesenchymal transitions in development and disease. *Stem Cells Int*. 2016;2016:1–2.
27. Zong H, Yin B, Zhou H, Cai D, Ma B, Xiang Y. Inhibition of mTOR pathway attenuates migration and invasion of gallbladder cancer via EMT inhibition. *Mol Biol Rep*. 2014;41:4507–4512.

28. Li S, Qin X, Li Y, et al. MiR-133a suppresses the migration and invasion of esophageal cancer cells by targeting the EMT regulator SOX4. *Am J Transl Res*. 2015;7:1390–1403.
29. Villegas-Comonfort S, Castillo-Sanchez R, Serna-Marquez N, Cortes-Reynosa P, Salazar EP. Arachidonic acid promotes migration and invasion through a PI3K/Akt-dependent pathway in MDA-MB-231 breast cancer cells. *Prostaglandins Leukot Essent Fatty Acids*. 2014;90:169–177.
30. Coulthard LR, White DE, Jones DL, Mcdermott MF, Burchill SA. p38 MAPK: Stress responses from molecular mechanisms to therapeutics. *Trends Mol Med*. 2009;15:369–379.
31. Cheng GZ, Chan J, Wang Q, Zhang W, Sun CD, Wang LH. Twist transcriptionally up-regulates AKT2 in breast cancer cells leading to increased migration, invasion, and resistance to paclitaxel. *Cancer Res*. 2007;67:1979–1987.
32. Ma XM, Shen ZH, Liu ZY, et al. Heparanase promotes human gastric cancer cells migration and invasion by increasing Src and p38 phosphorylation expression. *Int J Clin Exp Pathol*. 2014;7:5609–5621.
33. Liu Y, Zheng J, Zhang Y, et al. Fucoxanthin activates apoptosis via inhibition of pi3k/akt/mtor pathway and suppresses invasion and migration by restriction of p38-MMP-2/9 pathway in human glioblastoma cells. *Neurochem Res*. 2016;41:2728–2751.
34. Li F, Yin X, Luo X, et al. Livin promotes progression of breast cancer through induction of epithelial–mesenchymal transition and activation of AKT signaling. *Cell Signal*. 2013;25:1413–1422.
35. Liu L, Dai Y, Chen J, et al. Maelstrom promotes hepatocellular carcinoma metastasis by inducing epithelial-mesenchymal transition by way of Akt/GSK-3β/snail signaling. *Hepatology*. 2014;59:531–543.
36. Kolosova I, Nethery D, Kern JA. Role of Smad2/3 and p38 MAP kinase in TGF-β1-induced epithelial–mesenchymal transition of pulmonary epithelial cells. *J Cell Physiol*. 2011;226:1248–1254.

Examination of the antioxidant effects of pre-HSG melatonin use on ovarian surface epithelium in rats: An experimental study

Esra Saygılı Yılmaz[1,A–F], Tansel Sapmaz[2,3,B,C], Halil Kazgan[1,A,B], Şule Menziletoglu Yildiz[4,A,D], Derya Kocamaz[4,A,D], Nusret Akpolat[5,C,E], Ekrem Sapmaz[1,C,F]

[1] Department of Gynecology and Obstetrics, Adana Numune Training and Research Hospital, Turkey
[2] Department of Histology and Embryology, Institute of Medical Sciences, Imperial School of Medicine, Istanbul, Turkey
[3] Department of Histology and Embryology, Faculty of Medicine, Firat University, Elazig, Turkey
[4] Blood Center of Balcali Hospital, Faculty of Medicine, Çukurova University, Adana, Turkey
[5] Department of Pathology, Faculty of Medicine, Inonu University, Malatya, Turkey

A – research concept and design; B – collection and/or assembly of data; C – data analysis and interpretation; D – writing the article; E – critical revision of the article; F – final approval of the article

Advances in Clinical and Experimental Medicine, ISSN 1899–5276 (print), ISSN 2451–2680 (online) *Adv Clin Exp Med*. 2018;27(7):907–911

Address for correspondence
Esra Saygılı Yılmaz
E-mail: deryaserbes@gmail.com

Funding sources
None declared

Conflict of interest
None declared

Received on February 28, 2017
Reviewed on April 18, 2017
Accepted on April 27, 2017

Abstract

Background. There is no study of whether the dysplastic changes in the ovarian surface epithelium of X-ray-exposed rats during hysterosalpingography (HSG) decrease or not with the use of Lipiodol and melatonin given both intraperitoneally (i.p.) and into the suspensorium ovarii.

Objectives. We investigated the restorative effects of melatonin and Lipiodol administration during the HSG procedure on the dysplastic changes in the ovarian surface epithelium of X-ray-exposed rats.

Material and methods. A total of 50 Wistar rats with regular estrous cycles were randomly divided into 5 groups. Group 1 was the control group. In other groups, X-ray was applied (group 2), 0.1 mL Lipiodol was applied to each uterine horn (group 3), 20 mg/kg intraperitoneal melatonin application was followed by 0.1 mL Lipiodol administration to each uterine horn after 15 min (group 4), and 20 mg/kg melatonin was administered to the ligamentum suspensorium ovarii, followed by 0.1 mL Lipiodol application to each uterine horn after 15 min (group 5). The rats in groups 2–5 were exposed to whole body radiation 3 times. After 3 h, the abdomens of all rats were reopened and left oophorectomy was performed.

Results. The presence of nucleoli and mitosis values were found similar among the groups. All other parameters were significantly higher in group 2 compared to other groups, except for the presence of nucleoli and mitosis values ($p < 0.05$). The presence of hyperchromasia and the total score were found to be the highest in group 2, followed by group 3, when compared to other groups ($p < 0.05$). It was detected that the detrimental effects of X-ray exposure diminished with Lipiodol use, and were further reduced by the use of melatonin in combination.

Conclusions. We suggest that the use of melatonin and Lipiodol during HSG may prevent the carcinogenic changes exerted by radiation on the ovarian surface epithelium.

Key words: melatonin, hysterosalpingography, rats, radiation, Lipiodol

DOI
10.17219/acem/70810

Introduction

During the last decade, the number of women seeking infertility evaluation has increased significantly. Despite the development of other diagnostic procedures, such as magnetic resonance imaging, hysteroscopy and laparoscopy, hysterosalpingography (HSG) remains as the most valuable and commonly used gynecoradiological technique for the diagnosis of fallopian tube obstruction and uterine cavity abnormalities.[1]

In HSG studies that are performed under fluoroscopic control, various radioscopic exposures are effectuated to visualize the fallopian tubes and the uterine cavity, following the gradual introduction of the contrast medium.[2] As HSG involves radiation exposure of the gonadal region in women of reproductive capacity and the possibility for repeated examinations, concerns over radiation doses and the associated radiation risks have become an issue.[3] People are constantly exposed to low levels of radiation because of the common use of certain electronic devices, air travel and medical diagnostic exams. Scientific and technological advancements have further increased the radiation burden in humans.[4]

Ionizing radiation consists of energetic particles and electromagnetic radiation, which can easily penetrate the living tissues or cells. The absorbed energy of ionizing radiation can break chemical bonds and cause the ionization of water and different biologically important macromolecules, such as nucleic acids, membrane lipids and proteins.[5] Unstable and reactive free radicals, such as hydroxyl radical, superoxide anion and hydrogen peroxide, are produced more rapidly in ionized biological materials.[6] These free radicals cause the peroxidation of membrane lipids, inactivation of enzymes, depolymerization of polysaccharides, and degradation of nucleic acids. Free radicals can cause severe irreversible damage to the cell membrane.[7] Cells are well equipped to defend themselves against free radicals, with antioxidant enzymes and molecules.[8] These antioxidant systems consist of low-molecular-weight antioxidants, like glutathione and melatonin, and antioxidant enzymes, such as superoxide dismutase, catalase and glutathione peroxidase.[9]

The function of melatonin as an antioxidant and a free radical scavenger was first defined by Ianas et al. in 1991.[10] Melatonin, a derivative of amino acid tryptophan, is a neurohormone secreted from the pineal glands. However, other organs, such as the retina, ovaries, gastrointestinal tract, and lenses, are also capable of synthesizing melatonin.[11] Melatonin is considered a quite exceptional antioxidant, because it can easily cross the blood–brain barrier. Studies have shown that it neutralizes hydroxyl radicals, inhibits superoxide radicals through stimulating the mRNA levels for superoxide dismutase, increases glutathione reductase, glutathione peroxidase and glucose-6-phosphate dehydrogenase activities, and decreases the intracellular concentration of hydrogen peroxide.[12] Lipiodol is iodized ethyl esters of poppy-seed oil fatty acids and has been in use as an iodinated contrast agent since 1926.[13] It is a liquid, fiducial marker for image-guided radiation therapy (IGRT) used to mark the tumor beds.[14]

There is no study of whether the dysplastic changes in the ovarian surface epithelium of X-ray-exposed rats during HSG decrease or not with the use of Lipiodol and melatonin given both intraperitoneally and into the suspensorium ovarii. Therefore, the aim of this study was to histologically investigate the restorative effects of melatonin and Lipiodol administration during the HSG procedure on the dysplastic changes of the ovarian surface epithelium of rats.

Material and methods

Following the approval of the Ethics Committee of Firat University (Elazig, Turkey), all surgical procedures and care protocols used were planned and conducted in accordance with the "Guide for the Care and Use of Laboratory Animals". The experiments were performed on 50 female albino Wistar rats at the animal laboratory of Firat University. The rats were 5 months old, weighed approx. 200–230 g and had regular ovulation cycles. They were kept at 21–23°C, with 55–60% relative humidity, under controlled photo-periods (12:12 h light:dark) and were fed with a standard rodent chow and tap water. Feeding of the rats stopped 18 h prior to the experiment, only water was allowed. The rats that were detected to be in the estrus phase via vaginal cytology were anesthetized with chloral hydrate (400 mg/kg, intraperitoneally – i.p.). Each rat was placed on the operating table in a supine position, and the abdomen was opened through a midline incision. The rats were randomized into 5 groups of 10 rats each:

– group 1 (G1): the group in which the abdomen was opened and closed without any X-ray irradiation;

– group 2 (G2): the group in which the abdomen was opened and closed, and X-ray was applied;

– group 3 (G3): the group in which the abdomen was opened and 0.1 mL Lipiodol® amp. (Guerbet Lab, Aulnay-sous-bois, France) was applied to each uterine horn;

– group 4 (G4): the group in which the abdomen was opened and 20 mg/kg melatonin (Melatonin®, N-acetyl-5-metoksitriptamin; Sigma Chemicals, Deisenhofen, Germany) was administered i.p., followed by 0.1 mL Lipiodol® application to each uterine horn after 15 min;

– group 5 (G5): the group in which the abdomen was opened and 20 mg/kg melatonin (Melatonin®, N-acetyl-5-metoksitriptamin; Sigma Chemicals) was administered to the ligamentum suspensorium ovarii, followed by 0.1 mL Lipiodol® application to each uterine horn after 15 min.

After their abdomens were closed, the rats in G2, G3, G4, and G5 were exposed to whole body irradiation 3 times, leaving 2-minute intervals in between (total dose: 15–20 milirad, Villa-Genius HF-80 X-ray Generator; double table, double

Table 1. Examined parameters of all groups with respect to the changes in the ovarian surface epithelium

Parameter	G1	G2	G3	G4	G5
Stratification	0.0[a]	1.4 ±0.5[b*]	0.0[a]	0.0[a]	0.0[a]
Tufting	0.0[a]	1.0 ±0.4[b*]	0.0[a]	0.0[a]	0.0[a]
Chromatin irregularity	0.0[a]	1.1 ±0.3[b*]	0.0[a]	0.0[a]	0.0[a]
Nuclear contour irregularity	0.0[a]	1.4 ±0.5[b*]	0.4 ±0.5[a]	0.0[a]	0.0[a]
Increase in nucleus size	0.0[a]	1.9 ±0.3[b*]	0.4 ±0.5[a]	0.2 ±0.4[a]	0.1 ±0.3[a]
Increase in nucleus/cytoplasm ratio	0.0[a]	2.6 ±0.5[b*]	0.4 ±0.5[a]	0.2 ±0.4[a]	0.1 ±0.3[a]
Pleomorphism	0.0[a]	1.0 ±0.0[b*]	0.0[a]	0.0[a]	0.0[a]
Hyperchromasia	0.2 ±0.4[a]	2.3 ±0.8[b*]	1.0 ±0.0[c*]	0.2 ±0.4[a]	0.2 ±0.4[a]
Presence of nucleoli	0.0	0.0	0.0	0.0	0.0
Presence of mitosis	0.0	0.0	0.0	0.0	0.0
Total	0.2 ±0.4[a]	12.7 ±1.7[b*]	2.3 ±1.7[c*]	0.6 ±1.2[a]	0.4 ±0.9[a]

Values shown are means ± standard deviation (SD). The letters a–c indicate statistical differences among the groups ($p < 0.005$, Mann-Whitney U test); * groups with parameters significantly different from control (G1).

tube) (Del Medical, Milan, Italy). During the experiment, the blood pressure, heart rate and body temperature of the rats were monitored. After 3 h, the abdomens of all rats were reopened and left oophorectomy was performed. Samples from the left ovaries were embedded into paraffin blocks after fixing in 10% formaldehyde for histologic examination, and then sliced into 4-micrometer thick sections.

After the preparations were stained with hematoxylin-eosin, changes in the ovarian surface epithelium were examined according to the endometrium ablation scale.[15] According to the scale, 1. stratification; 2. tufting; 3. chromatin irregularity; 4. nuclear contour irregularity; 5. increase in nucleus size; 6. increase in nucleus/cytoplasm ratio; 7. pleomorphism; 8. presence of nucleoli; 9. mitosis; and 10. hyperchromasia changes in the ovarian surface epithelium were examined. For each parameter, a scale (none = 0 points, present = 1 point, considerably present = 2 points) was applied, and the total score was obtained based on the values of all the parameters in a preparation.

The Kruskal-Wallis variance test from the SPSS Package Software (IBM, Armonk, USA) was used in the statistical analysis of data. The Mann-Whitney U test with Bonferroni correction was applied for parameters with $p < 0.05$. A probability value of $p < 0.005$ was considered statistically significant.

Results

The presence of nucleoli and mitosis values were found similar in all groups ($p > 0.05$, Kruskal-Wallis variance test).

All parameters except nucleoli and mitosis values increased significantly in the X-ray exposed group compared to other groups ($p < 0.005$, Mann-Whitney U test).

The detrimental effects of X-ray application diminished with Lipiodol use and were further reduced by the use of melatonin in combination with Lipiodol.

The presence of hyperchromasia and the total score were found to be the highest in group 2, followed by group 3, compared to other groups ($p < 0.005$, Mann-Whitney U test). All examined parameters are listed in Table 1.

Discussion

The ovaries are a part of the female reproductive system that is very sensitive to radiation. Ovarian damage is a major complication observed in patients who receive long-term radiotherapy. High doses of radiotherapy damage the ovarian function of all ages, causing a decline in fertility.[16] Therefore, researchers' interest in rat estrus cycle studies has increased in order to prevent ovarian damage caused by radiation, to discuss the effects of radiotherapy and to evaluate normal ovarian function.

The total number of follicles is regarded as one of the most important parameters reflecting ovarian function.[17] Lee et al. investigated the damage in primordial and primary follicles by collecting the ovaries of female prepubertal mice exposed to 8.3 Gy gamma radiation after 3, 6 and 12 h after irradiation.[18] They reported that the most damage occurred after 3 h of irradiation, and the damage decreased as exposure time progressed. For this reason, in order to determine the dysplastic changes in the rat ovarian surface epithelium, the ovarian tissues were collected after 3 h of exposure and histologically evaluated for each group. Our study demonstrated that the radiation received during HSG treatment significantly increased stratification, tufting, chromatin irregularity, nuclear contour irregularity, nucleus size, nucleus/cytoplasm rate, pleomorphism, and hyperchromasia in the rat ovarian surface epithelium. Similarly, Pala et al. reported that markedly increased epithelial degeneration and obstruction was observed in the endometrial glands of rats that were exposed to X-ray irradiation with Lipiodol, as compared

to other groups.[19] Said et al. reported degeneration of the mucosal lining epithelial cell layers of the uteri in rats that were exposed to gamma radiation.[20] Radiation triggers carcinogenic changes in the ovarian surface epithelium. Our results were similar to the histological changes observed in radiation-exposed normal cells.[21,22]

Our study confirmed that the detrimental effects of X-ray application in the rat ovarian surface epithelium were significantly diminished with Lipiodol application. This may be due to the fact that linoleic acid, an antioxidant constituent of Lipiodol, has a cytotoxic effect on macrophages, reducing the production of reactive oxygen species (ROS) in the ovaries and having antiproliferative activity. Sapmaz and Akpolat reported that Lipiodol use significantly diminished the dysplastic changes in luminal epithelial cells of rats that were exposed to X-ray irradiation.[23] In previous studies, Lipiodol uptake by the cancer cells and by the endothelial cells was demonstrated on light and electron microscopy as early as 3 h after I-lipiodol application. Lipiodol is rapidly taken up and retained in the cells in the form of cytoplasmic bound vesicles.[24] It also has a role as a vehicle to carry other agents inside the cells.[25] Sapmaz et al. examined the effects of Lipiodol and Lipiodol combined with tetracycline against X-ray exposure during HSG treatment, and reported that Lipiodol use diminished the carcinogenic effects of radiation on ovarian surface epithelium, and were further reduced by the use of tetracycline in combination with Lipiodol.[15]

The protective effects of melatonin against oxidative stress have been established in in vitro and in vivo studies.[26–28] During antioxidant defense, melatonin not only neutralizes hydroxyl radicals, but also scavenges peroxyl radicals and singlet oxygen throughout peroxidation.[29] This implies that melatonin, which is lipophilic and hydrophilic, has effects not only at the cellular level, but also in the subcellular compartments.[30] Melatonin stimulates the activity of the detoxifying enzyme glutathione peroxidase and strengthens the antioxidant defense of the cells against oxidative stress.[31] That is how melatonin stimulates antioxidant defense or exhibits strengthening actions against ionizing radiation which causes genetic damage by increasing the production of free radicals.[32] In our study, changes in ovarian surface epithelium in rats treated with Lipiodol and melatonin were found to be similar to the control group. Sapmaz and Akpolat reported that the use of melatonin in combination with Lipiodol has a decreasing effect on congestion, endometrial ablation, fibrosis, and dysplastic changes to the control levels in X-ray-treated rats.[23] It is thought that this decreasing effect is due to the stimulation of the antioxidant defense system of the cells against the damage caused by ionizing radiation by elevated intracellular concentrations of melatonin with Lipiodol's action. Radiation causes arteritis in large vessels such as coronary, pulmonary, thoracic aorta, brachial, renal, and ilio-femoral vessels, and causes hypoxia and ischemia in the perfused organs.[33,34] In our study, the rats in the X-ray group may have developed a more severe radiation-associated ilio-femoral or uterine arteritis than the rats in the groups G3, G4 and G5. This may have led to a severe hypoxic effect and an increase in ROS production in G2, leading to the onset of carcinogenic changes in the ovarian surface epithelium. Even though other groups developed radiation-associated ilio-femoral or uterine arteritis of similar severity, it is thought that the combined use of Lipiodol and melatonin, which have antioxidant properties, was effective in reducing the detrimental effects of radiation. The study conducted by Badr et al. on rats confirmed that melatonin treatment 1 h before the X-ray irradiation prevented chromosomal damage, but no significant effect was observed when melatonin was given 1/2 h after the exposure.[30] Undeger et al. demonstrated that intraperitoneal pretreatment of rats with 100 mg/kg melatonin provided a significant decrease in the DNA strand breakage and lipid peroxidation in the brain tissue.[35] Canyılmaz et al. reported that 100 mg/kg intraperitoneal melatonin administration 1/2 h prior to a single dose of 6-Gy-gamma irradiation decreased the tubular atrophy and lipid peroxidation in the rat kidney tissues.[36] Sato et al. conducted a study in order to reduce the risk for postoperative acute liver failure, in which prostaglandin was administered either from the hepatic artery or superior mesenteric artery to patients who were undergoing major hepatic resections, and found that prostaglandin applied through the hepatic artery was infused more rapidly.[37] In our study, melatonin was administered in 2 different ways prior to irradiation, intraperitoneally (G4) and into the suspensorium ovarii (G5). Although both groups were at the control level, it was determined that the values of G5 were better than those of G4. This suggests that antioxidants may increase their protective effects if administered closer to the target organs. Pala et al. reported that there was no significant difference in epithelial degeneration and congestion in rats administered with Lipiodol combined with vitamin C and Lipiodol combined with vitamin E i.p. prior to irradiation, indicating that both groups were at the control level.[19] Sapmaz et al. reported that melatonin was more effective than oxytetracycline in their comparative study of the antioxidant effects of melatonin and oxytetracycline in autologous intraperitoneal ovary transplantation.[38] Histoenzymological and morphological studies suggested that melatonin was shown to act synergistically with chemotherapeutic agents or radiotherapy in order to increase the antitumor effects by promoting disease stabilization.[39] Therefore, it is believed that melatonin and Lipiodol administration to patients prior or during the HSG procedure can reduce the harmful effects of radiation. Based on the results of our work, it is thought that melatonin and Lipiodol administration may prevent the carcinogenic changes exerted by radiation on the ovarian surface epithelium.

References

1. Úbeda B, Paraira M, Alert E, Abuin RA. Hysterosalpingography: Spectrum of normal variants and nonpathologic findings. *ASSS*. 2001;177: 131–135.
2. Perisikanis K, Damilakis J, Grammatikakis J, Therocharopolus N, Gourtsayiannis N. Radiogenic risk from hysterosalpingography. *Eur Radiol*. 2003;13:1522–1528.
3. Yousef M, Tambul JY, Sulieman A. Radiation dose measurements during hysterosalpingography. *Sudan Medical Monitor*. 2014;9(1):15–19.
4. Jagetia GC, Reddy TK. Modulation of radiation-induced alteration in the antioxidant status of mice by naringin. *Life Sci*. 2005;77(7): 780–794.
5. Lett JT. Damage to cellular DNA from particulate radiations, the efficacy of its processing and the radiosensitivity of mammalian cells. Emphasis on DNA double strand breaks and chromatin breaks. *Radiat Environ Biophys*. 1992;31(4):257–277.
6. Robbins MEC, Zhao W. Chronic oxidative stress and radiation late normal tissue injury: A review. *Int J Radiat Biol*. 2004;80(4):251–259.
7. Yalinkilic O, Enginar H. Effect of X-radiation and lipid peroxidation and antioxidant system in rats treated with saponin-containing compound. *Photochem Photobiol*. 2008;84(1):236–242.
8. Jagetia GC, Vankatesha VA, Reddy TK. Naringin, a citrus flavonone, protects against radiation-induced chromosome damage in mouse bone marrow. *Mutagenesis*. 2003;18:337–343.
9. Jeon WY, Lee MY, Shin HS, Shin HK. Protective effects of the traditional herbal formula oryeongson water extract on ethanol-induced acute gastric mucosal injury in rats. *Evid Based Complement Alternat Med*. 2012;1–9. doi: 10.1155/2012/438191
10. Ianas O, Oliverscu R, Badescu I. Melatonin involvement in oxidative processes. *Rom J Endocrinol*. 1991;29:117–123.
11. Reiter RJ, Tan DX, Qi W, Manchester LC, Karbownik M, Calvo JR. Pharmacology and physiology of melatonin in the reduction of oxidative stress in vivo. *Biol Signals Recept*. 2000;9(3–4):160–171.
12. Ozcelik F, Erdem M, Bolu A, Gulsun M. Melatonin: General features and its role in psychiatric disorders. *Current Approach in Psychiatry*. 2013;5(2):179–203.
13. Freilich JM, Spiess PE, Biogoli ME, et al. Lipiodol as a fiducial marker for image-guided radiation therapy for bladder cancer. *Int Braz J Urol*. 2014;40(2):190–197.
14. Baumgarten AS, Emtage JB, Wilder RB, Biagioli AS, Gupta S, Spiesu PE. Intravesical lipiodol injection technique for image-guided radiation therapy for bladder cancer. *Urology*. 2014;83:946–950.
15. Sapmaz E, Akpolat N, Çelik A, Sapmaz T, Pala S, Hanay F. Examination of the effect of HSG procedure on ovarian surface epithelium: Experimental study. *J Turk Soc Obstet Gynecol*. 2006;3:112–117.
16. Bricaire L, Larache E, Bourcigoux N, Daradille B, Christin-Maitre S. Premature ovarian failure. *Presse Med*. 2013;42(11):1500–1507.
17. Zhang XF, Zhang LJ, Li L, et al. Diethylhexyl phthalate exposure impairs follicular development and affects oocyte maturation in the mouse. *Environ Mol Mutagen*. 2013;54:354–361.
18. Lee CJ, Park HH, Do BR, Yoon Y, Kim JK. Natural and radiation-induced degeneration of primordial and primary follicles in mouse ovary. *Anim Reprod Sci*. 2000;59(1–2):109–117.
19. Pala S, Atilgan R, Kuloglu T, et al. Protective effects of vitamin C and vitamin E against hysterosalpingography-induced epithelial degeneration and proliferation in rat endometrium. *Drug Des Devel Ther*. 2016;4079–4089.
20. Said RS, Nada AS, El-Demerdash E. Sodium selenite improves folliculogenesis in radiation-induced ovarian failure: A mechanistic approach. *PLoS One*. 2012;7(12):e50928.
21. Preston RJ. Radiation biology: Concepts for radiation protection. *Health Phys*. 2005;88(6):545–556.
22. Abe S, Otsuki M. Styrene maleic acid neocarzinostatin treatment for hepatocellular carcinoma. *Curr Med Chem Anticancer Agents*. 2002;2(6): 715–726.
23. Sapmaz E, Akpolat N. Examination of the effects of pre-HSG melatonin on endometrial ablation and uterine dysplasic cell development associated with radiation. *Fırat Tıp Dergisi*. 2012;17(1):1–5.
24. Al Mufti R, Pedley RB, Marshall D, et al. In vitro assessment of Lipiodol-targeted radiotheraphy for liver and colorectal cancer cell lines. *Br J Cancer*. 1999;79:1665–1671.
25. Kishimoto S, Miyazawa K, Fukushima S, Takeuchi Y. In vitro antitumor activity intracellular accumulation and DNA adduct formation of cis-[((1R,2R)-1,2-cyclohexanediamine-N,N')bis(myristato)] platinum (II) suspended in lipiodol. *Jpn J Cancer Res*. 2000;91(1):99–104.
26. Sewerynek E, Reiter RJ, Melchiorri D, Ortiz GG, Lewinski A. Oxidative damage in the liver induced by ischemia-reperfusion: Protection by melatonin. *Hepatogastroenterology*. 1996;43:898–905.
27. Princ FG, Juknat AA, Maxit AG, Cardalda C, Battle A. Melatonin's antioxidant protection against delta-aminolevulinic acid-induced oxidative damage in rat cerebellum. *J Pineal Res*. 1997;23:40–46.
28. Melchiorri D, Reiter RJ, Sewerynek E, Hara M, Chen L, Nistico G. Paraquat toxicity and oxidative damage. Reduction by melatonin. *Biochem Pharmacol*. 1996;51:1095–1099.
29. Reiter RJ. Functional pleiotropy of neurohormone melatonin: Antioxidant protection and neuroendocrine regulation. *Front Neuroendocrinol*. 1995;16(4):383–415.
30. Badr FM, El Habit OH, Harraz MM. Radioprotective effect of melatonin assessed by measuring chromosomal damage in mitotic and meiotic cells. *Mutat Res*. 1999;444(2):367–372.
31. Pablos MI, Chuang JI, Reiter RJ, et al. Time course of melatonin-induced increase in glutathione peroxidase activity in chick tissues. *Biol Signals*. 1996;4:324–330.
32. Melchiorri D, Ortiz GG, Reiter RJ, et al. Melatonin reduces paraquat-induced genotoxicity in mice. *Toxicol Lett*. 1998;95(2):103–108.
33. Rubin DI, Schomberg PJ, Shepherd RF, Panneton JM. Arteritis and brachial plexus neuropathy as delayed complications of radiation therapy. *Mayo Clin Proc*. 2001;76(8):849–852.
34. Bigot JM, Mathieu D, Reizine D. Radiation arteriopathies. *Ann Med Interne (Paris)*. 1983;134(5):411–415.
35. Undeger U, Giray B, Zorlu AF, Oge K, Bacaran N. Protective effects of melatonin on the ionizing radiation induced DNA damage in the rat brain. *Exp Toxicol Pathol*. 2004;5:379–384.
36. Canyılmaz E, Uslu GH, Bahat Z, et al. Comparison of the effects of melatonin and genistein on radiation induce nephrotoxicity results of an experimental study. *Biomed Rep*. 2016;4(1):45–50.
37. Sato T, Yasui O, Kurokawa T, Asanuma Y, Koyama K. Appraisal of intra-arterial infusion of prostaglandin E1 in patients undergoing major hepatic resection report of four cases. *Tohoku J Exp Med*. 2001;195(2): 125–133.
38. Sapmaz E, Ayar A, Celik H, Sapmaz T, Kilic N, Yasar MA. Effects of melatonin and oxytetracycline in autologous intraperitoneal ovary transplantation in rats. *Neuro Endocrinol Lett*. 2003;24(5):350–354.
39. Sener G, Atasoy BM, Ersoy Y, Arbak S, Sengoz M, Yegen BC. Melatonin protects against ionizing radiation induced oxidative damage in corpus cavernosum and urinary bladder in rats. *J Pineal Res*. 2004;37:241–246.

Ginkgolide B exerts anti-inflammatory and chondroprotective activity in LPS-induced chondrocytes

Hejia Hu[B–F], Yan Li[B,C,F], Zengfeng Xin[B,C,F], Xiangfeng Zhang[A–F]

Department of Orthopedics, Second Affiliated Hospital, School of Medicine, Zhejiang University, Hangzhou, China

A – research concept and design; B – collection and/or assembly of data; C – data analysis and interpretation;
D – writing the article; E – critical revision of the article; F – final approval of the article

Advances in Clinical and Experimental Medicine, ISSN 1899-5276 (print), ISSN 2451-2680 (online) *Adv Clin Exp Med.* 2018;27(7):913–920

Address for correspondence
Xiangfeng Zhang
E-mail: doctorzxiangfeng@163.com

Funding sources
None declared

Conflict of interest
None declared

Received on December 25, 2016
Reviewed on January 17, 2017
Accepted on April 12, 2017

Abstract

Background. Osteoarthritis (OA) is one of degenerative and chronic diseases of articular joints. Articular cartilage is an avascular tissue, and its primary cellular component are chondrocytes. The main characteristic of OA is non-classic inflammation and cartilage degeneration. Ginkgolide B (GB) is a component of *Ginkgo biloba* which has diverse bioactivities.

Objectives. The present study uses an in vitro experimental model to detect the underlying anti-inflammatory and chondroprotective effects of GB and provides a new way for future clinical therapy of OA.

Material and methods. Rat chondrocytes were isolated, cultured and treated with 1 μg/mL lipopolysaccharide (LPS) and/or different concentrations of GB. Cell Counting Kit-8 (CCK-8) was used to test the cell viability of chondrocytes, and chondrocytes apoptosis was detected using a cell apoptosis kit. Collagen-II and aggrecan expression were detected by immunohistochemistry. Relative expression of genes was detected by real-time PCR and western blot.

Results. Ginkolide B did not inhibit chondrocyte proliferation, and ginkgolide B inhibited LPS induced matrix-degradation in chondrocytes. Ginkgolide B also reversed LPS-induced collagen-II and aggrecan decreased in chondrocytes via upregulated synthesis-related gene expression and downregulated matrix-degrading enzyme gene expression. Furthermore, we found that ginkgolide B significantly inhibited LPS-induced MAPK pathway activation.

Conclusions. The results of our study suggest that ginkgolide B exerted anti-inflammatory and chondroprotective effects in LPS-induced chondrocytes, and might be an underlying therapy for OA afterwards.

Key words: osteoarthritis, anti-inflammatory, chondrocyte, ginkgolide B

DOI
10.17219/acem/70414

Introduction

Osteoarthritis (OA) is a chronic and degenerative disease of the articular joints. It is thought to cause pain and functional disability in the adult population.[1] According to a report, in America alone, 13% of women and 10% of men over the age of 60 have suffered from knee OA.[2]

Articular cartilage is an avascular tissue, and its primary cellular component is chondrocytes. Under normal physiological conditions, chondrocytes produce adequate extracellular matrix (ECM) for maintaining cartilage structure and function.[3] However, OA cartilage is characterized by a lack of proteoglycans and collagen, which are the main components of ECM. Aggrecan and collagen is degraded by aggrecanases or matrix metalloproteinases (MMPs) in OA cartilage.[4] Furthermore, in degenerative cartilage, there is evidence of cell death in chondrocytes, which will enhance the degenerative course.[5]

Due to the limited regenerative ability of articular cartilage, OA is one of the most challenging joint diseases. Current pharmacologic treatments include analgesics and nonsteroidal anti-inflammatory drugs (NSAIDs). These treatments provide symptomatic relief, however, they have no effect on OA disease prevention or modification, and substantial side effects of these treatments such as gastrointestinal, renal, and cardiovascular diseases are cause for concern, especially in long-term use.[6] Therefore, alternative strategies, including traditional Chinese medicine therapy, are becoming prevalent for their clinical curative effect without toxic side effects.

Ginkgolide B (GB) is a component of the ginkgo leaf, which has diverse bioactivities.[7] As a traditional Chinese drug, ginkgo leaf has commonly been used for treating asthma, cough and enuresis for a long time.[8] Previous studies have reported that GB has beneficial biological effects on the protection of endothelial cells.[9] In vitro and in vivo experiments have also shown that GB exerts an anti-inflammatory effect on different cells.[10–12] However, the effects and underlying mechanism of GB in OA have not yet been reported. To elucidate this question, the present study uses an in vitro experimental model to investigate the underlying chondroprotective and anti-inflammatory efficacy of GB and provides a new way for future clinical therapy of OA.

Material and methods

Reagents

GB was purchased from Sigma-Aldrich (St. Louis, USA) and was dissolved in dimethyl sulfoxide (DMSO) to 100 mM. The working concentration of GB is 50 and 100 μM.

Chondrocyte isolation and cell culture

Cell collection was approved by the Zhejiang University Animal Experimental Ethics Committee. Ten Sprague Dawley rats (6 weeks old) were euthanized by abdominally injecting a lethal dose of pentobarbital sodium, and then the hip cartilage was isolated. The cartilage was digested at 37˚C with 0.2% collagenase for 4 h. After filtration, chondrocytes were cultured in α-MEM (Hyclone, Tauranga, New Zealand) medium, mixed with 10% fetal bovine serum (FBS) (Gibco, Thermo-Fisher Scientific, Waltham, USA) and antibiotics (100 U/mL penicillin, 100 μg/mL streptomycin) (Sigma). Chondrocytes were used within 3 passages.

Measurement of cell viability

Cell viability was measured using a Cell Counting Kit-8 (CCK-8) (Dojindo, Japan). 1×10^4/mL cells were seeded onto 96-well plates and cultured with various concentrations of GB for 24 h after adherence. At the specified time point, the culture medium was discarded and phosphate buffered saline (PBS) was used to wash the cells. After incubation with CCK-8 solution at 37°C for 2.5 h, the optical density (OD) of the wells at 450 nm was measured using a microplate reader (Thermo Electron Corp., Waltham, USA). The cell viability to control was calculated using the following equation:

$$\text{cell viability to control (\%)} = OD_{\text{drug-treated group}}/OD_{\text{control group}}.$$

Apoptosis analysis

Chondrocyte apoptosis was detected using a Cell Apoptosis Kit (Becton Dickinson, Franklin Lakes, USA). Chondrocytes were cultured with various concentrations of GB and/or 1 μg/mL lipopolysaccharide (LPS) for 24 h. Then the cells were washed with cold PBS and resuspended with ×1 annexin-binding buffer. After that, all cells were stained with propidium iodide and fluorescein isothiocyanate (FITC). The apoptosis rate was measured by flow cytometry (FCM). Apoptotic events were indicated as FITC+/PI- (Q2 quadrant in flow cytometry (FCM) figure.

Gene expression

Chondrocytes were incubated with different doses of GB and 1 μg/mL LPS for 24 h. Total RNA was isolated by the Total RNA Miniprepkit (Axygen Scientific, Corning Inc., Corning, USA). A reverse transcription kit (iScript cDNA Synthesis Kit, Bio-Rad, Hercules, USA) was used to synthesize cDNA using the reverse transcriptional method. mRNA expression levels were evaluated by real-time PCR (Reagent Kit: SYBR® Premix ex TaqTM, TliRNase H Plus, Takara, Tokyo, Japan) according to the manufacturer's instructions. The PCR setting was as follows: 40 cycles at

Table 1. Sequences of primers used in real-time PCR

Gene	Primer sequences (5'-3')	
Collagen II	forward reverse	GGCCAGGATGCCCGAAAATTA ACCCCTCTCTCCCTTGTCAC
Aggrecan	forward reverse	CAGATGGCACCCTCCGATAC GACACACCTCGGAAGCAGAA
MMP3	forward reverse	TTTGGCCGTCTCTTCCATCC GCATCGATCTTCTGGACGGT
MMP13	forward reverse	ACCATCCTGTGACTCTTGCG TTCACCCACATCAGGCACTC
ADAMTS-4	forward reverse	ACCGATTACCAGCCTTTGGG CCGACTCCGGATCTCCATTG
ADAMTS-5	forward reverse	CCGAACGAGTTTACGGGGAT TGTGCGTCGCCTAGAACTAC
IL-1	forward reverse	ATCAGCACCTCACAGCTTCC TCTCCTCCCGATGAGTAGGC
IL-6	forward reverse	CACTTCACAAGTCGGAGGCT TCTGACAGTGCATCATCGCT
TNF-α	forward reverse	GGCTTTCGGAACTCACTGGA GGGAACAGTCTGGGAAGCTC
GAPDH	forward reverse	TGCCACTCAGAAGACTGTGG TTCAGCTCTGGGATGACCTT

MMP3 – matrix metalloproteinase 3; MMP13 – matrix metalloproteinase 13; IL-1 – interleukin 1; IL-6 – interleukin 6; TNF-a – tumor necrosis factor alpha; GAPDH – glyceraldehyde 3-phosphate dehydrogenase.

95°C for 5 s and 60°C for 34 s. The primers were designed and selected using BLAST. The primer sequences are listed in Table 1 and glyceraldehyde 3-phosphate dehydrogenase (GAPDH) was used as the internal control.

Western blot analysis

For aggrecan and collagen II protein assay, the cells were treated with different doses of GB and/or 1 μg/mL LPS for 5 or 8 days. For mitogen-activated protein kinase (MAPK) pathway protein assay, the cells were treated with different doses of GB and/or 1 μg/mL LPS for 24 h. At specific time points, the cells were washed with ×1 PBS, then total protein was extracted using radioimmunoprecipitation assay (RIPA) lysis buffer. The protein concentration was quantified using a bicinchoninic acid (BCA) Protein Assay Kit, 20 μg protein (each sample) was loaded into gel, and separated by 10% SDS-PAGE (sodium dodecyl sulfate polyacrylamide gel electrophoresis), then transferred to 0.22-μm PVDF (polyvinylidene difluoride) membranes (Millipore, Merck, Billerica, USA). The membranes were blocked for 1 h in Tris-buffered saline (TBS) containing 0.05% Tween 20 (TBST) and 5% nonfat milk powder and then incubated overnight with MAPK pathway-related antibodies, such as p-ERK, total-ERK, p-JNK, total-JNK, p-p38 and total-p38, and GAPDH overnight at 4°C (1:1000 dilution, Cell Signaling Technology, Danvers, USA). After 3 washes with TBST, the membranes were incubated with anti-rabbit IgG (1:5000 dilution, Cell Signaling Technology) at room temperature for 1 h. After 3 washes with TBST, the membranes were incubated in enhanced chemiluminescence (ECL) solution (Amersham Life Science, GE Healthcare Life Sciences, Little Chalfont, United Kingdom). GAPDH was used as the house-keeping gene.

Immunohistochemistry staining

Three 10^4/mL cells were seeded in 24-well plates and cultured with different doses of GB and/or 1 μg/mL LPS for 5 or 8 days. Cells were fixed with 4% paraformaldehyde before making cell slides. After fixation, the cells were treated with 0.1% Triton X-100 for 10 min, and blocked with 2% bovine serum albumin (Sigma-Aldrich, St. Louis, USA) for 1 h. Then, cells slides were incubated with an anti-collagen II antibody (1:200 dilution, Abcam, Cambridge, UK) and anti-aggrecan antibody (1:200 dilution, Abcam, Cambridge, UK) overnight at 4°C. For immunohistochemistry, cell slides were incubated with secondary antibody (1:200 dilution, Dako, Agilent Technologies, Santa Clara, USA), followed by color development with diaminobenzidine tetrahydrochloride (DAB, Dako). We used an inverted microscope microscopy (Olympus Life Science, Shinjuku, Tokyo, Japan) for observation and imaging. The integral optical density (IOD) of each picture was measured using the Image-Pro Plus 6.0 software (Media Cybernetics, Rockville, USA).

Statistical analysis

SPSS 19.0 (IBM Corp., Armonk, USA) was used for the statistical analysis. The data is expressed as mean ±SD. The significance of differences was assessed with one-way analysis of variance (ANOVA), followed by Duncan's post

hoc test. $P < 0.05$ was considered to indicate a statistically significant difference.

Results

Cell viability assay

To study the potential cytotoxicity of GB, we measured chondrocyte viability. After incubating with different concentrations of GB for 24 h, we used CCK-8 to assay the cell viability of chondrocytes. As shown in Fig. 1, GB did not inhibit chondrocyte proliferation at concentrations of 50 and 100 μM.

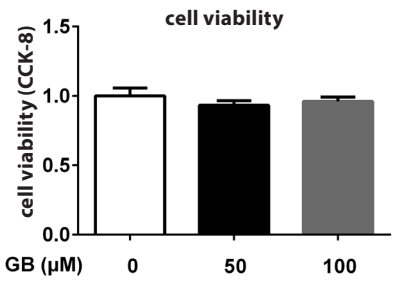

Fig. 1. Cell viability assay of chondrocytes

10000/mL cells were seeded onto 96-well plates and cultured with various concentrations of ginkgolide B for 24 h after adherence. Then, we used a CCK-8 to test the cell viability of the chondrocytes.

Ginkgolide B protected chondrocytes from inflammation-induced apoptosis

We examined the apoptosis rate of chondrocytes after treating with 1 μg/mL LPS for 24 h. Figure 2A shows LPS-induced chondrocyte apoptosis, while GB protected chondrocytes from inflammation-induced apoptosis at concentrations of 50 and 100 μM ($p < 0.05$) (Fig. 2B).

Ginkgolide B inhibited LPS-induced matrix-degradation in chondrocytes

Chondrocytes were incubated with 1 μg/mL LPS with or without GB (50 or 100 μM) for 5 or 8 days. After that, we detected extracellular matrix content by cell immunohistochemistry. Our results indicate that the expression of collagen-II and aggrecan increased over time in chondrocytes, while LPS strikingly reduced the aggrecan and collagen-II content ($p < 0.05$) (Fig. 3A). Immunohistochemistry staining showed GB significantly suppressed the degradation of aggrecan and collagen-II compared to the LPS group ($p < 0.05$) (Fig. 3A). The quantification of IOD also indicated that the GB groups gained more aggrecan and collagen-II staining (Fig. 3B,C).

After being incubated with LPS and various concentrations of GB for 5 or 8 days, we also used western blot to measure the collagen-II and aggrecan protein content. The result was similar to the immunohistochemistry staining. As shown in Fig. 4, LPS-induced collagen-II and aggrecan protein down-expression, and GB significantly attenuated the collagen-II and aggrecan loss. This effect was more obvious on day 8 ($p < 0.01$) (Fig. 4).

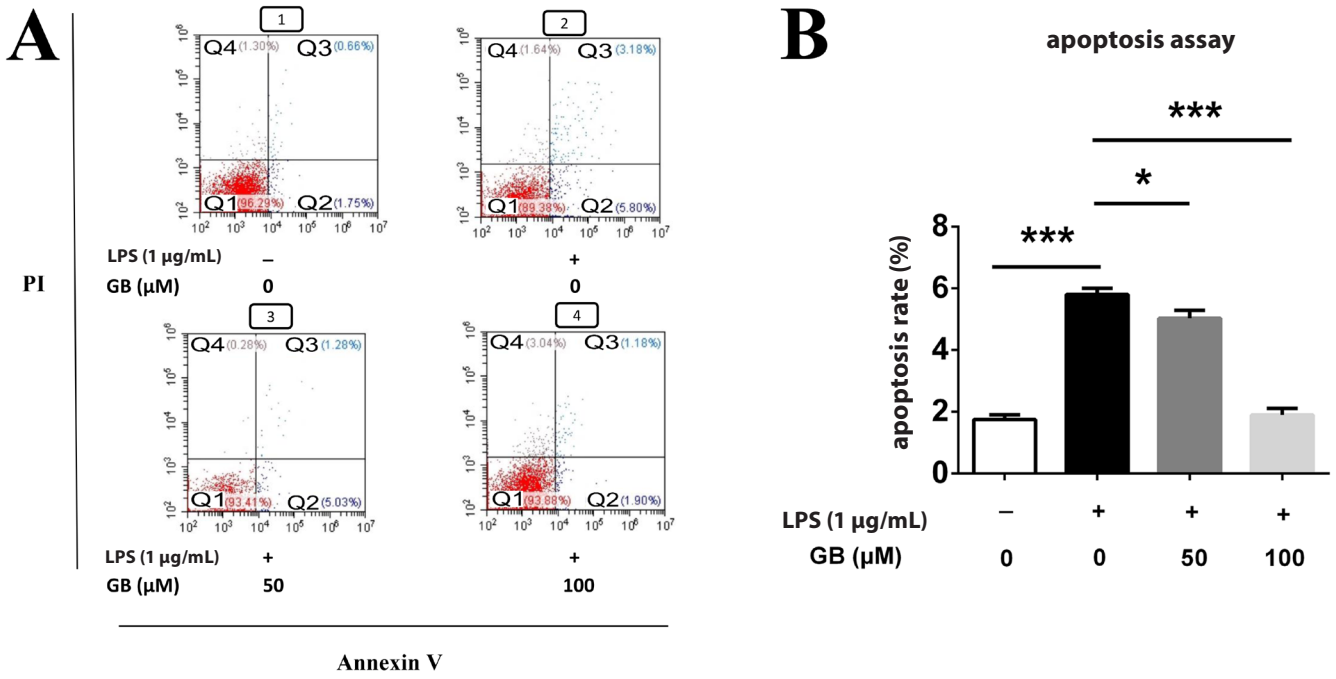

Fig. 2. Apoptosis assay of chondrocytes

A – after stimulation with or without 1 μg/mL LPS and different doses of ginkgolide B for 24 h, cells were stained with annexin V-FITC and propidium iodide and the apoptosis rate was measured via flow cytometry; B – the apoptosis rate (Q2) was calculated and compared; data is presented as the mean ± SD; *** indicates $p < 0.001$; ** indicates $p < 0.01$; * indicates $p < 0.05$ compared to the control group.

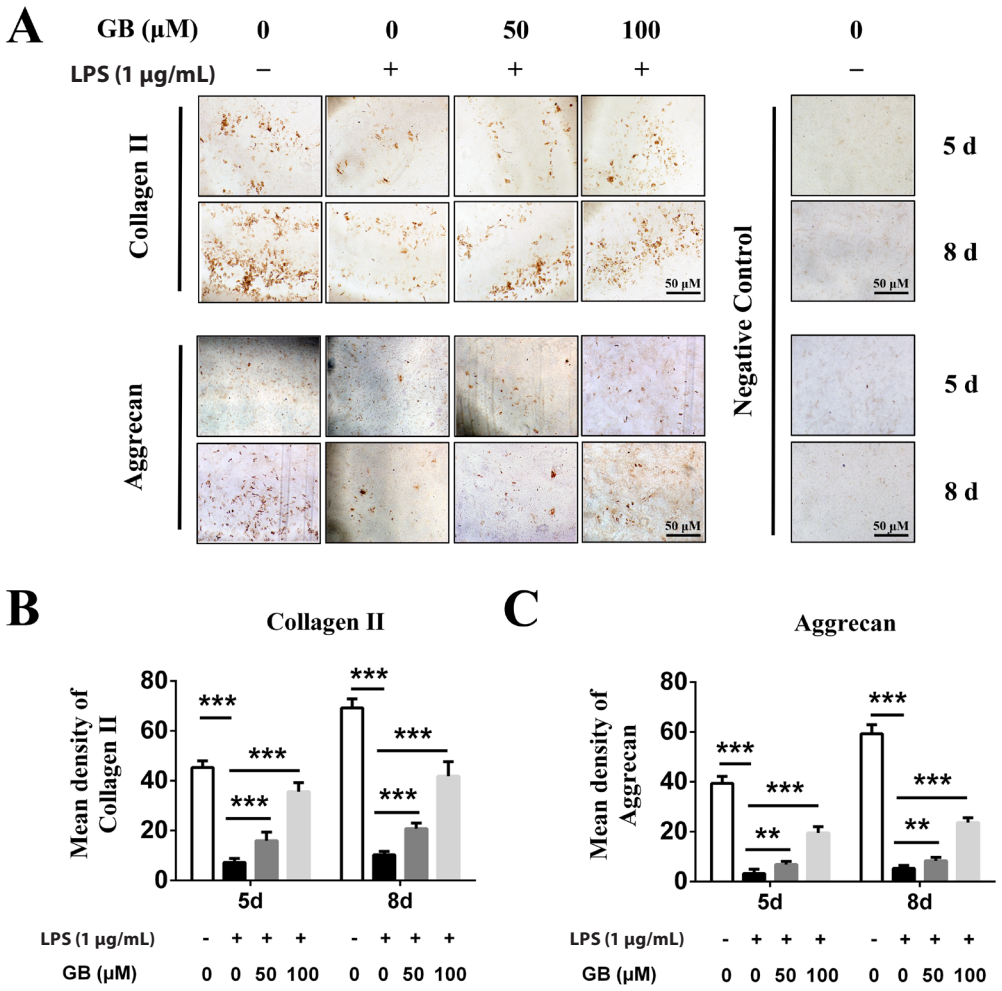

Fig. 3. Immunohistochemistry staining of chondrocytes

A – 30000/mL cells were seeded in 24-well plates and cultured with different doses of ginkgolide B and/or 1 g/mL LPS for 5 or 8 days, then cells were fixed with 4% paraformaldehyde and immunohistochemistry staining of aggrecan and collagen-II was performed; B, C – results of immunohistochemistry staining were quantified by integrated optical density (IOD); data is presented as the mean ± SD; *** indicates $p < 0.001$; ** indicates $p < 0.01$ compared to the control group.

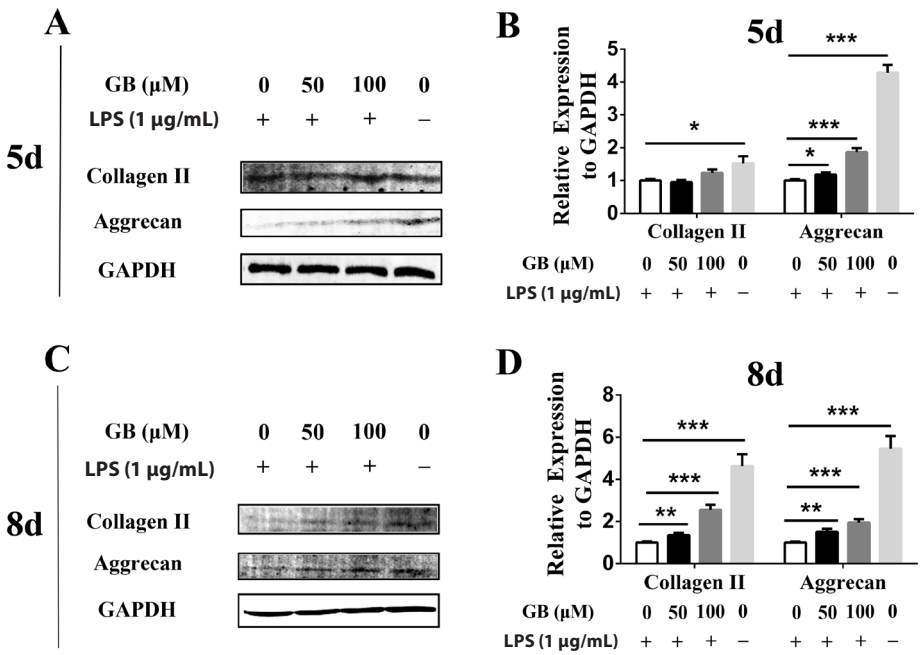

Fig. 4. Matrix-related protein expression of chondrocytes

We used western blot to measure aggrecan and collagen-II protein expression of chondrocytes. Cells were cultured with different doses of ginkgolide B and/or 1 μg/mL LPS for 5 or 8 days, then the total protein of cells was extracted using RIPA lysis buffer and western blot was performed. A, C – expression of collagen-II and aggrecan at 5 and 8 days; B, D – GAPDH was used as the house-keeping gene; data is presented as the mean ± SD; *** indicates $p < 0.001$; ** indicates $p < 0.01$; * indicates $p < 0.05$ compared to the control group.

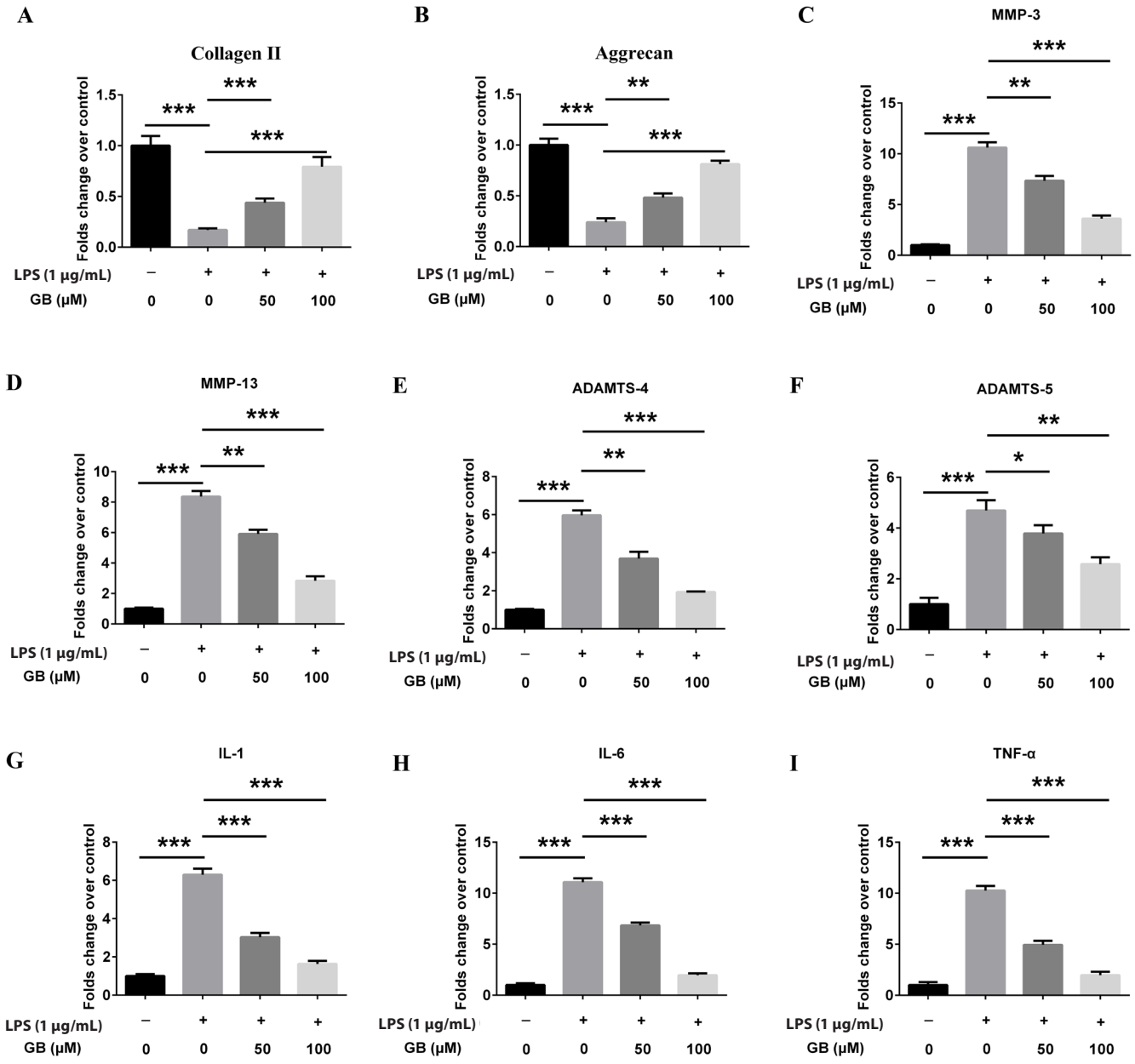

Fig. 5. Gene expression changes in chondrocytes

A–I – chondrocytes were treated with or without 1 μg/mL LPS and various concentrations of ginkgolide B for 24 h; total RNA was isolated, then the gene expression of collagen-II, aggrecan, MMP-13, MMP-3, ADAMTS-5, ADAMTS-4, IL-1, IL-6 and TNF-α were measured by real-time PCR; GAPDH was used as the internal control; data is presented as the mean ± SD; *** indicates $p < 0.001$; ** indicates $p < 0.01$; * indicates $p < 0.05$ compared to the control group.

Ginkgolide B reversed LPS-induced gene expression changes in chondrocytes

Chondrocytes were stimulated with 1 μg/mL LPS and 0, 50 or 100 μM GB, followed by real-time PCR assay. PCR results showed that LPS significantly up-regulated the gene expression of proinflammatory cytokines (IL-1, IL-6 and TNF-α). LPS also down-regulated the gene expression of collagen-II and aggrecan in chondrocytes, which was reversed by GB ($p < 0.01$) (Fig. 5A,B), and GB also inhibited multiple matrix-degrading enzyme (MMP-13, MMP-3, ADAMTS-5 and ADAMTS-4) gene over-expression induced by LPS in chondrocytes ($p < 0.05$) (Fig. 5C–F). IL-6, TNF-α and IL-1 were downregulated by GB ($p < 0.001$) (Fig. 5G–I), so GB has an anti-inflammatory effect in LPS-induced chondrocytes.

Ginkgolide B inhibited LPS-induced activation of MAPK pathway in chondrocytes

We measured the activation of MAPK pathway-related proteins by western blot to evaluate the potential mechanisms of the effects of GB on LPS-induced chondrocytes. Cells were pretreated with different doses of GB for 2 h, then treated with or without 1 μg/mL LPS for 30 min.

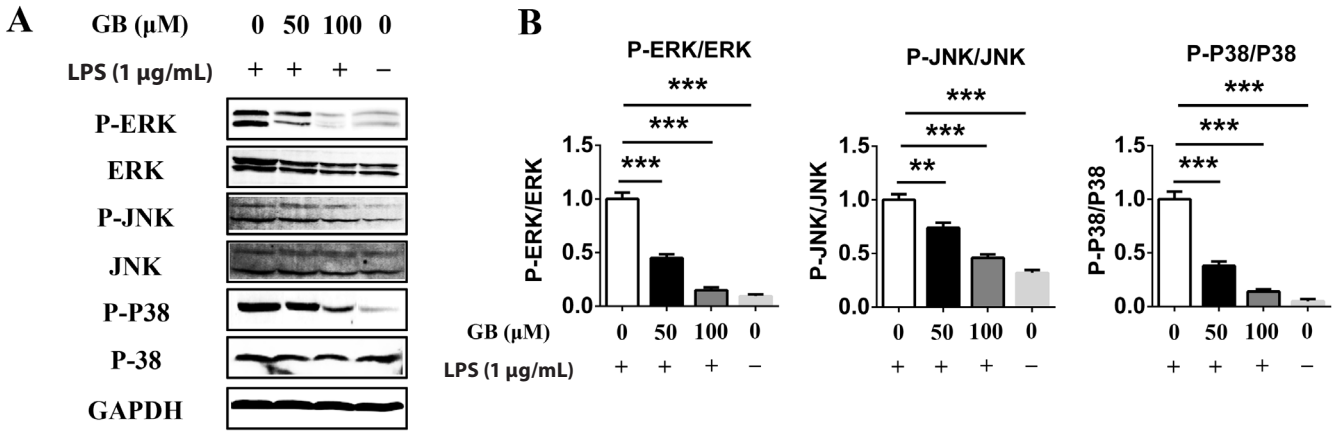

Fig. 6. Effect of ginkgolide B on LPS-induced activation of the MAPK pathway in chondrocytes

A – chondrocytes were pretreated with various concentrations of ginkgolide B for 2 h, then treated with or without 1 μg/mL LPS for 30 min; the expression of MAPK pathway proteins was measured by western blot; B – results were densitometrically quantified as the ratio of p-ERK to total-ERK, p-JNK to total-JNK and p-p38 to total-p38; data is presented as the mean ± SD; *** indicates $p < 0.001$; ** indicates $p < 0.01$; * indicates $p < 0.05$ compared to the control group.

The results showed that 1 μg/mL LPS significantly activated the MAPK pathways by promoting JNK, ERK and P38 protein phosphorylation (Fig. 6), and GB could inhibit the phosphorylation of JNK, ERK and P38 in a dose-dependent manner (Fig. 6). This result indicates the MAPK pathway was involved while GB exerted an anti-inflammatory effect in chondrocytes.

Discussion

Our study indicated that GB exhibited anti-inflammatory effects in chondrocytes for the first time.

Chondrocyte apoptosis plays a key role in the pathogenesis of OA.[13,14] Chondrocytes from normal donors did not show any apoptosis signs, while chondrocytes isolated from human OA cartilage exhibited multiple morphological evidence of apoptosis.[15,16] A proper balance between cell death and regeneration is essential for a healthy joint, and apoptosis excess is one of the reasons for tipping this balance.[17] As previously reported, treating chondrocytes with IL-1β could reduce chondrocyte viability and upregulate apoptotic-related proteins, and several anti-inflammatory agents had been believed to exert anti-apoptosis effects in chondrocytes.[13,18] The dose of GB used in different cells varies from 25–1000 μM, and in our study, we demonstrated that GB exerted anti-inflammation and anti-apoptosis effects in chondrocytes at doses of 50–100 μM.[7,10,12]

Previous studies have suggested that LPS markedly induces upregulation of genes and the generation of various matrix-degrading enzymes and proinflammatory cytokines, including IL-6, Cox-2, ADAMTS-5, ADAMTS-4, MMP-13 and MMP-3, in chondrocytes.[19] The expression of ADAMTSs and MMPs has been extensively detected in the process of OA. In the expression of MMP-13 associated with OA, as shown in recent studies, osteoarthritis progression was inhibited in MMP-13 knockout mice.[20] MMP-3 is a superior indicator of joint destruction that cleaves aggrecan, and the cartilage degradation is related to the activity of MMP-3 enzymes.[21–23] Besides MMPs, ADAMTSs are also believed to be involved in the OA process.[24] ADAMTS-4 and ADAMTS-5 are the most important aggrecanases among the 20 different ADAMTSs.[25] ADAMTS-5 was responsible for driving aggrecan loss in mice, which would result in cartilage damage, and an animal experiment also showed mouse with a knockin aggrecan mutated to have aggrecanase resistance successfully suppressed both meniscectomy-induced and antigen-induced arthritis.[26,27] The gene expression of both enzymes was upregulated by inflammatory stimuli such as TNF-α and oncostatin M in both human and mouse chondrocytes.[28,29] Moreover, inflammatory stimuli lead to matrix breakdown in chondrocytes.[30] The matrix of chondrocytes, which includes pericellular matrix (PCM) and ECM, conferred mechanical properties of cartilage. Loss of collagen II and proteoglycan significantly reduced chondron's mechanical properties.[31] Progressive breakdown of cartilage in OA involves proteolysis of both aggrecan and collagen II.[32] In our study, we demonstrated that GB could reverse the gene over-expression of MMP-13, MMP-3, ADAMTS-5 and ADAMTS-4 induced by LPS in chondrocytes, and GB also efficiently inhibited the collagen II and aggrecan loss of chondrocytes after stimulation with LPS.

Ginkolide B is a component of the ginkgo leaf, and EGb761, a commercial product of *Ginkgo biloba* extract, has been used in various diseases such as cardiovascular disease, hearing loss, and Alzheimer's disease.[33] Ginkolide B was proved to be an effective anti-inflammatory agent in different diseases.[10,11,34] MAPK is an important pathway that is involved in chondrocyte mechanical stress and inflammation.[35] The effect of inhibiting p38 in cartilage was tested in a previous study.[36] The results indicated that inhibition of p38 suppressed IL-1-induced MMP-1 and MMP-3 expression and collagen breakdown in cartilage. The role of the ERK pathway had also been investigated in a rabbit osteoarthritis model, and treatment with an EKR inhibitor

reduced cartilage lesion size and histological damage.[37] The JNK inhibitor SP600125 inhibited collagenase mRNA accumulation in synoviocytes after stimulation with IL-1, and JNK is a critical MAPK pathway for joint arthritis.[38] Our western blot results showed that GB inhibited the activation of the MAPK pathway in chondrocytes, thus exerting an anti-inflammation effect, which is consistent with previous reports.[34,39]

In conclusion, our results show that GB exerted anti-inflammatory and anti-apoptosis effects in chondrocytes. Ginkolide B may be a potential agent for treatment of OA. However, more research should be done in the future to further study the efficacy and mechanism of GB.

References

1. Lawrence RC, Felson DT, Helmick CG, et al. Estimates of the prevalence of arthritis and other rheumatic conditions in the United States. Part II. *Arthritis Rheum*. 2008;58:26–35.
2. Zhang Y, Jordan JM. Epidemiology of osteoarthritis. *Clin Geriatr Med*. 2010;26:355–369.
3. Caron MM, Emans PJ, Coolsen MM, et al. Redifferentiation of dedifferentiated human articular chondrocytes: Comparison of 2D and 3D cultures. *Osteoarthr Cartil*. 2012;20:1170–1178.
4. Stanton H, Melrose J, Little CB, Fosang AJ. Proteoglycan degradation by the ADAMTS family of proteinases. *Biochim Biophys Acta*. 2011;1812:1616–1629.
5. Musumeci G, Castrogiovanni P, Trovato FM, et al. Biomarkers of chondrocyte apoptosis and autophagy in osteoarthritis. *Int J Mol Sci*. 2015; 16:20560–20575.
6. Le Graverand-Gastineau MP. Disease modifying osteoarthritis drugs: Facing development challenges and choosing molecular targets. *Curr Drug Targets*. 2010;11:528–535.
7. Jiang W, Cong Q, Wang Y, Ye B, Xu C. Ginkgo may sensitize ovarian cancer cells to cisplatin: Antiproliferative and apoptosis-inducing effects of ginkgolide B on ovarian cancer cells. *Integr Cancer Ther*. 2012;13:NP10–NP17.
8. Chu X, Ci X, He J, et al. A novel anti-inflammatory role for ginkgolide B in asthma via inhibition of the ERK/MAPK signaling pathway. *Molecules*. 2011;16:7634–7648.
9. Zhou T, You WT, Ma ZC, et al. Ginkgolide B protects human umbilical vein endothelial cells against xenobiotic injuries via PXR activation. *Acta Pharmacol Sin*. 2016;37:177–186.
10. Gu JH, Ge JB, Li M, Wu F, Zhang W, Qin ZH. Inhibition of NF-kappaB activation is associated with anti-inflammatory and anti-apoptotic effects of Ginkgolide B in a mouse model of cerebral ischemia/reperfusion injury. *Eur J Pharm Sci*. 2012;47:652–660.
11. Wu F, Shi W, Zhou G, et al. Ginkgolide B functions as a determinant constituent of ginkgolides in alleviating lipopolysaccharide-induced lung injury. *Biomed Pharmacother*. 2016;81:71–78.
12. Liu X, Zhao G, Yan Y, Bao L, Chen B, Qi R. Ginkgolide B reduces atherogenesis and vascular inflammation in ApoE(-/-) mice. *PLoS One*. 2012;7:e36237. doi: 10.1371/journal.pone.0036237
13. Zhang X, Xu X, Xu T, Qin S. β-ecdysterone suppresses interleukin-1 beta-induced apoptosis and inflammation in rat chondrocytes via inhibition of NF-kappaB signaling pathway. *Drug Dev Res*. 2014;75: 195–201.
14. Musumeci G, Aiello FC, Szychlinska MA, Di Rosa M, Castrogiovanni P, Mobasheri A. Osteoarthritis in the XXIst century: Risk factors and behaviours that influence disease onset and progression. *Int J Mol Sci*. 2015;16:6093–6112.
15. Musumeci G, Loreto C, Carnazza ML, Martinez G. Characterization of apoptosis in articular cartilage derived from the knee joints of patients with osteoarthritis. *Knee Surg Sports Traumatol Arthrosc*. 2011;19:307–313.
16. Musumeci G, Loreto C, Carnazza ML, Strehin I, Elisseeff J. OA cartilage derived chondrocytes encapsulated in poly(ethylene glycol) diacrylate (PEGDA) for the evaluation of cartilage restoration and apoptosis in an in vitro model. *Histol Histopathol*. 2011;26:1265–1278.
17. Zhou PH, Liu SQ, Peng H. The effect of hyaluronic acid on IL-1beta-induced chondrocyte apoptosis in a rat model of osteoarthritis. *J Orthop Res*. 2008;26:1643–1648.
18. Zhang XH, Xu XX, Xu T. Ginsenoside Ro suppresses interleukin-1beta-induced apoptosis and inflammation in rat chondrocytes by inhibiting NF-kappaB. *Chin J Nat Med*. 2015;13:283–289.
19. Goldring MB, Otero M. Inflammation in osteoarthritis. *Curr Opin Rheumatol*. 2011;23:471–478.
20. Little CB, Fosang AJ. Is cartilage matrix breakdown an appropriate therapeutic target in osteoarthritis-insights from studies of aggrecan and collagen proteolysis? *Curr Drug Targets*. 2010;11:561–575.
21. Hiura K, Iwaki-Egawa S, Kawashima T, et al. The diagnostic utility of matrix metalloproteinase-3 and high-sensitivity C-reactive protein for predicting rheumatoid arthritis in anti-cyclic citrullinated peptide antibody-negative patients with recent-onset undifferentiated arthritis. *Rheumatol Int*. 2013;33:2309–2314.
22. Haller JM, Swearingen CA, Partridge D, McFadden M, Thirunavukkarasu K, Higgins TF. Intraarticular matrix metalloproteinases and aggrecan degradation are elevated after articular fracture. *Clin Orthop Relat Res*. 2015;473:3280–3288.
23. Voigt H, Lemke AK, Mentlein R, Schünke M, Kurz B. Tumor necrosis factor alpha-dependent aggrecan cleavage and release of glycosaminoglycans in the meniscus is mediated by nitrous oxide-independent aggrecanase activity in vitro. *Arthritis Res Ther*. 2009;11:R141.
24. Rosenthal AK. Crystals, inflammation, and osteoarthritis. *Curr Opin Rheumatol*. 2011;23:170–173.
25. Gendron C, Kashiwagi M, Lim NH, et al. Proteolytic activities of human ADAMTS-5: Comparative studies with ADAMTS-4. *J Biol Chem*. 2007; 282:18294–18306.
26. Echtermeyer F, Bertrand J, Dreier R, et al. Syndecan-4 regulates ADAMTS-5 activation and cartilage breakdown in osteoarthritis. *Nat Med*. 2009;15:1072–1076.
27. Little CB, Meeker CT, Golub SB, et al. Blocking aggrecanase cleavage in the aggrecan interglobular domain abrogates cartilage erosion and promotes cartilage repair. *J Clin Invest*. 2007;117:1627–1636.
28. Song RH, Tortorella MD, Malfait AM, et al. Aggrecan degradation in human articular cartilage explants is mediated by both ADAMTS-4 and ADAMTS-5. *Arthritis Rheum*. 2007;56:575–585.
29. Rogerson FM, Chung YM, Deutscher ME, Last K, Fosang AJ. Cytokine-induced increases in ADAMTS-4 messenger RNA expression do not lead to increased aggrecanase activity in ADAMTS-5-deficient mice. *Arthritis Rheum*. 2010;62:3365–3373.
30. Rainbow RS, Kwon H, Foote AT, Preda RC, Kaplan DL, Zeng L. Muscle cell-derived factors inhibit inflammatory stimuli-induced damage in hMSC-derived chondrocytes. *Osteoarthritis Cartilage*. 2013;21:990–998.
31. Guilak F, Alexopoulos LG, Upton ML, et al. The pericellular matrix as a transducer of biomechanical and biochemical signals in articular cartilage. *Ann N Y Acad Sci*. 2006;1068:498–512.
32. Little CB, Fosang AJ. Is cartilage matrix breakdown an appropriate therapeutic target in osteoarthritis-insights from studies of aggrecan and collagen proteolysis? *Curr Drug Targets*. 2010;11:561–575.
33. Nash KM, Shah ZA. Current perspectives on the beneficial role of Ginkgo biloba in neurological and cerebrovascular disorders. *Integr Med Insights*. 2015;10:1–9.
34. Chu X, Ci X, He J, et al. A novel anti-inflammatory role for ginkgolide B in asthma via inhibition of the ERK/MAPK signaling pathway. *Molecules*. 2011;16:7634–7648.
35. Goldring MB, Otero M, Plumb DA, et al. Roles of inflammatory and anabolic cytokines in cartilage metabolism: Signals and multiple effectors converge upon MMP-13 regulation in osteoarthritis. *Eur Cell Mater*. 2011;21:202–220.
36. Phitak T, Pothacharoen P, Settakorn J, Poompimol W, Caterson B, Kongtawelert P. Chondroprotective and anti-inflammatory effects of sesamin. *Phytochemistry*. 2012;80:77–88.
37. Prasadam I, Mao X, Shi W, Crawford R, Xiao Y. Combination of MEK-ERK inhibitor and hyaluronic acid has a synergistic effect on anti-hypertrophic and pro-chondrogenic activities in osteoarthritis treatment. *J Mol Med*. 2013;91:369–380.
38. Schepetkin IA, Kirpotina LN, Hammaker D, et al. Anti-inflammatory effects and joint protection in collagen-induced arthritis after treatment with IQ-1S, a selective c-Jun N-terminal kinase inhibitor. *J Pharmacol Exp Ther*. 2015;353:505–516.
39. Liu X, Yan Y, Bao L, Chen B, Zhao Y, Qi R. Ginkgolide B inhibits platelet release by blocking Syk and p38 MAPK phosphorylation in thrombin-stimulated platelets. *Thromb Res*. 2014;134:1066–1073.

PIK3R1 gene polymorphisms are associated with type 2 diabetes and related features in the Turkish population

Abdullah Hakan Karadoğan[1,A–C], Hilal Arikoglu[1,A,C–F], Fatma Göktürk[1,B], Funda İşçioğlu[2,C], Süleyman Hilmi İpekçi[3,B]

[1] Department of Medical Biology, Faculty of Medicine, Selçuk University, Konya, Turkey
[2] Department of Statistics, Faculty of Science, Ege University, Izmir, Turkey
[3] Department of Endocrinology, Faculty of Medicine, Selçuk University, Konya, Turkey

A – research concept and design; B – collection and/or assembly of data; C – data analysis and interpretation;
D – writing the article; E – critical revision of the article; F – final approval of the article

Advances in Clinical and Experimental Medicine, ISSN 1899-5276 (print), ISSN 2451-2680 (online) *Adv Clin Exp Med*. 2018;27(7):921–927

Address for correspondence
Hilal Arikoglu
E-mail: harikoglu@selcuk.edu.tr

Funding sources
This study was supported by the Selçuk University Research Foundation (13202033).

Conflict of interest
None declared

Acknowledgements
We would like to thank Dr. Sevim Karakas for her assistance in this study.

Received on February 22, 2016
Reviewed on July 22, 2016
Accepted on February 14, 2017

Abstract

Background. The phosphatidylinositol 3-kinase p85 alpha regulatory subunit 1 gene (*PIK3R1*) encodes the PIK3R1 protein, which plays a direct role in insulin signaling. PIK3R1 (p85 regulatory subunit) connects firmly with the p110 catalytic subunit, and together these proteins form the phosphatidylinositol 3-kinase (PI3K) protein. PI3K is a key protein in the Akt signaling pathway, which regulates cell survival, growth, differentiation, glucose trafficking, and utilization. Defects in the insulin signaling cascade play an important role in the development of insulin resistance, which shares a common genetic basis for metabolic diseases such as type 2 diabetes (T2D), obesity and cardiovascular diseases.

Objectives. In our study, we investigated the effect of single nucleotide polymorphisms (SNPs) rs3756668 in 3'UTR region, rs706713 and rs3730089 in exons 1 and 6, respectively, rs7713645 and rs7709243 in intron 1, and rs1550805 in intron 6 of *PIK3R1* gene on T2D.

Material and methods. This study enrolled a total of 840 individuals, including 427 diabetic individuals (206 obese and 221 non-obese) and 413 nondiabetic individuals (138 obese and 275 non-obese). The target SNPs were analyzed using real-time polymerase chain reaction (RT-PCR). Statistical analysis was performed using SPSS18.0 (IBM Corp., Armonk, USA). The p-values ≤ 0.05 were considered statistically significant.

Results. The SNPs rs706713 (Tyr73Tyr) and rs3730089 (Met326Ile) located in exons, and rs7713645, rs7709243 and rs1550805 located in introns were determined to be significantly associated with T2D and phenotypic features such as obesity, insulin resistance and the lipid parameters. The association with SNP rs3756668, which is located in the 3'UTR, was not significant.

Conclusions. Our study supports the role of *PIK3R1*, an important candidate gene due to its critical role in insulin signal transduction, in T2D development.

Key words: type 2 diabetes, single nucleotide polymorphisms, *PIK3R1* gene

DOI
10.17219/acem/68985

Introduction

Insulin is a major hormone that regulates processes such as cellular growth, differentiation and apoptosis, in addition to glucose metabolism. Insulin acts on target tissues, mainly liver, muscle and adipose tissues, by binding to its receptor on the cell surface, leading to the autoactivation of tyrosine residues. Once activated, receptor phosphorylates the downstream signaling proteins known as the insulin receptor substrate (IRS) family, which has Src Homology 2 (SH2) domain-containing proteins. Then, phosphorylated IRS proteins activate other SH2 domain-containing proteins, including the regulatory subunits of phosphatidylinositol 3-kinase (PI3K). PI3K catalyzes the conversion of phosphatidylinositol phosphate (PIP) 2 to PIP3, which activate Akt signaling, which itself regulates cell survival, growth, differentiation, glucose transporter type 4 (GLUT-4) trafficking, and glucose utilization.[1]

Impaired activation of the insulin signaling pathway results in the decreased responsiveness of target tissues to normal circulating levels of insulin, a condition known as insulin resistance. Insulin resistance is a common pathogenesis in several metabolic diseases, such as type 2 diabetes (T2D), obesity and cardiovascular diseases.

Insulin resistance generally occurs as a result of post-receptor defects.[2] Especially, it is suggested that reductions in both IRS-l phosphorylation and insulin-stimulated PI3K activation leads to impaired insulin signal transduction. Additionally, other signaling molecules in this transduction, insulin signaling inhibitors such as ENPP1, PTP1B, and INPPL1, lipid accumulation in target tissues, and abnormal lipid metabolism can also contribute to insulin resistance.[3,4]

The PI3K enzyme is composed of 2 subunits, the p110 catalytic subunit and regulatory p85α subunit.[5] The p85α subunit stabilizes the p110 catalytic subunit and determines the level of activity.[5] Polymorphisms in the *PIK3R1* gene, which encodes the p85 regulatory subunit of the PI3K enzyme, are associated with the development of diseases such as insulin resistance, obesity, T2D, and cancer.[6–8] In this study, we investigated the effects of single nucleotide polymorphisms (SNPs) rs3756668A→G (located in the 3'UTR region), rs706713C→T and rs3730089A→G (located in exons 1 and 6, respectively), rs7713645A→C and rs7709243C→T (both located in intron 1), and rs1550805C→T (located in intron 6) of the *PIK3R1* gene on T2D.

Material and methods

Clinical samples

This study enrolled a total of 840 individuals, including 427 diabetic individuals (206 obese and 221 non-obese) and 413 nondiabetic individuals (138 obese and 275 non-obese). These individuals were selected from patients admitted to the Selçuk University Hospital, Department of Endocrinology (Konya, Turkey). The individuals in the diabetic group, who were diagnosed according to the guidelines of the American Diabetes Association (ADA), were over 30 years old and did not use insulin. Other types of diabetes (type 1 diabetes, maturity onset diabetes of the young – MODY, latent autoimmune diabetes of adults – LADA, drug-related and other types) were excluded. Obesity criteria was considered as body mass index (BMI) ≥30. The control group in this study included age- and BMI-matched nondiabetic individuals with no family history of diabetes. Written informed consent was obtained from each individual before participation in the study. The study was approved by the Ethics Committee of the Selçuk University Medical Faculty (Konya, Turkey). An oral glucose tolerance test (OGTT) was performed on the individuals considered as pre-diabetic. Individuals with impaired glucose tolerance or insulin resistance were excluded from the study.

Clinical analyses

Fasting plasma glucose, fasting insulin, HbA1C, c-peptide, cholesterol, low density lipoprotein (LDL), high density lipoprotein (HDL), and triglyceride values were measured for both diabetic and control groups. Insulin resistance was determined using the homeostasis model assessment of insulin resistance (HOMA-IR) and was calculated as fasting plasma glucose (mmol/L) multiplied by fasting serum insulin (pmol/L) and divided by 22.5. An individual with a HOMA-IR value higher than 2.5 was considered resistant to insulin.

Genotyping

Genomic DNA was isolated from peripheral blood leukocytes using a standard proteinase K and sodium dodecyl sulphate (SDS) procedure. Target SNPs were analyzed using the real-time polymerase chain reaction (RT-PCR) technique and a TIB MolBiol LightSNiP kit (Roche, Basel, Switzerland). Six SNPs in the *PIK3R1* gene were previously reported to be associated with the disease in the literature. Information about these target SNPs is shown in Table 1.

Statistical analysis

Descriptive statistics were obtained for clinical and biochemical characteristics. Normally distributed parameters were compared using one-way analysis of variance (ANOVA), while parameters that did not show normal distributions were compared by Kruskal-Wallis test after transformation.

The differences between the patient and control groups in terms of genotype distribution or allele frequency were analyzed using Pearson's χ^2 test. A χ^2 goodness of fit test was used to evaluate Hardy-Weinberg equilibrium (HWE)

Table 1. Clinical and biochemical characteristics of study subjects

Variable	Obese		Non-obese		p-value			
	DM (1)	control (2)	DM (3)	control (4)	p (1–2)	p (1–3)	p (2–4)	p (3–4)
Number (840)	206	138	221	275	NA	NA	NA	NA
Age [years]	55.6 ±8.8	48.9 ±11.3	56.5 ±9.3	43.9 ±10.4	<0.001*	0.792	<0.001*	<0.001*
Gender (M/F)	154/52	120/18	86/135	182/93	NA	NA	NA	NA
BMI [kg/m^2]	35.14 ±4.23	34.57 ±3.92	26.74 ±2.74	26.08 ±3.01	0.445	NA	NA	0.162
Insulin[1] [µIU/mL]	11.89 (2.04–40.79)	10.85 (4.31–39.98)	7.90 (1.00–37.30)	7.33 (2.00–39.91)	0.270	<0.001*	<0.001*	0.297
C-peptide[1] [ng/mL]	3.07 (0.74–9.40)	2.51 (1.49–6.30)	2.00 (0.50–16.10)	2.13 (0.70–15.70)	0.292	<0.001*	0.013	0.067
FG[1] [mg/dL]	140 (64–377)	94 (76–113)	134 (59–363)	92 (58–114)	<0.001*	0.548	0.001*	<0.001*
A1c[1] (%)	7.1 (5.2–12.5)	5.6 (5.3–6.4)	7.1 (5.1–19.5)	5.5 (5.0–6.4)	<0.001*	0.915	0.212	<0.001*
TG[1] [mg/dL]	171 (59–674)	126 (52–380)	128 (41–457)	116 (40–478)	<0.001*	0.002*	0.029	0.055
Chol [mg/dL]	203 ±45	211 ±39	197 ±47	202 ±42	0.415	0.632	0.332	0.817
LDL[1] [mg/dL]	122 (52–276)	130 (78–239)	124 (35–271)	125 (39–294)	0.006*	0.929	0.169	0.257
HDL [mg/dL]	43 ±10	47 ±11	44 ±13	47 ±12	0.003*	0.786	0.991	0.055
HOMA-IR[1]	4.42 (0.79–18.00)	2.61 (0.83–9.90)	2.80 (0.42–17.00)	1.67 (0.40–12.00)	<0.001*	<0.001*	<0.001*	<0.001*

[1] Non-normally distributed parameters are shown as median (min–max); * statistically significant differences were found; NA – this data could not be evaluated for statistical significance because it was not found to be clinically significant. In post-hoc test, p-value = 0.008 was considered statistically significant for comparing 4 groups; DM – diabetes mellitus; FG – fasting glucose; TG – triglyceride; Chol – cholesterol; LDL – low-density lipoprotein; HDL – high-density lipoprotein; HOMA-IR – homeostasis model assessment of insulin resistance.

in the patient and control groups. Analyses were performed using dominant, additive and recessive models. Dominance was defined in terms of allele 2 effects. In dominant allele 2 models, homozygous individuals for allele 1 were compared with carriers of allele 2. In recessive allele 2 models, homozygous individuals for allele 2 were compared with carriers of allele 1. Association between genotypes and T2D was tested by conducting a case-control study. Allele frequencies of SNPs in the patient and control groups were evaluated using odds ratio (OR). We performed logistic regression analysis by considering not only dominant, additive and recessive models of SNP genotypes, but also sex and age.

We also investigated if there was any association between genotypes and biochemical characteristics of T2D. Therefore, we performed tests to determine the normality of the biochemical characteristics. Fasting plasma insulin and triglyceride variables were normalized by log transformation, and cholesterol was normalized by square root transformation, before ANOVA analysis. For the other characteristics (BMI, fasting glucose, c-peptide, HbA1C, LDL, HDL, and HOMA-IR), the Kruskal-Wallis test was performed. The SNP genotypes were coded as 11, 12 and 22. Then, a single point (single SNP) regression analysis model was fitted. Linkage disequilibrium (LD) analysis was performed with MIDAS software.[9]

All analyses were carried out using SPSS 18.0 (IBM Corp., Armonk, USA). In all analyses, p-value ≤0.05 was considered statistically significant.

Results

Characteristics of study subjects

A total of 840 individuals, including 427 diabetic individuals (206 obese and 221 non-obese) and 413 nondiabetic individuals (138 obese and 275 non-obese), were enrolled in this study. The clinical and biochemical characteristics of the individuals studied are shown in Table 2.

Association study

The genotype distribution and association analyses of SNPs are summarized in Table 3. The silent SNP rs706713 in exon 1 of the *PIK3R1* gene showed a significant association with T2D (OR 1.7 (95% confidence interval – CI: 1.09–2.40), p = 0.016 and OR 1.5 (95% CI: 1.054–2.233), p = 0.025, additive and dominant models, respectively) when individuals were considered as patient and control groups. When the obese and non-obese groups were evaluated separately, a strong relationship between SNP

Table 2. Genotype distribution of studied SNPs in the *PIK3R1* gene and their association analysis results in diabetics and controls

SNP	Genotype	Diabetic (n)	Control (n)	Dominant OR (CI %) p-value	Additive OR (CI %) p-value	Recessive OR (CI %) p-value
rs3756668	G/G G/A A/A	162 196 69	187 160 66	1.3 (0.94–1.88) p = 0.108	0.8 (0.52–1.10) p = 0.149	1.2 (0.73–1.96) p = 0.472
rs706713	C/C C/T T/T	219 176 32	254 135 24	1.5 (1.05–2.23) p = 0.025	1.7 (1.09–2.40) p = 0.016	0.9 (0.43–1.98) p = 0.825
rs7713645	A/A A/C C/C	137 202 74	135 192 86	1.08 (0.77–1.53) p = 0.648	0.9 (0.59–1.45) 0.727	1 (0.70–1.1.53) p = 0.872
rs77092243	C/C C/T T/T	131 226 70	138 190 85	1 (0.70–1.45) p = 0.959	0.9 (0.62–1.34) p = 0.629	0.7 (0.46–1.09) p = 0.114
rs3730089	G/G G/A A/A	316 103 8	318 80 15	0.9 (0.63–1.40) p = 0.752	0.8 (0.54–1.25) p = 0.363	3.5 (1.02–11.76) p = 0.047
rs1550805	C/C C/T T/T	320 102 5	309 89 11	1 (0.72–1.55) p = 0.770	1 (0.68–1.49) p = 0.968	0.5 (0.12–1.92) p = 0.303

SNPs – single nucleotide polymorphisms; OR – odds ratio; CI – confidence interval.

Table 3. Genotype distribution of studied SNPs in the *PIK3R1* gene and their association analysis results in obese and non-obese diabetics and controls

SNP	Geno-type	Obese		Non-obese		Obese			Non-obese		
		DM n	control n	DM n	control n	dominant OR (CI %) p-value	additive OR (CI %) p-value	recessive OR (CI %) p-value	dominant OR (CI %) p-value	additive OR (CI %) p-value	recessive OR (CI %) p-value
rs3756668	G/G G/A A/A	82 91 33	57 60 21	80 105 36	130 100 45	0.9 (0.54–1.40) p = 0.540	1 (0.58–1.60) p = 0.876	1.6 (0.80–3.35) p = 0.179	1.5 (0.87–2.45) p = 0.157	0.9 (0.44–2.03) p = 0.875	0.8 (0.41–1.74) p = 0.649
rs706713	C/C C/T T/T	113 74 19	86 39 13	106 102 13	168 96 11	1.4 (0.58–1.60) p = 0.244	0.7 (0.38–1.14) p = 0.139	1.4 (0.53–3.58) p = 0.513	1.8 (1.01–3.13) p = 0.047*	0.6 (0.16–2.09) p = 0.398	1.4 (0.38–4.90) p = 0.627
rs7713645	A/A A/C C/C	74 95 37	44 57 37	63 107 51	91 135 49	1.2 (0.72–1.93) p = 0.527	2 (1.08–3.77) p = 0.028*	2 (1.10–3.51) p = 0.022*	1.4 (0.85–2.31) p = 0.191	2 (1.081–3.906) p = 0.03*	1.9 (1.079–3.235) p = 0.03*
rs77092243	C/C C/T T/T	75 99 32	43 58 37	56 127 38	95 132 48	1.3 (0.80–2.24) p = 0.257	2.5 (1.24–4.89) p = 0.01*	2.4 (1.31–4.42) p = 0.005*	0.8 (0.44–1.31) p = 0.320	0.8 (0.44–1.38) p = 0.395	1.22 (0.64–2.35) p = 0.537
rs3730089	G/G G/A A/A	153 47 6	108 24 6	163 56 2	210 56 9	0.7 (0.50–1.58) p = 0.892	2 (0.49–8.83) p = 0.320	2.2 (0.52–9.25) p = 0.288	0.9 (0.52–1.64) p = 0.798	0.8 (0.44–1.46) p = 0.476	0.1 (0.12–1.38) p = 0.90
rs1550805	C/C C/T T/T	151 53 2	108 30 –	169 49 3	201 59 11	1.4 (0.79–2.43) p = 0.261	0.7 (0.42–1.29) p = 0.280	0 p = 1	1.6 (0.92– 2.74) p = 0.097	1.5 (0.87–2.73) p = 0.138	1.9 (0.38–9.64) p = 0.433

SNP – single nucleotide polymorphism; DM – diabetes mellitus; OR – odds ratio; CI – confidence interval; * statistically significant.

rs706713 and T2D was also identified in the non-obese group (OR 1.8 (95% CI: 1.006–3.128), p = 0.05, dominant model). The groups were in HWE for this SNP when considered either together or separately (p > 0.05).

The SNP rs3730089 in exon 6 causes an amino acid substitution in the protein, and was significantly associated with T2D (OR 3.5 (95% CI: 1.015–11.762), p = 0.047, recessive model). The genotype distribution for this SNP was found to deviate from HWE in the control groups (p < 0.05).

While the intronic SNP rs7709243 was associated with T2D in the obese group (OR 2.5 (95% CI: 1.239–4.891), p = 0.01 and OR 2.4 (95% CI: 1.309–4.418), p = 0.005, additive and recessive models, respectively), the rs7713645 SNP was associated with the disease in both the obese group (OR 2 (95% CI: 1.081–3.773), p = 0.03 and OR 2 (95% CI: 1.101–3.514), p = 0.022, additive and recessive models, respectively) and the non-obese group (OR 2 (95% CI: 1.081–3.906), p = 0.03 and OR 1.9 (95% CI: 1.079–3.235), p = 0.03, additive and recessive models, respectively). With the exception of the genotype distribution of SNP rs7709243 in the non-obese diabetic group, both of the SNPs located in intron 1 were in HWE.

Neither the SNP rs1550805 in intron 6 nor the SNP rs3756668 in the 3'UTR of the *PIK3R1* gene were associated with T2D ($p > 0.05$) when the groups were assessed together or separately. The genotype distributions of both SNPs showed deviation from HWE in the control groups.

Additionally, linkage disequilibrium was calculated for the 6 SNPs and r^2 values were used to provide evidence of pairwise LD between the SNPs. Only the rs7709243 and rs7713645 SNPs located in intron 1 were found to be in strong LD ($D' = 0.85$; $r^2 = 0.7$). The LD between the other variants was weak.

Genotype–phenotype relationship

The effects of the SNPs on phenotypic characteristics such as fasting glucose, insulin, c-peptide, hemoglobin A1C levels, triglycerides, cholesterol, LDL and HDL levels, BMI, and HOMA-IR value as an insulin resistance marker were analyzed in this study. The SNP rs706713 in exon 1 had a strong effect on HOMA-IR ($p = 0.018$). The intronic SNP rs7709243 showed an effect on LDL level ($p = 0.028$) and cholesterol ($p = 0.008$), while the other intronic SNP, rs1550805, had a strong effect on c-peptide level ($p = 0.023$) and BMI ($p = 0.007$).

Discussion

Insulin has both metabolic and growth-stimulating effects, and its metabolic effect occurs through the PI3K/Akt pathway.[10] Although other growth factors also activate PI3K via distinct receptor tyrosine kinases, PI3K activation, which occurs only through insulin effect, has been found to regulate metabolic homeostasis.[11] In adipocyte cell cultures, it was revealed that both insulin and platelet-derived growth factor (PDGF) activate PI3K, and that insulin stimulates GLUT4 translocation to the plasma membrane, while PDGF does not.[12]

Insulin resistance develops as a result of the reduced responsiveness of target tissues to insulin due to decreased receptor and/or downstream signaling protein activity, rather than a reduced circulating insulin level.[13,14]

PI3K/Akt plays a central role in several pathway-related energy homeostases, including leptin, pro-opiomelanocortin (POMC), TNF-α, adiponectin, and cytokine stimulation.[15–18] PI3K consists of a catalytic subunit (p110) and a regulatory subunit (p85α).[5] The p85α subunit provides stability and maintains the activity of the p85α/p110 complex.[1,5]

In addition, the monomer p85α is in competition with the p85α/p110 complex for binding to IRS1 or allosteric interaction with p110, provide negative regulation of the p85α/p110 complex.[19] The overexpression of p85α by hormonal or experimental induction weakens signal transmission and causes insulin resistance by disrupting the activity of the p85α/p110 complex and the connection between PI3K and IRS1.[20,21]

This study found that the SNPs localized in the *PIK3R1* gene, encoding p85α regulatory subunit of PI3K which plays a critical role in signal transduction, are associated with T2D, obesity and related phenotypic characteristics. Reports have indicated that SNPs rs706713 (Tyr73Tyr) and rs3730089 (Met326Ile) in exons 1 and 6, respectively, have reduced protein activity and are associated with T2D.[22,23] Additionally, we also detected a significant association between rs706713 and T2D ($p < 0.05$). When the patients were divided into obese and non-obese groups, rs706713 was associated with the disease in the non-obese group ($p = 0.05$). The patient and control groups were in HWE for the SNP rs706713. We also found that this SNP had an effect on HOMA-IR ($p = 0.018$) and c-peptide ($p = 0.007$) levels, although no effect was found on obesity, glucose or insulin levels, a finding that is consistent with a report from Jamshidi et al.[23] This silent substitution might be interacting with other known and unknown variants.

Many studies have reported conflicting results regarding the association between the Met326Ile (rs3730089) variant in exon 6 of the *PIK3R1* gene and insulin resistance and T2D. While this SNP was not found to be a risk factor for diabetes in a Danish population, it was associated with the disease in a Chinese population.[24,25] This inconsistency in results may be due to differences in sample size and the studied populations. There is evidence that European and Asian populations have different allele frequencies, risk allele profiles, risk genes, and so on.[26]

We also observed a strong association between Met326Ile and the disease ($p < 0.05$). This missense variation is located between the N-terminal-Src homology region (N-SH2) and the BH region which has homology with GTPase activating protein (GAP). The SH2 domains include tyrosine residues and mediate binding to phosphotyrosine residues in the YXXM motif in receptor and adaptor molecules.[27] Therefore, the Met326Ile variation may alter protein activity by affecting binding to its receptor and adaptor molecules. In our study, the genotype distributions of Met326Ile deviated from HWE in the control groups ($p < 0.05$). This deviation should be taken into account while assessing the results for Met326Ile. Future studies are needed to reanalyze the results after increasing the sample size to reach equilibrium.

Jamshidi et al. investigated intronic SNPs in the *PIK3R1* gene, specifically rs7713645 and rs7709243 in intron 1 and rs1550805 in intron 6, showing that SNPs rs7713645 and rs7709243 were associated with BMI, fasting glucose level and glucose level during the 2nd hour of oral glucose application and that rs1550805 was significantly associated with BMI, body weight and central adiposity.[23] These results indicate the existence of a strong link between these intronic SNPs, especially rs1550805, and obesity.

In our study, we observed strong associations between the SNPs rs7709243 and rs7713645, and T2Din obese patients ($p < 0.05$) and between the SNP rs7713645 and T2D in non-obese patients ($p < 0.05$). In addition, the rs7709243

variant was determined to have an effect on cholesterol (p = 0.008) and LDL (p = 0.028) levels.

On the other hand, we did not detect any association between the intronic SNP rs1550805 and T2D. However, this SNP had an effect on c-peptide (p = 0.023) and BMI (p = 0.007). These results support the hypothesis that the intronic SNPs in the *PIK3R1* gene have significant effects on BMI and lipid parameters. Because this significant association with T2D was especially observed in the obese group, one could suggest that the rs7709243 and rs7713645 substitutions play a role in the development of T2D through the development of obesity. Additionally, the genotype distributions of these T2D-associated intronic SNPs were in HWE in all groups. Moreover, according to LD analysis, we detected significant linkage only between SNPs rs7709243 and rs7713645 (D' = 0.85; r^2 = 0.7). Localization at the same intron of both variants might explain this linkage.

Since 2007, more than 60 variants have been shown to be associated with T2D by genome wide association (GWA) analysis, which was performed in numerous populations with large samples. It is noteworthy that the vast majority of these variants are intronic variants. These SNPs do not cause any changes in protein structure but show a strong association with type 2 diabetes, suggesting that they are intronic enhancers.[28] Additionally, it has been proposed that these variants can be haplotyped with other functional variants.[29]

It has been reported that the SNPs in the noncoding UTR sequence of the *PIK3R1* gene, especially SNP rs3756668 in the 3'UTR region, are associated with a high risk of diabetes and elevated BMI as well as increased risk for insulin resistance.[30] Additionally, the same study revealed that this SNP also has an effect on fasting glucose and fasting insulin levels.[30] However, our study did not identify a relationship between SNP rs3756668 and T2D or its phenotypes in obese and non-obese individuals in the Turkish population. We suspect that the deviation from HWE in the control group may have influenced our results. Reassessing these results after increasing the population size to reach equilibrium will increase reliability.

Jamshidi et al. investigated the association between the tag SNPs including rs706713, rs7713645, rs7709243, rs251406, rs40318, rs1550805, rs831125 and rs3730089 of the *PIK3R1* gene, and BMI, serum leptin level, and glucose/insulin homeostasis in a large population of female twins.[23] According to their report, rs1550805 in particular was determined to have a strong relationship with serum leptin level and BMI (p < 0.05). Consistently, in our study, only rs1550805 was associated with BMI, supporting the findings of Jamshidi et al.[23]

Our study is the 1st to show that SNPs rs706713 (Tyr73Tyr) and rs3730089 (Met326Ile), which are located in exons, and SNPs rs7713645, rs7709243 and rs1550805, which are located in introns, are significantly associated with T2D and have effects on phenotypic features such as obesity, insulin resistance and lipid parameters in a Turkish population. The only exception was SNP rs3756668, which is located in the 3'UTR. Our research findings support the idea that SNPs located in the *PIK3R1* gene can affect insulin signaling transduction and thus may play a role in the development of T2D through the development of insulin resistance.

References

1. Klippel A, Reinhard C, Kavanaugh WM, Apell G, Escobedo MA, Williams LT. Membrane localization of phosphatidylinositol 3-kinase is sufficient to activate multiple signal-transducing kinase pathways. *Mol Cell Biol*. 1996;16(8):4117–4127.
2. Rojek A, Niedziela M. Insulin receptor and its relationship with different forms of insulin resistance. *Adv Cell Biol*. 2010;2:59–90.
3. Honardoost M, Sarookhani MR, Arefian E, Soleimani M. Insulin resistance associated genes and miRNA. *Appl Biochem Biotechnol*. 2014;174(1):63–80.
4. Virtue S, Vidal-Puig A. Adipose tissue expandability, lipotoxicity and the metabolic syndrome – an allostatic perspective. *Biochim Biophys Acta*. 2010;1801(3):338–349.
5. Yu J, Zhang Y, McIlroy J, Rordorf-Nikolic T, Orr GA, Backer JM. Regulation of the p85/p110 phosphatidylinositol 3-kinase: Stabilization and inhibition of the p110a catalytic subunit by the p85 regulatory subunit. *Mol Cell Biol*. 1998;18(3):1379–1387.
6. Małodobra M, Pilecka A, Gworys B, Adamiec R. Single nucleotide polymorphisms within functional regions of genes implicated in insulin action and association with the insulin resistant phenotype. *Mol Cell Biochem*. 2011;349(1–2):187–193.
7. Chen JM, Férec C, Cooper DN. A systematic analysis of disease-associated variants in the 30 regulatory regions of human protein-coding genes II: The importance of mRNA secondary structure in assessing the functionality of 30 UTR variants. *Hum Genet*. 2006;120(3):301–333.
8. Nelsoe RL, Hamid YH, Pociot F, et al. Association of a microsatellite in FASL to type 2 diabetes and of the FAS-670G>A genotype in insulin resistance. *Genes Immun*. 2006;7:316–321.
9. Gaunt TR, Rodriguez S, Zapata C, Day IN. MIDAS: Software for analysis and visualisation of interallelic disequilibrium between multiallelic markers. *BMC Bioinformatics*. 2006;27:227. doi: 10.1186/1471-2105-7-227
10. Kahn CR. The molecular mechanism of insulin action. *Annu Rev Med*. 1985;36:429–451.
11. Dhe-Paganon S, Ottinger EA, Nolte RT, Eck MJ, Shoelson SE. Crystal structure of the pleckstrin homology-phosphotyrosine binding (PH-PTB) targeting region of insulin receptor substrate 1. *Proc Natl Acad Sci*. 1999;96(15):8378–8383.
12. Isakoff SJ, Taha C, Rose E, Marcusohn J, Klip A, Skolnik EY. The inability of phosphatidylinositol 3-kinase activation to stimulate GLUT4 translocation indicates additional signaling pathways are required for insulin-stimulated glucose uptake. *Proc Natl Acad Sci USA*. 1995; 92(22):10247–10251.
13. Perry RJ, Shulman GI. Treating fatty liver and insulin resistance. *Aging*. 2013;5(11):791–792.
14. Knights AJ, Funnell AP, Pearson RC, Crossley M, Bell-Anderson KS. Adipokines and insulin action: A sensitive issue. *Adipocyte*. 2014; 3(2):88–96.
15. Hotamisligil GS, Peraldi P, Budavari A, Ellis R, White MF, Spiegelman BM. IRS-1-mediated inhibition of insulin receptor tyrosine kinase activity in TNF-alpha- and obesity-induced insulin resistance. *Science*.1996; 271(5249):665–668.
16. Bogan JS, Lodish HF. Two compartments for insulin-stimulated exocytosis in 3T3-L1 adipocytes defined by endogenous ACRP30 and GLUT4. *J Cell Biol*. 1999;146(3):609–620.
17. Chagnon YC, Rankinen T, Snyder EE, Weisnagel SJ, Pe'russe L, Bouchard C. The human obesity gene map: The 2002 update. *Obes Res*. 2003;11(3):313–367.
18. Bokarewa M, Nagaev I, Dahlberg L, Smith U, Tarkowski A. Resistin, an adipokine with potent proinflammatory properties. *J Immunol*. 2005;174(9):5789–5795.

19. Ueki K, Yballe CM, Brachmann SM, et al. Increased insulin sensitivity in mice lacking p85 beta subunit of phosphoinositide 3-kinase. *PNAS*. 2002;99(1):419–424.
20. Barbour LA, Shao J, Qiao L, et al. Human placental growth hormone increases expression of the P85 regulatory unit of phosphatidylinositol 3-kinase and triggers severe insulin resistance in skeletal muscle. *Endocrinology*. 2004;145(3):1144–1150.
21. Giorgino F, Pedrini MT, Matera L, Smith RJ. Specific increase in p85a expression in response to dexamethasone is associated with inhibition of insulin-like growth factor-1 stimulated phosphatidylinositol 3-kinase activity in cultured muscle cells. *J Biol Chem*. 1997;272(11):7455–7463.
22. Rai E, Sharma S, Kaul S, et al. The interactive effect of SIRT1 promoter region polymorphism on type 2 diabetes susceptibility in the north Indian population. *Plos One*. 2012;7(11):e48621. doi: 10.1371/journal.pone.0048621
23. Jamshidi Y, Snieder H, Wang X, et al. Phosphatidylinositol 3-kinase p85 alpha regulatory subunit gene PIK3R1 haplotype is associated with body fat and serum leptin in a female twin population. *Diabetologia*. 2006;49(11):2659–2667.
24. Hansen L, Zethelius B, Berglund L, et al. In vitro and in vivo studies of a naturally occurring variant of the human p85a regulatory subunit of the phosphoinositide 3-kinase. Inhibition of protein kinase b and relationships with type 2 diabetes, insulin secretion, glucose disappearance constant, and insulin sensitivity. *Diabetes*. 2001;50:691–693.
25. Chen S, Yan W, Huang J, Ge D, Yao Z. Association analysis of the variant in the regulatory subunit of phosphoinositide 3-kinase (p85a) with type 2 diabetes mellitus and hypertension in the Chinese Han population. *Diabet Med*. 2005;22(6):737–743.
26. Hancock AM, Witonsky DB, Gordon AS, et al. Adaptations to climate in candidate genes for common metabolic disorders. *PLoS Genet*. 2008;4(2):e32. doi: 10.1371/journal.pgen.0040032
27. Fruman DA, Cantley LC. Phosphoinositide 3-kinase in immunological systems. *Semin Immunol*. 2002;14(1):7–18.
28. Pang DX, Smith AJP, Humphries SE. Functional analysis of TCF7L2 genetic variants associated with type 2 diabetes. *Nutr Metab Cardiovasc Dis*. 2013;23(6):550–556.
29. Hossain S, Islam S, Khatun T, Sapon A. Type 2 diabetes mellitus: Impact of genetics and environment. *Int J Curr Sci*. 2014;12:110–127.
30. Małodobra M. The role of single nucleotide polymorphisms of untranslated regions (Utrs) in insulin resistance pathogenesis in patients with type 2 diabetes. In: Croniger C, ed. *Medical Complications of Type 2 Diabetes*. London, UK: InTech; 2011:165–188.

Assessment of markers expressed in human hair follicles according to different skin regions

Arzu Yay[1,A–E], Özge Göktepe[1,B,C], Anzel Bahadir[2,D,E], Saim Özdamar[1,A], Ibrahim Suat Öktem[3,B], Atilla Çoruh[4,B], Münevver Baran[5,C,D]

[1] Department of Histology and Embryology, Faculty of Medicine, Erciyes University, Kayseri, Turkey
[2] Department of Biophysics, Faculty of Medicine, Düzce University, Turkey
[3] Department of Neurosurgery, Faculty of Medicine, Erciyes University, Kayseri, Turkey
[4] Department of Plastic and Reconstructive Surgery, Faculty of Medicine, Erciyes University, Kayseri, Turkey
[5] Department of Pharmaceutical Basic Science, Faculty of Pharmacy, Erciyes University, Kayseri, Turkey

A – research concept and design; B – collection and/or assembly of data; C – data analysis and interpretation;
D – writing the article; E – critical revision of the article; F – final approval of the article

Advances in Clinical and Experimental Medicine, ISSN 1899-5276 (print), ISSN 2451-2680 (online) *Adv Clin Exp Med*. 2018;27(7):929–939

Address for correspondence
Arzu Yay
E-mail: arzu.yay38@gmail.com

Funding sources
None declared

Conflict of interest
None declared

Acknowledgements
This work was supported by the Scientific Research Project Coordination Unit of Erciyes University (Project number: EUBAP, TCD-4517).

Received on February 4, 2017
Reviewed on May 23, 2017
Accepted on June 5, 2017

Abstract

Background. Body region-dependent hair follicle (HF) characteristics are concerned with follicular size and distribution, and have been demonstrated to have characteristics for each region of the body.

Objectives. The aim of the present study was to investigate the expression patterns of the markers called cytokeratin 15 (K15), cytokeratin 6 (K6) and monoclonal antibody Ki-67, and also apoptosis in HFs, which can be observed in different parts of the human body.

Material and methods. In this study, healthy human HFs were taken by biopsy from 5 various donor sites of the human body: the scalp, the leg, the abdomen, the back and waist. HF-containing skin specimens taken using cryosection were stained with hematoxylin & eosin (H&E) and K15, K6, Ki-67 and terminal deoxynucleotidyl transferase-mediated digoxigenin-dNTP nick end-labelling (TUNEL) immunofluorescence staining protocol was performed.

Results. Different skin regions from the human body were examined histologically. While the HFs of scalp tissue showed anatomically obvious hair layers, some hair sections from other regions, like the leg, the abdomen, back and waist, were not as distinct as in the scalp region. According to our findings, K15 expression was highest in the scalp. In addition, the immunoreactivity (IR) intensity of K15 was significantly decreased in the HFs on the waist and abdominal regions, compared to the scalp and back regions ($p < 0.001$). However, the IR intensity of K6 in the scalp region was statistically significantly higher than the IR intensity of K6 in the abdomen region ($p < 0.05$). Moreover, we showed intraepithelial apoptosis and proliferation of keratinocytes in the bulge of HF. In the study, Ki-67-positive and TUNEL-positive cell numbers were not statistically significant ($p > 0.05$).

Conclusions. Our findings are important for further investigation of molecular aspects of the human hair follicle stem cells compartments in health and disease, which might be a promising model for comparative studies with different human diseases.

Key words: monoclonal antibody Ki-67, terminal deoxynucleotidyl transferase-mediated digoxigenin-dNTP nick end-labelling, hair follicle, cytokeratin 15, cytokeratin 6

DOI
10.17219/acem/74429

Introduction

Hair follicles (HFs) as a functional mini-organ, form a very complex structure which consists of mesenchyme-derived dermal papilla and 3 distinct epithelial layers: the outer root sheath (ORS) (the outer layer), the inner root sheath (IRS) (the middle layer) and the hair shaft (the central layer).[1] The mammalian hair follicle contains a heterogeneous cell population, including hair follicle stem cells (HFSCs) and epithelial cells, such as keratinocytes.[2] The diversity of the morphologic differentiation pathway of the hair follicle is partly reflected by the respective keratin protein patterns. The HF keratin patterns are mainly composed of the epithelial keratins.[3] These keratins belong to a heterogeneous family of intermediate filaments that are essential to the epidermis, where they are expressed in a cell-type and differentiation-specific manner during epithelial development and differentiation.[4,5] In humans, keratins generally present in epithelial cells as keratinocytes.[6] The main function of keratins is the maintenance of cell and tissue structure.[5,7] Expression of specific keratins and changes in the expression profile temporally and spatially reflect the differentiation status of epidermal cells both in development and in mature epidermal tissue.[8]

The expression of cytokeratin 15 (K15) is thought to have stem cell characteristics[9,10] and enrichment has been observed in the HF bulge region where multipotential epidermal stem cells are located.[11,12] The HFSCs sustain growth and cycling of the HF and they are known to play a major role in maintaining skin homeostasis.[13] Actually, human HF bulge is an important niche for HFSCs and several authors have described K15 as a putative epidermal stem cell marker.[12,14,15] In humans, cytokeratin 6 (K6), which is expressed in epithelial appendages, has distinct tissue expression patterns, and it is the dominant form in epithelial tissue. K6 is expressed in the inner bulge layer and is implicated in maintaining HFSC quiescence, whereas strong K6 expression was observed in the interfollicular epidermis but not in the bulge region.[16] The expression of the human Ki-67 protein is properly associated with cell proliferation and this makes it an excellent marker for determining the growth fraction of a given cell population.[17] Indeed, Ki-67 immunoreactivity (IR) is a useful tool for cell proliferation in HF matrix keratinocytes below the widest part of the dermal papilla and bulge. The onset of catagen is characterized by a noticeable reduction in the percentage of Ki-67-positive matrix keratinocytes, with virtually no Ki-67-positive HF keratinocytes present in late catagen.[18]

Over the years, both human and mouse disorders have shown additional complex functional roles for cytoskeleton keratins, which are involved in the modulation of apoptosis, cell growth, tissue polarity, wound response and tissue remodeling.[5,7,19] The HF is an established tissue source for cell-based therapy. The skin stem cells of HF are in clinical set up for a long period of time and many cell-based applications are there for the management of disorders. Thus, some investigators have used HFSCs for cell-based clinical needs such as vitiligo.[20] In this context, the results of many studies have suggested that an abnormal stem cell marker, such as K15 expression, potentially plays a role in the pathogenesis.[21]

Previous studies have shown body region-dependent HF characteristics concerning follicular size and follicular distribution, and demonstrated that each region of the body disposes of its own hair follicle characteristics. In these studies, the hair follicle density on the forehead, cheek, chest and back of the human body has been determined.[22] Nevertheless, the expression patterns of useful markers used in HF studies in different skin regions are poorly understood. However, the determination of these markers in different skin regions and a comparison of expression intensities can be an important contribution to treatments for skin injury, cancers and hair loss. Hence, we aimed in this preliminary study to evaluate the expression intensities of markers such as K15 and K6 identified in hair follicle cells found in different skin regions. Moreover, to the best of our knowledge, this is the 1st study to evaluate apoptosis and proliferation of keratinocytes in the HF bulge of different skin regions.

Material and methods

The study was approved by the clinical research ethics committee of Faculty of Medicine, Erciyes University, Kayseri, Turkey (number: 197). All volunteers gave written informed consent and the protocol was approved by the institutional review board.

Specimens

Human healthy hair skin biopsy specimens were taken from each routine surgery from 5 various donor sites (scalp, leg, abdomen, back and waist). This process was conducted with written consent, under the same conditions, i.e., at the same room temperature and humidity. The voluntary donors were all patients from the Neurosurgery Department and the Plastic and Reconstructive Surgery Department at the Erciyes University, Kayseri, Turkey. All experiments were carried out according to the Helsinki guidelines, in compliance with national regulations for the experimental use of human material. We examined 38 samples of healthy skin from various donor sites and their description is shown in Table 1. None of the volunteers suffered from any kind of skin disease, hormonal dysregulation or adiposity. Also, they did not have any diseases such as cancer or autoimmune diseases. The excised hair skin biopsies were transported in Williams E medium (Biochrom, Cambridge, UK) on ice and transferred to the laboratory of histology and embryology immediately.

Table 1. Classifications of healthy skin specimens gathered from various donor sites of the body according to individual's gender and age range

Body region	Female [n]	Male [n]	Total [n]	Age range [years]
Scalp	6	5	11	22–60
Leg	3	10	13	24–72
Back	6	4	10	30–75
Abdomen	5	3	8	31–69
Waist	5	4	9	29–58

n – number of examined healthy individuals.

Tissue preparation and histochemistry analysis

Normal hair skin tissue specimens were first shaved using a scalpel and dissected into approx. 0.5 cm^2 pieces before being washed 1–3 times with phosphate-buffered saline (PBS) to remove cell debris. The skin biopsies were embedded in Shandon Cryomatrix (Thermo Fisher Scientific, Waltham, USA), snap-frozen in liquid nitrogen, and stored at –80°C until use. All specimens were covered with poly-L-lysine and the sections were placed on slides for examination. Cryosections (7 µm thick) were first air-dried for 10 min, fixed in acetone at –20°C for 10 min, and then air-dried again for 10 min. Longitudinally cut hair skin specimens were stained by hematoxylin & eosin (H&E). The hair skin sections were studied using light microscopy (Olympus BX51 fluorescent microscope; Olympus, Tokyo, Japan). Photos were taken using a Olympus DP71 (Olympus, Tokyo, Japan) digital camera.

Immunofluorescence staining

Immunofluorescence staining was used to detect K15, K6, Ki-67 and terminal deoxynucleotidyl transferase-mediated digoxigenin-dNTP nick end-labelling (TUNEL) IRs in the HFs.

K15 immunofluorescence staining

To identify the IR of K15 in the bulge region of the HFs in human skin via immunofluorescence staining, we used the tyramide signal amplification method, according to Kloepper et al.[23] After fixation, the cryosections were washed 3 times by using a TNT (Tris-HCl NaCl Tween) buffer for 5 min. Next, horseradish peroxidase was blocked by washing with 3% H_2O_2 in PBS for 15 min. The sections were incubated with avidin and biotin for 15 min. Preincubation was performed in 5% goat normal serum in TNT for 30 min. Primary antibodies (K15) diluted in TNT (1:400 dilution Chemicon CBL; Merck, Billerica, USA) were incubated overnight at 4°C, followed by a biotinylated secondary antibody goat anti-mouse (1:200 dilution in TNT) for 45 min at room temperature (RT). For the next steps, a tyramide signal amplification kit (TSA kit; Perkin-Elmer, Boston, USA) was administered (1:100 dilution in TNT) for 30 min at RT. The reaction was amplified by tetramethylrhodamine-tyramide amplification reagent at RT for 5 min. The cryosections were counterstained with 4;6-diamidino-2-phenylindole (DAPI) (Sigma, St. Louis, USA) for nuclear staining for 1 min and mounted with Fluoromount-G (Southern Biotechnologies, Birmingham, USA).

K6 immunofluorescence staining

Cryosections (7 µm) stored at –80°C were first air-dried for 10 min, fixed in acetone at –20°C for 10 min and then air-dried again for 10 min at RT. After the slides were washed 3 times for 5 min with tris-buffered saline (TBS), they were preincubated with normal goat serum (10% in tris-buffered saline) for 20 min. Primary antibody K6 (1:400 in TBS) (Progen, Heidelberg, Germany) was applied directly on the sections and the slides were incubated overnight at 4°C in a humidity chamber. After washing 3 times for 5 min in TBS, the sections were stained with goat anti-mouse secondary antibody and conjugated with fluorescein isothiocyanate (FITCH) (1:200 dilution in TBS; Jackson ImmunoResearch, Cambridgeshire, UK) for 45 min at RT. The slides were again washed 3 times for 5 min in TBS. Following each step, the cryosections were counterstained with DAPI (Sigma, St. Louis, USA) for 1 min. The slides were mounted by using Fluoromount-G (Southern Biotechnologies, Birmingham, USA). For immunostaining assays, primary antibodies were omitted as a negative control.

Ki-67 and TUNEL double staining assay

To compare proliferation and apoptosis of human HFs in the various hair cycles of different body regions, Ki-67 and in situ terminal deoxynucleotidyl transferase-mediated digoxigenin-dNTP nick end-labelling (TUNEL) double staining method were used. The TUNEL method was utilized to show the apoptotic cells of human HF, while the Ki-67 marker was used for detecting proliferating cells. For double immunofluorescence staining of TUNEL-positive cells and Ki-67 IR, the protocol for the TUNEL technique was combined with the manufacturer's protocol for Ki-67 immunofluorescence.[24] The TUNEL apoptosis detection kit (ApopTag Fluorescein in Situ Apoptosis detection kit; Millipore, Berlin, Germany) was used according to the manufacturer's protocol. TUNEL staining was performed using standard protocols. Briefly, 7 µm frozen tissue sections were air-dried for 15 min and postfixed in ethanol-acetic acid (–20°C) for 5 min, followed by incubation with digoxigenin-dUTP in the presence of TdT (terminal deoxynucleotidyl transferase) for 1 h at 37°C. TUNEL-positive cells were visualized by anti-digoxigenin fluorescence unconjugated antibody. Subsequently, the sections were pre-saturated with normal goat serum and incubated with the primary Ki-67 antibody (mouse anti-human 1:100 in PBS) (DAKO, Carpinteria, USA) overnight

at 4°C. The cryosections were incubated with a secondary rhodamine-labelled goat anti-mouse antibody (1:200 dilution in PBS; Jackson ImmunoResearch, Newmarket, UK) for 45 min at RT after a washing step. Nuclear counter staining was performed with DAPI (Sigma, St. Louis, USA) to stain the cell nuclei and mounted with Fluoromount-G (Southern Biotechnologies, Birmingham, USA). Negative controls were performed by omitting TdT and the Ki-67 antibody. Images were visualized under an Olympus BX51 fluorescence microscope (Olympus, Tokyo, Japan).

Histomorphometry and statistical analysis

The immunostaining intensity levels for the selected examined antigens were compared by quantitative immunohistochemistry using Image J software (ImageJ, National Institute of Health, USA). The IR intensities of K15 and K6 of at least 3 HFs randomly defined for 5 different groups were evaluated from each individual. The mean of the IR intensities for K15 and K6 was calculated by using Image J software at high power fields (×400 magnification). To obtain numbers for Ki-67 and TUNEL-positive cells, 3–7 hair follicles per each region were analyzed. The numbers of the Ki-67 and TUNEL-positive cells in the bulge regions of each HF were counted by Image J software, irrespective of the follicular cycle.

For evaluating statistical significance, these measurements were pooled and the mean ± standard deviation values were calculated. All statistical procedures were performed by statistical analysis software SPSS v. 15.0 (SPSS Inc., Chicago, USA). One-way analysis of variance (ANOVA) compared the staining intensity values between groups. When the p-value from one-way ANOVA test statistics was statistically significant, a post hoc Tukey HSD nonparametric multiple comparison test was used to determine which group differed from which others. The results were considered significant if the p-value was <0.05.

Results

Histological findings

A comparison of HF samples originating from different donor sites showed the same features as those known from the histologic examination. In the study, primarily the histological structures of HFs were examined in hairy skin specimens taken from different regions of the human body, and the HFs were evaluated histologically. Staining the HF sections with H&E allows a clear visualization of the different follicular compartments. Histological images from HFs of different skin regions are shown in Fig. 1. From the histological examination, it was observed that HFs from scalp tissue showed a complete histological stratification, whereas HFs from other regions (leg, abdomen, back and waist) did not show complete stratification.

Immunofluorescence findings

In this part of the study, K15, K6, Ki-67 and TUNEL immunofluorescence staining used in HF hair follicle studies were selected and expression intensities in the HFs from different skin regions of these antibodies were calculated. K15-positive IR was observed in the outermost layer of the outer root sheath in the bulge of HFs, corresponding to the human bulge region in all regions of HFs. When the HFSCs with K15 IR intensities were compared with other regions, it was observed that the highest expression was in the HFSCs taken from the scalp tissue. Interestingly, when K15 expression was evaluated, the HFSCs in the back and leg region showed almost as much as the HFSCs in the scalp (Table 2). In our study, the decrease in IR intensity of K15 was statistically significant in the HFs on the waist and abdominal regions, compared to the scalp and back regions ($p < 0.001$). Additionally, there were no significant differences between in the HFs taken from the scalp region and the back or leg regions in terms of K15 IR intensity ($p > 0.05$) (Fig. 2).

Moreover, K6 expression was present in the keratinocyte cells of all HFs when the HFs in different skin regions were evaluated in terms of K6 expression levels. However, it was determined that the IR intensity of K6 differed according to the region of the HF. The HFs with the most intensive K6 expression was observed in the scalp tissue. Immunoreactivity intensity of K6 was higher in the scalp region than the abdomen region, and this difference was statistically significant ($p < 0.05$). According to our results, while the HFs in the back region showed similar K6 expression to the scalp HFs, K6 levels were not statistically significantly different between the scalp and back regions, as shown in Table 2 ($p > 0.05$) (Fig. 3).

Table 2. Immunoreactivity intensity of K15, K6 and Ki-67 terminal deoxynucleotidyl transferase-mediated digoxigenin-dNTP nick end-labelling (TUNEL)-positive cell number in HFs of different skin regions

Markers	Scalp	Leg	Abdomen	Back	Waist	p-value
K6	74.67 ±13.35*	70.90 ±11.12	68.63 ±16.99	73.35 ±13.33	70.34 ±11.01	0.020
Ki-67	17.85 ±6.92	15.47 ±5.77	14.67 ±5.08	14.67 ±5.08	14.61 ±5.04	0.354
K15	38.58 ±9.80**	33.17 ±8.43	30.88 ±8.52	35.27 ±8.57**	32.73 ±7.91	<0.001
TUNEL	6.93 ±3.50	6.31 ±3.35	6.33 ±3.55	6.23 ±4.00	6.17 ±3.95	0.984

Data is expressed as mean ± standard deviation. Comparisons: * scalp region vs abdomen region ($p < 0.05$); ** scalp region vs abdomen and waist regions ($p < 0.001$). One-way analysis of variance (ANOVA) and post hoc Tukey test statistical analyses were used.

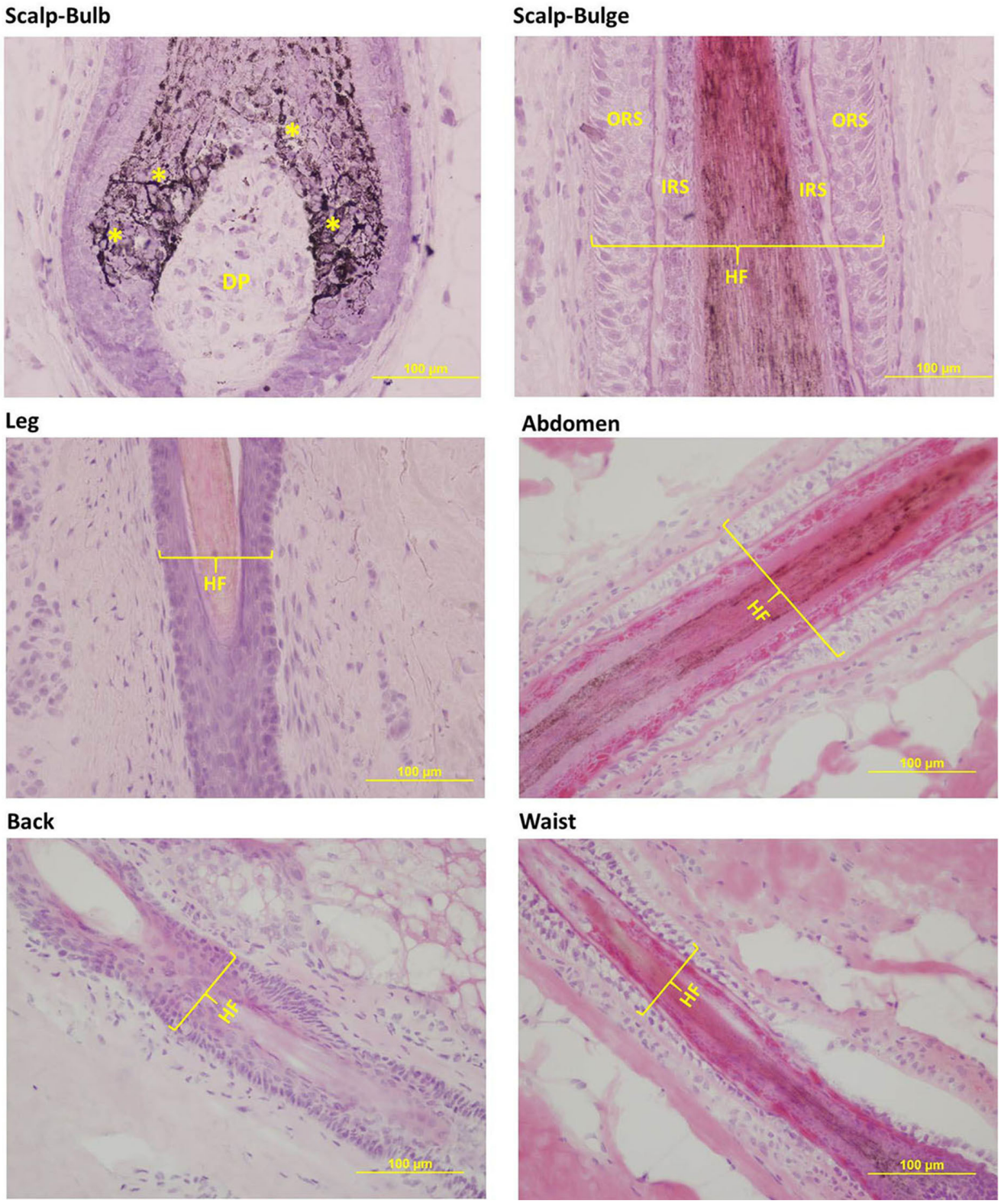

Fig. 1. Hematoxylin and eosin histochemistry: the overview of bulb and bulge regions of a HF of scalp tissue and the section of HFs taken from other skin regions

* melanocytes; DP – dermal papilla; HS – hair shaft; IRS – inner root sheath; ORS – outer root sheath; original magnification (×400).

The cell apoptosis in the outer root sheath is most frequently assessed by the addition of synthetic, detectable nucleotides (dUTP) at DNA breaks by terminal transferase activity, that is TUNEL immunofluorescence, properly in conjunction with Ki-67 IR. It provides information to simultaneously show both proliferative and apoptotic cells by this method. Therefore, TUNEL and Ki-67 documented massive intraepithelial apoptosis and proliferation of keratinocytes in the bulge. In the Ki-67 and TUNEL double-staining, whereas TUNEL-positive

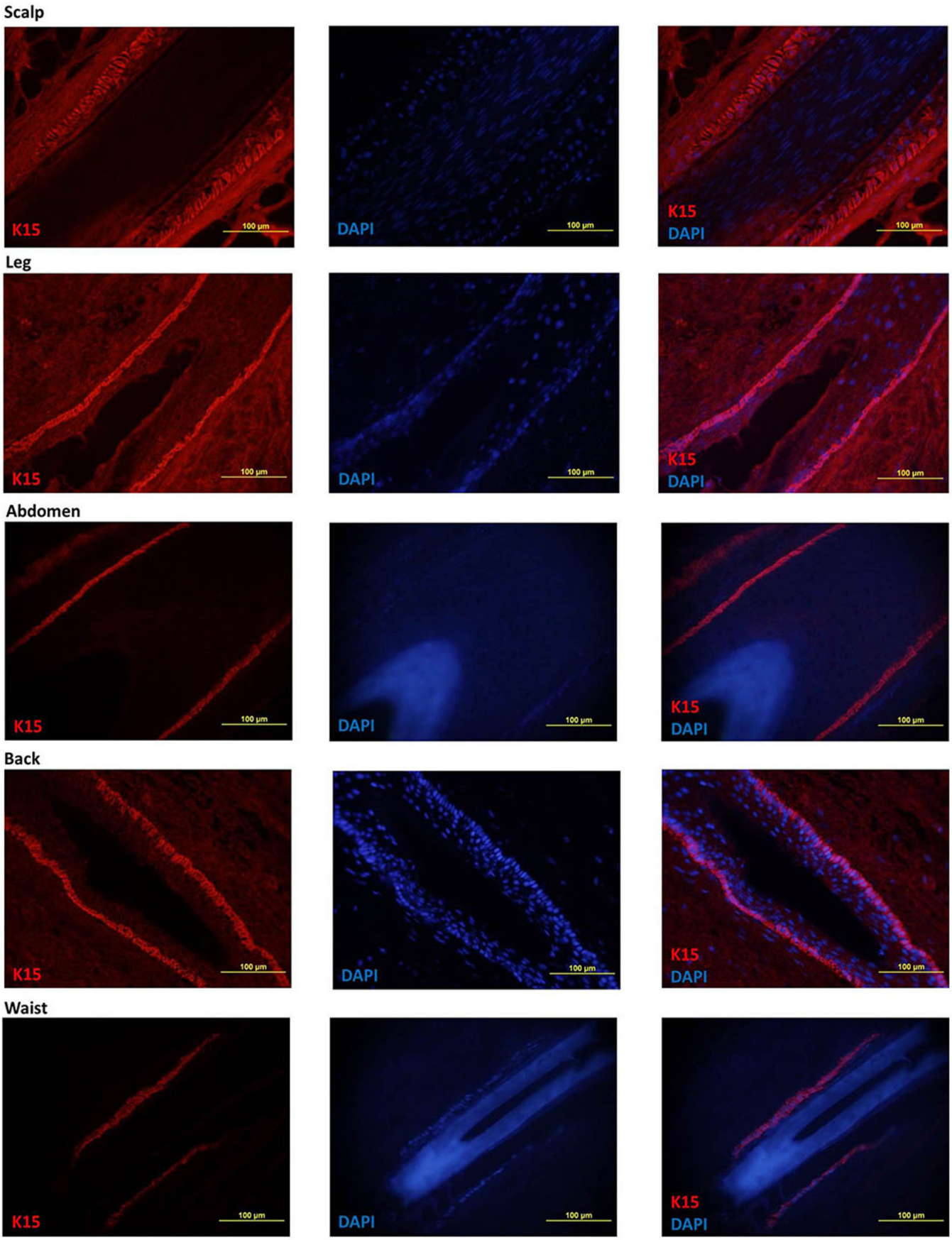

Fig. 2. The HF stem cells in the bulge region of the HFs from all different skin regions showing K15 IR. K15 immunofluorescence staining Original magnification (×400); DAPI – 4;6-diamidino-2-phenylindole.

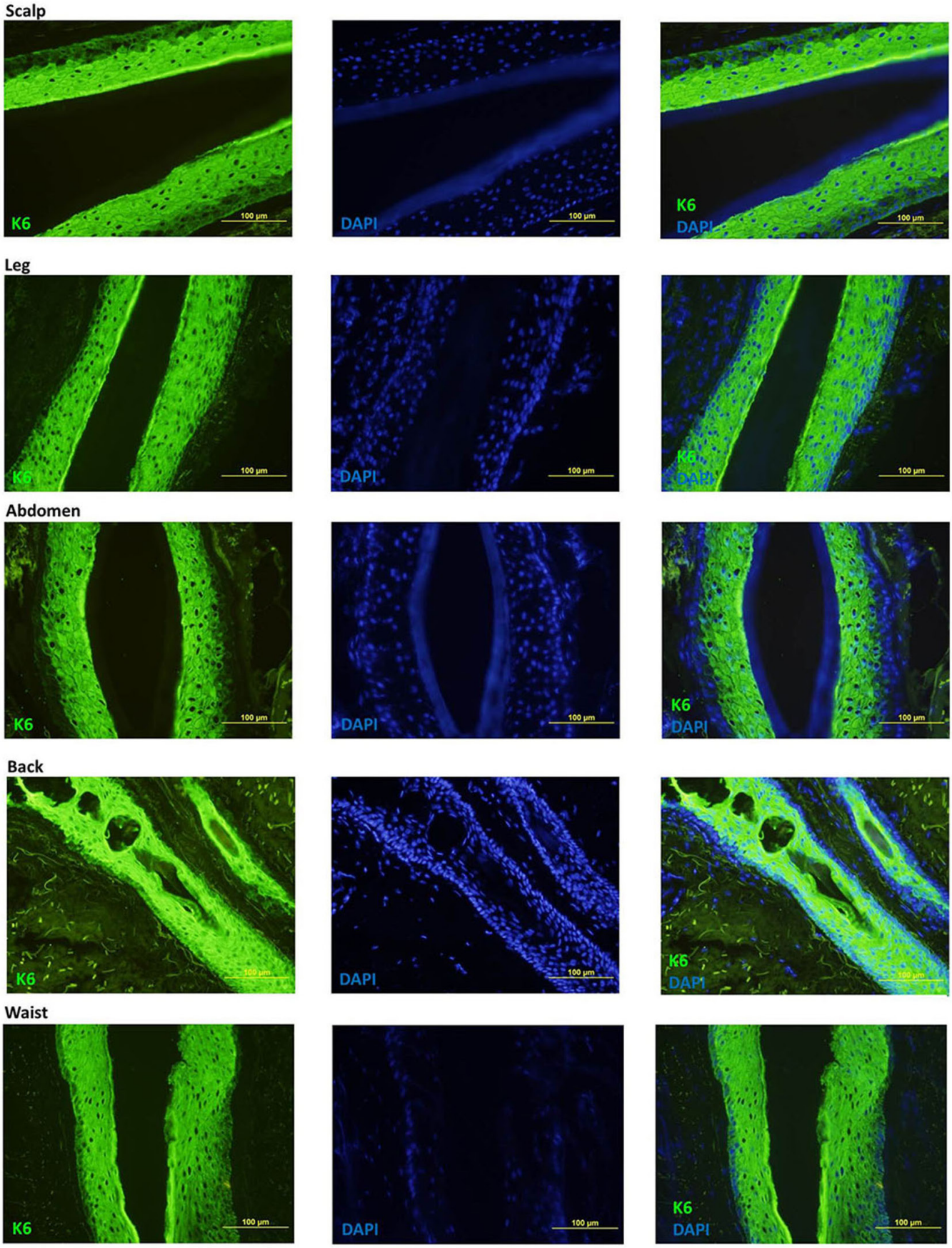

Fig. 3. Immunoreactivity intensity of K6 in the HFs of different body regions. K6 immunofluorescence staining

Original magnification (×400); DAPI – 4;6-diamidino-2-phenylindole.

cells seemed bright green, Ki-67-positive cells had bright red nuclei. The number of Ki-67-positive cells was highest in HFs of the scalp region, whereas the lowest Ki-67-positive cell number was observed in HFs of the abdomen region. However, this difference was not statistically significant ($p > 0.05$). The number of TUNEL-positive cells was the highest in the HFs of scalp tissue, compared to the bulge regions of HFs obtained from other regions. There were TUNEL-positive cells in the bulge of HFs from different skin regions, but no significant difference between the scalp region and other regions in terms of the TUNEL-positive cell numbers ($p > 0.05$) (Table 2, Fig. 4).

Discussion

Cytokeratins play a critical role in differentiation and tissue specialization, and function to maintain the overall structural integrity of epithelial cells. They are useful markers of tissue differentiation and also define the anatomical location of the niche, especially K15. Previous studies of the IR pattern of human HFSCs indicate that K15 IR is upregulated in the scalp human bulge compared with other regions of the ORS. The HFSCs were shown by immunostaining and microarray analyses, which demonstrated K15 upregulation in mice and human HF bulge cells.[14] Under normal conditions, the epithelial compartments of the HF and interfollicular epidermis remain discrete, with K15-positive and bulge stem cells contributing progeny for HF reconstruction during the hair cycle. Garcin et al. have suggested that bulge cells only respond to epidermal wounding during later stages of repair.[25] In our study, we investigated the outer root sheath of human HFs taken from 5 different skin regions, the head, leg, abdomen, back and waist, by using the K15 marker. We demonstrated that the highest expression was in the HFSCs taken from the scalp tissue. Furthermore, the HFSCs in the back and leg region showed nearly the same HFSCs as in the scalp, as opposed to in the waist and abdominal regions. This finding suggests that these regions may be as suitable as HFs taken from scalp tissue for stem cell isolation.

Additionally, suprabasal expression of K15 has also been reported in both normal and diseased tissues, which is incompatible with its role as a stem cell marker.[26] Many disorders of the skin, such as cancer, chronic wounds, skin atrophy and fragility, hirsutism, and alopecia, can be investigated as disorders of adult stem cells. Because stem cells in the epidermis and HF serve as an excellent source of cells, understanding the control of their proliferation and differentiation is crucial to fully understand the disorders associated with the disruption in these processes.[27] K15 has been indicated to be expressed in variants of human basal cell carcinoma and other neoplasms of skin appendages such as sebaceous neoplasms and trichoepithelioma.[28] A study by Quist et al. showed that expression of potential stem cell markers of the epidermis and HF was observed in the skin tumors of appendages and human basal cell carcinomas.[29] Also, they demonstrated that many of these markers appeared to be downregulated during tumor progression. These studies have expressed the importance of general HF markers in that it can change expression levels in some pathological conditions. Therefore, it is important to determine the expression levels of specific markers in HFs taken from different skin regions. Although there are numerous immunohistochemical and immunofluorescence studies of HF specific markers on both normal and pathologic skin, expression patterns in the HFs of the different skin regions has been not been addressed. Our study is the 1st one to investigate this hypothesis. We investigated the expression patterns of K15, K6 and proliferative cell number with Ki-67 in different skin regions. In the present study, the HFSCs showed K15-positive expression in all of the HFs taken from different skin regions in the ORS of the follicle. According to our results, K15 IR intensity was higher in the HFSCs of the scalp tissue than in other tissues.

It may be considered that the role of constitutive K6 expression is one reinforcement needed only to withstand increased mechanical stress. It is a marker for the proliferating epithelial layer and is exudative in keratinocytes in the specialized epithelium of the HF. In the current study, the HF keratinocytes taken from different skin regions were determined by K6 immunofluorescent staining method and K6 IR was present in all HFs taken from different skin regions, especially the innermost cells surrounding the hair shaft as is supported by other studies.[2,16] Some lesions reflect a loss of the structural support function shared by K6, other keratins or intermediate filament proteins. In our study, most of the K6 expression was observed in the HFs belonging to the scalp tissue, whereas the HFs of the back region showed a K6 expression density close to scalp tissue. Additionally, in the HF sections of the other regions (leg, abdomen, and waist) there was less expression intensity of K6 than the densities of expression in the back and scalp region, but these results were not statistically significantly different.

The proliferative and apoptotic cell numbers of the HFSCs in different skin regions are also important, considering the studies on HFSCs. Ki-67, a cell proliferation marker, is a useful component for gaining information on cell proliferation in cryosections and is commonly used in HF studies. During anagen, Ki-67 IR is most prominent in hair matrix keratinocytes below the widest part of the dermal papilla. The onset of catagen is described by a marked reduction in the percentage of Ki-67-positive matrix keratinocytes, with virtually no Ki-67-positive HF keratinocytes present in late catagen.[18] Contrary to conventional information, even in telogen HFs, some keratinocytes still enter into the cell cycle.[30] In our study, we performed Ki-67 and TUNEL double staining to show cell proliferation and apoptosis. The number of Ki-67-positive cells was observed in keratinocytes

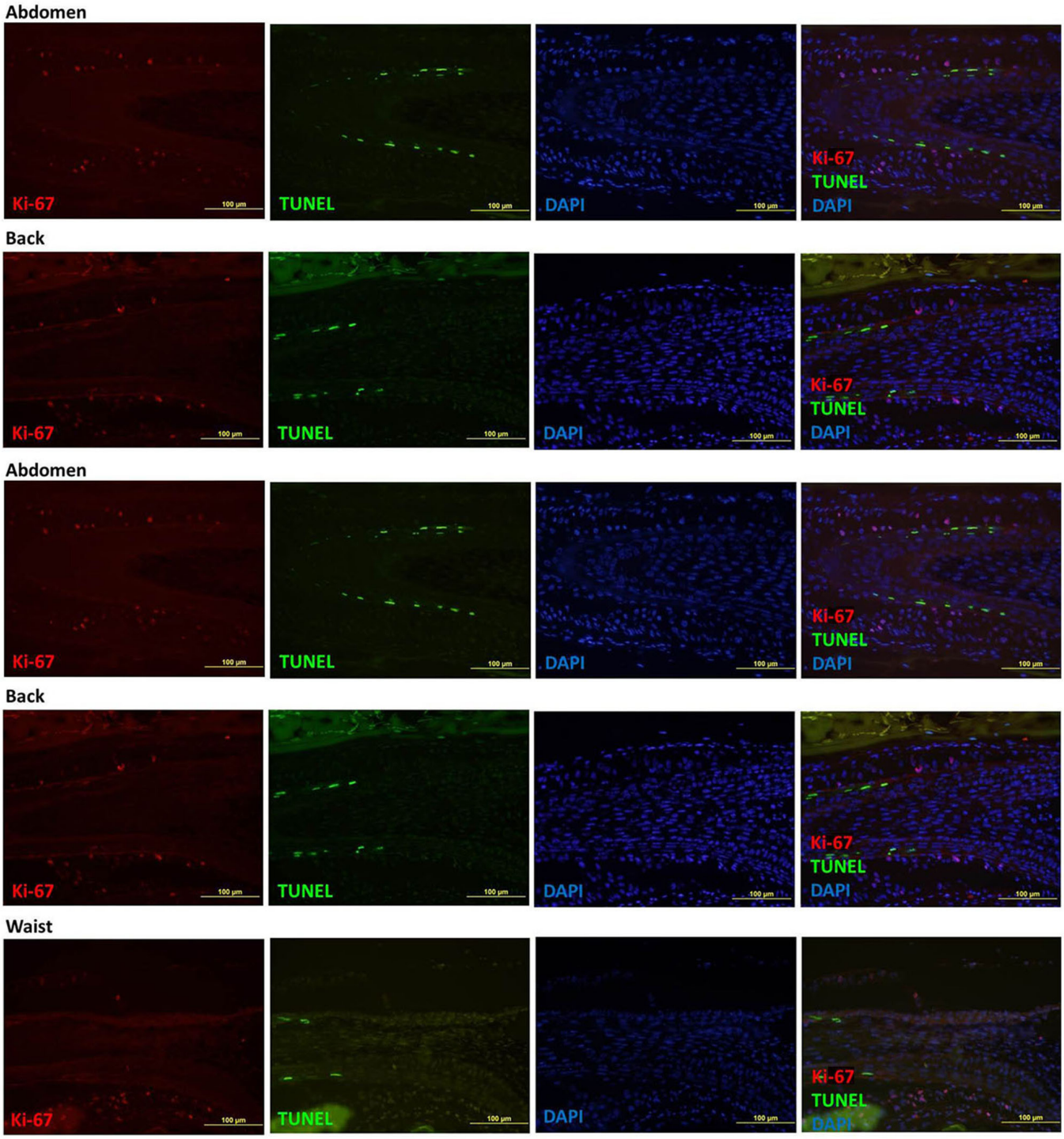

Fig. 4. While apoptotic cells were labeled with TUNEL, proliferative cells were determined with Ki-67 in ORS keratinocytes of HF bulges from different skin regions. TUNEL-positive cells reflect green immunofluorescence, whereas Ki-67-positive cells reflect red immunofluorescence

TUNEL – terminal deoxynucleotidyl transferase-mediated digoxigenin-dNTP nick end-labelling; ORS – outer root sheath; DAPI – 4;6-diamidino-2-phenylindole.

in the bulge of all HFs taken from different skin regions. Additionally, apoptosis was also viewed in some cells that form the HF bulge of different skin regions. In this study, there was no significant difference in the Ki-67 and TUNEL-positive cell numbers in the keratinocytes of the HF bulge regions taken from different skin regions.

In recent years, cell-based therapies, particularly those using stem cells, for improving survival, have emerged as a promising approach for the treatment of severe diseases. The conversion of stem cells to other cells has also increased the interest in these cells. The ease of tissue harvesting and multipotent nature of the resident stem cells in the HF has encouraged basic and clinical research in this area. As a novel cell source, mesenchymal stem cells separated from human HFs are appropriate to obtain, have no age limit, and are easily accessible.[31] These results have

increased the interest especially in working on HFSCs. However, it may also be important to know which skin regions the HF should be taken from in such studies.

There have been many studies on the size and diameter of the HF and also the volume of the dermal papillae in different body regions.[22,32,33] Otberg et al. showed the diversity of HF sizes in different body regions in their study, which emphasizes the importance of understanding and calculating the follicular penetration and permeability processes of HF density and size.[22] Only a few studies have been performed for the determination of vellus HF density on the human body.[11,22] A study by Blume et al. determined the HF density on the forehead, cheek, chest, and back.[32] In this study, an average density of 423 follicles per cm^2 was identified on the forehead and a mean density of 92 follicles on the back. Additionally, Pagnoni et al. found a density of 455 HFs on the lateral forehead and the highest density on the nasal wing, with 1220 follicles per cm^2.[33] However, because of the relatively lower growth of the head in comparison to the extremities, the HFs are much more numerous on the face and scalp than on the legs and arms.[33] On the other hand, Otberg et al. stated that the highest HF density and percentage of follicular orifices on the skin and infundibular surfaces were observed on the forehead, whereas the highest average size of the follicular orifices was measured in the calf region.[22] In their study, the highest infundibular volume, and therefore a potential follicular reservoir, was calculated for the forehead and the calf region, although the calf region showed the lowest HF density.

Studies on the functions, molecular mechanisms and hormonal controls of HFSCs continue. In the research literature, there were no studies on the expression of HF specific markers in vellus type HFs in different regions of the human body as well as terminal HFs. Therefore, the knowledge of IR intensity of specific markers in the HFs obtained from different areas can be important for understanding the characteristics of the isolated HF. This was a preliminary study that investigated the IR of specific markers in the HFs according to different skin regions. Here, we have shown that the IR of HF specific markers can vary according to different skin regions. These findings might play a crucial role for tissue sample diagnosis and prognosis of being both biologically and clinically important in the future, and could be exploited for research and therapeutic purposes. Further studies are required to address whether the differences in the expression patterns of molecular markers is a result of an age-related dissociation or a site-specific differentiation at the tissue and cellular levels in humans.

References

1. Niemann C, Watt FM. Designer skin: Lineage commitment in postnatal epidermis. *Trends Cell Biol.* 2002;12:185–192.
2. Blanpain C, Lowry WE, Geoghegan A, et al. Self-renewal, multipotency, and the existence of two cell populations within an epithelial stem cell niche. *Cell.* 2004;118:635–648.
3. Langbein L, Rogers MA, Winter H, et al. The catalog of human hair keratins. II. Expression of the six type II members in the hair follicle and the combined catalog of human type I and II keratins. *J Biol Chem.* 2001;276:35123–35132.
4. Magin TM, Vijayaraj P, Leube RE. Structural and regulatory functions of keratins. *Exp Cell Res.* 2007;313:2021–2032.
5. Moll R, Divo M, Langbein L. The human keratins: Biology and pathology. *Histochem Cell Biol.* 2008;129:705–733.
6. Langbein L, Schweizer J. Keratins of the human hair follicle. *Int Rev Cytol.* 2005;243:1–78.
7. Schweizer J, Bowden PE, Coulombe PA, et al. New consensus nomenclature for mammalian keratins. *J Cell Biol.* 2006;174:169–174.
8. Troy TC, Arabzadeh A, Turksen K. Re-assessing K15 as an epidermal stem cell marker. *Stem Cell Rev.* 2011;7(4):927–934.
9. Liu Y, Lyle S, Yang Z, et al. Keratin 15 promoter targets putative epithelial stem cells in the hair follicle bulge. *J Invest Dermatol.* 2003;121:963–968.
10. Webb A, Li A, Kaur P. Location and phenotype of human adult keratinocyte stem cells of the skin. *Differentiation.* 2004;72:387–395.
11. Pontiggia L, Biedermann T, Meuli M, et al. Markers to evaluate the quality and self-renewing potential of engineered human skin substitutes in vitro and after transplantation. *J Invest Dermatol.* 2009;129:480–490.
12. Roh C, Roche M, Guo Z, et al. Multi-potentiality of a new immortalized epithelial stem cell line derived from human hair follicles. *In Vitro Cell Dev Biol Anim.* 2008;44:236–244.
13. Blanpain C, Fuchs E. Epidermal homeostasis: A balancing act of stem cells in the skin. *Nat Rev Mol Cell Biol.* 2009;10:207–217.
14. Ohyama M, Terunuma A, Tock CL, et al. Characterization and isolation of stem cell-enriched human hair follicle bulge cells. *J Clin Invest.* 2006;116:249–260.
15. Omoto M, Miyashita H, Shimmura S, et al. The use of human mesenchymal stem cell-derived feeder cells for the cultivation of transplantable epithelial sheets. *Invest Ophthalmol Vis Sci.* 2009;50:2109–2115.
16. Hsu YC, Pasolli HA, Fuchs E. Dynamics between stem cells, niche, and progeny in the hair follicle. *Cell.* 2011;144:92–105.
17. Scholzen T, Gerdes J. The Ki-67 protein: From the known and the unknown. *J Cell Physiol.* 2000;182:311–322.
18. Kloepper JE, Sugawara K, Al-Nuaimi Y, et al. Methods in hair research: How to objectively distinguish between anagen and catagen in human hair follicle organ culture. *Exp Dermatol.* 2010;19:305–312.
19. Chamcheu JC, Siddiqui IA, Syed DN, et al. Keratin gene mutations in disorders of human skin and its appendages. *Arch Biochem Biophys.* 2011;508:123–137.
20. Mohanty S, Kumar A, Dhawan J, et al. Noncultured extracted hair follicle outer root sheath cell suspension for transplantation in vitiligo. *Br J Dermatol.* 2011;164:1241–1246.
21. Harries MJ, Meyer KC, Chaudhry IH, et al. Does collapse of immune privilege in the hair-follicle bulge play a role in the pathogenesis of primary cicatricial alopecia? *Clin Exp Dermatol.* 2010;35:637–644.
22. Otberg N, Richter H, Schaefer H, et al. Variations of hair follicle size and distribution in different body sites. *J Invest Dermatol.* 2004;122:14–19.
23. Kloepper JE, Tiede S, Brinckmann J, et al. Immunophenotyping of the human bulge region: The quest to define useful in situ markers for human epithelial hair follicle stem cells and their niche. *Exp Dermatol.* 2008;17:592–609.
24. Foitzik K, Hoting E, Förster T, et al. L-carnitine–L-tartrate promotes human hair growth in vitro. *Exp Dermatol.* 2007;16:936–945.
25. Garcin CL, Ansell DM, Headon DJ, et al. Hair follicle bulge stem cells appear dispensable for the acute phase of wound re-epithelialisation. *Stem Cells.* 2016;34:1377–1385.
26. Bose A, Teh MT, Mackenzie IC, et al. Keratin K15 as a biomarker of epidermal stem cells. *Int J Mol Sci.* 2013;14:19385–19398.
27. Stenn KS, Cotsarelis G. Bioengineering the hair follicle: Fringe benefits of stem cell technology. *Curr Opin Biotechnol.* 2005;16:493–497.
28. Evangelista MT, North JP. Comparative analysis of cytokeratin 15, TDAG51, cytokeratin 20 and androgen receptor in sclerosing adnexal neoplasms and variants of basal cell carcinoma. *J Cutan Pathol.* 2015;42:824–831.
29. Quist SR, Eckardt M, Kriesche A, et al. Expression of epidermal stem cell markers in skin and adnexal malignancies. *Br J Dermatol.* 2016;175:520–530.

30. Geyfman M, Plikus MV, Treffeisen E, et al. Resting no more: Re-defining telogen, the maintenance stage of the hair growth cycle. *Biol Rev Camb Philos Soc*. 2015;90:1179–1196.
31. Xu S, Shuang L, Xia H, et al. Differentiation of hepatocytes from induced pluripotent stem cells derived from human hair follicle mesenchymal stem cells. *Cell Tissue Res*. 2016;366:89–99.
32. Blume U, Ferracin J, Verschoore M, et al. Physiology of the vellus hair follicle. Hair growth and sebum excretion. *Br J Dermatol*. 1991;124:21–28.
33. Pagnoni AP, Kligman AM, Gammal SEL, et al. Determination of density of follicles on various regions of the face by cyanoacrylate biopsy: Correlation with sebum output. *Br J Dermatol*. 1994;131:862–865.

Differential altered expression of let-7a and miR-205 tumor-suppressor miRNAs in different subtypes of breast cancer under treatment with Taxol

Faezeh Asghari[1,2,A–D], Navideh Haghnavaz[1,A,B], Darioush Shanehbandi[1,B,C], Vahid Khaze[1,C], Behzad Baradaran[1,A], Tohid Kazemi[1,A,B,E,F]

[1] Immunology Research Center, Tabriz University of Medical Sciences, Iran
[2] Student Research Committee, Tabriz University of Medical Sciences, Iran

A – research concept and design; B – collection and/or assembly of data; C – data analysis and interpretation; D – writing the article; E – critical revision of the article; F – final approval of the article

Advances in Clinical and Experimental Medicine, ISSN 1899-5276 (print), ISSN 2451-2680 (online) *Adv Clin Exp Med*. 2018;27(7):941–945

Address for correspondence
Tohid Kazemi
E-mail: tkazemi@gmail.com

Funding sources
This study was performed with a grant from the Immunology Research Center, Tabriz University of Medical Sciences, Iran (grant No. 93-86).

Conflict of interest
None declared

Received on December 16, 2016
Reviewed on January 12, 2017
Accepted on April 26, 2017

Abstract

Background. MicroRNAs (miRNAs) are small non-coding RNAs which have been considered as major players in the process of carcinogenesis and drug responsiveness of breast cancer.

Objectives. In this study, we aimed to investigate the expression pattern of let-7a and miR-205 tumor-suppressor miRNAs in breast cancer cell lines under treatment with paclitaxel.

Material and methods. The half maximal inhibitory concentration (IC_{50}) of paclitaxel was determined for 4 breast cancer cell lines, including MCF-7, MDA-MB-231, SKBR-3, and BT-474 by an MTT assay. The expression level of let-7a and miR-205, and their targets, *K-RAS* and *HER3*, was determined before and after treatment with paclitaxel, using quantitative reverse transcriptase real-time polymerase chain reaction (qRT-PCR).

Results. After treatment, the expression level of both let-7a and miR-205 was significantly increased in *HER2*-overexpressing cell line BT-474 (26.4- and 7.2-fold, respectively). In contrast, the *HER2*-negative cell lines MCF-7 and MDA-MB-231 showed a significantly decreased expression of both let-7a (30.3- and 13.5-fold, respectively) and miR-205 (20- and 18.1-fold, respectively). Controversially, SKBR-3 revealed a significantly decreased expression of both let-7a (1.3-fold) and miR-205 (1.3-fold). The expression level of *K-RAS* as a target of let-7a decreased in all cell lines significantly, but the pattern of alteration in the expression level of *HER3* as a target of miR-205 in all cell lines was the reverse of the pattern of alteration in the expression level of miR-205.

Conclusions. Our results confirmed a better response of *HER2*-overexpressing breast cancer to paclitaxel at the miRNA level. One putative reason could be the upregulation of tumor-suppressor miRNAs after treatment with paclitaxel. On the other hand, *HER2*-negative breast cancer cell lines showed a significantly decreased expression of tumor-suppressor miRNAs, a putative mechanism of resisting the therapy.

Key words: breast cancer, microRNA, tumor-suppressor, Taxol

DOI
10.17219/acem/70745

Introduction

During the past decades, breast cancer has been the most frequent type of carcinoma and the second most fatal cancer among women worldwide. Importantly, both the prevalence and mortality of breast cancer is increasing[1]; it has been estimated that 249,260 new cases and 40,890 deaths due to breast cancer will occur in the United States in 2016.[2] Breast cancer occurs as a result of a collection of genetic alterations and environmental factors.[3] Among the well-known genetic loci related to breast cancer are: breast cancer susceptibility gene 1 (*BRCA1*) and breast cancer susceptibility gene 2 (*BRCA2*), human epidermal growth factor receptor-2 (*HER-2*) and tumor protein p53 (*TP53*).[4–6] Dietary habits like consuming fat-rich foods, presence of chemical substances in food, long exposure to estrogen, e.g., excessive use of steroids, and use of alcohol are examples of environmental risk factors.[3,7] Breast cancer is a heterogenic disease which includes molecular subtypes, characterized by immunohistochemical expression of estrogen receptor (*ER*), progesterone receptor (*PR*) and *HER-2*. These molecular subtypes differ in response to treatment, progression and preferential organs to metastasis.[8,9] The treatment approaches for breast cancer are surgery, radiation and chemotherapy with different agents, such as taxanes, anthracyclines, hormone-based drugs, and also targeted therapy with monoclonal antibodies.[10]

Taxol (paclitaxel) is a member of the taxane family with a plant origin that is among the effective chemotherapy agents in the treatment of breast cancer. The mechanism of its action is the induction of dimerization and the prevention of depolymerization of tubulins. Cells lose their flexibility and cannot divide, thus, the tumor progression is stopped. Paclitaxel can be used alone or in combination with other chemotherapy or immunological agents as first-line and also salvage therapy in advanced tumors. Particularly, the use of paclitaxel in a regimen including anthracycline significantly improves the chance of survival.[11]

MicroRNAs (miRNAs) are a group of conserved non-coding RNAs which regulate gene expression through the regulation of targeted mRNAs or the prevention of their translation. They play an essential role in cellular processes, and subsequently various physiological and pathological conditions, such as cancer.[12,13] The first study related to the importance of miRNAs in breast cancer was done in 2005, and it demonstrated a significant deregulation of 5 miRNAs in breast cancer.[14] Since then, studies have been improved in this context and shown the importance of miRNAs in the prognosis, metastasis and drug resistance of different subtypes of breast cancer. As a general rule, the miRNAs involved in breast cancer include 2 groups: oncomirs with oncogenic nature (which are upregulated during carcinogenesis) and tumor-suppressor ones with the ability to prevent breast cancer initiation, progression and metastasis (downregulated in malignancy). Several miRNAs have been introduced in breast cancer as tumor-suppressors which target the mRNAs of oncogenes. Among the best-known tumor suppressor miRNAs are the let-7 family and miR-205.[15] Let-7 is the second identified miRNA in *Caenorhabditis elegans* and the first one in humans. The let-7 family contains 13 members encoded from different loci. The role of this family of miRNAs is promoting differentiation, and their expression is low in embryonic and cancerous cells because of poor differentiation.[16] As the let-7 family of miRNAs target mRNAs of some important oncogenes, such as *RAS* and *HMGA2*, several studies have introduced this family of miRNAs as tumor-suppressor miRNAs in breast cancer.[17–21] MiR-205 is located in 1q32.2 and plays a role in the evolution of 3 organs: the breast, prostate and thymus.[22] Studies on the relation of this miRNA to breast cancer have demonstrated the tumor-suppressing nature of miR-205.[19] Among the oncogenes targeted by miR-205 are *HER-3* and vascular endothelial growth factor-A (*VEGF-A*), with roles in promoting cell proliferation, angiogenesis and metastasis.[23]

Because of the role of tumor-suppressor miRNAs in preventing breast cancer progression and the usefulness of them in predicting the outcome and response of cancer to treatment, the aim of this study was to investigate the effect of the anticancer drug paclitaxel on the expression levels of let-7a and miR-205 and their targets in different subtypes of breast cancer cell lines.

Material and methods

Cell culture

The human breast cancer cell lines MCF-7, MDA-MB-231, SKBR3, and BT-474 were purchased from the national cell bank of Iran (Pasteur Institute, Tehran, Iran) and cultured in RPMI1640 (Gibco; Thermo Fisher, Waltham, USA) medium supplemented with 10% fetal bovine serum (FBS) (Gibco), penicillin (100 IU/mL) and streptomycin (100 mg/mL) at 37°C with 5% CO_2 and humidified air.

MTT assay

The inhibitory concentration 50% (IC_{50}) of paclitaxel was determined for each cell line with an MTT assay. Briefly, 15×10^3 cells of each cell line were seeded in 96-well plates. After reaching 70–80% confluency, the cells were treated with different concentrations of paclitaxel. After 24 h of treatment, MTT dye (Sigma-Aldrich, St. Louis, USA), and subsequently its dissolvers, dimethyl sulfoxide (DMSO) and Sorenson's buffer, were added. The optical density (OD) of each concentration was measured at 570 nm and IC_{50} was calculated using Prism v. 6.0 software (Graphpad Software, La Jolla, USA). The MTT assay was performed in 2 steps. First, all cell lines were treated with concentrations of 0.1 nM, 1 nM, 10 nM, 100 nM, 1 µM, 10 µM, and 100 µM. According to the data from step 1 and

determining the narrower range of paclitaxel concentration, the cells were treated with limited concentration ranges (for MCF-7: 125 nM, 250 nM, 500 nM, 1000 nM, 2000 nM, 4000 nM, and 8000 nM; for MDA-MB-231: 153 nM, 306 nM, 612 nM, 1225 nM, 2450 nM, 4900 nM, and 9800 nM; for SKBR3: 100 nM, 1000 nM, 10,000 nM, 25,000 nM, 50,000 nM, 100,000 nM, and 250,000 nM; for BT-474: 0.1 nM, 1 nM, 10 nM, 25 nM, 50 nM, 100 nM, and 250 nM). All assays were done in triplicate.

RNA extraction and complementary DNA synthesis

In the study, 10^5 cells were seeded in a 6-well plate overnight, and paclitaxel was added to the wells in IC_{50} concentrations determined by the MTT assay. After 24 h, total RNA was extracted from both untreated (as a control group) and treated cells by RNX-PLUS reagent (SinaClon; Vivantis, Tehran, Iran) according to the manufacturer's instructions. The quality and quantity of the extracted RNAs were evaluated using spectrophotometry and agarose gel electrophoresis. For miRNA detection, complementary DNA (cDNA) samples were prepared by Universal cDNA Synthesis Kit II (Exiqon A/S, Vedbæk, Denmark) according to kit instructions.

The cDNA synthesis for the quantification of the expression level of target mRNAs was performed as described elsewhere.[24]

Quantitative real-time polymerase chain reaction

The expression levels of all miRNAs and mRNAs in each cell line before and after treatment with paclitaxel were assessed using SYBR green-based quantitative reverse transcriptase real-time polymerase chain reaction (qRT-PCR) (Yekta Tajhiz Azma, Tehran, Iran). We used U6 as an internal control to normalize the miRNAs level expression and β-actin (for cell lines MCF-7, MDA-MB-231 and SKBR3) and glyceraldehyde 3-phosphate dehydrogenase (*GAPDH*) (for BT-474) to normalize real-time PCR data for the expression level of the mRNAs of target genes. The sequences of primers used and annealing temperatures are listed in Table 1.

Statistical analysis

Statistical analysis was performed with Prism v. 6.0 software (Graphpad Software). We used a multiple t-test to compare the data of the 2 groups (treated and untreated); p-values <0.05 were considered statistically significant.

Results

Inhibitory concentration 50% of paclitaxel for breast cancer cell lines

To determine IC_{50} concentration of paclitaxel for each cell line, the MTT assay was run in 2 steps, first with a larger range, and then with a limited range. Our results showed specific IC_{50} concentrations of paclitaxel for each cell line: 3.5 μM for MCF-7, 0.3 μM for MDA-MB-231, 4 μM for SKBR3, and 19 nM for BT-474.

The effect of paclitaxel on the expression levels of let-7a and miR-205, and their targets

The results from quantitative real-time PCR and subsequent statistical analysis showed differential effects of paclitaxel on the expression levels of let-7a and miR-205, and their targets, *K-RAS* and *HER-3*. *HER-2* overexpressing BT-474 cell line showed a different pattern of altered expression of both miRNAs, i.e., paclitaxel caused a significant overexpression of let-7a (26.4-fold) and miR-205 (7.2-fold) (Fig. 1A,1C). Inversely, SKBR-3, MCF-7 and MDA-MB-231 showed a significant downregulation of both miRNAs. It is important to note that this effect is much less pronounced in the *HER-2* positive SKBR-3 cell line (1.3-fold for both miRNAs, let-7a and miR-205) in comparison to the

Table 1. Sequences of primers and annealing temperatures used for quantitative real-time PCR

Target gene	Primer sequence	Annealing temperature [°C]
*Let-7a**	5′-UGAGGUAGUAGGUUGUAUAGUU-3′	60
*miR-205**	5′-UCCUUCAUUCCACCGGAGUCUG-3′	60
*U6**	5′-GGG CAG GAA GAG GGC CTA T-3′	60
K-RAS	F: 5′-CTCCCTGTGTCAGACTGCTCTTT-3′ R: 5′-GGCCTTGCAACCTTGGTCTCTTG-3′	60
HER-3	F: 5′-TCTACTCTACCATTGCCCAACC-3′ R: 5′-GGAACCATCGGGAACTGACC-3′	59
β-actin	F: 5′-TCCCTGGAGAAGAGCTACG-3′ R: 5′-GTAGTTTCGTGGATGCCACA-3′	59
GAPDH	F: 5′-CAAGATCATCACCAATGCCT-3′ R: 5′- CCCATCACGCCACAGTTTCC-3′	59

PCR – polymerase chain reaction; * sequence for target gene.

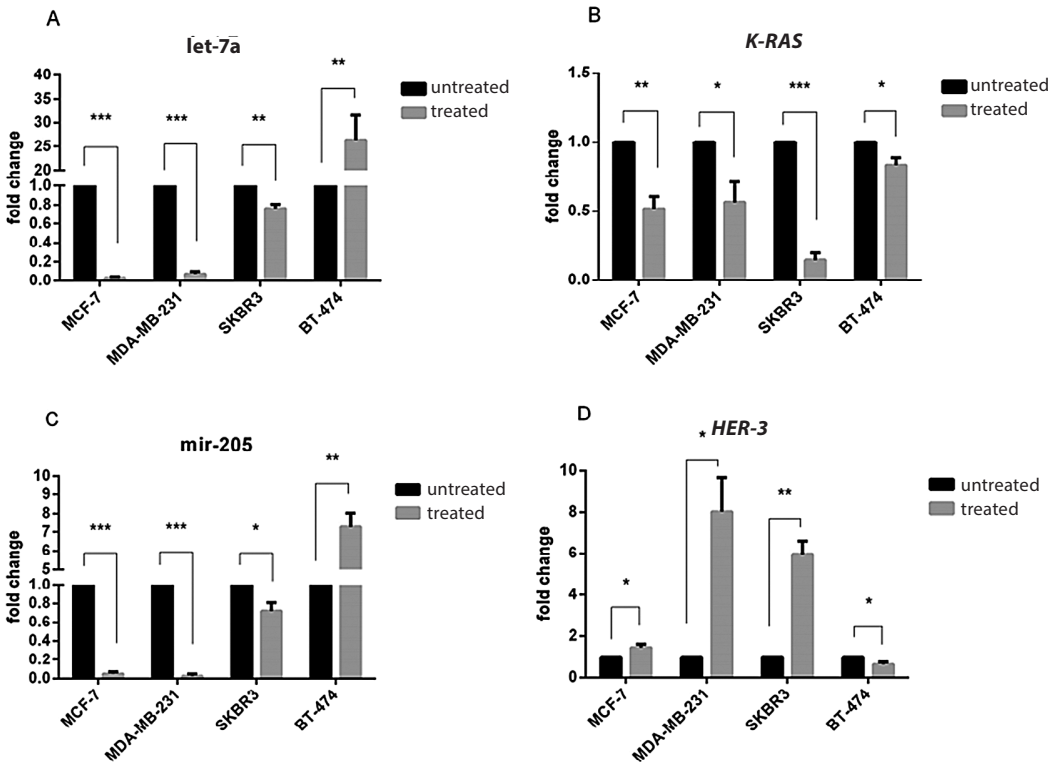

Fig. 1. Alterations in the expression level of miRNAs and targeted mRNAs

The expression level of let-7a (A) and its target, *K-RAS* (B), miR-205 (C) and its target, *HER-3* (D) was quantitatively evaluated before and after treatment of the MCF-7, MDA-MB-231, SKBR3, and BT-474 cell lines with paclitaxel, using quantitative real-time PCR. The expression levels of the 2 miRNAs were significantly decreased in 3 cell lines – MCF-7, MDA-MB-231 and SKBR3 – and significantly increased in BT-474. *K-RAS* showed significantly decreased levels in all cell lines, but *HER-3* was upregulated except for in the BT-474 cell line. * $p < 0.05$; ** $p < 0.005$; *** $p < 0.0005$.

HER-2 negative MCF-7 (30.3-fold for let-7a and 20-fold for miR-205) and MDA-MB-231 (13.5-fold for let-7a and 38.4-fold for miR-205) cell lines (Fig. 1A,1C).

Altered expression of *K-RAS* and *HER-3* as targets for let-7a and miR-205, respectively, was found controversial. K-RAS showed a significantly reduced expression in BT-474 (1.2-fold), SKBR-3 (7.4-fold), MCF-7 (1.96-fold), and MDA-MB-231 (1.76-fold) (Fig. 1B). On the other hand, *HER-3* showed an altered expression level related to miR-205. *HER-3* was downregulated in BT-474 (1.58-fold), but upregulated in SKBR-3 (5.9-fold), MCF-7 (1.4-fold) and MDA-MB-231 (8.03-fold) (Fig. 1D).

Discussion

It has been proposed that the altered expression of miRNAs participates in various aspects of cancer, including initiation, progression, metastasis, and drug responsiveness/resistance.[12,25,26] It has been demonstrated that the pattern of miRNA expression can be changed in response to treatment with doxorubicin, 5-fluorouracil and trastuzumab, and this alteration can be useful for predicting the outcome of the therapy.[26–28] However, there is no clear knowledge of the molecular mechanism of paclitaxel with regards to its effect on miRNAs expression. For that reason, we aimed in this study to evaluate the expression level of 2 tumor-suppressor miRNAs, let-7a and miR-205, before and after treatment with paclitaxel. Our results showed that the expression of the miRNAs were significantly altered in response to paclitaxel, but these alterations were different in each subtype of breast cancer.

In our study, the expression level of both tumor-suppressor miRNAs, let-7a and miR-205, showed a significant decrease in 2 *HER-2* negative cell lines, MCF-7 and MDA-MB-231, which was in opposition to the anticancer feature of the drug. Rossi et al. demonstrated that the expression level of miR-21, as an oncomir in various types of cancer, is increased after the administration of 5-fluorouracil in resistant cells of colon cancer. They described this observation as a defense mechanism to resist the chemotherapy.[29] According to the studies done by Konecny et al. and Hayes et al., *HER-2* negative breast tumors show more resistance in response to paclitaxel in comparison to *HER-2* positive ones.[30,31] Our study showed that one of the probable molecular mechanisms of the resistance and a poor response to paclitaxel in *HER-2* negative tumors could be a decreased expression of tumor-suppressor miRNAs let-7a and miR-205.

In contrast, we observed a significant increase in the expression level of both miRNAs in the BT-474 cell line, with the overexpression of the *HER-2* receptor. According to the studies mentioned above, breast cancers with a high expression level of the *HER-2* receptor respond better to paclitaxel therapy, and one molecular mechanism could be the overexpression of tumor-suppressor miRNAs, as we showed.[30,32]

In our study, SKBR-3, which also expresses the *HER-2* receptor, showed a decreased expression of both miR-205 and let-7a after treatment with paclitaxel. According to Ichikawa et al., the genome amplification of the *HER-2* receptor is high, but the expression of this receptor is poor in SKBR-3 in comparison to BT-474.[27] This could justify our results that showed a decreased expression of let-7a and

miR-205 in contrast to BT-474, and much less underexpression than the *HER-2* negative MCF-7 and MDA-MB-231 cell lines. Collectively, our results showed a dependence of the altered expression of let-7a and miR-205 and *HER2*-positivity.

For more evaluation of the molecular aspects of treatment with paclitaxel, we also determined the alterations of expression of *K-RAS* as the target of let-7a and *HER-3* as the target of miR-205.[17,23] Treatment with paclitaxel caused a significant underexpression of *K-RAS* in 4 studied cell lines. It has been previously shown that the downregulation of *K-RAS* is one of the molecular mechanisms of the effect of paclitaxel, and our results confirmed this finding.[33] However, except for in BT-474, the underexpression of let-7a was not in agreement with a decreased expression of *K-RAS* (Fig. 1A,1B). One possible explanation could be multiple regulatory mechanisms for controlling the expression of *K-RAS*, one of the best-known and important oncogenes in most types of cancer.

HER-3, on the other hand, showed a consistent altered expression with the expression of miR-205 in all cell lines (Fig. 1C,1D), albeit with a little inconsistency in the fold change.

Conclusions

Conclusively, treatment of breast cancer cells causes alterations in the expression level of let-7a and miR-205, and also in their targets, *K-RAS* and *HER-3*. The pattern of such alterations is different, depending on the molecular subtype of breast cancer. Such findings could be a molecular reason for the different responsiveness of different subtypes of breast cancer. However, more extensive studies are needed to find the exact and detailed molecular markers for predicting response to therapy.

References

1. Bombonati A, Sgroi DC. The molecular pathology of breast cancer progression. *J Pathol*. 2011;223(2):308–318.
2. Siegel RL, Miller KD, Jemal A. Cancer statistics, 2016. *CA Cancer J Clin*. 2016;66(1):7–30.
3. Kamińska M, Ciszewski T, Łopacka-Szatan K, Miotła P, Starosławska E. Breast cancer risk factors. *Prz Menopauz*. 2015;14(3):196.
4. Ford D, Easton D, Stratton M, et al. Genetic heterogeneity and penetrance analysis of the *BRCA1* and *BRCA2* genes in breast cancer families. *Am J Hum Genet*. 1998;62(3):676–689.
5. Press MF, Pike MC, Chazin VR, et al. Her-2/neu expression in node-negative breast cancer: Direct tissue quantitation by computerized image analysis and association of overexpression with increased risk of recurrent disease. *Cancer Res*. 1993;53(20):4960–4970.
6. Walerych D, Napoli M, Collavin L, Del Sal G. The rebel angel: Mutant p53 as the driving oncogene in breast cancer. *Carcinogenesis*. 2012; 33(11):2007–2017.
7. Nelson HD, Zakher B, Cantor A, et al. Risk factors for breast cancer for women aged 40 to 49 years: A systematic review and meta-analysis. *Ann Intern Med*. 2012;156(9):635–648.
8. Polyak K. Heterogeneity in breast cancer. *J Clin Invest*. 2011;121(10): 3786.
9. Yang XR, Chang-Claude J, Goode EL, et al. Associations of breast cancer risk factors with tumor subtypes: A pooled analysis from the Breast Cancer Association Consortium studies. *J Natl Cancer Inst*. 2011;103(3):250–263.
10. DeSantis CE, Lin CC, Mariotto AB, et al. Cancer treatment and survivorship statistics, 2014. *CA Cancer J Clin*. 2014;64(4):252–271.
11. Patt D, Gauthier M, Giordano S. Paclitaxel in breast cancer. *Womens Health (Lond)*. 2006;2(1):11–21.
12. Jansson MD, Lund AH. MicroRNA and cancer. *Mol Oncol*. 2012;6(6): 590–610.
13. Pritchard CC, Cheng HH, Tewari M. MicroRNA profiling: Approaches and considerations. *Nat Rev Genet*. 2012;13(5):358–369.
14. Iorio MV, Ferracin M, Liu C-G, et al. MicroRNA gene expression deregulation in human breast cancer. *Cancer Res*. 2005;65(16):7065–7070.
15. Kent O, Mendell J. A small piece in the cancer puzzle: MicroRNAs as tumor suppressors and oncogenes. *Oncogene*. 2006;25(46): 6188–6196.
16. Roush S, Slack FJ. The let-7 family of microRNAs. *Trends Cell Biol*. 2008; 18(10):505–516.
17. Johnson SM, Grosshans H, Shingara J, et al. RAS is regulated by the let-7 microRNA family. *Cell*. 2005;120(5):635–647.
18. Mayr C, Hemann MT, Bartel DP. Disrupting the pairing between let-7 and Hmga2 enhances oncogenic transformation. *Science*. 2007;315 (5818): 1576–1579.
19. Asghari F, Haghnavaz N, Baradaran B, Hemmatzadeh M, Kazemi T. Tumor suppressor microRNAs: Targeted molecules and signaling pathways in breast cancer. *Biomed Pharmacother*. 2016;81:305–317.
20. Oliveras-Ferraros C, Cufí S, Vazquez-Martin A, et al. Micro (mi) RNA expression profile of breast cancer epithelial cells treated with the anti-diabetic drug metformin: Induction of the tumor suppressor miRNA let-7a and suppression of the TGFβ-induced oncomiR miRNA-181a. *Cell Cycle*. 2011;10(7):1144–1151.
21. Yu F, Yao H, Zhu P, et al. let-7 regulates self renewal and tumorigenicity of breast cancer cells. *Cell*. 2007;131(6):1109–1123.
22. Shingara J, Keiger K, Shelton J, et al. An optimized isolation and labeling platform for accurate microRNA expression profiling. *RNA*. 2005; 11(9):1461–1470.
23. Wu H, Zhu S, Mo Y-Y. Suppression of cell growth and invasion by miR-205 in breast cancer. *Cell Res*. 2009;19(4):439–448.
24. Kazemi T, Asgarian-Omran H, Memarian A, et al. Low representation of Fc receptor-like 1–5 molecules in leukemic cells from Iranian patients with acute lymphoblastic leukemia. *Cancer Immunol Immunother*. 2009;58(6):989–996.
25. Hemmatzadeh M, Mohammadi H, Karimi M, Musavishenas MH, Baradaran B. Differential role of microRNAs in the pathogenesis and treatment of esophageal cancer. *Biomed Pharmacother*. 2016;82: 509–519.
26. Kovalchuk O, Filkowski J, Meservy J, et al. Involvement of microRNA-451 in resistance of the MCF-7 breast cancer cells to chemotherapeutic drug doxorubicin. *Mol Cancer Ther*. 2008;7(7):2152–2159.
27. Ichikawa T, Sato F, Terasawa K, et al. Trastuzumab produces therapeutic actions by upregulating miR-26a and miR-30b in breast cancer cells. *PLoS ONE*. 2012;7(2):e31422.
28. Shah MY, Pan X, Fix LN, Farwell MA, Zhang B. 5-fluorouracil drug alters the microRNA expression profiles in MCF-7 breast cancer cells. *J Cell Physiol*. 2011;226(7):1868–1878.
29. Rossi L, Bonmassar E, Faraoni I. Modification of miR gene expression pattern in human colon cancer cells following exposure to 5-fluorouracil in vitro. *Pharmacol Res*. 2007;56(3):248–253.
30. Konecny GE, Thomssen C, Lück HJ, et al. Her-2/neu gene amplification and response to paclitaxel in patients with metastatic breast cancer. *J Natl Cancer Inst*. 2004;96(15):1141–1151.
31. Hayes DF, Thor AD, Dressler LG, et al. HER2 and response to paclitaxel in node-positive breast cancer. *N Engl J Med*. 2007;357(15):1496–1506.
32. Roukos DH. HER2 and response to paclitaxel in node-positive breast cancer. *N Engl J Med*. 2008;358(2):197.
33. Thissen JA, Gross JM, Subramanian K, Meyer T, Casey PJ. Prenylation-dependent association of Ki-Ras with microtubules: Evidence for a role in subcellular trafficking. *J Biol Chem*. 1997;272(48):30362–30370.

Myeloid-derived suppressor cell accumulation in renal cell carcinoma is correlated with CCL2, IL-17 and IL-18 expression in blood and tumors

Xiaodong Guan[1,A–D], Zhiyu Liu[2,A,C–E], Jianhua Zhang[3,A,D,E], Xunbo Jin[1,A,C–F]

[1] Shandong Provincial Hospital, Shandong University, Jinan, China
[2] Department of Urinary Surgery, Second Hospital of Dalian Medical University, China
[3] Yuncheng Central Hospital, China

A – research concept and design; B – collection and/or assembly of data; C – data analysis and interpretation;
D – writing the article; E – critical revision of the article; F – final approval of the article

Advances in Clinical and Experimental Medicine, ISSN 1899-5276 (print), ISSN 2451-2680 (online) *Adv Clin Exp Med*. 2018;27(7):947–953

Address for correspondence
Xunbo Jin
E-mail: xunbojn@gmail.com

Funding sources
None declared

Conflict of interest
None declared

Received on January 5, 2017
Reviewed on February 28, 2017
Accepted on March 30, 2017

Abstract

Background. Myeloid-derived suppressor cells (MDSC) play an important role in tumor-mediated immune evasion. Levels of MDSC in peripheral blood are increased in patients with cancer, correlating with cancer stage and outcome. Studies have confirmed the associations between MDSC and various cytokines in the peripheral blood of murine and human cancer hosts. However, little is known about the association between parenchymal MDSC subsets and cytokines, or the mechanism drawing MDSC into tumor parenchyma.

Objectives. The aim of this study was to analyze the correlation between MDSC subsets and tumor grade as well as stage in renal cell carcinoma (RCC) patients. The expression of chemokine (C-C motif) ligand 2 (CCL2), interleukin 17 (IL-17) and interleukin 18 (IL-18) in the peripheral blood and parenchyma of RCC patients was also detected to explore its correlation with MDSC accumulation.

Material and methods. Total MDSC, granulocytic MDSC (G-MDSC), monocytic MDSC (M-MDSC), and immature MDSC (I-MDSC) from the blood and parenchyma were isolated and analyzed by flow cytometry. Cytokines were detected by the enzyme-linked immunosorbent assay (ELISA), real-time polymerase chain reaction (PCR) and western blot in blood and tumors.

Results. Parenchymal levels of MDSC had a positive correlation with levels of CCL2, IL-17, and IL-18, suggesting these cytokines may attract MDSC into the parenchyma. Moreover, peripheral total MDSC, G-MDSC and I-MDSC were shown to correlate with tumor grade and stage. Gene and protein expression of CCL2, IL-17, and IL-18 was significantly increased in blood and tumors of RCC patients.

Conclusions. Our study has provided potential new targets for the risk stratification of patients with limited stages of renal carcinoma, in addition to elucidating a possible association between MDSC subsets and cytokine-induced migration into the tumor tissue.

Key words: chemokine (C-C motif) ligand 2, renal cell carcinoma, interleukin 17, interleukin 18, myeloid-derived suppressor cells

DOI
10.17219/acem/70065

Introduction

Renal cell carcinoma (RCC) is a kidney cancer originating in the lining of the proximal convoluted tubule and is the most common type of kidney cancer in adults, responsible for approx. 90–95% of cases. It accounts for approx. 3% of adult malignancies, with close to 64,000 new cases diagnosed every year and with a consistent increase in the incidence rate.[1] It is well-known that tumor-mediated immunosuppression of the microenvironment and immune evasion contribute to decreased clinical efficacy of immune and targeted therapy.[2,3] Various cell types are involved in tumor-mediated immune suppression, such as regulatory T cells (T_{reg}), tumor-associated macrophages (TAMs), and myeloid-derived suppressor cells (MDSC).[4,5] In particular, as a heterogeneous cell population, MDSC have become the focus of intense study in recent years because of their important role in tumor-associated immune suppression.[6]

Arising from myeloid progenitor cells, MDSC fail to differentiate into mature dendritic cells, granulocytes or macrophages, with the capacity to suppress T cell and natural killer (NK) cell function.[7] These mechanisms to suppress antitumor immunity by MDSC include depletion of L-arginine to arrest T cells in mitosis, cystine sequestration to decrease proliferation, induction of $FOXP3^+$ T_{reg} cells, down-regulation of CD4 and CD8 T cell homing to lymph nodes, etc.[8,9]

Levels of MDSC in peripheral blood are significantly increased in patients with cancer, and correlate with metastatic burden and clinical cancer stage.[10] Granulocytic MDSC (G-MDSC) additionally express CD15 with CD14 negative, whereas monocytic MDSC (M-MDSC) express CD14 with CD15 negative, and immature MDSC (I-MDSC) express neither CD14 nor CD15.[11]

Granulocytic MDSC are the dominant population in peripheral blood in RCC, and have been associated with decreased overall survival (OS) time. Monocytic MDSC levels have also been shown to inversely correlate with OS, and have been described as an independent risk factor for recurrence in hepatocellular carcinoma.[12–14] However, all of these studies pertained only to peripheral MDSC, and to our knowledge, no correlation has been made between intratumoral MDSC levels.

While associations have been confirmed between MDSC and various cytokines in the peripheral blood of murine and human cancer hosts, little is known about the mechanism drawing MDSC directly into the tumor parenchyma.[15] Studies have shown that inflammatory cytokines such as interleukin-17 (IL-17), interleukin-18 (IL-18) and chemokine (C-C motif) ligand 2 (CCL2) are related to stimulation of myeloid cells including tumor-promoting MDSC, inducing the accumulation of MDSC and enhancing their suppression of T cells.[16–21] However, the association of cytokine production and accumulation of MDSC in RCC has not been fully investigated.

Here, we analyzed the relationship between circulating or intratumoral levels of MDSCs and tumor grade and stage in patients with RCC. In addition, we determined the correlation between MDSC subsets and levels of IL-17, IL-18, and CCL2 expression in the parenchyma and peripheral blood in patients with primary RCC tumors. This study elucidates some of the factors that might promote MDSC accumulation and lead to tumor immunosuppression.

Material and methods

Renal cell carcinoma tumor lysates

Primary RCC tumor samples were collected from 55 patients prior to nephrectomy according to the IRB (institutional review board)-approved protocol. A portion of the tumor sample was flash frozen to make lysates using FastPrep-24 (MP Biomedicals, Santa Ana, USA) according to the manufacturer's manual. Briefly, tumor tissue was placed in lysing matrix D tubes with RIPA buffer (Thermo Fisher Scientific, Waltham, USA), protease inhibitor (Sigma-Aldrich, St. Louis, USA) and Halt phosphatase inhibitors (Thermo Fisher), incubated and processed in the FastPrep-24. The lysates were then aliquoted and frozen at –80°C.

Phenotype analysis of myeloid-derived suppressor cells subsets from tumor

Phenotyping of MDSC was performed on fresh tumor samples. Granulocytic MDSC, M-MDSC and I-MDSC from the parenchyma of 55 RCC nephrectomy samples were phenotyped using flow cytometry. The tumor was cut into small fragments followed by digestion for 15 min with enzyme cocktail (collagenase 1 mg/mL, DNase 0.1 mg/mL, and hyaluronidase 2.5 U/mL; Sigma-Aldrich), and then filtered using 70 µm cell strainers (BD Falcon; BD, Franklin Lakes, USA). The single cell suspension was subjected to 30% percoll gradient over 70% percoll gradient to enrich for mononuclear cells, followed by staining cells with anti-CD33 APC, anti-HLA-DR FITC, anti-CD15 PE and anti-CD14 PerCP antibodies, along with appropriate isotype controls (all from BD) for flow cytometry analysis (BD FACSCalibur; BD) and computer analysis (CellQuest Pro; BD). Total MDSC were defined as $CD33^+$ $HLA\text{-}DR^{low/-}$; G-MDSC were defined as $CD33^+$ $HLA\text{-}DR^{low/-}$ $CD14^-CD15^+$; M-MDSC were defined as $CD33^+$ $HLA\text{-}DR^{low/-}$ $CD14^+$ $CD15^-$, and I-MDSC were defined as $CD33^+$ $HLA\text{-}DR^{low/-}$ $CD14^-$ $CD15^-$.

Phenotype analysis of myeloid-derived suppressor cells subsets from peripheral blood

Peripheral blood was obtained prior to surgery from 55 patients with tumors, and 15 controls from healthy donors, in accordance with the IRB protocol. The blood was

subjected to Ficoll-Hypaque density centrifugation and the buffy layer containing peripheral blood mononuclear cells (PBMC), including MDSC, was stained with the same antibodies as the tumor for flow cytometry analysis. The flow data was presented as the percentage of MDSC subsets in the PBMC buffy layer.

Cytokine levels from tumor and peripheral blood

The enzyme-linked immunosorbent assay (ELISA) (R&D Systems, Minneapolis, USA) was used to quantitate levels of IL-17, IL-18 and CCL2 in tumor lysates and plasma according to the manufacturer's instructions. Protein was quantitated by the bicinhoninic acid assay (BCA) (Thermo Fisher) on both parenchymal and peripheral blood samples to ensure that equal amounts of protein were aliquoted in each well. Myeloid-derived suppressor cells subsets were screened with corresponding beads from the tumor lysates.

Quantitative real-time reverse transcription polymerase chain reaction

Samples from the patients and healthy donors were collected and placed in 100 µL of TRIzol reagent (Thermo Fisher) to extract the total RNA. Total RNA from samples was pooled together. Complementary DNA was generated by adding 1 µg of the total RNA to SuperScript master mix (Thermo Fisher) and performing reverse transcription. Quantitative polymerase chain reaction (PCR) and melt-curve analyses were performed using iQ SYBR Green Supermix (Bio-Rad Laboratories, Hercules, USA). The comparative C_t value method was used to quantify the expression of genes of interest in different samples. The mRNA levels were normalized to that of a housekeeping gene, *Rpl19* mRNA.

Western blot

Total cellular protein from the samples of the patients and healthy donors was pooled together and quantified with the BCA protein assay kit. After boiling, equal amounts of protein (50 µg) from each sample were subjected to electrophoresis on a 10% (v/v) sodium dodecyl sulfate (SDS)-polyacrylamide gel. The protein was then electroblotted from gel to a polyvinylidene difluoride (PVDF) membrane. The membrane was blocked with phosphate buffered saline-Tween 20 (PBS-T), containing 5% non-fat milk at room temperature for 1 h, and incubated with the indicated primary antibodies (anti-CCL2 rabbit pAb ab9669, 1:2000; anti-IL-17 rabbit pAb ab79056, 1:1000; anti-IL-18 rabbit pAb ab68435, 1:1000; anti-glyceraldehyde 3-phosphate dehydrogenase (anti-GAPDH) rabbit pAb SC-25778, 1:2000) at 4°C overnight, followed by incubating with the goat-anti-rabbit horseradish peroxidase-conjugated secondary antibody for 1 h. After incubation, the membrane was washed 3 times, and the antigen–antibody complexes were visualized using the enhanced chemiluminescence system.

Statistical analysis

Categorical variables were summarized as frequency counts and percentages. The Wilcoxon rank-sum and Jonckheere-Terpstra tests were used for the comparison of MDSC between patient groups. Spearman rank correlations were used to assess the association between MDSC and inflammatory factors in tumor samples and blood. A p-value <0.05 was considered as significant difference. SAS v. 9.1 software (SAS Institute, Cary, USA) was used for all analyses.

Ethics

The present study was approved by the institutional Human Investigations and Ethics Committee in Shandong Provincial Hospital Affiliated to Shandong University and was conducted in accordance with the Helsinki Declaration. Written informed consent was obtained from patients and healthy donors.

Results

Patient characteristics

The present cohort included 55 patients with RCC prior to nephrectomy. Median age was 62 (range: 43–68), and 42 patients (76%) were male. 52 patients (94%) had clear cell carcinoma, and 3 patients had papillary carcinoma. 13 patients (24%) had grade 2 histology, 25 (45%) had grade 3, and 17 (31%) had grade 4 histology. 28 patients (51%) had stage

Table 1. Patient characteristics

Factor	N (%) or median (range)
Age (range) at diagnosis [years]	62 (43–68)
Gender	
Male	42 (76%)
Female	13 (24%)
Histology	
Clear cell	52 (95%)
Papillary carcinoma	3 (5%)
Grade	
2	13 (24%)
3	25 (45%)
4	17 (31%)
Stage	
1	25 (45%)
2	3 (6%)
3	18 (33%)
4	9 (16%)

I–II, 18 (33%) had stage III, and 9 patients (16%) had metastatic (stage IV) disease at the time of nephrectomy (Table 1). Of the 9 patients with metastases, 5 had lung, lymph node or adrenal involvement, 3 had liver metastasis, and 1 had bone metastasis. No patient had received any systemic anti-cancer treatment prior to nephrectomy. The peripheral blood analysis of MDSC subsets in RCC patients was compared to the same populations in the PBMC fraction from healthy donors.

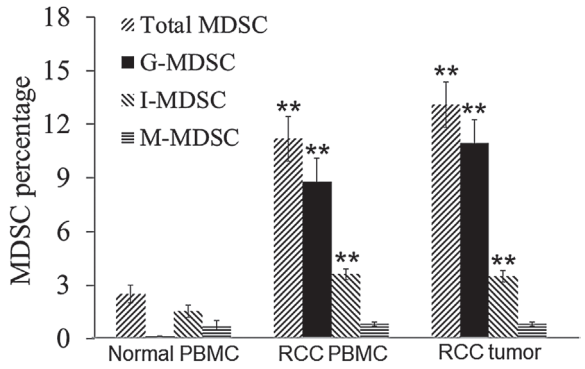

Fig. 1. Percentage of MDSC subsets from normal individuals, RCC patients' PBMC and tumors. Compared to healthy donors, the percentage of MDSC, particularly the G-MDSC and I-MDSC subsets, is significantly increased in the peripheral blood of RCC patients

The data was expressed as mean ±SEM; ** $p < 0.01$ vs normal PBMC; PBMC – peripheral blood mononuclear cells; RCC – renal cell carcinoma; MDSC – myeloid-derived suppressor cells; G-MDSC – granulocytic myeloid-derived suppressor cells; M-MDSC – monocytic myeloid-derived suppressor cells; I-MDSC – immature myeloid-derived suppressor cells.

Myeloid-derived suppressor cells subset levels were increased in renal cell carcinoma patients

Gates were set up for analysis of MDSC subsets based on staining for CD33, HLA-DR, CD15 and CD14. Compared to healthy donor PBMC (n = 15), the number of total MDSC, G-MDSC and I-MDSC was significantly increased in RCC patients (Fig. 1).

Peripheral blood was available from 55 patients with tumors, and 15 normal controls (Table 2). Comparing MDSC subset levels in each cohort, we found that total MDSC were 5.6% (median) in patients vs 2.3% in controls (a 2.43-fold increase, $p < 0.001$). In addition, G-MDSC were 23.75-fold elevated in RCC patients compared to controls (1.9% vs 0.08%, respectively; $p < 0.001$). Immature MDSC

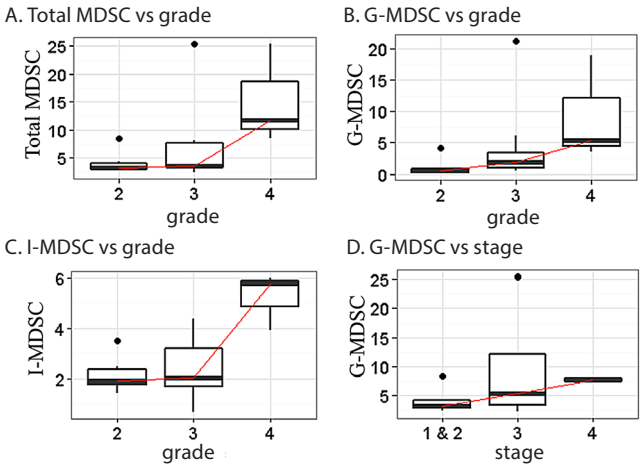

Fig. 2. Peripheral blood MDSC vs grade and stage in RCC patients

RCC – renal cell carcinoma; MDSC – myeloid-derived suppressor cells; G-MDSC – granulocytic myeloid-derived suppressor cells; M-MDSC – monocytic myeloid-derived suppressor cells; I-MDSC – immature myeloid-derived suppressor cells.

were also elevated in patients compared to controls (2.7% vs 1.14%, a 2.37-fold increase; $p < 0.001$). There was no significant difference in the levels of M-MDSC between the 2 cohorts.

Myeloid-derived suppressor cells levels correlate with tumor grade

Increasing peripheral levels of MDSC correlated with higher tumor grade. Specifically, total MDSC, G-MDSC and I-MDSC in the periphery of RCC patients correlated with increasing tumor grade ($p < 0.05$, $p < 0.01$ and $p < 0.05$, respectively) (Fig. 2 A–C). There was no correlation between peripheral M-MDSC level and tumor grade. Moreover, the peripheral level of G-MDSC correlated with higher tumor stage ($p < 0.05$) (Fig. 2 D).

Cytokines were increased in renal cell carcinoma patients

Gene and protein expression of CCL2, IL-17 and IL-18 in PBMC and tumors was detected by real-time PCR and western blot. The results showed that both gene and protein expression was significantly increased in the RCC patients comparing to the healthy donors (Fig. 3–4).

Table 2. Comparison of MDSC subsets in peripheral blood between patients with cancer and healthy donors

Factor	Controls (n = 15)	Patients (n = 55)	p-value*
Total MDSC	2.3 (0.53, 6.8)	5.6 (2.6, 36.8)	<0.001
G-MDSC	0.08 (0.02, 0.35)	1.9 (0.06, 25.7)	<0.001
M-MDSC	0.41 (0.05, 3.4)	0.48 (0.12, 2.8)	0.55
I-MDSC	1.14 (0.36, 4.9)	2.7 (0.73, 7.8)	<0.001

*Wilcoxon rank-sum test; MDSC – myeloid-derived suppressor cells; G-MDSC – granulocytic myeloid-derived suppressor cells; M-MDSC – monocytic myeloid-derived suppressor cells; I-MDSC – immature myeloid-derived suppressor cells; results expressed as medians.

Table 3. Correlation between MDSC and IL-17, IL-18 and CCL2 expression in tumor samples from patients with RCC

Tumor lysate	Cytokines					
	IL-17		IL-18		CCL2	
	COF	p-value	COF	p-value	COF	p-value
Total MDSC	0.71	<0.01	0.62	<0.01	0.49	<0.01
G-MDSC	0.68	<0.01	0.66	<0.01	0.56	<0.01
M-MDSC	–0.21	0.22	–0.28	0.15	–0.17	0.46
I-MDSC	0.39	<0.05	0.12	0.32	0.65	<0.01

COF – coefficient; MDSC – myeloid-derived suppressor cells; G-MDSC – granulocytic myeloid-derived suppressor cells; M-MDSC – monocytic myeloid-derived suppressor cells; I-MDSC – immature myeloid-derived suppressor cells; IL-17 – interleukin-17; IL-18 – interleukin-18; CCL2 – chemokine (C-C motif) ligand 2.

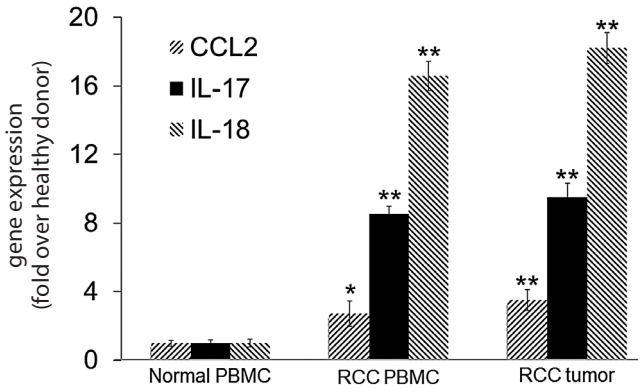

Fig. 3. Cytokine gene expression was increased in the PBMC and tumor lysate of RCC patients

* $p < 0.05$; ** $p < 0.01$ vs normal PBMC; PBMC – peripheral blood mononuclear cells; RCC – renal cell carcinoma; IL-17 – interleukin-17; IL-18 – interleukin-18; CCL2 – chemokine (C-C motif) ligand 2.

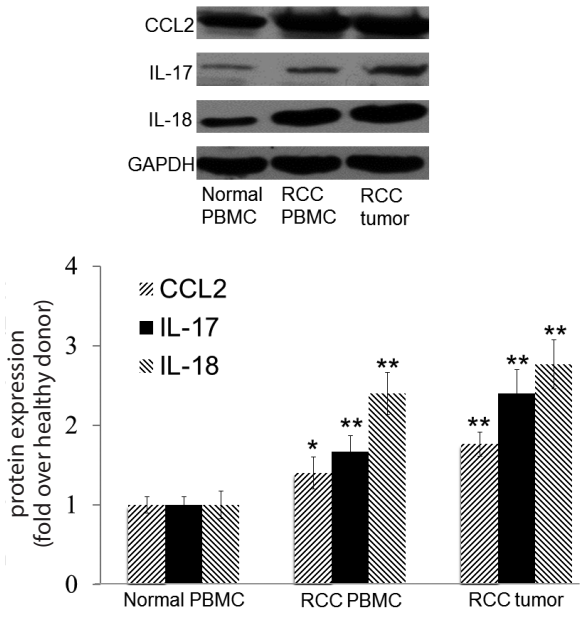

Fig. 4. Cytokine protein expression was increased in the PBMC and tumor lysate of RCC patients

* $p < 0.05$; ** $p < 0.01$ vs normal PBMC; PBMC – peripheral blood mononuclear cells; RCC – renal cell carcinoma; IL-17 – interleukin-17; IL-18 – interleukin-18; CCL2 – chemokine (C-C motif) ligand 2; GAPDH – glyceraldehyde 3-phosphate dehydrogenase.

Myeloid-derived suppressor cells subsets correlate with cytokines

Renal cell carcinoma tumor tissue was examined for expression of cytokines known to promote the trafficking of MDSC and neutrophils. The results showed that parenchymal levels of total MDSC and G-MDSC had a positive correlation with IL-17 ($p < 0.01$), IL-18 ($p < 0.01$) and CCL2 ($p < 0.01$) (Table 3). In addition, levels of I-MDSC correlated positively with IL-17 ($p < 0.05$) and CCL2 ($p < 0.01$), but not IL-18 (Table 3).

Discussion

Myeloid-derived suppressor cells have emerged as key effectors in the tumor microenvironment in many solid tumors, and the factors that influence MDSC recruitment and function continue to expand. In this study, MDSC subset levels in the peripheral blood of RCC patients vs healthy donors were compared and the results showed that total MDSC, as well as G-MDSC and I-MDSC, are elevated in patients, which is consistent with several other studies.[22,23] The levels of M-MDSC did not change significantly, probably due to its lowest subset proportion or its potential differentiation into G-MDSC or TAMs.[24,25] Total MDSC, G-MDSC and I-MDSC in the peripheral blood of RCC patients correlated with increasing tumor grade. Moreover, peripheral levels of G-MDSC correlated with higher tumor stage ($p < 0.05$). Although several other studies have shown a correlation between peripheral MDSC levels and patient outcomes, to the best of our knowledge, this is the first time a correlation has been shown between MDSC subset levels and tumor grade in RCC patients.

Granulocytic MDSC derived from the peripheral blood have been shown to suppress T cell production of interferon gamma (IFN-γ) and T cell proliferation, whose mechanism of suppression is partly dependent on the arginase pathway.[8,12,26] These findings support the idea that G-MDSC have the potential to block the development of an effective antitumor immunity, thereby promoting tumor progression. Another study showed that G-MDSC promoted immune suppression and reduced the

effectiveness of anti-PD-1 antibody therapy in tumor bearing mice. The reduction of G-MDSC with anti-CXCR2 antibody treatment decreased tumor growth and significantly improved in vivo activity of anti-PD-1 treatment.[27] Tumor-associated inflammation contributes to cancer growth and spread, and intratumoral immune cells influence patient prognosis and survival. Various immunomodulatory factors have been linked to increased cancer metastatic potential.[28]

By recruiting monocytes, memory T cells and dendritic cells to the sites of inflammation, CCL2 has been shown to be a chemoattractant for MDSC and functions as a neoplastic factor that regulates MDSC accumulation and function and fosters a tumor permissive microenvironment that influences early-stage carcinogenesis. Chemokine (C-C motif) ligand 2 contributes intratumoral MDSC accumulation and influences MDSC-mediated suppression of $CD4^+$ and $CD8^+$ T cells via distinct pathways. Constitutive deletion or antibody-mediated neutralization of CCL2 halts neoplastic progression in an inflammation-associated tumor model.[20,29]

Interleukin-17 is a pro-inflammatory cytokine that is thought to promote neutrophil chemotaxis and degranulation, and increased expression of IL-17 has been shown in cancer cells and TAMs, suggesting it may play an important role in the regulation of the tumor microenvironment. Previous studies have suggested a causal relationship between IL-17 production and the level of circulating MDSC. Indeed, in addition to IL-6 and tumor necrosis factor alpha (TNF-α), IL-17 has been shown to be significantly increased in RCC tissue, and its expression is dependent on the degree of malignancy.[16,30–32] Here, we showed that parenchymal levels of IL-17 correlate with increased total MDSC ($p < 0.01$), G-MDSC ($p < 0.01$) and I-MDSC ($p < 0.05$). While this data is associative, it again suggests that IL-17 plays an important role in immune modulation of the tumor microenvironment.

Interleukin-18 has been reported to stimulate expression of hematopoietic cytokines and growth factors such as IL-3, IL-6, G-CSF and GM-CSF, which regulate the development of neutrophils and differentiation of hematopoietic cells. Many studies have demonstrated the pivotal role of IL-18 in immune cell activation and tumor progression. Interleukin-18 supplementation significantly enhances the immunosuppressive activity of MDSC.[6,33] As MDSC have a wide range of effects in cancer progression and metastasis, we hypothesized that IL-18 may have certain effects on MDSC biology in RCC.

Although MDSC accumulation correlated with cytokine expression in this study, our sample size was small, which may have led to type II error, such as the inability to discern the difference between chemokine levels in the patients and healthy donors. Moreover, one PBMC sample from a healthy donor and 2 PBMC samples from patients with RCC used for chemokine analysis had been re-thawed one time, which may have led to inter-sample variability. However, based on our experience and results, the difference of chemokine analysis between fresh samples and re-thawed samples is negligible and it does not undermine the reliability of our results. Despite these limitations, our results showed that total MDSC, G-MDSC and I-MDSC were significantly increased in the blood and tumors of RCC patients, and total MDSC, G-MDSC and I-MDSC in peripheral blood correlated with tumor grade. Myeloid-derived suppressor cells were found to correlated with intratumoral levels of IL-17, IL-18 and CCL2, suggesting that these cytokines promote accumulation of MDSC in the parenchyma of the RCC host and MDSC were drawn into the RCC tumor parenchyma by these factors in the tumor milieu. Blocking these cytokines may inhibit MDSC recruitment and delay tumor progression.

Conclusions

Our study has provided potential new targets for the risk stratification of patients with limited stage renal carcinoma, in addition to elucidating a possible association between MDSC subsets and cytokine-induced migration into the tumor tissue. Targeting these cytokines may reduce MDSC number and function, which could enhance the efficacy of immunotherapy and targeted therapy approaches, including immune checkpoint blockade in RCC patients.

References

1. Tsiatas M, Grivas P. Immunobiology and immunotherapy in genitourinary malignancies. *Ann Transl Med*. 2016;4:270–281.
2. Schatton T, Frank MH. Antitumor immunity and cancer stem cells. *Ann N Y Acad Sci*. 2009;1176:154–169.
3. Wilkie KP, Hahnfeldt P. Tumor-immune dynamics regulated in the microenvironment inform the transient nature of immune-induced tumor dormancy. *Cancer Res*. 2013;73:3534–3544.
4. Gabrilovich DI, Nagaraj S. Myeloid-derived suppressor cells as regulators of the immune system. *Nat Rev Immunol*. 2009;9:162–174.
5. Ostrand-Rosenberg S. Myeloid-derived suppressor cells: More mechanisms for inhibiting antitumor immunity. *Cancer Immunol Immunother*. 2010;59:1593–1600.
6. Lim HX, Hong HJ, Cho DH, Kim TS. IL-18 enhances immunosuppressive responses by promoting differentiation into monocytic myeloid-derived suppressor cells. *J Immunol*. 2014;193:5453–5460.
7. Najjar YG, Finke JH. Clinical perspectives on targeting of myeloid-derived suppressor cells in the treatment of cancer. *Front Oncol*. 2013; 3:49. doi: 10.3389/fonc.2013.00049
8. Rodriguez PC, Hernandez CP, Quiceno D, et al. Arginase I in myeloid suppressor cells is induced by COX-2 in lung carcinoma. *J Exp Med*. 2005;202:931–939.
9. Serafini P, Mgebroff S, Noonan K, Borrello I. Myeloid-derived suppressor cells promote cross-tolerance in B-cell lymphoma by expanding regulatory T cells. *Cancer Res*. 2008;68:5439–5449.
10. Diaz-Montero CM, Salem ML, Nishimura MI, Garrett-Mayer E, Cole DJ, Montero AJ. Increased circulating myeloid-derived suppressor cells correlate with clinical cancer stage, metastatic tumor burden, and doxorubicin-cyclophosphamide chemotherapy. *Cancer Immunol Immunother*. 2009;58:49–59.
11. Gabrilovich DI, Ostrand-Rosenberg S, Bronte V. Coordinated regulation of myeloid cells by tumours. *Nat Rev Immunol*. 2012;12:253–268.
12. Ko JS, Rayman P, Ireland J, et al. Direct and differential suppression of myeloid-derived suppressor cell subsets by sunitinib is compartmentally constrained. *Cancer Res*. 2010;70:3526–3536.

13. Zea AH, Rodriguez PC, Atkins MB, et al. Arginase-producing myeloid suppressor cells in renal cell carcinoma patients: A mechanism of tumor evasion. *Cancer Res*. 2005;65:3044–3048.
14. Arihara F, Mizukoshi E, Kitahara M, et al. Increase in $CD14^{+}HLA\text{-}DR^{-/low}$ myeloid-derived suppressor cells in hepatocellular carcinoma patients and its impact on prognosis. *Cancer Immunol Immunother*. 2013;62:1421–1430.
15. Serafini P, De Santo C, Marigo I, et al. Derangement of immune responses by myeloid suppressor cells. *Cancer Immunol Immunother*. 2004;53:64–72.
16. Yazawa T, Shibata M, Gonda K, et al. Increased IL-17 production correlates with immunosuppression involving myeloid-derived suppressor cells and nutritional impairment in patients with various gastrointestinal cancers. *Mol Clin Oncol*. 2013;1:675–679.
17. Cua DJ, Tato CM. Innate IL-17-producing cells: The sentinels of the immune system. *Nat Rev Immunol*. 2010;10:479–489.
18. Park S, CHeon S, Cho D. The dual effects of interleukin-18 in tumor progression. *Cell Mol Immunol*. 2007;4:329–335.
19. Elkabets M, Ribeiro VS, Dinarello CA, et al. IL-1b regulates a novel myeloid-derived suppressor cell subset that impairs NK cell development and function. *Eur J Immunol*. 2010;40:3347–3357.
20. Qian BZ, Li J, Zhang H, et al. CCL2 recruits inflammatory monocytes to facilitate breast-tumour metastasis. *Nature*. 2011;475:222–225.
21. McClellan JL, Davis JM, Steiner JL, et al. Linking tumor-associated macrophages, inflammation, and intestinal tumorigenesis: Role of MCP-1. *Am J Physiol Gastrointest Liver Physiol*. 2012;303:1087–1095.
22. Solito S, Falisi E, Diaz-Montero CM, et al. A human promyelocytic-like population is responsible for the immune suppression mediated by myeloid-derived suppressor cells. *Blood*. 2011;118: 2254–2265.
23. Gabitass RF, Annels NE, Stocken DD, Pandha HA, Middleton GW. Elevated myeloid-derived suppressor cells in pancreatic, esophageal and gastric cancer are an independent prognostic factor and are associated with significant elevation of the Th2 cytokine interleukin-13. *Cancer Immunol Immunother*. 2011;60:1419–1430.
24. Youn JI, Kumar V, Collazo M, et al. Epigenetic silencing of retinoblastoma gene regulates pathologic differentiation of myeloid cells in cancer. *Nat Immunol*. 2013;14:211–220.
25. Corzo CA, Condamine T, Lu L, et al. HIF-1alpha regulates function and differentiation of myeloid-derived suppressor cells in the tumor microenvironment. *J Exp Med*. 2010;207:2439–2453.
26. Ko JS, Zea AH, Rini BI, et al. Sunitinib mediates reversal of myeloid-derived suppressor cell accumulation in renal cell carcinoma patients. *Clin Cancer Res*. 2009;15:2148–2157.
27. Highfill SL, Cui Y, Giles AJ, et al. Disruption of CXCR2-mediated MDSC tumor trafficking enhances anti-PD1 efficacy. *Sci Transl Med*. 2014;6: 237ra67. doi: 10.1126/scitranslmed.3007974
28. Galon J, Angell HK, Bedognetti D, Marincola FM. The continuum of cancer immunosurveillance: Prognostic, predictive, and mechanistic signatures. *Immunity*. 2013;39:11–26.
29. Chun E, Lavoie S, Michaud M, et al. CCL2 promotes colorectal carcinogenesis by enhancing polymorphonuclear myeloid-derived suppressor cell population and function. *Cell Rep*. 2015;12:244–257.
30. Li L, Huang L, Vergis AL, et al. IL-17 produced by neutrophils regulates IFN-gamma-mediated neutrophil migration in mouse kidney ischemia-reperfusion injury. *J Clin Invest*. 2010;120:331–342.
31. Wu P, Wu D, Ni C, et al. γδT17 cells promote the accumulation and expansion of myeloid-derived suppressor cells in human colorectal cancer. *Immunity*. 2014;40:785–800.
32. König B, Steinbach F, Janocha B, et al. The differential expression of proinflammatory cytokines IL-6, IL-8 and TNF-alpha in renal cell carcinoma. *Anticancer Res*. 1999;19:1519–1524.
33. Ogura T, Ueda H, Hosohara K, et al. Interleukin-18 stimulates hematopoietic cytokine and growth factor formation and augments circulating granulocytes in mice. *Blood*. 2001;98:2101–2107.

L-FABP and IL-6 as markers of chronic kidney damage in children after hemolytic uremic syndrome

Katarzyna Lipiec[1,A–D,F], Piotr Adamczyk[2,C,D,F], Elżbieta Świętochowska[3,B,C], Katarzyna Ziora[2,E], Maria Szczepańska[2,A,C,E,F]

[1] Department of Pediatric Nephrology with Dialysis Division for Children, Zabrze, Poland
[2] Department and Clinic of Pediatrics, SMDZ in Zabrze, SUM in Katowice, Poland
[3] Chair and Department of Medical and Molecular Biology, SMDZ in Zabrze, SUM in Katowice, Poland

A – research concept and design; B – collection and/or assembly of data; C – data analysis and interpretation;
D – writing the article; E – critical revision of the article; F – final approval of the article

Advances in Clinical and Experimental Medicine, ISSN 1899-5276 (print), ISSN 2451-2680 (online) *Adv Clin Exp Med*. 2018;27(7):955–962

Address for correspondence
Maria Szczepańska
E-mail: szczep57@poczta.onet.pl

Funding sources
Grant KNW-1-150/k/310 from the Medical University of Silesia in Katowice, Poland.

Conflict of interest
None declared

Received on October 16, 2016
Reviewed on March 22, 2017
Accepted on April 20, 2017

Abstract

Background. Hemolytic-uremic syndrome (HUS) is a form of thrombotic microangiopathy, in the course of which some patients may develop chronic kidney disease (CKD). From a clinical point of view, it is important to search for markers that allow for early identification of patients at risk of a poor prognosis.

Objectives. The study evaluated the serum and urine levels of liver-type fatty acid binding protein (L-FABP) and interleukin 6 (IL-6).

Material and methods. The study was conducted in 29 children with a history of HUS. The relationship between L-FABP and IL-6 and anthropometric measurements, the value of estimated glomerular filtration rate (eGFR) and albuminuria were additionally evaluated.

Results. In children after HUS, L-FABP and IL-6 concentration in both serum and urine was significantly higher in comparison to the control group. No differences in L-FABP and IL-6 concentration in serum and urine depending on the type of HUS and gender were noted. Correlation between L-FABP and IL-6 in serum and urine with eGFR and urine albumin-creatinine ratio (ACR) in the total group of patients after HUS was not detected. In the group of children after 6 month observation after HUS, a negative correlation of L-FABP concentration with eGFR was found.

Conclusions. The results indicate that the higher concentration of L-FABP in serum and urine of children with a history of HUS can be the result of protracted injury initiated during the acute phase of the disease. Lack of correlation of L-FABP concentration with the ACR may be associated with a short (less than 6 months) observation after acute renal failure or merely temporary renal tubular damage in the acute phase of the disease. In contrast, higher levels of IL-6 in serum and urine in children after HUS compared to healthy children and the negative correlation of L-FABP concentration and eGFR in children after 6 month observation after HUS may confirm their participation in CKD. Thus, L-FABP and IL-6 seem to be good biomarkers of chronic kidney damage in survivors of the acute phase of HUS.

Key words: children, interleukin 6, chronic kidney disease, hemolytic-uremic syndrome, liver-type fatty acid binding protein

DOI
10.17219/acem/70567

Introduction

Hemolytic uremic syndrome (HUS) is the leading cause of acute kidney injury in previously healthy infants and younger children. It is characterized by a triad of symptoms – hemolytic anemia, thrombocytopenia, and acute kidney injury.[1] The most common form of HUS is a typical form, which traditionally is expected to represent up to 90% of cases of the disease.[1–3] A factor responsible for its occurrence is a bacterial toxin called verotoxin (VTEC) or Shiga-like toxin, produced by enterohemorrhagic *Escherichia coli* strains (STEC).[2,4–6]

Atypical hemolytic-uremic syndrome (aHUS) is a mixed group of disorders related to disturbances in the coagulation cascade and immune system.[4] aHUS in most cases is characterized by abnormal activation of the complement system (the alternative pathway), caused by, among other factors, the mutation of genes encoding protein components of the complement system (C3 protein, factor H, I, and B, membrane cofactor protein – MCP, thrombomodulin) and the presence of antibodies against factor H. There are also mutations in other genes, e.g. mutations of the gene encoding diacylglycerol kinase (DGKE).[7] Some patients may have more than one causative mutation in different genes.[8] aHUS is characterized by a poor long-term prognosis, is burdened with significant mortality, reaching 25%, and 50% of the patients require chronic renal replacement therapy.[1,9]

Prognosis in the typical form of HUS is much better since renal replacement therapy had become widely available and mortality does not exceed 10%. In the majority of patients, the recovery of renal function with normal glomerular filtration rate is observed. However, in some patients the disease has consequences which may lead to developing chronic kidney disease (CKD) and even end-stage renal failure (ESRF).[10] Children with a history of HUS require continuous monitoring, since the features of reduced renal function may appear many years after the outbreak of the illness. Commonly used diagnostic tools such as serum creatinine measurement (with calculation of estimated glomerular filtration rate – eGFR), albuminuria assessment (including the urine albumin/creatinine ratio – ACR) or ultrasound examination of the kidneys do not give the opportunity for early detection of chronic kidney injury. There is a need to look for sensitive and specific markers that would be sufficient to identify initial stages of kidney damage. It seems that liver-type fatty acid binding protein (L-FABP) and interleukin 6 (IL-6) may be among those markers.

The first marker chosen by us for testing in the HUS group, whose predictive value in renal diseases has recently attracted considerable attention, was L-FABP. It is a cytoplasmic protein belonging to the family of fatty acid binding proteins (FABPs).[11,12] Fatty acid binding proteins are responsible for binding to an excess of accumulated free long-chain fatty acids and directing them to appropriate intracellular sites of utilization.[13] L-FABP facilitates fatty-acid metabolism via β-oxidation and causes the excretion of lipid peroxidation products, which result in attenuating the release of inflammatory factors and inhibiting damage of tubulointerstitial tissue. L-FABP belongs to effective endogenous antioxidants. This protein, due to its low molecular weight (14 kDa), high tissue specificity, abundance in the tissue and rate of release into the blood stream, can serve as a specific marker of kidney damage.[14] The L-FABP gene is located on chromosome 2 and encodes 127 amino acids.[15] L-FABP is present in proximal tubule cells of the kidney.[16] The circulating fraction of L-FABP is filtered by the glomeruli and afterwards reabsorbed in the proximal renal tubules, which explains the increase of its concentration in the urine when proximal tubule cell injury occurs.[17,18] The increase in the concentration of L-FABP excreted in the urine in the course of kidney disease was confirmed in numerous clinical trials in adult patients.[19–21]

The second of the markers analyzed by us was IL-6, one of the main factors regulating the body's defense mechanisms via multidirectional action.[17] The most important role of IL-6 function covers its involvement in the immune response, hematopoiesis, and inflammatory processes.[17,22] Many clinical trials carried out in adults and children have confirmed the association of elevated levels of IL-6 with kidney disease severity, especially chronic kidney disease progression.[23–25] The cause of this phenomenon is believed to be ongoing chronic inflammation within the kidney tissue, which is a characteristic feature of kidney damage due to different reasons.[26] Interleukin 6, one of the major proinflammatory human cytokines, is also involved in such processes, which may explain the increase in serum level of this cytokine in the course of chronic kidney damage.

Objectives

The aim of the study was to evaluate the concentration of L-FABP and IL-6 in serum and urine in children with a past history of HUS and to compare the obtained results to a control group of healthy age-matched children. The relationship between the 2 selected markers and anthropometric measurements, the value of estimated glomerular filtration rate (eGFR) and albuminuria (expressed as ACR and daily urinary albumin excretion) were also evaluated.

Material and methods

The study group (HUS) consisted of 29 patients (9 girls and 20 boys) aged 1 to 15 years with a past history of HUS treated at the Department and Clinic of Pediatrics in Zabrze, Medical University of Silesia in Katowice. The children were also divided into 2 groups regarding the cause of HUS: typical HUS – 14, and atypical HUS – 15 children. In the group of children with a history of HUS,

86% required renal replacement therapy in the acute phase of the disease; 62% – were treated with peritoneal dialysis, 14% – hemodialysis, 10% – both peritoneal dialysis and hemodialysis and 14% of the children did not require dialysis. The mean anuria period observed in 12 children lasted for 4.6 ±4.0 days. Mean acute kidney injury (AKI) duration was 28.6 ±15.0 days (range 2–60 days) with final mean eGFR 71.9 ±23.6 mL/min/1.73 m^2. Mean duration of renal recovery was 37.2 ±21.4 days with mean eGFR at renal recovery of 95.0 ±34.3 mL/min/1.73 m^2. Two children progressed to CKD. All the children from the study group were treated pharmacologically: diuretics (4 children), calcium channel blocking agents (21 children), angiotensin converting enzyme inhibitors (ACEI) (14 children), supplementation of alkali (4 children), iron formulas (1 child), and folic acid (8 children). On admission, weight, height and blood pressure were taken and routine biochemical tests were performed. Body mass index (BMI) was calculated using the formula BMI = body weight (kg)/height (m^2). Estimated glomerular filtration rate (eGFR) was calculated according to the Schwartz formula (mL/min/1.73 m^2).[27] Additionally, albuminuria (mg/day) using 24 h urine collection was evaluated.

The control group consisted of 21 healthy children (11 girls and 10 boys) aged 1–15 years with monosymptomatic nocturnal enuresis or presented with surgical procedures of one-day surgery, without any signs of kidney diseases. All children participating in the study were in good clinical condition, without signs of acute infection. The study was approved by the Bioethics Committee of the Medical University of Silesia in Katowice (resolution No. CDF/0022/KB1/111/13 of 10.22.2013) and written consent from parents or legal guardians, and/or the patients was obtained.

Anthropometric measurements and the age of the study subjects and controls are presented in Table 1. The average age, weight, height and BMI in the study group and the control group did not differ significantly. The average age of children in the study group at HUS onset was 3.42 ±3.49 years, while the average time from the HUS outbreak and acute kidney injury until the current examinations was 4.94 ±3.94 years (range 1 month–13.9 years), including 24 from 29 patients more than 6 months after the onset of acute phase of the disease..

Laboratory tests

Blood samples (3–5 mL) for laboratory tests were drawn in Eppendorf tubes in the morning (8:00–9:00) during examination related to periodic control in the outpatient clinic. After centrifugation 1000 × for 15 min at 4°C, the serum was stored at –20°C until assayed. Urine samples (50–100 mL) were collected at the same time as the blood samples, and also kept at –20°C until evaluated. Determination of concentrations of L-FABP and IL-6 was performed in the Chair and Department of Medical and Molecular Biology, SMDZ in Zabrze, SUM in Katowice.

The concentration of IL-6 in serum and urine was performed by ELISA using a Diaclone (Besancon Cedex, France) set according to the manufacturer's protocol. Determination of concentrations of L-FABP was carried out using a kit from BioVendor (Brno, Czech Republic) according to the manufacturer's protocol.

Statistical analysis

A database was prepared in a Microsoft Excel spreadsheet. For statistical calculations, licensed v. 10.0 STATISTICA software (StatSoft Inc., Tulsa, USA) was used. In the statistical analysis, the level of significance at $p \leq 0.05$ was assumed. As the parameters of descriptive statistics, the arithmetic mean, median, minimum and maximum value, lower and upper quartile and standard deviation were chosen. For all parameters, the compatibility of their distributions with a normal distribution were checked with a Shapiro-Wilk test. For variables with

Table 1. Clinical characteristics of children evaluated after HUS and from control group

Parameter	HUS group					Control group
	total group (n = 29)	girls (n = 9)	boys (n = 20)	atypical HUS (n = 15)	typical HUS (n = 14)	total group (n = 21)
Age [years]	8.4 ±4.3	10.0 ±4.3	7.6 ±4.2	7.7 ±5.1	9.0 ±3.4	8.4 ±4.1
Height [cm]	128.7 ±25.5	142.5 ±23.7	122.5 ±24.3*	125.8 ±29.7	131.4 ±21.6	128.2 ±25.2
Height SDS	0.45 ±0.93	0.92 ±0.73	0.35 ±1.30	0.47 ±1.14	0.43 ±0.75	–0.06 ±1.10
Body weight [kg]	30.3 ±17.1	42.5 ±19.8	24.7 ±12.7*	29.5 ±19.0	30.9 ±15.7	31.9 ±16.5
Weight SDS	0.15 ±0.82	0.85 ±0.68	–0.17 ±0.68*	0.25 ±0.92	0.07 ±0.74	0.11 ±1.3
BMI [kg/m^2]	16.7 ±3.6	19.6 ±4.7	15.4 ±2.0*	16.7 ±3.6	16.8 ±3.8	15.4 ±2.08
BMI SDS	–0.20 ±1.00	0.45 ±0.86	–0.52 ±0.92*	0.04 ±0.86	–0.42 ±0.09	0.32 ±1.02
Age at HUS onset [years]	3.4 ±3.5	5.0 ±4.7	2.7 ±2.6	3.4 ±3.9	3.4 ±3.1	–
Time after HUS [years]	4.9 ±4.0	5.0 ±5.0	4.9 ±3.5	4.3 ±4.3	5.6 ±3.7	–

Data is presented as mean ± standard deviation; HUS – hemolytic-uremic syndrome; BMI – body mass index; SDS – standard deviation score; $p > 0.05$ HUS vs control group; * $p < 0.05$ girls after HUS vs boys after HUS.

normal distribution, parametric tests were used (t-test for independent variables in comparative analyses and Pearson's test for analyses of correlation). For other variables, nonparametric tests were applied (Mann-Whitney U-test for comparisons and Spearman's rank correlation test for analyses of correlation).

Results

The results of laboratory tests and mean arterial pressure values in the group of children after HUS are reported in Table 2. In children with a history of HUS, daily urine albumin excretion of 52.69 ±108.4 mg/24 h and expressed as ACR 122.0 ±378.7 mg/g were noted. The average value of eGFR in the study group was 96.5 ±19.8 mL/min/1.73 m^2, and in the majority of children remained within the normal range. Girls after HUS had higher mean arterial pressure than boys after HUS. Children with atypical HUS showed higher values of serum urea as compared to children with typical HUS.

Serum and urine concentrations of L-FABP and IL-6, as the CKD markers in the group of children after HUS, are shown in Table 3. A significantly higher concentration of L-FABP in serum and urine was found as compared to healthy children. IL-6 level was also significantly higher in serum and urine in the study group in contrast to the control group. In the whole HUS group, no correlation between the studied markers in serum and urine and eGFR or albuminuria expressed as ACR was found, except the value of eGFR at the end of AKI, which positively correlated with serum IL-6 concentration (Table 4). For additional analyses, the subgroup of children after HUS limited to subjects with a minimal time period since resolution of the disease onset until sample collection established at 6 months was extracted. In this subgroup (n = 24), a negative correlation between the concentration of L-FABP in the serum and eGFR, as well as between the concentration of L-FABP in urine and eGFR were documented (Fig. 1, 2). The concentration of L-FABP in serum and urine positively correlated with standard deviation score (SDS) for growth in children with a history of HUS,

Table 2. Biochemical parameters and mean arterial pressure in children after HUS

Parameter	HUS total group (n = 29)	HUS girls (n = 9)	HUS boys (n = 20)	aHUS (n = 15)	Typical HUS (n = 14)
Serum albumin [g/L]	45.1 ±4.34	44.08 ±4.52	45.56 ±4.3	44.1 ±3.87	46.32 ±4.7
Total proteins [g/L]	68.87 ±5.45	70.54 ±3.76	68.88 ±5.39	69.35 ±6.05	69.44 ±3.86
Total cholesterol [mmol/L]	4.18 ±0.88	4.02 ±0.8	4.25 ±0.92	3.98 ±0.87	4.37 ±0.88
Triglycerides [mmol/L]	1.12 ±0.59	1 ±0.32	1.17 ±0.68	1.18 ±0.78	1.05 ±0.33
Creatinine [mmol/L]	50.27 ±11.95	53.44 ±12.02	48.85 ±11.95	53.1 ±14.2	47.67 ±9.14
Uric acid [mmol/L]	251 ±61.7	260.89 ±74.0	247.85 ±56.9	259.36 ±74.9	244.9 ±48.4
Urea [mmol/L]	4.3 ±1.97	3.63 ±1.12	4.61 ±2.21	5.12 ±2.41	3.54 ±1.03#
Daily urine albumin excretion [mg/24 h]	52.69 ±108.4	26.99 ±25.99	62.97 ±127.0	81.45 ±161.6	35 ±58.72
Albuminuria [mg/L]	56.46 ±157.3	17.4 ±19.35	71.11 ±183.5	106.47 ±254.46	27.89 ±51.63
ACR [mg/g]	122.04 ±378.69	40.43 ±33.77	152.6 ±443.5	257.6 ±624.1	44.6 ±64.83
eGFR [mL/min/1.73 m^2]	96.53 ±9.84	99.29 ±14.38	95.28 ±2.08	90.43 ±2.44	102.2 ±15.75
Mean arterial pressure [mm Hg]	76.93 ±8.94	82.4 ±10.15	74.47 ±7.35*	78.83 ±8.33	75.16 ±9.41

Data is presented as mean ± standard deviation (min–max); HUS – hemolytic-uremic syndrome; ACR – urine albumin/creatinine ratio; eGFR – estimated glomerular filtration rate; * $p < 0.05$ girls after HUS vs boys after HUS; # $p < 0.05$ aHUS vs typical HUS.

Table 3. Mean concentration of examined markers in children after HUS and in control group

Parameter	Children after HUS (n = 29)	Girls after HUS (n = 29)	Boys after HUS (n = 29)	aHUS	Typical HUS	Control group (n = 21)
Serum IL-6 [ng/mL]	79.96 ±26.68 (32.9–161.3)	65.7 ±22.51 (32.9–93.9)	86.39 ±26.38 (39.6–161.3)	82.18 ±30.44 (32.9–161.3)	77.89 ±23.55 (39.6–101.6)	7.34 ±1.43* (4.77–9.61)
Urine IL-6 [ng/mL]	97.64 ±15.46 (73.8–121.5)	97.62 ±16.96 (73.8–117.6)	97.65 ±15.2 (39.6–161.3)	102.3 ±13.53 (75.9–121.5)	93.27 ±16.29 (73.8–118.9)	36.87 ±12.01* (18.6–55.7)
Serum L-FABP [ng/mL]	72.49 ±18.53 (44.3–100.1)	75.61 ±16.75 (49.9–93.8)	71.08 ±19.52 (44.3–100.1)	74.66 ±18.33 (48.5–96.6)	70.47 ±19.11 (44.3–100.1)	2.65 ±0.75* (1.1–3.75)
Urine L-FABP [ng/mL]	11.54 ±4.32 (4.9–7.6)	11.80 ±3.51 (5.8–15.7)	11.42 ±4.72 (4.7–19.6)	11.62 ±3.74 (5.9–16.7)	11.46 ±4.93 (4.7–19.6)	2.76 ±0.63* (1.9–4.1)

Data is presented as mean ± standard deviation (min–max); HUS – hemolytic-uremic syndrome; L-FABP – liver-type fatty acid binding protein; * $p < 0.05$ children after HUS vs control group.

Table 4. Correlation between studied markers of chronic kidney disease and results of anthropometric measurements and biochemical parameters

Parameter	Examined children with HUS n = 29 (HUS)			
	IL-6 serum	IL-6 urine	L-FABP serum	L-FABP urine
Body weight [kg]	r = –0.009 p = 0.951	r = –0.04 p = 0.782	r = –0.05 p = 0.752	r = 0.0006 p = 0.997
Height [cm]	r = 0.034 p = 0.817	r = 0.009 p = 0.948	r = –0.029 p = 0.843	r = –0.004 p = 0.979
Age [years]	r = 0.112 p = 0.44	r = 0.073 p = 0.615	r = 0.022 p = 0.882	r = –0.079 p = 0.584
Age at HUS onset [years]	r = 0.07 p = 0.715	r = 0.168 p = 0.385	r = 0.029 p = 0.493	r = 0.189 p = 0.327
Time from HUS onset [years]	r = 0.095 p = 0.623	r = –0.17 p = 0.376	r = –0.133 p = 0.493	r = –0.12 p = 0.535
MAP [mm Hg]	r = –0.206 p = 0.283	r = –0.157 p = 0.416	r = 0.088 p = 0.65	r = –0.029 p = 0.882
GPT [U/L]	r = –0.007 p = 0.973	r = –0.036 p = 0.852	r = –0.103 p = 0.597	r = –0.057 p = 0.768
Serum albumin [g/L]	r = 0.299 p = 0.138	r = –0.08 p = 0.695	r = –0.132 p = 0.519	r = –0.0007 p = 0.997
Total proteins [g/L]	r = –0.21 p = 0.274	r = 0.147 p = 0.446	r = –0.011 p = 0.953	r = 0.219 p = 0.254
Total cholesterol [mmol/L]	r = –0.215 p = 0.262	r = –0.367 p = 0.05	r = –0.119 p = 0.54	r = –0.0005 p = 0.998
Triglycerides [mmol/L]	r = –0.138 p = 0.483	r = –0.211 p = 0.280	r = 0.215 p = 0.270	r = 0.205 p = 0.295
Creatinine [mmol/L]	r = 0.035 p = 0.858	r = –0.264 p = 0.166	r = 0.055 p = 0.777	r = 0.103 p = 0.593
Uric acid [mmol/L]	r = –0.046 p = 0.813	r = –0.134 p = 0.487	r = 0.058 p = 0.763	r = 0.057 p = 0.770
Urea [mmol/L]	r = –0.064 p = 0.741	r = –0.115 p = 0.553	r = 0.168 p = 0.385	r = 0.069 p = 0.720
ACR [mg/g]	r = –0.146 p = 0.515	r = 0.156 p = 0.487	r = –0.084 p = 0.712	r = –0.119 p = 0.598
eGFR [mL/min/1.73 m^2]	r = 0.01 p = 0.957	r = 0.187 p = 0.332	r = –0.245 p = 0.2	r = –0.261 p = 0.171
AKI time [days]	r = –0.1433 p = 0.458	r = –0.2717 p = 0.154	r = –0.0975 p = 0.615	r = –0.1604 p = 0.406
eGFR at the end of AKI [mL/min/1.73 m^2]	r = 0.4661* p = 0.011*	r = 0.242 p = 0.206	r = –0.3496 p = 0.063	r = –0.2419 p = 0.206
Renal recovery time [days]	r = –0.2842 p = 0.151	r = 0.0012 p = 0.995	r = –0.0344 p = 0.865	r = –0.043 p = 0.831
eGFR renal recovery [mL/min/1.73 m^2]	r = 0.3145 p = 0.110	r = 0.3642 p = 0.062	r = 0.2384 p = 0.231	r = 0.3503 p = 0.073

* significant correlation coefficients $p < 0.05$; AKI – acute kidney injury; HUS – hemolytic-uremic syndrome; L-FABP – liver-type fatty acid binding protein; MAP – mean arterial pressure; GPT – glutamic pyruvic transaminase; ACR – urine albumin/creatinine ratio; eGFR – estimated glomerular filtration rate.

in which the time since the disease resolution was longer than 6 months ($r = 0.5534$; $p < 0.005$ and $r = 0.5194$; $p < 0.01$, respectively).

Discussion

A large number of reports published in recent years has proved that the concentration of L-FABP in urine could serve as a useful marker for the diagnosis of early stage kidney damage, especially acute kidney injury (AKI).[21,28] L-FABP is a protein found in the cytoplasm of the proximal tubule cells in the kidney, both healthy and injured.[15] Various pathological conditions such as proteinuria, hyperglycemia, hypertension and toxin-induced injury to the proximal tubule cells may result (directly or through the regulation of gene expression) in the increase of the excretion of urine derived L-FABP.[11,15] Recent studies have demonstrated that L-FABP can play an important role in injury and repair processes in the kidneys, and that

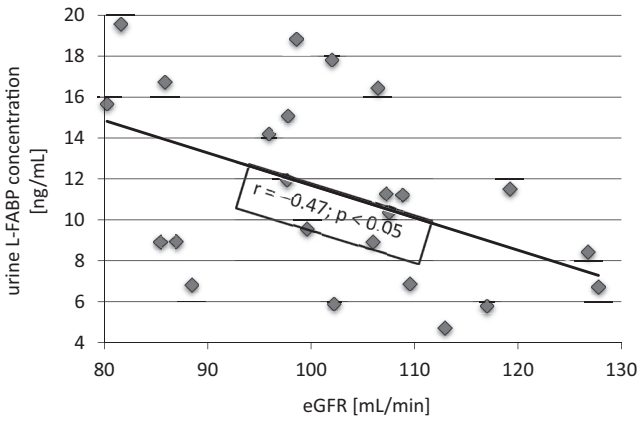

Fig. 1. Analysis of correlation results in examined children (> 6 months after HUS)

HUS – hemolytic-uremic syndrome; L-FABP – liver-type fatty acid binding protein; eGFR – estimated glomerular filtration rate.

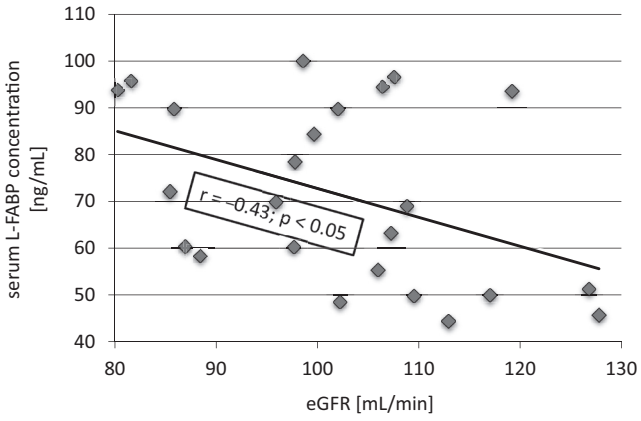

Fig. 2. Analysis of correlation results in examined children (> 6 months after HUS)

HUS – hemolytic-uremic syndrome; L-FABP – liver-type fatty acid binding protein; ACR – urine albumin/creatinine ratio; eGFR – estimated glomerular filtration rate.

the monitoring of urine L-FABP concentration may make it possible to predict the occurrence and severity of various renal diseases.[21,29] In the literature there is no data on the urine/serum concentration of L-FABP in children with HUS. In our retrospective study, we assessed in a single evaluation the concentration of L-FABP after the acute phase of HUS, and a significant increase in both plasma (30-fold) and urine (5-fold) concentrations was recorded. A negative correlation of L-FABP concentration and eGFR in the group of children with more than 6 month observation after HUS may confirm L-FABP participation in CKD. Single evaluation is a limitation of our study. Further studies are needed, with prospective assessment of the parameters in a few time intervals to confirm that patients with the highest concentration of L-FABP shortly after HUS should present decreasing eGFR in the longer follow-up. We also did not find a relationship between AKI or renal recovery time duration and FABP serum and urine concentration, which also could be the result of only single measurement.

Parr et al. in their study evaluated biomarkers for early detection of AKI in 152 adult patients with known baseline serum creatinine concentration.[21] They considered that, in the case of only a slight increase in serum creatinine, L-FABP concentration can help in determination of outcome, and could even predict the progression of kidney damage in patients at risk of AKI.[21] The role of the concentration of L-FABP in urine was also examined as potentially useful for the assessment of prognosis in renal transplant recipients.[12,20] Pajek et al., in a group of 71 adult patients after kidney transplantation, confirmed that the determination of L-FABP in urine may be helpful for the prediction of graft function within the 1st week, and especially after 48 h from transplantation surgery.[20] Acute kidney injury is a common and serious postoperative complication of cardiac surgery. In studies carried out in adult patients after cardiac surgery, the usefulness of L-FABP as a marker of AKI in the postoperative period was also assessed.[19,30] Kokot et al. demonstrated that increased L-FABP levels may lead to the detection of very early stages of AKI, and thereby identify patients in imminent danger of complications after abdominal aortic aneurysm surgery.[19] In a study carried out by Hwang et al. in 26 children after cardiac catheterization, the authors proved that urine concentration of L-FABP was useful in the diagnosis of a subclinical form of contrast induced nephropathy.[31] In patients with CKD, some studies confirm that the concentration of L-FABP in urine accurately reflects the degree of kidney damage and is correlated with the rate of progression of renal disease.[32] Xie et al. demonstrated this relationship in a group of 90 patients with obstructive nephropathy.[33] They also showed that the concentration of L-FABP in urine is more sensitive than albuminuria in predicting the progression of CKD.[34] However, in our study the relationship of urine L-FABP and albuminuria has not been proved. The interesting finding was that the concentration of L-FABP in serum and urine positively correlated with SDS for growth in children with a history of HUS. The girls in our study tended to be older and thus grew better than the younger boys, however without significant difference in SDSs, while renal function expressed as eGFR was similar.

In terms of CKD, data from the literature has documented the usefulness of L-FABP as a marker for diabetic kidney disease. Kamijo-Ikemori et al., in animal experiments, showed that expression of L-FABP increased significantly in the group of diabetic mice compared to control mice group.[35] Also, in studies in humans it was shown that L-FABP is an indicator of development of diabetic kidney disease, regardless of its stage.[36] Mou et al. confirmed the correlation between the level of L-FABP in urine and development of renal impairment in patients with chronic glomerulonephritis, and showed that L-FABP excreted in the urine may be a good marker of progression of chronic glomerulonephritis.[37] In Japan, the determination of L-FABP

in urine has been recognized as a novel biomarker for renal damage and in that country the use of a rapid kit for measuring the concentration of L-FABP in urine has been introduced for clinical use.[38]

The second marker investigated in our study was IL-6, which is considered as one of the major pro-inflammatory cytokines.[17] We have confirmed high serum and urine levels of IL-6 in the group of children after HUS. As already mentioned above, CKD is accompanied by local inflammation, regardless of CKD cause and the stage, as well as the age of the patient. The intensity of the inflammation negatively correlates with current kidney function.[26] A fundamental role in the development and progression of chronic nephropathy is attributed to inflammation mediators (including cytokines), which are released as a result of the action of kidney-damaging agents. Pro-inflammatory cytokines potentiate the activity of adhesion molecules in endothelial cells of capillaries. In turn, adhesion molecules bind to the receptors of activated T cells, which lead to the formation of inflammatory infiltrates in the interstitium of the kidneys and stimulation of fibroblasts, fibrosis development and progression of CKD.[39] Research studies in recent years have confirmed the elevated IL-6 levels in serum of CKD patients compared to healthy controls and a strong correlation with reduced eGFR.[23–25] In a population-based study with 4926 Caucasian adults enrolled and followed over 15 years, Shankar et al. found that IL-6 levels were positively related to the presence of CKD in both the baseline and long term observation.[24] Gupta et al. in a group of 3939 adult patients with CKD showed higher levels of IL-6 in the serum of patients with lower eGFR.[23] We have also confirmed higher serum IL-6 levels in children after HUS with positive correlation with final eGFR at the end of AKI. Repeated examinations of serum IL-6 concentration in these patients during follow-up would be needed to validate this finding. Sikorska et al., in a cross-sectional study involving 96 patients diagnosed with CKD stages 1–5 of various etiology, found that an increased proportion of patients with elevated IL-6 levels was observed from the earliest stages of CKD, which highlighted the role of severity of inflammation.[25] Perlman et al. evaluated diabetic patients at different stages of development of diabetic kidney disease and found that IL-6 concentration in the serum increased with the progression of CKD.[40] Rodriquez et al., in a study of 32 children, have shown that patients who have developed renal scarring after suffering from urinary tract infection (UTI) in childhood have a higher concentration of pro-inflammatory IL-6 in the blood during a recurrence of an acute episode of UTI. Moreover, it can be concluded that children with a high concentration of IL-6 coexisting with high CRP level during infection are at higher risk of kidney scarring, and consequently the development of CKD.[41] There are also many studies demonstrating the role of IL-6 in the pathogenesis of AKI.[42,43] Greenberg et al., in a group of 106 children undergoing cardiac surgery, demonstrated that children with high levels of IL-6 in the serum before surgery have a higher risk of postoperative AKI.[43] Zhang et al., in studies involving 960 adult patients after cardiac surgery, have shown that the concentration of serum IL-6 preoperative was not significantly associated with an increased risk of AKI, in contrast to the 1st postoperative concentrations of the interleukins.[44] The role of IL-6 in the development of acute renal failure and its predictive value in the diagnosis of AKI is not fully understood. Most of the studies assume IL-6 as a good, but imperfect marker for AKI development.[45]

Conclusions

The results indicate that the higher concentration of L-FABP in the serum and urine of children with a history of HUS can be the result of protracted injury initiated during the acute phase of the disease. Lack of correlation of L-FABP concentration with ACR may be associated with a short (less than 6 months) observation after acute renal failure or merely temporary renal tubular damage in the acute phase of the disease. In contrast, higher levels of IL-6 in the serum and urine in children after HUS compared to healthy children, and the negative correlation of L-FABP concentration and eGFR in the group of children after 6-month observation after HUS may confirm their participation in CKD. Thus, L-FABP and IL-6 seem to be good biomarkers of chronic kidney damage in survivors of the acute phase of HUS.

References

1. Adamczuk D, Bieroza I, Roszkowska-Blaim M. Zespół hemolityczno-mocznicowy. *Nowa Pediatr*. 2009;2:63–67.
2. Franchini M. Atypical hemolytic uremic syndrome: From diagnosis to treatment. *Clin Chem Lab Med*. 2015;53:1679–1688.
3. Żurowska A. Zespół hemolityczno-mocznicowy u dzieci i młodzieży. *Forum Nefrol*. 2012;5:283–288.
4. Jander A, Krakowska A, Tkaczyk M. Atypowy zespół hemolityczno-mocznicowy – opis przypadku. *Med Og Nauk Zdr*. 2013;19:75–77.
5. Nester CM, Barbour T, de Cordoba SR, et al. Atypical aHUS: State of the art. *Mol Immunol*. 2015;67:31–42.
6. Picard C, Burtey S, Bornet C, Curti C, Montana M, Vanelle P. Pathophysiology and treatment of typical and atypical hemolytic uremic syndrome. *Pathol Biol*. 2015;63:136–143.
7. Loirat C, Fakhouri F, Ariceta G, et al. An international consensus approach to the management of atypical hemolytic uremic syndrome in children. *Pediatr Nephrol*. 2016;31:15–39.
8. Wong E, Challis R, Sheerin N, Johnson S, Kavanagh D, Goodship TH. Patient stratification and therapy in atypical haemolytic uraemic syndrome (aHUS). *Immunobiology*. 2016;221:715–718.
9. Loirat C, Fremeaux-Bacchi V. Atypical hemolytic uremic syndrome. *Orphanet J Rare Dis*. 2011;6:60.
10. Lumbreras Fernández J, Cruz Rojo J, Iñigo Martín G, Muley Alonso R, Vara Martín J. Hemolytic uremic syndrome: Long term renal injury. *Ann Pediatr*. 2010;72:309–316.
11. Choromańska B, Myśliwiec P, Dadan J, Hady HR, Chabowski A. Znaczenie kliniczne białek wiążących kwasy tłuszczowe (FABPs). *Postepy Hig Med Dosw*. 2011;65:759–763.
12. Yamamoto T, Noiri E, Ono Y, et al. Renal L-type fatty acid binding protein in acute ischemic injury. *J Am Soc Nephrol*. 2007;18:2894–2902.

13. Kalinowska A, Harasim E, Łukaszuk B, Chabowski A. Białka transportujące kwasy tłuszczowe a metabolizm lipidów w mięśniu sercowym. *Czyn Ryz*. 2009;4:43–49.
14. Funaoka H, Kanda T, Fujii H. Intestinal fatty acid-binding protein (I-FABP) as a new biomarker for intestinal diseases. *Rinsho Byori*. 2010; 58:162–168.
15. Xu Y, Xie Y, Shao X, Ni Z, Mou S. L-FABP: A novel biomarker of kidney disease. *Clin Chim Acta*. 2015;445:85–90.
16. Kamijo-Ikemori A, Sugaya T, Matsui K, Yokoyama T, Kimura K. Roles of human liver type fatty acid binding protein in kidney disease clarified using hL-FABP chromosomal transgenic mice. *Nephrol* (*Carlton*). 2011;16:539–544.
17. Łukaszewicz M, Mroczko B, Szmitkowski M. Clinical significance of interleukin-6 (IL-6) as a prognostic factor of cancer disease. *Pol Arch Med Wewn*. 2007;117:247–251.
18. Moore E, Bellomo R, Nichol A. Biomarkers of acute kidney injury in anesthesia, intensive care and major surgery: From the bench to clinical research to clinical practice. *Minerva Anestesiol*. 2010;76: 425–440.
19. Kokot M, Biolik G, Ziaja D, et al. Assessment of subclinical acute kidney injury after abdominal aortic aneurysm surgery using novel markers L-FABP and H-FABP. *Nefrologia*. 2014;34:628–636.
20. Pajek J, Škoberne A, Šosterič K, et al. Non-inferiority of creatinine excretion rate to urinary L-FABP and NGAL as predictors of early renal allograft function. *BMC Nephrol*. 2014;15:117.
21. Parr SK, Clark AJ, Bian A, et al. Urinary L-FABP predicts poor outcomes in critically ill patients with early acute kidney injury. *Kidney Int*. 2015;87:640–648.
22. Culig Z, Steiner H, Bartsch G, Hobisch A. Interleukin-6 regulation of prostate cancer cell growth. *J Cell Biochem*. 2005;95:497–505.
23. Gupta J, Mitra N, Kanetsky PA, et al. Association between albuminuria, kidney function, and inflammatory biomarker profile in CKD in CRIC. *Clin J Am Soc Nephrol*. 2012;7:1938–1946.
24. Shankar A, Sun L, Klein BE, et al. Markers of inflammation predict the long-term risk of developing chronic kidney disease: A population-based cohort study. *Kidney Int*. 2011;80:1231–1238.
25. Sikorska D, Szkudlarek M, Kłysz P, et al. Cross-sectional assessment of relationship between the stage of chronic kidney disease, chronic inflammation indicators and selected markers of cardiovascular damage. *Now Lek*. 2013;82:197–203.
26. Oberg BP, Mc Menamin E, Lucas FL, et al. Increased prevalence of oxidant stress and inflammation in patients with moderate to severe chronic kidney disease. *Kidney Int*. 2004;65:1009–1016.
27. Janeczko M, Niedzielska E, Pietras W. Evaluation of renal function in pediatric patients after treatment for Wilms' tumor. *Adv Clin Exp Med*. 2015;24:497–504.
28. Portilla D, Dent C, Sugaya T, et al. Liver fatty acid-binding protein as a biomarker of acute kidney injury after cardiac surgery. *Kidney Int*. 2008;73:465–472.
29. Yang J, Choi HM, Seo MY, et al. Urine liver-type fatty acid-binding protein predicts graft outcome up to 2 years after kidney transplantation. *Transplant Proc*. 2014;46:376–380.
30. Krawczeski CD, Goldstein SL, Woo JG, et al. Temporal relationship and predictive value of urinary acute kidney injury biomarkers after pediatric cardiopulmonary bypass. *J Am Coll Cardiol*. 2011;58:2301–2309.
31. Hwang YJ, Hyun MC, Choi BS, Chun SY, Cho MH. Acute kidney injury after using contrast during cardiac catheterization in children with heart disease. *J Korean Med Sci*. 2014;29:1102–1107.
32. Kamijo A, Sugaya T, Hikawa A, et al. Urinary liver-type fatty acid binding protein as a useful biomarker in chronic kidney disease. *Mol Cell Biochem*. 2006;284:175–182.
33. Xie Y, Xue W, Shao X, et al. Analysis of a urinary biomarker panel for obstructive nephropathy and clinical outcomes. *PLoS One*. 2014;9: e112865. https://doi.org/10.1371/journal.pone.0112865
34. Kamijo A, Sugaya T, Hikawa A, et al. Clinical evaluation of urinary excretion of liver-type fatty acid-binding protein as a marker for the monitoring of chronic kidney disease: A multicenter trial. *J Lab Clin Med*. 2005;145:125–133.
35. Kamijo-Ikemori A, Sugaya T, Sekizuka A, Hirata K, Kimura K. Amelioration of diabetic tubulointerstitial damage in liver-type fatty acid-binding protein transgenic mice. *Nephrol Dial Transplant*. 2009;24: 788–800.
36. Panduru NM, Forsblom C, Saraheimo M; FinnDiane Study Group, et al. Urinary liver-type fatty acid-binding protein and progression of diabetic nephropathy in type 1 diabetes. *Diabetes Care*. 2013;36: 2077–2083.
37. Mou S, Wang Q, Li J, Shi B, Ni Z. Urinary excretion of liver-type fatty acid-binding protein as a marker of progressive kidney function deterioration in patients with chronic glomerulonephritis. *Clin Chim Acta*. 2012;413:187–191.
38. Sato R, Suzuki Y, Takahashi G, Kojika M, Inoue Y, Endo S. A newly developed kit for the measurement of urinary liver-type fatty acid-binding protein as a biomarker for acute kidney injury in patients with critical care. *J Infect Chemother*. 2015;21:165–169.
39. Zajączkowska MM, Bieniaś B. Aktualny stan wiedzy na temat patogenezy, diagnostyki i leczenia przewlekłej choroby nerek. *Med Og Nauk Zdr*. 2013;19:1–7.
40. Perlman AS, Chevalier JM, Wilkinson P, et al. Serum inflammatory and immune mediators are elevated in early stage diabetic nephropathy. *Ann Clin Lab Sc*i. 2015;45:256–263.
41. Rodríguez LM, Robles B, Marugán JM, et al. Do serum C-reactive protein and interleukin-6 predict kidney scarring after urinary tract infection? *Indian J Pediatr*. 2013;80:1002–1006.
42. Dennen P, Altmann C, Kaufman J, et al. Urine interleukin-6 is an early biomarker of acute kidney injury in children undergoing cardiac surgery. *Crit Care*. 2010;14:R181.
43. Greenberg JH, Whitlock R, Zhang WR, et al. Interleukin-6 and interleukin-10 as acute kidney injury biomarkers in pediatric cardiac surgery. *Pediatr Nephrol*. 2015;30:1519–1527.
44. Zhang WR, Garg AX, Coca SG, et al. Plasma IL-6 and IL-10 concentrations predict AKI and long-term mortality in adults after cardiac surgery. *J Am Soc Nephrol*. 2015;26:3123–3132.
45. Miklaszewska M, Korohoda P, Zachwieja K, et al. Serum interleukin 6 levels as an early marker of acute kidney injury on children after cardiac surgery. *Adv Clin Exp Med*. 2013;22:377–386.

PIK3CA mutation in gastric cancer and the role of microsatellite instability status in mutations of exons 9 and 20 of the *PIK3CA* gene

Karol Polom[1,6,A-F], Daniele Marrelli[1,A–F], Giandomenico Roviello[2,3,A–F], Valeria Pascale[1,B,E,F], Costantino Voglino[1,B,C,E,F], Carla Vindigni[4,B,E,F], Daniele Generali[5,C,E,F], Franco Roviello[1,A–F]

[1] Unit of General Surgery and Surgical Oncology, University of Siena, Italy
[2] Department of Oncology, Medical Oncology Unit, San Donato Hospital, Arezzo, Italy
[3] Department of Medical, Surgery and Health Sciences, University of Trieste, Italy
[4] Department of Pathology, Hospital Department of University of Siena, Italy
[5] Department of Medical, Surgery and Health Sciences, University of Trieste, Italy
[6] Department of Surgical Oncology, Medical University of Gdansk, Poland

A – research concept and design; B – collection and/or assembly of data; C – data analysis and interpretation; D – writing the article; E – critical revision of the article; F – final approval of the article

Advances in Clinical and Experimental Medicine, ISSN 1899-5276 (print), ISSN 2451-2680 (online) *Adv Clin Exp Med*. 2018;27(7):963–969

Address for correspondence
Karol Polom,
E-mail: polom.karol@gmail.com

Funding sources
Istituto Toscano Tumori (ITT) grant entitled "Gene expression profiles and therapy of gastric cancer" – (grant No. ITT-2007) European Union's Seventh Framework Programme (FP7), GastricGlyco-Explorer under grant agreement No. [316929] (Karol Polom, Franco Roviello).

Conflict of interest
None declared

Received on September 21, 2016
Reviewed on February 13, 2017
Accepted on April 27, 2017

Abstract

Background. A better understanding of molecular gastric cancer (GC) entities may help in tailored treatments of that neoplasm. The *PIK3CA* mutation is one of the most important in many cancers.

Objectives. We performed a comparison of clinical and pathological data of the *PIK3CA* mutation in GC patients.

Material and methods. The analysis was done on 472 patients operated on in 1 center. Polymerase chain reaction (PCR) was used for the screening of *PIK3CA* (exon 9 and 20). For microsatellite instability (MSI) we used 5 quasi-monomorphic mononucleotide repeats — BAT-26, BAT-25, NR-24, NR-21, and NR-27. The clinical and pathological data was analyzed.

Results. *PIK3CA* mutation was observed in 10 out of 472 GC patients (2.1%). Nine out of 10 were MSI (9 of 111 MSI patients – 8.1%). Half of the 10 patients had mutations in exon 9 and the other half in exon 20. A majority of patients with the *PIK3CA* mutation had MSI ($p < 0.001$). The 5-year survival of MSI patients with the *PIK3CA* mutation was 40% and without the mutation, 70.4% ($p = 0.309$). For patients with the mutation in exon 9, the 5-year survival was 0%, and for those with the mutation in exon 20, 80% ($p = 0.031$). The Cox proportional hazards regression analysis did not show that *PIK3CA* is statistically correlated with a worse overall survival.

Conclusions. *PIK3CA* mutation in GC is a rare finding. It is strongly associated with the MSI molecular subgroup, presenting a worse outcome than other MSI patients. A completely different outcome is associated with the mutation in exon 9 compared to the mutation in exon 20, with the latter being more favorable.

Key words: gastric cancer, *PIK3CA*, mutation, microsatellite instability, exon

DOI
10.17219/acem/70795

Introduction

Gastric cancer (GC) is a disease that is characterized by multiple molecular, genetic, and epigenetic events.[1] Mutation in a signaling pathway is one such event and the phosphoinositide 3-kinase (PI3K)/AKT/mammalian target of the rapamycin pathway (PI3K/AKT/mTOR pathway) is one example of the mutation mechanism.[2] A fundamental step in this pathway is the creation of phosphatidylinositol-3,4,5-triphosphatate (PIP3), catalyzed by PI3K. This pathway is important in the cancer-related functions of cell proliferation, catabolism, cell adhesion, apoptosis, and autophagy.[3] It also plays an important role in motility and glucose homeostasis.[4] The mutations of this pathway have frequently been seen in cancers such as ovarian, breast, thyroid, and cervical. Many studies have revealed that this pathway is not of highest importance in GC patients. The *PIK3CA* gene is located on chromosome 3p26.3.[5] The most common mutations are seen in exon 9 and 20, representing different hotspots of mutations.[4]

In the current literature, *PIK3CA* mutations in colorectal cancer (CRC) are associated with female gender, proximal position, well-differentiated tumors, and mucinous histology, but these findings are not consistent.[6] Some studies have shown a significant coexistence of *PIK3CA* and *KRAS* mutations, while other studies have failed to show such a coexistence. Other contradictory data presented a link between the *PIK3CA* mutation and MSI or CpG island methylator phenotype (CIMP).[6] Another inconclusive study showed worse outcome for early stage resectable disease, but other studies did not prove this finding.[6] Such conflicting findings can be explained by important differences between cancers that have the mutation in exon 9 vs those with the mutation in exon 20.[6,7] Exon 20 has a mutual relationship with *BRAF* mutation, CIMP high/low and MSI-H, and exon 9 is linked with KRAS mutations.[7] In the study by Mao et al., authors showed that mutations in exon 20 are associated with resistance to anti-EGFR antibody therapy. This was not seen for mutations in exon 9.[8] Tapia et al. reported that PI3K and AKT are overexpressed in GC with lymph node spread.[9]

New molecular classifications of gastric cancer have recently been proposed.[1,10] We are witnessing huge advances in our understanding of cancer from a molecular, immunological, diagnostic and even bioinformatical standpoint, all contributing to better tailored treatments for patients.[1,10–15] In both classifications, microsatellite instability (MSI) is a distinct molecular subgroup of GC. In the available studies, MSI is associated with older age, female gender, intestinal histotype, non-cardia tumors, lower number of metastatic lymph nodes, and better survival.[16–18] It seems that the MSI subgroup is not homogenous and other genetic and molecular factors may play an important role for these particular patients.

The aim of the study was to compare the clinical and pathological data of *PIK3CA* mutation in GC patients. We divided *PIK3CA* mutations into 2 categories based on the hotspot mutation sites at exon 9 and exon 20. In addition, we investigated the coexistence of this mutation with MSI status and *KRAS* mutations.

Material and methods

Patients

The analysis was performed on a group of 472 GC patients treated in the General Surgery and Surgical Oncology Department, University of Siena, Italy. We used tissue material stored in our biobank collected from patients who were operated on between 1990–2011. None of these patients received neoadjuvant treatment. We used tumoral and healthy tissues for comparative analysis. All samples were collected just after resection in the operating theatre.

PIK3CA sample preparation

Genomic DNA was extracted by tumoral and constitutional fresh frozen sample tissues using a standard protocol (Gentra Systems, Minneapolis, USA). The DNA concentration was calculated by spectrophotometry.

Polymerase chain reaction (PCR) is used for the screening of *PIK3CA* (exon 9 and 20).

To search for somatic alterations of the *PIK3CA* gene, exons 9 and 20 were sequenced according to the protocol described in detail by Velho et al.[19] PCR reactions were carried out in a volume of 20 µL containing 100 ng/µL genomic DNA template, 1X Reaction Buffer, 0.5 µM of each PCR primer, $MgCl_2$ 1.25 mM, 0.15 mM of each dNTPs, *Taq* polymerase 0.5 U/µL (Euroclone, Pero, Italy). The reactions were performed in programmable thermocyclers according to the standard protocol.

A 5 µL aliquot of each PCR reaction was run on a 2% agarose gel to confirm the size, quantity, and purity of each PCR product. The remaining 15 µL of PCR amplified bands were extracted from the gel with the Invisorb® Spin DNA Extraction Kit (Invitek, Stratec Biomedical Systems, Birkenfeld, Germany). Samples were then purified and 2 µL aliquot of purified PCR product was cycle sequenced using a BigDye Terminator Kit (Applied Biosystems, Foster City, USA) in a total volume of 20 µL. Samples were then purified and sequenced using an automated DNA sequencer ABI PRISM 310 Genetic Analyzer (Applied Biosystems, Milan, Italy) according to the protocol of the manufacturer. Sequencing was performed in both strands. All sequence alterations in these genes were validated with a second independent PCR.

Pentaplex polymerase chain reaction and microsatellite analysis

A detailed description of MSI analysis was described in our previous paper.[18] In short, we used 5 quasi-monomorphic

mononucleotide repeats, namely, BAT-26, BAT-25, NR-24, NR-21, and NR-27. Following the definition of the National Cancer Institute workshop on MSI for cancer, we considered a tumor as MSI when 2 or more markers showed instability on 5 loci (MSI-H).[20]

A detailed description of the pathological, clinical, surgical and follow-up data was also given in our previous publication.[18]

Statistical analysis

Statistical analysis was performed with the χ^2 test or Fisher exact test to compare categorical variables. The Mann-Whitney U test was used to compare continuous variables not normally distributed. Cumulative survival was calculated by the life table method of Kaplan and Meier, and the log-rank test was used to distinguish significant differences. Statistical significance was determined at p-value < 0.05.

Survival curves estimated using the Kaplan-Meier method were compared using a log-rank test, considering death from cancer as the end-point (cancer-related survival).

The Kaplan-Meier estimation was used to plot survival curves, and log-rank tests were used to calculate the difference of overall survival (OS) between groups.

Multivariate Cox proportional hazard regression analysis was used to investigate independent prognostic factors for overall survival between groups. The variables including *PIK3CA* status, age, sex, tumor location, MSI status, Lauren histotype, type of resection, T, N, M status, and adjuvant therapy were used as covariates. Statistical analysis was done using commercially available statistical software (SPSS 20.0 for Windows SPSS Inc., Chicago, USA).

Results

PIK3CA mutation was observed in 10 of 472 GC patients (2.1%). Half of the 10 patients had mutations in exon 9 and the other half in exon 20. For exon 9 mutations, we found 2 mutations of *E542K*, 1 mutation of *E545K*, 1 of *N515S*, and 1 of *E545G*. All 5 patients with a mutation in exon 20 had mutation of *H1047R*.

Interestingly, 9 of 10 patients were also MSI positive. In 2 patients (20%), we observed *KRAS* mutation and *PIK3CA* mutation in exon 20. Both patient showed *KRAS* mutation -12D and were associated with better prognosis.

A clinicopathological comparison of *PIK3CA* patients and wild-type (wt) *PIK3CA* patients is presented in Table 1. The only statistically significant factor associated with *PIK3CA* mutations was MSI status. We also performed an analysis of *PIK3CA* mutation on the MSI positive subgroup. The clinicopathological analysis is presented in Table 2. Here, the only statistically significant factor was tumor position.

Table 1. *PIK3CA* wild type vs mutations in all GC group

Clinico-pathological characteristic	*PIK3CA* wt		*PIK3CA* mut		p-value
Patient (n)	462		10		–
Age (years, median)	70		75		0.058
Sex (male, female)	280:182 (60.6:39.4)		3:7 (30:70)		0.051
pT					0.657
1	42	9.1%	0	0%	–
2	74	16%	1	10%	–
3	95	20.6%	3	30%	–
4	251	54.3%	6	60%	–
pN					0.471
0	130	28.1%	3	30%	–
1	75	16.2%	2	20%	–
2	100	21.6%	4	40%	–
3a	74	16%	0	0%	–
3b	83	18%	1	10%	–
Tumor site					0.256
Non cardia	386	83.5%	7	70%	–
Cardia	76	16.5%	3	30%	–
MSI status					<0.001
MSS	360	77.9%	1	10%	–
MSI-H	102	22.1%	9	90%	–
Lauren					0.078
Diffuse/mixed	153	33.1%	0	0%	–
Intestinal	305	66%	10	100%	–
Unclassified	4	0.9%	0	0%	–
UICC-R					0.345
R0	339	73.4%	6	60%	–
R+	123	26.6%	4	40%	–
Stage					0.389
I	74	16%	1	10%	–
II	108	23.4%	3	30%	–
III	194	42%	6	60%	–
IV	86	18.6%	0	0%	–
M					0.131
M0	376	81.4%	10	100%	–
M1	86	18.6%	0	0%	–
WHO histological type*					0.132
Papillary	15	3.2%	0	0%	–
Poorly differentiated	146	31.6%	5	50%	–
Signet ring cell & mucinous	138	29.9%	0	0%	–
Tubular (well/mod. diff.)	153	33.1%	4	40%	–
Adjuvant					0.406
No	216	46.8%	6	60%	–
Yes	246	53.2%	4	40%	–

* 11 cases with unclassified WHO histotype are excluded ; MSS – microsatellite stable; MSI-H – microsatellite instable; M – metastases; pT – pathological tumor status; pN – pathological lymph node status.

Table 2. MSI status patients and *PIK3CA* mutations

Clinico-pathological characteristic	*PIK3CA* wt		*PIK3CA* mut		p-value
Patient (n)	102		9		–
Age (years, median)	75		76		0.559
Sex (male, female)	44:58 (43.1: 56.9)		2:7 (22.2:77.8)		0.222
pT					0.744
1	5	4.9%	0	0%	–
2	20	19.6%	1	11.1%	–
3	36	35.3%	3	33.3%	–
4	41	40.2%	5	55.6%	–
pN					0.309
0	44	43.1%	3	33.3%	–
1	18	17.6%	2	22.2%	–
2	19	18.6%	4	44.4%	–
3a	10	9.8%	0	0%	–
3b	11	10.8%	0	0%	–
Tumor site					0.008
Non-cardia	99	97.1%	7	77.8%	–
Cardia	3	2.9%	2	22.2%	–
Lauren					0.069
Diffuse/mixed	28	27.5%	0	0%	–
Intestinal	74	72.5%	9	100%	–
UICC-R					0.289
R0	83	81.4%	6	66.7%	–
R+	19	18.6%	3	33.3%	–
Stage					0.584
I	17	16.7%	1	11.1%	–
II	40	39.2%	3	33.3%	–
III	36	35.3%	5	55.6%	–
IV	9	8.8%	0	0%	–
M					0.353
M0	93	91.2%	9	100%	–
M1	9	8.8%	0	0%	–
WHO histological type*					0.287
Papillary	1	1%	0	0%	–
Poorly differentiated	42	41.2%	4	44.4%	–
Signet ring cell & Mucinous	23	22.5%	0	0%	–
Tubular (well/mod diff.)	34	33.3%	4	44.4%	–
Adjuvant					0.756
No	73	71.6%	6	66.7%	–
Yes	29	28.4%	3	33.3%	–

* 3 cases with unclassified WHO histotype are excluded ;
MSS – microsatellite stable; MSI-H – microsatellite instability;
pT – pathological tumor status; pN – pathological lymph node status;
UICC-R – Union Internationale Contre le Cancer Resection margin.

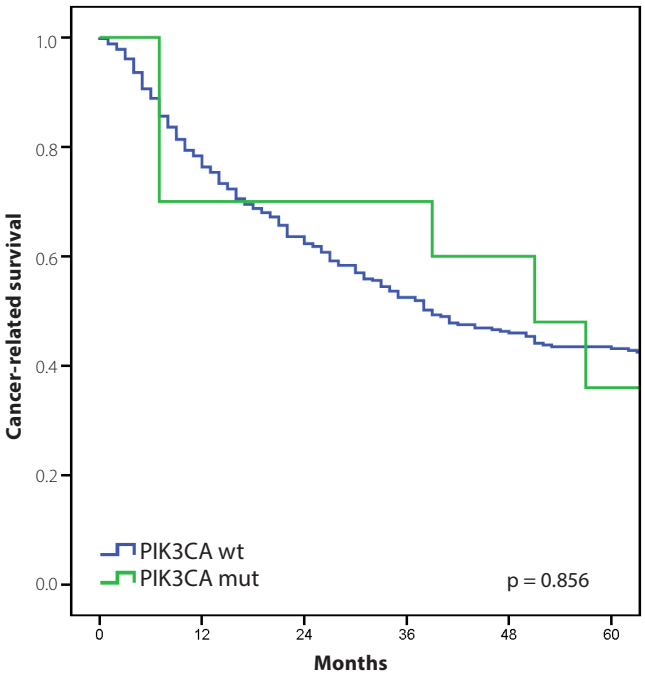

Fig. 1. Cancer-related survival of patients with or without mutation in *PIK3CA*

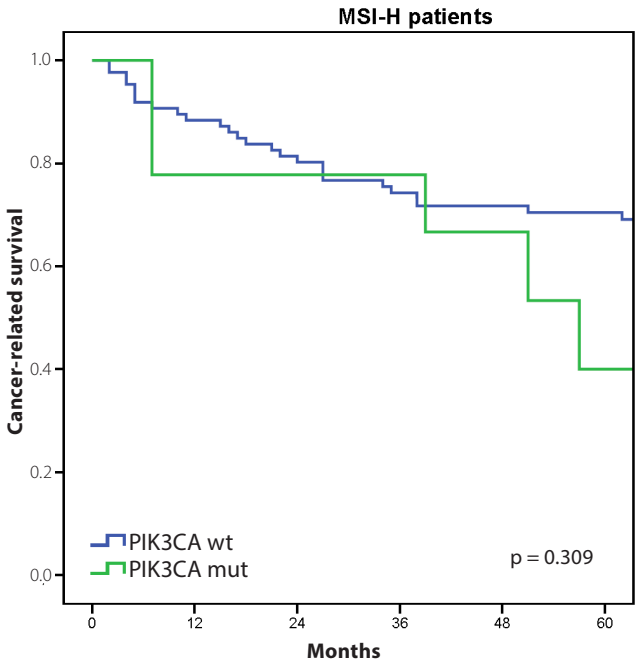

Fig. 2. Cancer-related survival of patients with MSI status with or without *PIK3CA* mutation

Interestingly all ten patients showed Lauren intestinal histotype.

We also analyzed cancer-related survivals. The first comparison was performed between all patients with or without *PIK3CA* mutation (Fig. 1). 5-year survival for *PIK3CA* wt patients was 43.2% and for *PIK3CA* mutation, 36% (p = 0.856). Secondly, we analyzed the group of MSI GC patients (Fig. 2). The 5-year survival of the MSI patients presenting with *PIK3CA* mutation was 40% and

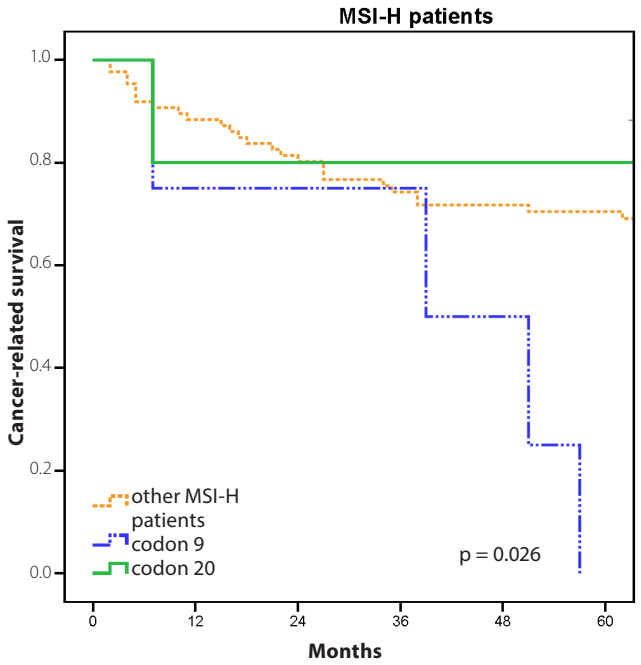

Fig. 3. Comparison of cancer-related survival of patients with different *PIK3CA* exon mutations together with a survival curve of MSI GC patients without *PIK3CA* mutation

Table 3. Cox proportional hazards regression analysis

Clinico-pathological characteristic	B	Exp (B)	95% CI	p-value
PIK3CA	–0.113	0.893	0.440–1.815	0.755
MSI status	–0.592	0.553	0.405–0.7554	<0.001
Age	0.032	1.032	1.018–1.047	<0.001
Gender	0.363	1.437	1.130–1.829	0.003
Lauren histotype	0.064	1.066	0.823–1.381	0.629
Tumor location	0.027	1.028	0.758–1.394	0.860
"T" parameter	0.602	1.826	1.322–2.522	<0.001
"N" parameter	0.675	1.965	1.354–2.850	<0.001
"M" parameter	0.060	1.062	0.770–1.463	0.715
Radicality of resection	1.098	2.999	2.264–3.972	<0.001
Adjuvant therapy	–0.033	0.967	0.683–1.370	0.851

PIK3CA status expressed as *PIK3CA* wt = 0 and *PIK3CA* mutation = 1; MS status expressed as MSS = 0 and MSI = 1; gender expressed as F = 0 an M = 1; Lauren histotype expressed as intestinal = 0 and non-intestinal = 1; tumor location expressed as non-cardias = 0 and cardias = 1; "T" parameter expressed as T1–T2 = 0 and T3–T4 = 1; "N" parameter expressed as N– = 0 and N+ = 1; "M" parameter expressed as negative = 0 and positive = 1; radicality of resection expressed as R0 = 0 and R1–R2 = 1; adjuvant therapy expressed as yes = 1 and no = 0;
MSI status – microsatellite instability; T parameter – pathological tumor status; N parameter – pathological lymph node status; M parameter – metastases status.

without the mutation, 70.4% (p = 0.309). We also checked the difference in survival of patients with the *PIK3CA* mutation in different exons (Fig. 3). For mutation in exon 9, the 5-year survival was 0% and for mutation in exon 20 – 80% (p = 0.031). For better visualization of these differences between the 2 mutation locations, we added a survival curve for MSI patients without *PIK3CA* mutation (p = 0.026) – Fig. 3.

The Cox proportional hazards regression analysis showed that age, sex, MSI status, "T" parameter, "N" parameter and type of "R" resection were the only prognostic factors statistically correlated with a worse overall survival (Table 3).

Discussion

In previous reports, the frequency of GC *PIK3CA* mutations varies from 4% to 13.2%.[21,22] In our paper, *PIK3CA* mutation occurred in 8.1% of the MSI group. In total, only a frequency of 2.1% was observed, lower in comparison with previous studies. The debate about *PIK3CA* mutation and its prognosis for different cancers is unresolved. Some authors suggest *PIK3CA* mutation is associated with a better prognosis in the case of breast cancer, while other authors showed worse prognosis in cancers like colorectal, endometrial, and lung cancers.[8,23–25] Warneke et al. presented interesting data for gastric cancer, showing worse survival in *PIK3CA* exon 20 mutation with intestinal histotype and better survival for the same mutation with diffuse histotype.[26] These results were statistically significant. In our study, it was impossible to analyze this factor because we did not observe diffuse/mixed histotype in our sample. *PIK3CA* mutation in exon 20 was found to be an independent prognostic factor of survival for intestinal pathology. Also, our results show that mutation in exon 20 presented improved patient survival.

In the paper by Fang et al., they found *PIK3CA* mutation in 57/432 of patients (13.2%).[22] They analyzed PIK3/AKT mutations together and found that in the intestinal histotype, patients presenting mutation in that gene showed tumors located mostly in the lower third of the stomach. In diffuse histotype, the location of the tumor was in the upper third of the stomach and patients showed a higher rate of hematogenous metastases. The authors did not find any difference in survival between patients presenting or not presenting *PIK3/AKT* mutation.

The authors also searched for a link between the *PIK3CA* mutation and Epstein-Barr virus (EBV) infection. The rate of EBV infection was higher only in the situation where the tumor was situated in the middle part of the stomach for GC patients with *PIK3CA* mutation.[22]

In a paper by Barbie et al., the authors also analyzed *PIK3CA* mutation in GC and its association with GC and MSI.[27] Only 8 of 39 MSI GC cases harbored the *H1047R* mutation. They found that this finding did not correlate with survival or any other clinical or pathological features linked with MSI GC. This is similar to our results on the exon 20 mutation in MSI patients, in which similar survival results were observed. A worse outcome was only observed in the case of exon 9 mutation, which was not observed in the above-mentioned study.[28]

In our study, we observed that *PIK3CA* patients were older and showed intestinal histotype more often but without statistical significance. Analyzing the subgroup of MSI GC patients, the only differences were tumor position (p = 0.008) and Lauren histotype (p = 0.069) – *PIK3CA* mutations were more commonly seen in the upper third of the stomach and also showed only intestinal histology. We did not observe any difference in survival between wild-type and mutated *PIK3CA* GC patients; however, in the MSI GC subgroup of patients, those with *PIK3CA* mutation had a worse 5-year survival rate (40%) than those without the mutation (70.4%).

PIK3CA mutations are also observed in head and neck squamous cell carcinoma (HNSCC) for 6–21% of patients.[4] Interestingly, this mutation was absent across German, Vietnamese, and Greek patients.[28,29] Likely, some ethnic, environmental, and/or other unknown factors are associated with this finding. A paper by Seiwert et al. pointed out that *PIK3CA* mutations are more commonly associated with human papillomavirus (HPV) positive HNSCC cancers.[30] This finding did not reach statistical significance but can be an example of a factor that may play an important role in developing this mutation. In our study, we observed one of the smallest incidences of *PIK3CA* mutation in GC patients – 2.1%.

In a CRC study by Day et al., it was found that *PIK3CA* exon 20 mutations were associated with proximal tumors and a sessile-serrated pathway (MSI-H/CIMP high/BRAF mutations), and *PIK3CA* exon 9 mutations were linked with the traditional serrated pathway of tumorigenesis (CIMP-low/KRAS mutations).[6] *PIK3CA* mutations were significantly associated with older age, proximal tumor site and mucinous histology, and *KRAS* mutation.[6] Comparison between wt *PIK3CA* and either exon 9 or 20 mutations showed some significant results. Mucinous histology was associated with exon 20, and for exon 9, factors like older age and *KRAS* mutations were associated. The direct comparison of exon 9 and 20 mutations did not reach statistical significance. In a study by Sukawa et al., MSI status was observed in 50% of *PIK3CA* GC patients.[21] Similarly, our results show a statistically significant link between *PIK3CA* mutation and MSI status. In fact, almost all of our GC patients presenting with a *PIK3CA* mutation were also MSI positive. *KRAS* mutation was observed only in the exon 20 mutation group (2 of 5 patients – 40%).

In breast cancer, *PIK3CA* mutations are seen in 40% of cases.[4] The presence of this mutation is associated with better prognosis in this cancer. Also, clinicopathological factors show higher rates of small tumor size, low grade, and positive estrogen receptor much more frequently in this group of patients.[24] Importantly, these patients also showed better survival.[24] In other cancers like colorectal, endometrial, or lung cancer, *PIK3CA* mutation is associated with worse prognosis.[23,25] We did not find any difference in survival between patients with and without *PIK3CA* mutations. The difference was observed when we analyzed subgroups according to the type of exon mutation.

Our study was limited by the small number of patients with *PIK3CA* mutations in our GC patient pool. We presented a link between different *PIK3CA* exon mutations and MSI GC that present completely different prognoses depending on the type of mutation. The MSI subtype of GC is a relatively new molecular subgroup and requires further analysis of different mutations that may have a positive or negative impact on patient outcome.

Our research leads to some important conclusions about *PIK3CA* mutations. Firstly, *PIK3CA* mutations in GC is rare. It is strongly associated with the MSI molecular subgroup, presenting a worse outcome than wt PIK3CA MSI GC patients. A completely different outcome is associated with mutation in exon 9 vs exon 20, with the latter being more favorable. The role of this mutation must be further studied with larger groups of patients.

References

1. Cristescu R, Lee J, Nebozhyn M, et al. Molecular analysis of gastric cancer identifies subtypes associated with distinct clinical outcomes. *Nat Med*. 2015;21(5):449–456.
2. Wadhwa R, Song S, Lee JS, Yao Y, Wei Q, Ajani JA. Gastric cancer-molecular and clinical dimensions. *Nat Rev Clin Oncol*. 2013;10: 643–655.
3. Willems L, Tamburini J, Chapuis N, Lacombe C, Mayeux P, Bouscary D. PI3K and mTOR signaling pathways in cancer: New data on targeted therapies. *Curr Oncol Rep*. 2012;14:129–138.
4. Lai K, Killingsworth MC, Lee CS. Gene of the month: PIK3CA. *J Clin Pathol*. 2015;68:253–257.
5. Volinia S, Hiles I, Ormondroyd E, et al. Molecular cloning, cDNA sequence, and chromosomal localization of the human phosphatidylinositol 3-kinase p110 alpha (PIK3CA) gene. *Genomics*. 1994;24: 472–477.
6. Day FL, Jorissen RN, Lipton L, et al. PIK3CA and PTEN gene and exon mutation-specific clinicopathologic and molecular associations in colorectal cancer. *Clin Cancer Res*. 2013;19(12):3285–3296.
7. Whitehall VL, Rickman C, Bond CE, et al. Oncogenic PIK3CA mutations in colorectal cancers and polyps. *Int J Cancer*. 2012;131: 813–820.
8. Mao C, Yang ZY, Hu XF, Chen Q, Tang JL. PIK3CA exon 20 mutations as a potential biomarker for resistance to anti-EGFR monoclonal antibodies in KRAS wild-type metastatic colorectal cancer: A systematic review and meta-analysis. *Ann Oncol*. 2012;23:1518–1525.
9. Tapia O, Riquelme I, Leal P, et al. The PI3K/AKT/mTOR pathway is activated in gastric cancer with potential prognostic and predictive significance. *Virchows Arch*. 2014;465:25–33.
10. Cancer Genome Atlas Research Network. Comprehensive molecular characterization of gastric adenocarcinoma. *Nature*. 2014;513(7517): 202–209.
11. Isa N. Evidence based radiation oncology with existing technology. *Rep Pract Oncol Radiother*. 2014;19(6):259–266.
12. Polom W, Markuszewski M, Rho YS, Matuszewski M. Usage of invisible near infrared light (NIR) fluorescence with indocyanine green (ICG) and methylene blue (MB) in urological oncology. Part 1. *Cent European J Urol*. 2014;67(2):142–148.
13. Subhash VV, Yeo MS, Tan WL, Yong WP. Strategies and advancements in harnessing the immune system for gastric cancer immunotherapy. *J Immunol Res*. 2015;308574. doi: 10.1155/2015/308574
14. Alocci D, Mariethoz J, Horlacher O, Bolleman JT, Campbell MP, Lisacek F. Property Graph vs RDF triple store: A comparison on glycan substructure search. *PLoS One*. 2015;10(12):e0144578. doi: 10.1371/journal.pone.0144578
15. Mereiter S, Magalhães A, Adamczyk B, et al. Glycomic analysis of gastric carcinoma cells discloses glycans as modulators of RON receptor tyrosine kinase activation in cancer. *Biochim Biophys Acta*. 2016; 1860(8):1795–1808.

16. Beghelli S, de Manzoni G, Barbi S, et al. Microsatellite instability in gastric cancer is associated with better prognosis in only stage II cancers. *Surgery*. 2006;139:347–356.
17. Corso G, Pedrazzani C, Marrelli D, Pascale V, Pinto E, Roviello F. Correlation of microsatellite instability at multiple loci with long-term survival in advanced gastric carcinoma. *Arch Surg*. 2009;144: 722–727.
18. Marrelli D, Polom K, Pascale V, et al. Strong prognostic value of microsatellite instability in intestinal type non-cardia gastric cancer. *Ann Surg Oncol*. 2016;23(3):943–950.
19. Velho S, Oliveira C, Ferreira A, et al. The prevalence of *PIK3CA* mutations in gastric and colon cancer. *Eur J Cancer*. 2005;41:1649–1654.
20. Boland CR, Thibodeau SN, Hamilton SR, et al. A National Cancer Institute workshop on microsatellite instability for cancer detection and familial predisposition: Development of international criteria for the determination of microsatellite instability in colorectal cancer. *Cancer Res*. 1998;58(22):5248–5257.
21. Sukawa Y, Yamamoto H, Nosho K, et al. Alterations in the human epidermal growth factor receptor 2-phosphatidylinositol 3-kinase-v-Akt pathway in gastric cancer. *World J Gastroenterol*. 2012;18(45): 6577–6586. doi: 10.3748/wjg.v18.i45.6577
22. Fang WL, Huang KH, Lan YT, et al. Mutations in *PI3K/AKT* pathway genes and amplifications of *PIK3CA* are associated with patterns of recurrence in gastric cancers. *Oncotarget*. 2016;7(5):6201–6220. doi: 10.18632/oncotarget.6641
23. Catasus L, Gallardo A, Cuatrecasas M, Jaime P. *PIK3CA* mutations in the kinase domain (exon 20) of uterine endometrial adenocarcinomas are associated with adverse prognostic parameters. *Mod Pathol*. 2008;21:131–139.
24. Kalinsky K, Jacks LM, Heguy A, Patil S, Prat J. *PIK3CA* mutation associates with improved outcome in breast cancer. *Clin Cancer Res*. 2009; 15:5049–5059.
25. Janku F, Garrido-Laguna I, Petruzelka LB, Stewart DJ, Kurzrock R. Novel therapeutic targets in non-small cell lung cancer. *J Thorac Oncol*. 2011;6:1601–1612.
26. Warneke VS, Behrens HM, Haag J, et al. Prognostic and putative predictive biomarkers of gastric cancer for personalized medicine. *Diagn Mol Pathol*. 2013;22(3):127–137. doi: 10.1097/PDM0b013e318284188e
27. Barbi S, Cataldo I, De Manzoni G, et al. The analysis of *PIK3CA* mutations in gastric carcinoma and metaanalysis of literature suggest that exon-selectivity is a signature of cancer type. *J Exp Clin Cancer Res*. 2010;16:29–32.
28. Kostakis GC, Papadogeorgakis N, Koumaki V, Kamakari S, Koumaki D, Alexandridis C. Absence of hotspot mutations in exons 9 and 20 of the *PIK3CA* gene in human oral squamous cell carcinoma in the Greek population. *Oral Surg Oral Med Oral Pathol Oral Radiol Endod*. 2010;109:e53–58. doi: 10.1016/j.tripleo.2010.01.015
29. Fenic I, Steger K, Gruber C, Arens C, Woenckhaus J. Analysis of *PIK-3CA* and Akt/protein kinase B in head and neck squamous cell carcinoma. *Oncol Rep*. 2007;18:253–259.
30. Seiwert, TY, Zuo Z, Keck MK, et al. Integrative and comparative genomic analysis of HPV-positive and HPV-negative head and neck squamous cell carcinomas. *Clin Cancer Res*. 2015;21(3):632–641. doi: 10.1158/1078-0432.CCR-13-3310

Evaluation of the secretion and release of vascular endothelial growth factor from two-dimensional culture and three-dimensional cell spheroids formed with stem cells and osteoprecursor cells

Hyunjin Lee[A–F], Sung-Il Lee[A–F], Youngkyung Ko[A–F], Jun-Beom Park[A–F]

Department of Periodontics, College of Medicine, Catholic University of Korea, Seoul, Republic of Korea

A – research concept and design; B – collection and/or assembly of data; C – data analysis and interpretation;
D – writing the article; E – critical revision of the article; F – final approval of the article

Advances in Clinical and Experimental Medicine, ISSN 1899-5276 (print), ISSN 2451-2680 (online) *Adv Clin Exp Med*. 2018;27(7):971–977

Address for correspondence
Jun-Beom Park
E-mail: jbassoonis@yahoo.co.kr

Funding sources
This research was supported by the Basic Science Research Program through the National Research Foundation of Korea (NRF) funded by the Ministry of Science, Information and Communication Technology & Future Planning (NRF-2017R1A1A1A05001307).

Conflict of interest
None declared

Received on October 26, 2016
Reviewed on January 19, 2017
Accepted on April 26, 2017

Abstract

Background. Co-culture has been applied in cell therapy, including stem cells, and has been reported to give enhanced functionality.

Objectives. In this study, stem-cell spheroids were formed in concave micromolds at different ratios of stem cells to osteoprecursor cells, and the amount of secretion of vascular endothelial growth factor (VEGF) was evaluated.

Material and methods. Gingiva-derived stem cells and osteoprecursor cells in the amount of 6×105 were seeded on a 24-well culture plate or concave micromolds. The ratios of stem cells to osteoprecursor cells included: 0:4 (group 1), 1:3 (group 2), 2:2 (group 3), 3:1 (group 4), and 4:0 (group 5).

Results. The morphology of cells in a 2-dimensional culture (groups 1–5) showed a fibroblast-like appearance. The secretion of VEGF increased with the increase in stem cells, and a statistically significant increase was noted in groups 3, 4 and 5 when compared with the media-only group ($p < 0.05$). Osteoprecursor cells formed spheroids in concave microwells, and no noticeable change in the morphology was noted with the increase in stem cells. Spheroids containing stem cells were positive for the stem-cell markers SSEA-4. The secretion of VEGF from cell spheroids increased with the increase in stem cells.

Conclusions. This study showed that cell spheroids formed with stem cells and osteoprecursor cells with different ratios, using microwells, had paracrine effects on the stem cells. The secretion of VEGF increased with the increase in stem cells. This stem-cell spheroid may be applied for tissue-engineering purposes.

Key words: vascular endothelial growth factor, osteoblast, co-culture techniques, cellular spheroids, stem cell research

DOI
10.17219/acem/70789

Introduction

Co-culture has been applied in cell therapy, including stem cells, and has been reported to give enhanced functionality. Spheroids formed with primary hepatocytes and hepatic stellate cells showed a higher secretion of albumin than mono-culture hepatospheres.[1] Additionally, the enzymatic activity of co-cultured heterospheres was higher than the activity of a mono-culture.[1] Primary pancreatic islets and hepatocytes were applied as spheroids for the 3-dimensional co-culture model.[2] It was shown that the 2 different types of cells supported each other's functionality when compared with a mono-culture.

Our group isolated and characterized human mesenchymal stem cells from the gingiva.[3] Gingiva-derived stem cells have been suggested as candidates in the tissue-engineering field.[4] In this study, stem-cell spheroids were formed in concave micromolds at different ratios of stem cells to osteoprecursor cells, and the amount of secretion of vascular endothelial growth factor (VEGF) was evaluated. To the best of the authors' knowledge, this report is the first to evaluate the secretion of VEGF from cell spheroids formed with human gingiva-derived stem cells and osteoprecursor cells.

Material and methods

Isolation and culturing of gingiva-derived stem cells

Gingiva-derived stem cells were obtained using a previously reported method.[4] The Institutional Review Board of Seoul St. Mary's Hospital, College of Medicine, Catholic University of Korea approved this study (KC11SISI0348). All participants signed informed consent.

Gingival tissues were de-epithelialized, minced into 1–2 mm^2 fragments and digested in an alpha-modified, minimal essential medium (α-MEM; Gibco, Grand Island, USA) containing dispase (1 mg/mL; Sigma-Aldrich, St. Louis, USA) and collagenase IV (2 mg/mL; Sigma-Aldrich). The cells were incubated in a humidified incubator at 37°C. The non-adherent cells were washed with phosphate-buffered saline (PBS) (Welgene, Daegu, South Korea) and replaced with a fresh medium every 2–3 days.

Co-culture of gingiva-derived stem cells and osteoprecursor cells

Gingiva-derived stem cells and murine calvarial osteoprecursor cells (MC3T3-E1) (ATCC, Manassas, USA) in the amount of 6×10^5 were seeded on a 24-well culture plate and grown with a growth medium α-MEM. The ratios of stem cells to osteoprecursor cells included: 0:4 (group 1), 1:3 (group 2), 2:2 (group 3), 3:1 (group 4), and 4:0 (group 5).

Formation of cell spheroids with human gingiva-derived stem cells and osteoprecursor cells

Stem-cell spheroids were formed in polydimethylsiloxane-based concave micromolds (Prosys® StemFit 3D; Prodizen Inc., Seoul, South Korea) of a diameter of 600 μm (Fig. 1). Gingiva-derived stem cells and MC3T3-E1 cells in the amount of 6×10^5 were at the ratios of 0:4 (group 1), 1:3 (group 2), 2:2 (group 3), 3:1 (group 4), and 4:0 (group 5). Cell aggregation and cell-spheroid formation were observed under an inverted microscope (Leica DM IRM; Leica Microsystems, Wetzlar, Germany).

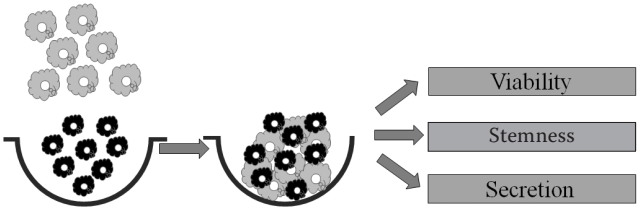

Fig. 1. Schematic illustration of the study using gingival-derived stem cells

Determination of cell viability

The viability of the cell spheroids was analyzed qualitatively by a Live/Dead Kit assay (Molecular Probes, Eugene, USA) on day 3. The cell spheroids were washed twice with PBS, followed by suspension in 1 mL of α-MEM, containing 2 μL of 50 mM calcein acetoxymethyl ester working solution and 4 μL of 2 mM ethidium homodimer-1, for 15 min at room temperature. The spheroids stained with calcein acetoxymethyl ester and ethidium homodimer-1 were observed under a confocal laser microscope (LSM800 with Airyscan; Carl Zeiss, Jena, Germany). The viable cells produced intense, uniform, green fluorescence; dead cells showed red fluorescence with this assay.

Evaluation of maintenance of expression of stem cell markers

The spheroids were retrieved on day 3 to evaluate the expression of stem cell markers. The spheroids were incubated with human SSEA-4 (Clone MC-813-70) conjugated to NHL493 (green) and human TRA-1-60(R) (Clone TRA-1-60) conjugated to NL557 (red) (R&D Systems, Minneapolis, USA) after dilution to 1 × concentration. The spheroids were visualized under a confocal laser microscope (LSM800 with Airyscan; Carl Zeiss). These antibodies were used as positive markers of human stem cells.

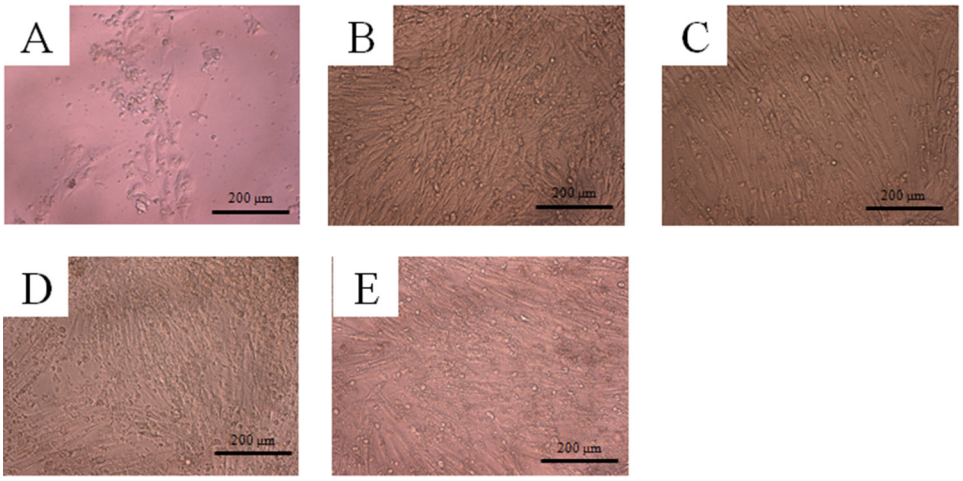

Fig. 2. Morphology of 2-dimensional stem cells cultured with osteoprecursor cells on day 3

A – group 1; B – group 2; C – group 3; D – group 4; E – group 5.

Evaluation of secretion of human vascular endothelial growth factor

The determination of human VEGF from 2- and 3-dimensional systems was performed using a commercially available kit (Quantikine® ELISA; R&D Systems). All reagents and samples were prepared according to the manufacturer's recommendations. A media group served as the control.

Statistical analysis

A test of normality was performed with the Shapiro-Wilk test, and a one-way analysis of variance with Tukey's post hoc test was performed to analyze the differences between the groups, using a commercially available program (SPSS 12 for Windows; SPSS, Chicago, USA), with the level of significance set at 0.05.

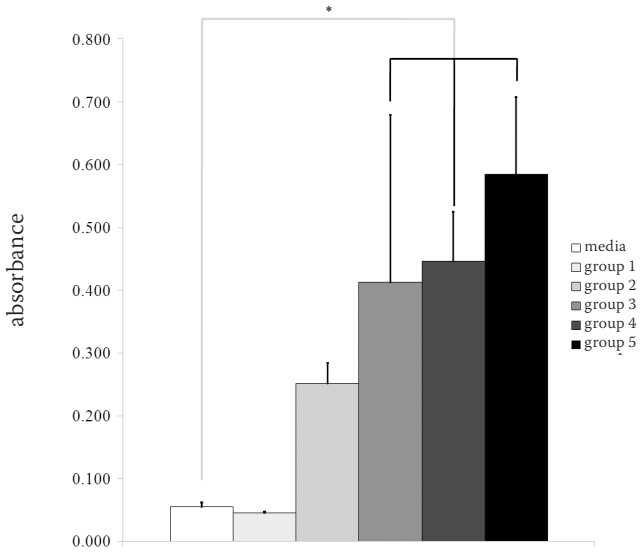

Fig. 3. Secretion of VEGF from 2-dimensional culture

One-way analysis of variance with Tukey's post hoc test was performed to determine the differences between the groups; * statistically significant differences were noted when compared with the media-only group.

Results

Evaluation of 2-dimensional culture

The morphology of the osteoprecursor cells showed a fibroblast-like appearance on day 3 (Fig. 2A). No significant difference in the morphology was noted when the culture with gingiva-derived stem cells was at different ratios of stem cells to osteoprecursor cells: 1:3 (group 2), 2:2 (group 3), 3:1 (group 4), and 4:0 (group 5) (Fig. 2B, 2C, 2D, and 2E, respectively).

Secretion of human vascular endothelial growth factor from 2-dimensional culture

The secretion of VEGF was noted in groups 2, 3, 4, and 5 (Fig. 3), and it increased with the increase in stem cells. A statistically significant increase was noted in groups 3, 4 and 5 when compared with the media-only group ($p < 0.05$).

Evaluation of spheroid morphology

The morphology of the spheroids on day 3 is shown in Fig. 4. Osteoprecursor cells formed spheroids in concave microwells (Fig. 4A). Gingiva-derived stem cells and osteoprecursor cells also formed spheroids (Fig. 4B–E). No significant change in the morphology was noted with the increase in stem cells, at different ratios of stem cells to osteoprecursor cells: 1:3 (group 2), 2:2 (group 3), 3:1 (group 4), and 4:0 (group 5) (Fig. 4B, 4C, 4D, and 4E, respectively).

Determination of cell viability and maintenance of expression of stem cell markers

Most of the cells in the spheroids emitted green fluorescence; a small portion of red fluorescence was also noted (Fig. 5). Spheroids containing stem cells were positive for

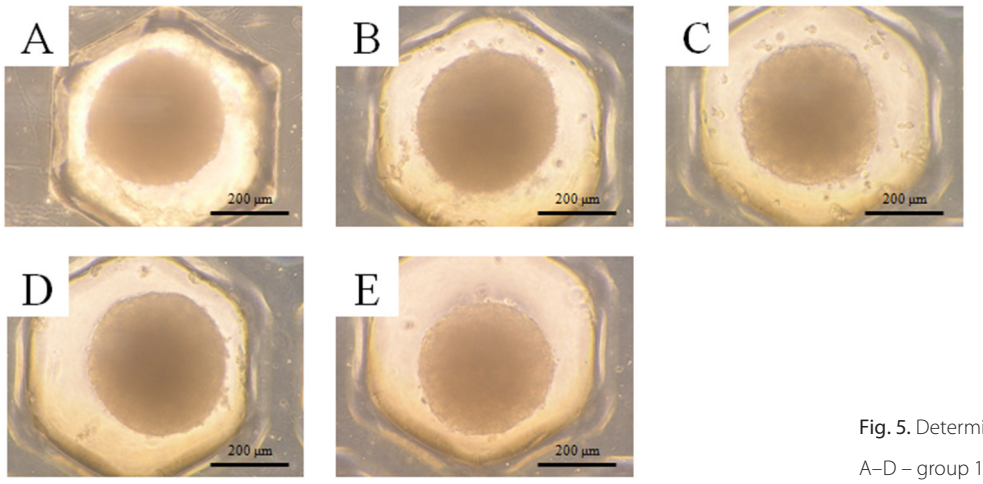

Fig. 4. Morphology of 3-dimensional stem cells cultured with osteoprecursor cells on day 3 (osteoprecursor cells formed spheroids in concave microwells)

A – group 1; B – group 2; C – group 3; D – group 4; E – group 5; no significant change in the morphology was noted with the increase in stem cells, at different ratios of stem cells to osteoprecursor cells: 0:4, 1:3, 2:2, and 3:1.

Fig. 5. Determination of cell viability of cell spheroids

A–D – group 1; E–H – group 2; I–L – group 3; M–P – group 4; Q–T – group 5.

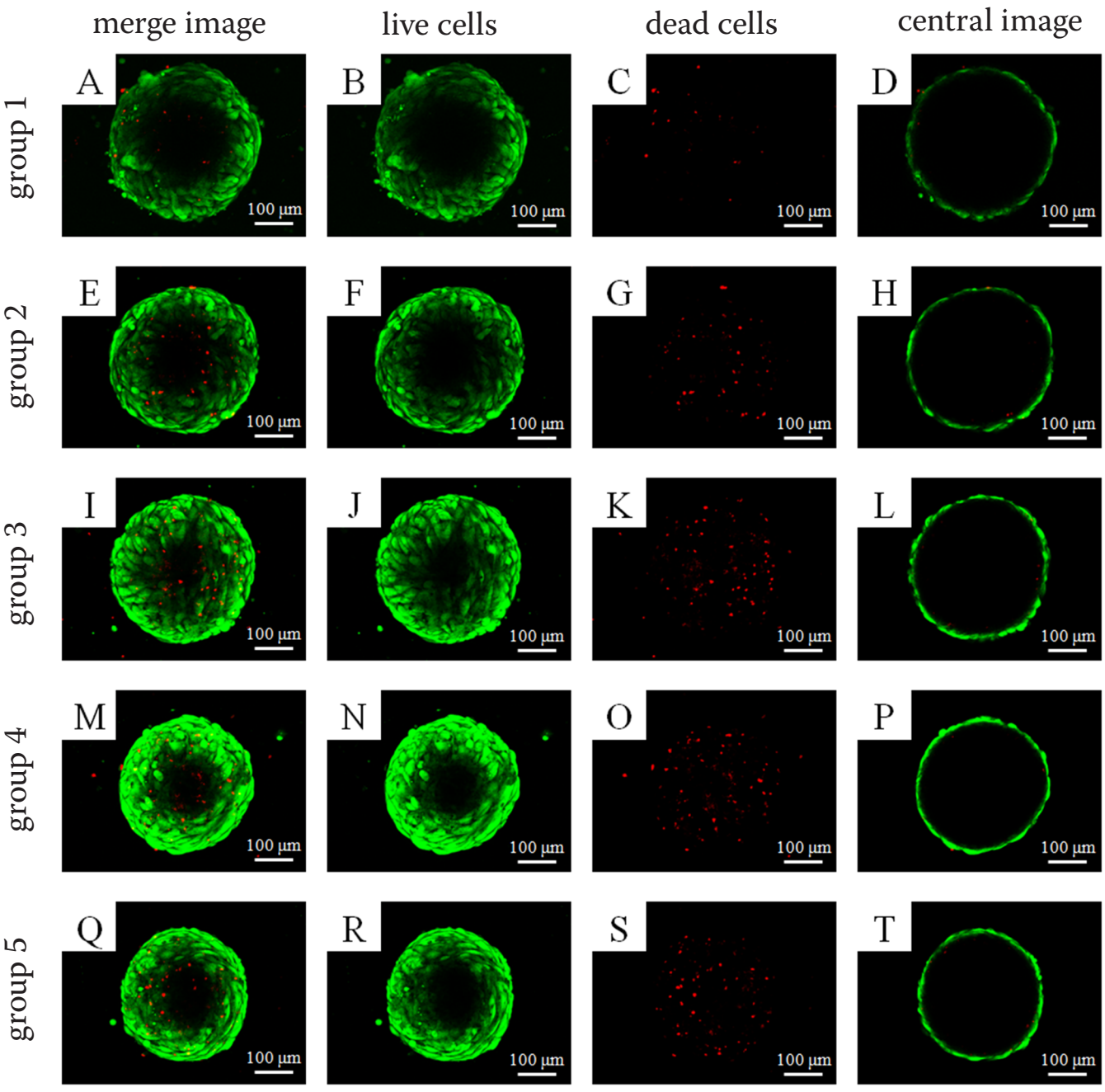

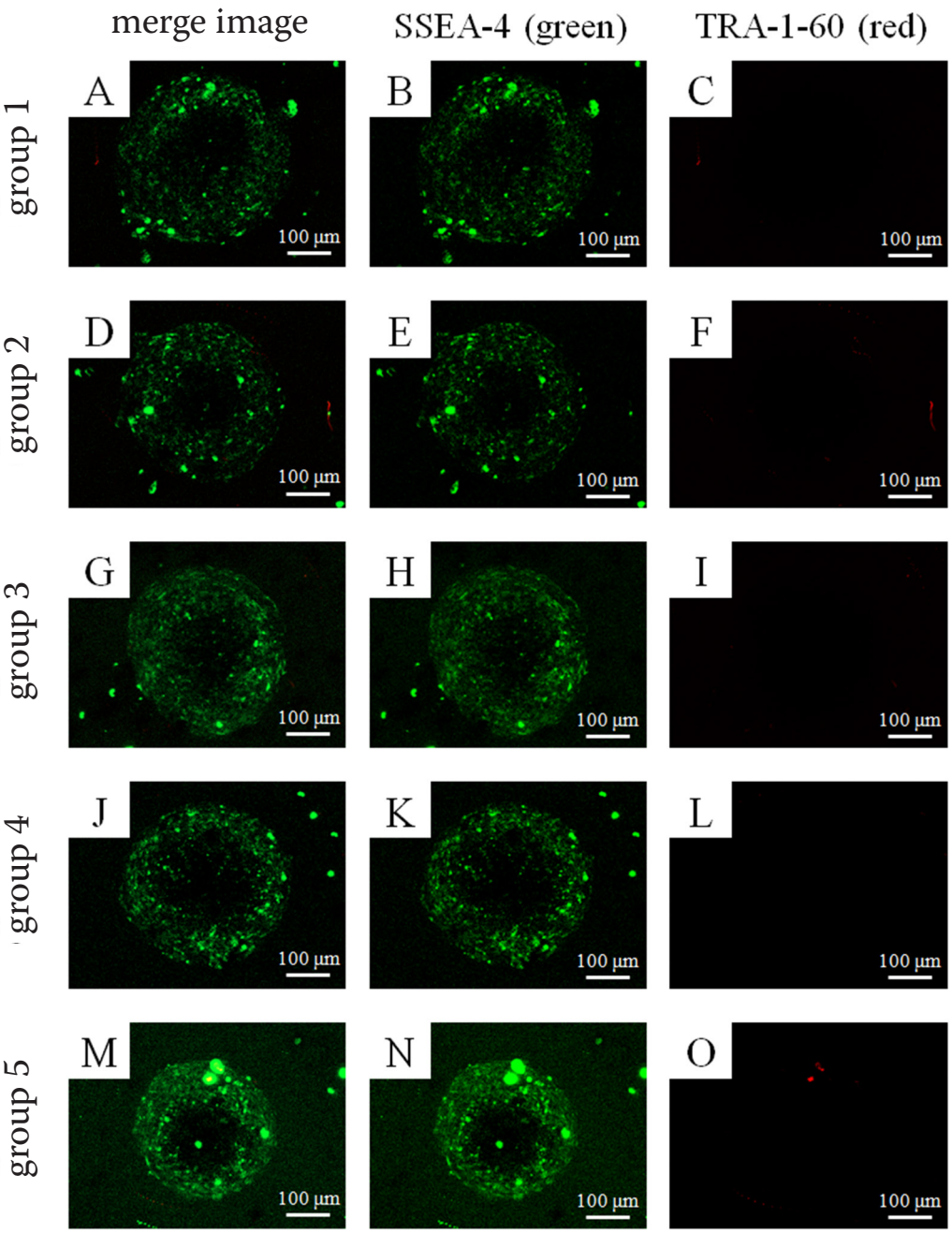

Fig. 6. Evaluation of maintenance of expression of stem cell markers of cell spheroids (spheroids containing stem cells were positive for the stem-cell markers SSEA-4)

A–C – group 1; D–F – group 2; G–I – group 3; J–L – group 4; M–O – group 5.

the stem-cell markers SSEA-4 and TRA-1-60(R) (Fig. 6). The green fluorescence showed a more intense assay with a higher number of stem cells.

Secretion of human vascular endothelial growth factor from spheroids

The secretion of VEGF from the spheroids was noted in groups 2, 3, 4, and 5 (Fig. 7), and it increased with the increase in the number of stem cells. A statistically significant increase in the secretion of VEGF was noted in groups 2, 3, 4 and 5 when compared with the media-only group ($p < 0.05$).

Discussion

In this report, stem cell spheroids were fabricated using microwells, and the paracrine effects of the stem cell spheroids were evaluated. This study showed that cell spheroids formed with stem cells and osteoprecursor cells with different ratios, using microwells, had different paracrine effects on the stem cells. It also proved that the secretion of VEGF increased with the increase in stem cells.

More recently, it has been shown that the beneficial effects of stem cells were reported to come from both cell restoration and paracrine effects.[5] Mesenchymal stem cells were reported to secrete a vast array of proteins, including growth factors, cytokines, chemokines, and extracellular

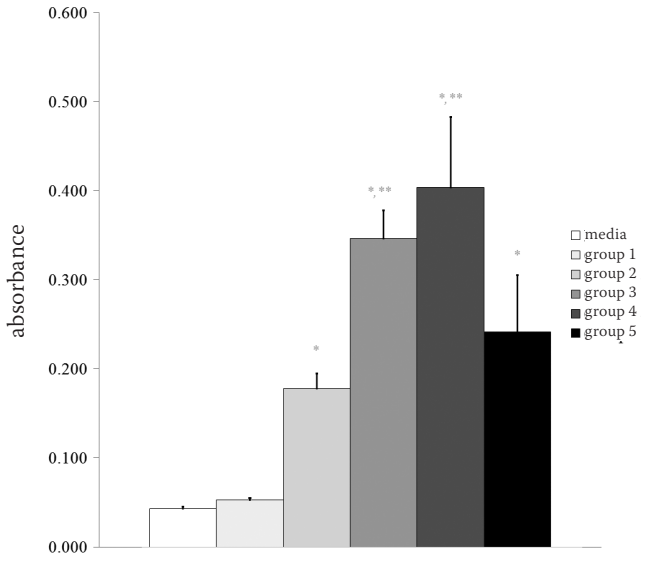

Fig. 7. Secretion of VEGF from cell spheroids

VEGF – vascular endothelial growth factor; differences between the groups were evaluated using a one-way analysis of variance with Tukey's post hoc test; * statistically significant differences were noted when compared with the media-only group; ** significant differences were seen when compared with group 2.

matrix metalloproteinases.[6] Various growth factors, e.g., vascular endothelial, fibroblast and hepatocyte growth factors, were secreted from mesenchymal stem cells, and previous reports showed that the growth of endothelial cells was stimulated by a conditioned medium of mesenchymal stem cells in a dose-dependent manner.[7,8]

Vascular endothelial growth factor is reported to be an important angiogenesis factor that mesenchymal stem cells release.[9] It also regulates endothelial cell survival, differentiation and angiogenesis.[10] The release of VEGF was demonstrated by the analysis of the mesenchymal stem cell-conditioned media.[11] This study showed that mesenchymal stem cell-conditioned media enhanced the proliferation of endothelial stem cells in a dose-dependent manner, and anti-vascular endothelial growth factor antibodies partly attenuated this effect. This study clearly proved that the secretion of VEGF from 3-dimensional stem cell spheroids increased with the increase in stem cells. However, it should be noted that the different method of culturing mesenchymal stem cells and the variety of the paracrine factors may produce different results.[6]

The paracrine effects of stem cells may be applied for the treatment of various diseases. Stem cells from the vertebral body were reported to enhance the regeneration of the intervertebral disc by paracrine interaction.[12] In a previous report, the transplanted stem cells released soluble factors that – acting in a paracrine fashion – contributed to cardiac repair and regeneration.[13] Another report showed that adult neural stem cells exerted neuroprotective effects on cortical neurons following neurotoxic insult by paracrine effects.[14] Adipose tissue-derived stem cells were applied for the treatment of erectile dysfunction due to the paracrine effect on surrounding tissues.[15] The improvements of glucose intolerance were achieved from the factors secreted from dental pulp stem cells by increasing pancreatic β-cell function in streptozotocin-induced diabetic mice.[16]

This study applied a 3-dimensional culture system. In a previous study, 3-dimensional stem cell spheroids were generated from gingiva-derived stem cells with concave microwells.[17] Recently, a 3-dimensional human stem cell construct has been built by applying bioprinting.[18] A 3-dimensional stem cell system may extend the knowledge about the structure–function relationship.[19] It was suggested that the 3-dimensional system simulates reality more closely when compared to the 2-dimensional one.[20] Additionally, it was suggested that 3-dimensional spheroids of mesenchymal stem cells showed enhanced survival effects.[21]

Stem cells may be obtained from bone marrow, peripheral blood, adipose tissue, and umbilical cord blood.[22–25] Stem cells from bone marrow are widely applied, but this may have limitations due to the low number of stem cells, pain of extraction and morbidity.[26,27] Umbilical cord blood may be a good source, but the supply is very limited.[28] Stem cells can be also obtained from the oral and maxillofacial area, including the maxilla and mandible.[29] The gingiva can be considered a favorable source of stem cells, because the tissue can be obtained from daily dental procedures under local anesthesia.[3]

This study showed that cell spheroids formed with stem cells and osteoprecursor cells with different ratios, using microwells, had paracrine effects on the stem cells. The secretion of VEGF increased with the increase in stem cells. This stem cell spheroid may be applied for tissue engineering purposes.

References

1. Wong SF, No da Y, Choi YY, Kim DS, Chung BG, Lee SH. Concave microwell based size-controllable hepatosphere as a three-dimensional liver tissue model. *Biomaterials*. 2011;32:8087–8096.
2. Jun Y, Kang AR, Lee JS, et al. 3D co-culturing model of primary pancreatic islets and hepatocytes in hybrid spheroid to overcome pancreatic cell shortage. *Biomaterials*. 2013;34:3784–3794.
3. Jin SH, Lee JE, Yun JH, Kim I, Ko Y, Park JB. Isolation and characterization of human mesenchymal stem cells from gingival connective tissue. *J Periodontal Res*. 2015;50:461–467.
4. Jin SH, Kweon H, Park JB, Kim CH. The effects of tetracycline-loaded silk fibroin membrane on proliferation and osteogenic potential of mesenchymal stem cells. *J Surg Res*. 2014;192:1–9.
5. Baraniak PR, McDevitt TC. Stem cell paracrine actions and tissue regeneration. *Regen Med*. 2010;5:121–143.
6. Chan JK, Lam P. Soluble factors from human fetal bone marrow-derived mesenchymal stem cells: Preparation of conditioned medium and its effect on tumor cells. *Methods Mol Biol*. 2016;1416:467–475.
7. Liang X, Ding Y, Zhang Y, Tse HF, Lian Q. Paracrine mechanisms of mesenchymal stem cell-based therapy: Current status and perspectives. *Cell Transplant*. 2014;23:1045–1059.
8. Tang Y, Li Q, Meng F, et al. Therapeutic potential of HGF-expressing human umbilical cord mesenchymal stem cells in mice with acute liver failure. *Int J Hepatol*. 2016;2016:5452487.

9. Yang Y, Hu S, Xu X, et al. The vascular endothelial growth factors-expressing character of mesenchymal stem cells plays a positive role in treatment of acute lung injury in vivo. *Mediators Inflamm*. 2016;2016:2347938.
10. Hoeben A, Landuyt B, Highley MS, Wildiers H, Van Oosterom AT, De Bruijn EA. Vascular endothelial growth factor and angiogenesis. *Pharmacol Rev*. 2004;56(4):549–580.
11. Kinnaird T, Stabile E, Burnett MS, et al. Local delivery of marrow-derived stromal cells augments collateral perfusion through paracrine mechanisms. *Circulation*. 2004;109:1543–1549.
12. Shim EK, Lee JS, Kim DE, et al. Autogenous mesenchymal stem cells from the vertebral body enhance intervertebral disc regeneration by paracrine interaction: An in vitro pilot study. *Cell Transplant*. 2016; 25(10):1819–1832.
13. Gnecchi M, Zhang Z, Ni A, Dzau VJ. Paracrine mechanisms in adult stem cell signaling and therapy. *Circ Res*. 2008;103:1204–1219.
14. Geranmayeh MH, Baghbanzadeh A, Barin A, et al. Paracrine neuroprotective effects of neural stem cells on glutamate-induced cortical neuronal cell excitotoxicity. *Adv Pharm Bull*. 2015;5:515–521.
15. Gokce A, Peak TC, Abdel-Mageed AB, Hellstrom WJ. Adipose tissue-derived stem cells for the treatment of erectile dysfunction. *Curr Urol Rep*. 2016;17:14.
16. Izumoto-Akita T, Tsunekawa S, Yamamoto A, et al. Secreted factors from dental pulp stem cells improve glucose intolerance in streptozotocin-induced diabetic mice by increasing pancreatic beta-cell function. *BMJ Open Diabetes Res Care*. 2015;3:e000128.
17. Lee SI, Yeo SI, Kim BB, Ko Y, Park JB. Formation of size-controllable spheroids using gingiva-derived stem cells and concave microwells: Morphology and viability tests. *Biomed Rep*. 2016;4:97–101.
18. Gu Q, Tomaskovic-Crook E, Lozano R, et al. Stem cell bioprinting: Functional 3D neural mini-tissues from printed gel-based bioink and human neural stem cells. *Adv Healthc Mater*. 2016;5(12):1428.
19. Seo S, Na K. Mesenchymal stem cell-based tissue engineering for chondrogenesis. *J Biomed Biotechnol*. 2011;2011:806891.
20. Valarmathi MT, Yost MJ, Goodwin RL, Potts JD. The influence of proepicardial cells on the osteogenic potential of marrow stromal cells in a three-dimensional tubular scaffold. *Biomaterials*. 2008;29:2203–2216.
21. Xu Y, Shi T, Xu A, Zhang L. 3D spheroid culture enhances survival and therapeutic capacities of MSCs injected into ischemic kidney. *J Cell Mol Med*. 2016;20(7):1203–1213.
22. Zhu HX, Gao JL, Zhao MM, et al. Effects of bone marrow-derived mesenchymal stem cells on the autophagic activity of alveolar macrophages in a rat model of silicosis. *Exp Ther Med*. 2016;11:2577–2582.
23. Sheashaa H, Lotfy A, Elhusseini F, et al. Protective effect of adipose-derived mesenchymal stem cells against acute kidney injury induced by ischemia-reperfusion in Sprague-Dawley rats. *Exp Ther Med*. 2016;11:1573–1580.
24. Cui B, Li E, Yang B, Wang B. Human umbilical cord blood-derived mesenchymal stem cell transplantation for the treatment of spinal cord injury. *Exp Ther Med*. 2014;7:1233–1236.
25. Fu Q, Tang NN, Zhang Q, et al. Preclinical study of cell therapy for osteonecrosis of the femoral head with allogenic peripheral blood-derived mesenchymal stem cells. *Yonsei Med J*. 2016;57:1006–1015.
26. Sakaguchi Y, Sekiya I, Yagishita K, Muneta T. Comparison of human stem cells derived from various mesenchymal tissues: Superiority of synovium as a cell source. *Arthritis Rheum*. 2005;52:2521–2529.
27. Zuk PA, Zhu M, Ashjian P, et al. Human adipose tissue is a source of multipotent stem cells. *Mol Biol Cell*. 2002;13:4279–4295.
28. Fu L, Liu Y, Zhang D, Xie J, Guan H, Shang T. Beneficial effect of human umbilical cord-derived mesenchymal stem cells on an endotoxin-induced rat model of preeclampsia. *Exp Ther Med*. 2015;10:1851–1856.
29. Sunil P, Manikandhan R, Muthu M, Abraham S. Stem cell therapy in oral and maxillofacial region: An overview. *J Oral Maxillofac Pathol*. 2012;16:58–63.

The clinical importance of changes in Treg and Th17 lymphocyte subsets in splenectomized patients after spleen injury

Witold Zgodziński[1,A–F], Ewelina Grywalska[2,A–F], Dorota Siwicka-Gieroba[3,B,F], Agata Surdacka[2,B,F], Krzysztof Zinkiewicz[1,B,E,F], Dariusz Szczepanek[4,B,F], Grzegorz Wallner[1,E,F], Jacek Roliński[2,E,F]

[1] 2nd Department of General, Gastrointestinal Surgery and Surgical Oncology of the Alimentary Tract, Medical University of Lublin, Poland
[2] Department of Clinical Immunology and Immunotherapy, Medical University of Lublin, Poland
[3] Department of Anesthesiology, Medical University of Lublin, Poland
[4] Department of Neurosurgery and Pediatric Neurosurgery, Medical University of Lublin, Poland

A – research concept and design; B – collection and/or assembly of data; C – data analysis and interpretation; D – writing the article; E – critical revision of the article; F – final approval of the article

Advances in Clinical and Experimental Medicine, ISSN 1899-5276 (print), ISSN 2451-2680 (online) *Adv Clin Exp Med*. 2018;27(7):979–986

Address for correspondence
Ewelina Grywalska
E-mail: ewelina.grywalska@gmail.com

Funding sources
This study was supported by the National Science Center, Poland (grant Nos.: UMO-2011/01/N/NZ6/01762 and UMO-2012/05/B/NZ6/00792).

Conflict of interest
None declared

Received on March 11, 2017
Reviewed on April 5, 2017
Accepted on May 15, 2017

Abstract

Background. Splenectomized patients are more prone to bacterial infections due to their immunocompromised status. Little is known about the role of T helper 17 (Th17) and T regulatory cells (Treg) in the immune system of patients after the removal of the spleen.

Objectives. The aim of the present study was to analyze possible changes in CD4+ lymphocyte T subsets, especially Treg and Th17, in patients who had undergone splenectomy.

Material and methods. The study included a group of 67 male patients (41.74 ±16.22 years). All patients had undergone splenectomy because of spleen injury. Mean time elapsed from splenectomy to analysis was 9.1 ±4.6 years. Control samples were obtained from 20 male healthy volunteers. The percentages and absolute counts of Th17 and Treg were measured using the flow cytometry method.

Results. The analysis of the antibody titer against 23 serotypes of *Streptococcus pneumoniae* (*S. pneumoniae*) in the splenectomized patients revealed its elevated values compared to controls ($p = 0.0016$). Higher percentages and absolute counts of Treg cells were found in the splenectomized group vs controls ($p < 0.000007$). Lower percentages and absolute counts of the Th17 subset were found in the study group vs controls ($p < 0.000002$ and $p < 0.00006$, respectively). The Treg cell percentage was positively correlated with the antibody titer against *S. pneumoniae* ($p < 0.02$). Th17 cells were reversely correlated with the antibody titer ($p < 0.004$ and $p < 0.001$ for absolute counts and percentage values, respectively). The Th17 subset values were significantly lower in the splenectomized patients who reported a higher frequency of upper respiratory tract infections (URTI) ($p < 0.0001$). No correlations were found between the time elapsed since splenectomy and the Treg or Th17 cell values in the study group.

Conclusions. Splenectomy results in an important deterioration of the Treg/Th17 cell balance with a predominance of immunoregulatory Tregs, which can contribute to insufficient immune response to infection.

Key words: immune response, T helper 17 cells, T regulatory cells, splenectomy

DOI
10.17219/acem/73734

Introduction

In 1919, Morris and Bullock reported on a preliminary study indicating the importance of the spleen in resistance to infection.[1] Further studies on animal models have shown significant relationships between splenectomy and the peripheral leukocyte count.[2]

After splenectomy, mechanisms that play important roles in bacterial clearance are impaired, which leads to an increased risk of severe infections. The absence of the phagocytic function of the spleen and the long-term impairment of humoral response to encapsulated bacteria are the main reasons for the overwhelming postsplenectomy infection (OPSI) syndrome. This severe infection occurs at an estimated incidence of 0.23–0.42% per year, with a lifetime risk of 5%.[3,4] The course of OPSI can be life-threatening, with a mortality rate of 38–69%.[3,5,6] Early diagnosis and aggressive therapy can decrease the number of fatal outcomes to 10–40%.[7] The highest risk of infection occurs during the first 3 years after splenectomy, particularly in children younger than 5 years.[8,9] OPSI is most commonly induced by encapsulated bacteria and *Streptococcus pneumoniae* (*S. pneumoniae*) is responsible for 50–90% of all cases of OPSI.[3,7] This has been attributed to the absence of marginal zone B cells in these patients.[10] Each patient should be vaccinated for *S. pneumoniae* both before and after splenectomy to minimize the risk of infection. According to the guidelines from the Centers for Disease Control and Prevention (CDCs), it is recommended to vaccinate for *S. pneumoniae* and *Haemophilus influenzae* type b (*H. influenzae*) at least 14 days before surgery, and to vaccinate for *S. pneumoniae*, *H. influenzae* and *Neisseria meningitidis* after splenectomy. Vaccination for influenza is also recommended once a year in this group of patients.[11] In cases of urgent splenectomy, vaccination before surgery is not applicable. In these cases, it is important to follow the guidelines for vaccination after surgery. However, post-splenectomy vaccinations, especially in urgent cases, seem to be less effective.[8] The lack of the spleen causes significant disorders in humoral immune response.[12] Despite a significant amount of evidence on B-lymphocyte function impairment, little is known about the distribution of separate populations of T-lymphocytes in splenectomized patients. CD4+ T cells are essential for directing immune responses during host defense and for the pathogenesis of inflammatory diseases. Recently, more attention has been paid to T regulatory cells (Treg cells) and the positive effects they exert by regulating immune response to self-antigens. Treg cells are a subset of phenotypically and functionally specific T lymphocytes which play an important role in the maintenance of immune tolerance. Foxp3, a member of the forkhead/winged-helix family of the transcription factor, has been identified as the best marker of Treg cells.[13] The dysfunction of Treg cells is observed in a variety of autoimmune diseases such as systemic lupus erythematosus (SLE) and rheumatoid arthritis.[14,15] T helper 17 (Th17) IL-17A+CD3+CD4+ cells represent a subset of T helper cells that can play an active role in several inflammatory and autoimmune diseases.[16] It has been demonstrated that human Th17 cells express IL-17A, IL-17F, IL-22, IL-26, IFN-γ, the chemokine CCL20, the transcription factor ROR-γt, and IL-23R.[17] It has been shown that the balance of Treg/Th17 controls immune response as an important factor in regulating the Th cell function relating to the Th1/Th2 shift in the graft vs host disease.[18] The Treg/Th17 imbalance contributes to the development of autoimmune diseases, such as SLE,[19] primary nephrotic syndrome[20] and idiopathic thrombocytopenic purpura.[21]

The aim of the present study was to analyze possible changes in the CD4+ lymphocyte T subsets, especially Treg and Th17, in patients who had undergone splenectomy, and to assess the relationships between increased susceptibility to infections and the Treg/Th17 status in this group.

Material and methods

Study and control groups

Between 2012 and 2013, a group of 67 male patients, with an average age of 41.74 ±16.22 years, was recruited. All patients enrolled were splenectomized because of an abdominal trauma with spleen injury. Mean time elapsed from splenectomy to analysis was 9.1 ±4.6 years. Control samples of peripheral blood were obtained from 20 healthy male volunteers (aged 42.95 ±15.3 years). None of the patients or controls had been receiving drugs affecting the immune system; none showed any signs of infection (within the last 2 months before the study) or any signs of autoimmune or allergic diseases, and none had received blood transfusions. None had been receiving immunosuppressive or immunomodulative treatment within the previous 3 months. To avoid hormonal changes during menstrual cycles, only male patients and controls were enrolled for the study. Fifty-nine patients (88.05%) reported more frequent upper respiratory tract infections (URTI) after splenectomy (4 or more cases of infection treated with antibiotics per year) and 8 patients (11.94%) did not observe any change in the prevalence of URTI. The peripheral blood (PB) samples were drawn from the basilic vein for the following tests: 1. serum specific pneumococcal antibody titers before vaccination (3 mL of peripheral blood collected to tubes with a clotting activator); 2. frequencies of selected lymphocyte subsets (5 mL of peripheral blood collected to tubes with the anticoagulant ethylenediaminetetraacetic acid – EDTA). Serum samples were stored at –70°C until the time of specific pneumococcal antibody titer analysis. The percentages of lymphocyte subsets were assessed on fresh peripheral blood samples from patients and healthy volunteers. This study was carried out

in accordance with the Code of Ethics of the World Medical Association (Declaration of Helsinki) for experiments involving humans. The Local Ethics Committee approved the research and patients gave their prior written consent.

The isolation of peripheral blood mononuclear cells and the detection of Th17 and Treg cells

The isolation of peripheral blood mononuclear cells (PBMCs) and the detection of Th17 and Treg cells were performed as described previously.[22]

The peripheral blood was diluted 1:1 with a 0.9% phosphate-buffered saline (PBS) without calcium (Ca^{2+}) or magnesium (Mg^{2+}) ions (Biochrome AG, Berlin, Germany). The diluted material was then overlaid on 3 mL of Gradisol L preparation (Aqua Medic, Łódź, Poland) with a specific gravity of 1.077 g/mL and subjected to density gradient centrifugation at 700 × g for 20 min. The obtained fraction of PBMCs was collected with a Pasteur pipette and washed twice in PBS without Ca^{2+} and Mg^{2+} ions for 5 min. Next, the cells were suspended in 1 mL of PBS without Ca^{2+} and Mg^{2+}, and counted in the Neubauer chamber, and their viability was determined by a trypan blue dye exclusion assay (0.4% Trypan Blue Solution; Sigma-Aldrich, St. Louis, USA).

For the detection of Th17 cells, PBMCs were resuspended in RPMI-1640 culture medium (Sigma-Aldrich) containing 10% heat-inactivated fetal calf serum (FCS, Sigma-Aldrich), 2 mM l-glutamine, 100 U/mL penicillin (Sigma-Aldrich), and 100 µg/mL streptomycin (Sigma-Aldrich). Mononuclear cells were stimulated for 5 h at 37°C in 5% CO_2 with 25 ng/mL of phorbol 12-myristate 13-acetate (PMA, Sigma Chemical, St. Louis, USA) and 1 µg/mL of ionomycin (Sigma Aldrich) in the presence of 10 µg/mL of brefeldin A (Sigma-Aldrich), which blocks the intracellular transport processes resulting in the accumulation of cytokine proteins on the Golgi complex. Next, PBMCs were collected, washed with PBS solution and prepared at a final concentration of 106 cells/mL. The number of viable leukocytes was determined using a 1% trypan blue dye exclusion assay. Later, the mononuclear cells were stained with anti-CD3 CyChrome and anti-CD4 fluorescein-isothiocyanate (FITC) conjugated monoclonal antibodies (Becton Dickinson, San Diego, USA). The permeabilization of cell membranes was achieved with a Cytofix/Cytoperm Kit (BD Pharmingen, San Jose, USA), which was added for 15 min at a temperature of 4°C. Next, the cells were washed twice with PBS. The permeabilized cells were stained with a phycoerythrin (PE)-conjugated anti-human IL-17A monoclonal antibody (eBioscience, San Diego, USA). Then, cells were washed twice with PBS again.

For the detection of Treg CD4+CD25+Foxp3+ cells, the cell surface and intracellular antigens were determined on fresh cells at the time of sample submission by cell staining according to the manufacturer's protocols. A total of 500 µL of cell suspensions were added to 5 µL of an appropriate solution of anti-human CD25 PE and anti-human CD4 PE-Cy5-conjugated antibodies (BioLegend, San Diego, USA). Next, the mixture of cells and antibodies was incubated for 30 min at 4°C in the dark, centrifuged, washed twice by adding 1 mL of cold PBS to each tube with 1% sodium azide and 1% FCS, and centrifuged again at 400 × g for 10 min. After the standard incubation with antibodies directed against surface markers, the incubation by fixation and permeabilization with FoxP3 Fix/Perm Buffer and FoxP3 Perm Buffer (BioLegend) was performed. Then, the incubation with antibodies directed against the intracellular protein FoxP3 – anti-human FoxP3 (Pacific Blue) monoclonal antibody (BioLegend) was carried out. Later, the supernatant was separated and, after washing, each sample was suspended in 200 µL of PBS.

The cells were immediately analyzed with a Becton Dickinson Canto II flow cytometer and analyzed by using FACSDiva™ software (Becton Dickinson). The results were presented as the percentage of CD45+ cells stained with the antibody. The percentage of positive cells was calculated via a comparison with the control. Background fluorescence was determined using isotype-matched, directly conjugated mouse anti IgG1/IgG2α monoclonal antibodies. The samples were gated on forward scatter vs side scatter to exclude debris and cell aggregates.[22] An example of a cytometric analysis is presented in Fig. 1.

The assessment of basic lymphocyte subsets

Three-color immunofluorescence analyzes were performed using a FACS Calibur flow cytometer (Becton Dickinson) equipped with a 488 nm argon laser. A minimum of 10,000 events were acquired and analyzed using CellQuest software (Becton Dickinson). The percentage of cells expressing surface markers was analyzed. The cells were phenotypically characterized by incubation (20 min in the dark at room temperature) with a combination of relevant FITC- PE- and CyChrome-labeled monoclonal antibodies. Immunofluorescence studies were performed using a combination of the following mAbs: CD3 FITC/CD19 PE and CD8 FITC/CD4 PE (Becton Dickinson).[23]

Serum pneumococcal antibody assessment

The serum pneumococcal antibody assessment was performed on all subjects. The amount of anti-capsular polysaccharide antibody specific to 23 pneumococcal serotypes (1, 2, 3, 4, 5, 6B, 7F, 8, 9N, 9V, 10A, 11A, 12F, 14, 15B, 17F, 18C, 19A, 19F, 20, 22F, 23F, 33F) was determined using a commercial ELISA test (ELIZEN Pneumococcus IgG Assay; Zentech, Liege, Belgium). Each of the serum samples was pre-adsorbed with 10 µg/mL polysaccharide C (C-PS; Statens Serum Institut, Copenhagen, Denmark) for 1 h at 37°C before quantification to increase the specificity

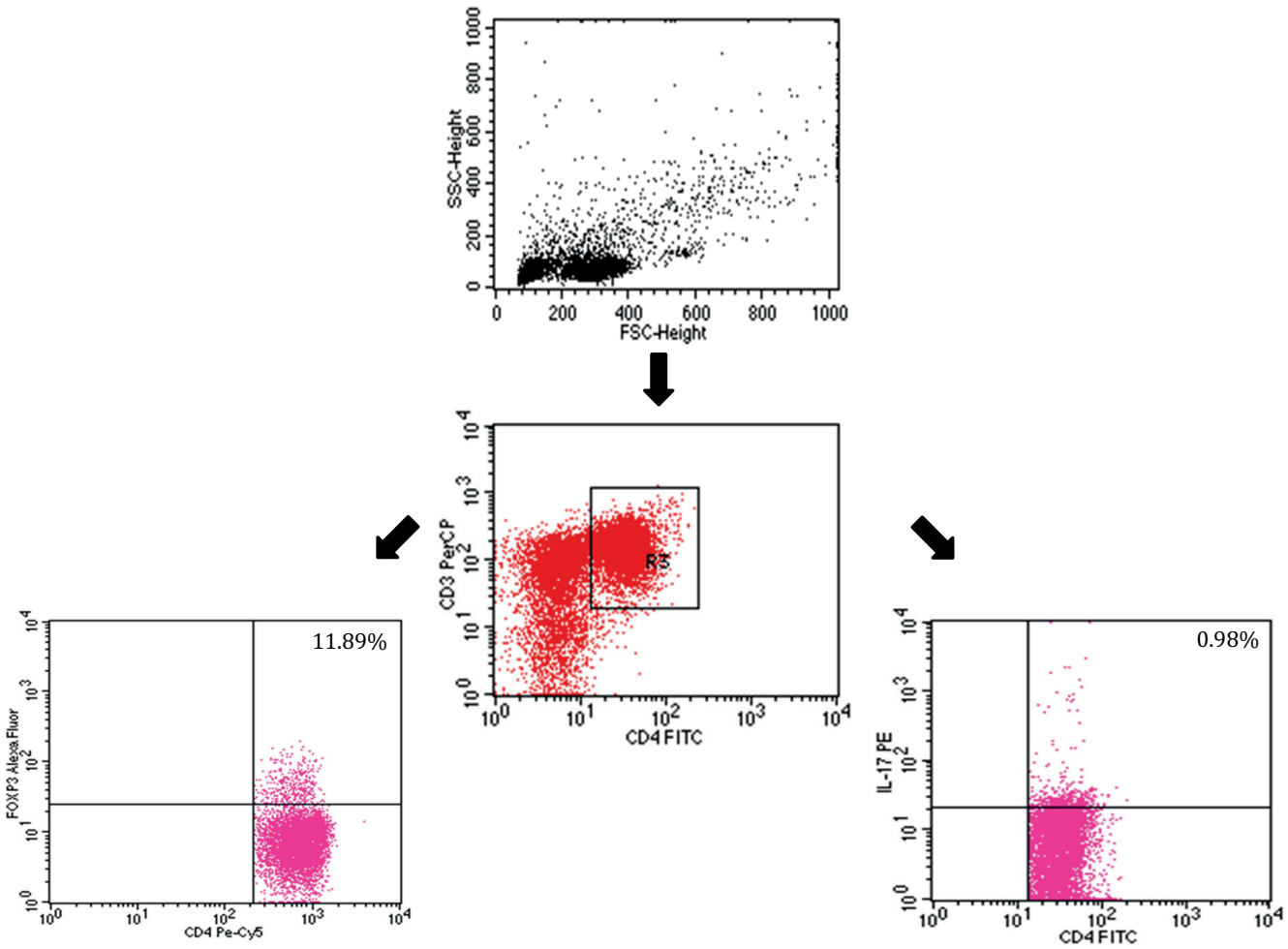

Fig. 1. An example of a 3-color flow cytometry analysis of lymphocytes from a splenectomized patient

The upper dot-plot shows the forward scatter/side scatter (FSC/SSC) distribution and the gate used to select lymphocytes for analysis. The lower left flow cytometry dot-plot shows the analysis of the percentage of Treg cells; the analysis was based on gating a subpopulation of FoxP3-positive Treg cells among T CD4-positive lymphocytes. The lower right flow cytometry dot-plot shows the analysis of the percentage of Th17 cells; the analysis was based on gating a subpopulation of Th17 cells among T CD4-positive lymphocytes. The number in the upper right quadrant in the dot-plots represents the percentage of Treg cells (bottom left dot-plot) and the percentage of Th17 cells (bottom right dot-plot).

of the test. The evaluation procedure was followed according to the manufacturer's instructions and an automatic VICTOR3 reader (Perkin Elmer, San Diego, USA) was used for result interpretation.[24]

Statistical analysis

The normal distribution of continuous variables was verified with the Shapiro-Wilk test. Categorical variables were presented as percentages and were compared using the χ^2 test. Continuous variables were presented as means and standard deviations (SD). The U Mann-Whitney test and the Student's t-test were applied for intergroup comparisons of the variables, according to the distribution. Pearson's linear correlation coefficient (r) was calculated to disclose relationships between the variables. All calculations were conducted using STATISTICA v. 10 software (StatSoft, Tulsa, USA). A p-value <0.05 was considered statistically significant.

Results

The analysis of the blood samples taken from the splenectomized patients revealed elevated antibody titer against *S. pneumoniae* compared to the healthy control group (833.68 ±535.98 vs 284.6 ±182.02; p = 0.0016) (Fig. 2). In the study group, a lower percentage of CD4+ cells was noted compared to the controls (median 37.89% vs 44.43%; p < 0.00128) and a higher percentage and quantity of CD19+ cells compared to the controls (median 11.6% vs 8.79%, p < 0.00001 and mean 0.328 ±0.156 vs 0.274 ±0.241, p < 0.006, respectively). In the Treg subset, a significantly higher percentage (median 9.85%) and total amount (mean $0.285 \times 10^3/mm^3$ ±0.133) were noted in the study group vs controls (5.22%, p < 0.000001 and $0.128 \times 10^3/mm^3$ ±0.057, p < 0.000007, respectively) (Fig. 3). In the Th17 subset, a significantly lower percentage (median 0.85%) and total amount (mean $0.027 \times 10^3/mm^3$ ±0.021) were found in the study group vs controls (2.64%, p < 0.000002 and

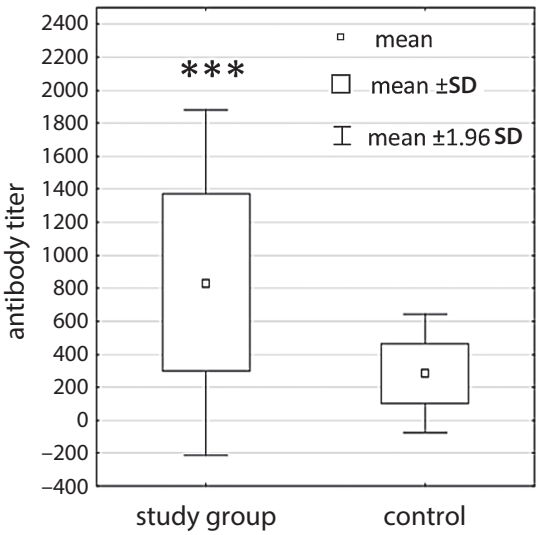

Fig. 2. The difference in antibody titer between splenectomized patients (study group) and controls

*** p = 0.0016.

$0.072 \times 10^3/mm^3 \pm 0.058$, $p < 0.00006$, respectively) (Fig. 4). Mean percentage values and mean quantity values of lymphocyte subsets in the study (splenectomized) population and the control group are presented in Table 1.

In the study group, the Treg cell percentage was positively correlated with antibody titer ($r = 0.467595$, $p < 0.02$) (Fig. 5 A). Conversely, there was a negative correlation between Th17 cells and antibody titer ($r = -0.628008$, $p < 0.001$ and $r = -0.580325$, $p < 0.004$ for percentage and total quantity values, respectively) (Fig. 5 B,C).

In the study group, among patients who reported a higher incidence of URTI, in the Th17 subset, the quantity (mean $0.019 \times 10^3/mm^3 \pm 0.0099$) and percentage values (median 0.69%) were significantly lower compared to those of the patients who did not report a higher URTI frequency ($0.064 \times 10^3/mm^3 \pm 0.021$, $p < 0.000001$ and 1.81%, $p < 0.00005$, respectively) (Fig. 6). The patients with a higher incidence of URTI also had a significantly higher

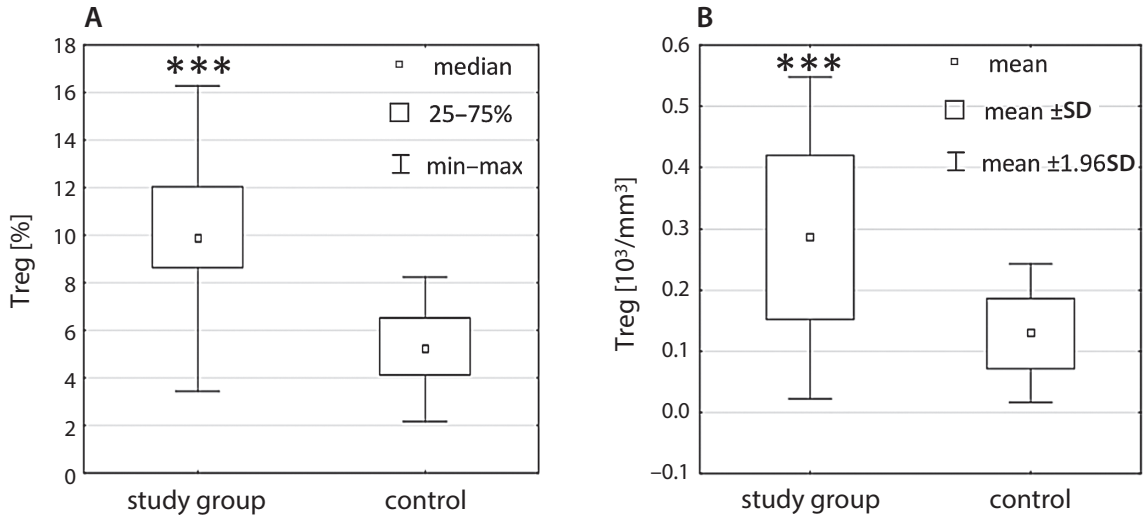

Fig. 3. The differences in the percentage of the Treg subset between splenectomized patients (study group) and controls (*** $p < 0.000001$) (A); the differences in the total amount of the Treg subset between splenectomized patients (study group) and controls (*** $p < 0.000007$) (B)

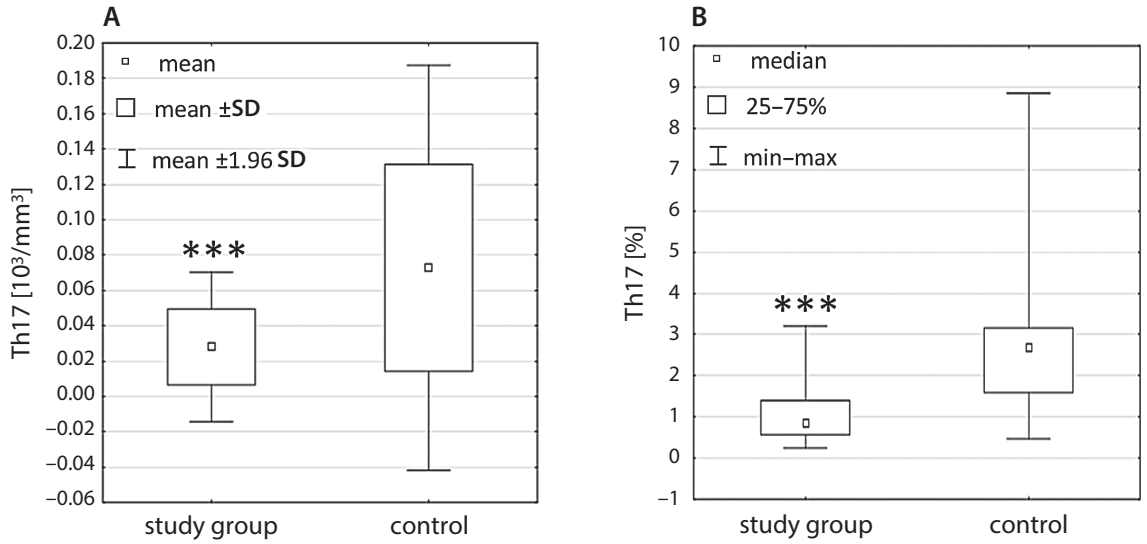

Fig. 4. The differences in the total amount of the Th17 subset between splenectomized patients (study group) and controls. (*** $p < 0.00006$) (A); the differences in the percentage of the Th17 subset between splenectomized patients (study group) and controls (*** $p < 0.000002$)

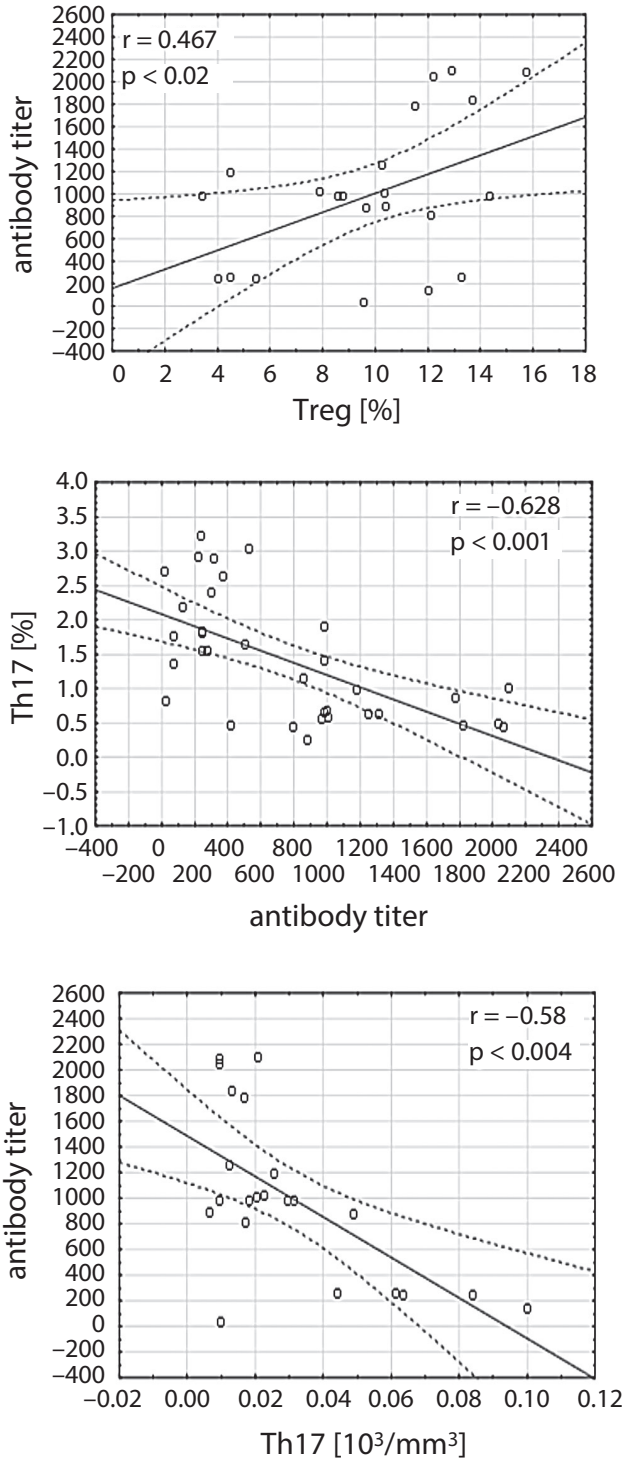

Fig. 5. Scatter diagrams presenting the positive correlation between the percentage of Treg cells and antibody titer against *S. pneumoniae* in splenectomized patients (A); the negative correlation between the percentage of Th17 cells (B), the quantity of Th17 cells (C) and antibody titer against *S. pneumoniae* in splenectomized patients

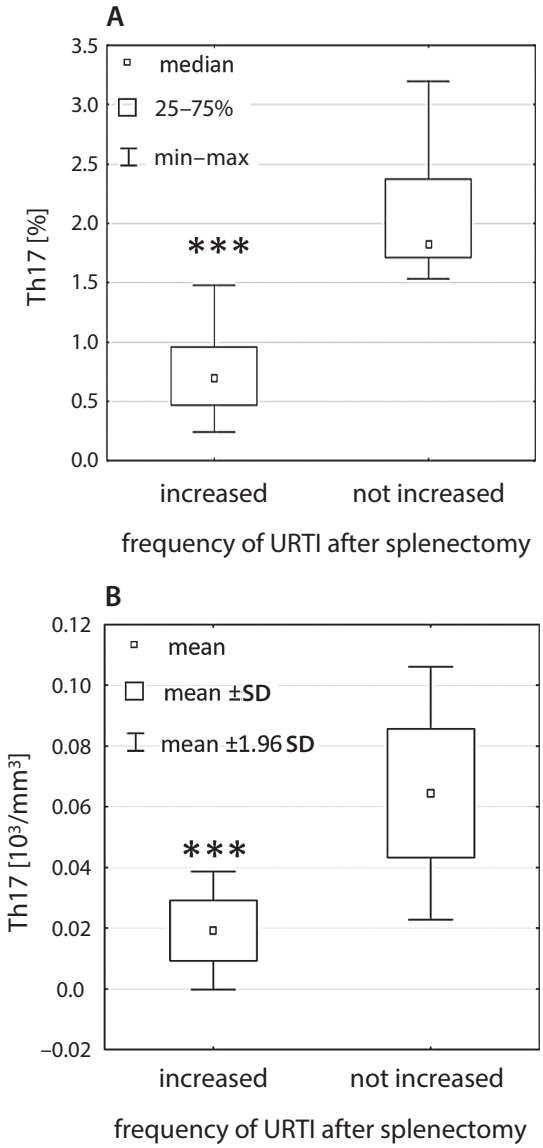

Fig. 6. The difference in the Th17 subset values – percentage (*** $p < 0.00005$) (A) and quantity (*** $p < 0.000001$) (B) – between splenectomized patients who reported a higher incidence of upper respiratory tract infections (URTI) and those who did not report a higher URTI frequency

antibody titer (955.94 ±514.13 vs 235.85 ±49.94; $p < 0.0007$) (Fig. 7). No statistically significant correlation was found between the time elapsed since splenectomy and the Treg or Th17 cell values in the study group.

Discussion

The aim of the present study was to assess the relationship between the lack of the spleen and the quantity of separate subpopulations of T lymphocytes as well as the number of specific antibodies against *S. pneumoniae*. Our study facilitates an understanding of the mechanisms which are behind weakened immune response in patients after splenectomy. The higher levels of specific antibodies against *S. pneumoniae* and values of CD19+ cells in the splenectomized patients compared to the control group suggest an increased exposure to antigens in bacterial capsules. It can be assumed that these patients reveal a higher exposure to bacterial antigens; thus, they are more susceptible to infections induced by this pathogen. This is in accordance with the results of previous studies indicating higher morbidity

Table 1. Mean percentage and quantity values of lymphocyte subsets in the study population (splenectomized) and healthy control group

Lymphocyte subsets	Study group n = 67		Control group n = 20		p-value
	mean	standard deviation	mean	standard deviation	
T CD3+ [%]	66.18727	8.482736	65.74850	13.25141	n.s.
T CD3+ [10^3/mm^3]	1.70540	0.610206	1.60591	0.52374	n.s.
B CD19+ [%]	12.74493	3.589680	11.33450	8.94963	0.00001
B CD19+ [10^3/mm^3]	0.32872	0.156565	0.27496	0.24151	0.006
T CD4+ [%]	37.05227	9.676037	44.04050	3.40697	0.00128
T CD4+ [10^3/mm^3]	0.93664	0.360878	1.07664	0.27880	n.s.
Treg [%]	9.817632	3.006509	5.230500	1.692536	0.000001
Treg [10^3/mm^3]	0.285388	0.133895	0.128761	0.057754	0.00026
Th17 [%]	1.018684	0.656494	2.833500	1.836078	0.000001
Th17 [10^3/mm^3]	0.027888	0.021533	0.072838	0.058360	0.00006
T CD8+ [%]	26.08621	9.130860	30.43050	7.18799	n.s.
T CD8+ [10^3/mm^3]	0.68469	0.381220	0.73060	0.21428	n.s.

n.s. – non-significant.

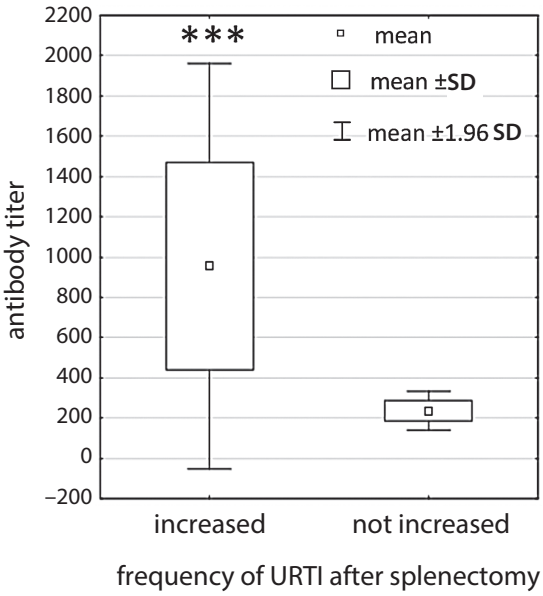

Fig. 7. The difference in antibody titer against *S. pneumoniae* between splenectomized patients who reported a higher incidence of upper respiratory tract infections (URTI) and those who did not report a higher URTI frequency (***p < 0.0007)

in splenectomized patients for *S. pneumoniae*-related infections.[7] In unvaccinated patients, the increase in the percentage of Treg lymphocytes, which also correlates with high levels of specific antibodies, seems to be distressing. The association with low levels of pro-inflammatory Th17 lymphocytes and higher antibody titer in splenectomized patients suggests that inflammatory response to *S. pneumoniae* capsule antigens is suppressed, and thus ineffective in this group.[25,26] In healthy, immunocompetent patients, the preservation of an appropriate balance between Th17 and Treg cells is one of the conditions for the best inflammatory response. There is a search for the reasons of the disruption of this balance to the benefit of Th17 lymphocytes, as this is one of the causes of autoimmune diseases or chronic inflammatory disorders.[27] The prevalence of regulatory T-lymphocytes is associated with immunosuppression, which results from their natural role in the immunotolerance of the body.[28] Therefore, the balance between regulatory T-lymphocytes and Th17 lymphocytes plays a significant role in the development of an effective inflammatory response.[27] Changes observed in this relation in patients after splenectomy may suggest that inflammatory response to the antigens contained in the *S. pneumoniae* capsula is suppressed, and thus ineffective. Therefore, despite the evidence of antigen stimulation, there is no effective immunological response from the immune system. These conclusions seem to be confirmed by the results of the quantity and percentage assessment of Th17 cells in the group of splenectomized patients reporting a higher incidence of URTI. Previous observations have demonstrated a positive correlation between the time elapsed since splenectomy and the percentage of peripheral blood CD4+ cells in the group of patients splenectomized because of an abdominal trauma.[23] Findings observed in the present study show that CD4+ cells comprise a smaller subset of lymphocytes compared to controls, but there is a tendency to rebuild this population over time. In the present research, we only enrolled patients splenectomized due to spleen injury. Elective splenectomy is generally performed on patients with idiopathic thrombocytopenic purpura; however, these patients are referred to pre-surgery vaccination that may influence the status of lymphocyte subsets. This study group is homogenous and vaccination-naive, and the results are free of any possible impact from the vaccine. Future studies are needed to assess the possible effects of vaccination on CD4+ cell frequency in splenectomized patients.

Conclusions

This research shows for the first time that substantial changes are occurring in the immunological system after splenectomy. Splenectomy has a significant effect on the quantitative distribution of lymphocyte subsets. Patients who undergo splenectomy reveal a strong reverse balance between Treg and Th17 lymphocytes. Certainly, this is one of the factors leading to a deterioration in the immunity response of the body against bacterial antigens. The high level of specific antibodies in these patients does not correlate with effective immunity.

References

1. Morris DH, Bullock FD. The importance of the spleen in resistance to infection. *Ann Surg*. 1919;70:513–521.
2. Bessler H, Bergman M, Salman H, Beilin B, Djaldetti M. The relationship between partial splenectomy and peripheral leukocyte count. *J Surg Res*. 2004;122:49–53.
3. Davidson RN, Wall RA. Prevention and management of infections in patients without a spleen. *Clin Microbiol Infect*. 2001;7:657–660.
4. Shatz DV. Vaccination practices among North American trauma surgeons in splenectomy for trauma. *J Trauma*. 2002;53:950–956.
5. Aguilar RB, Keister KJ, Russell AC. Prevention of sepsis after splenectomy. *Dimens Crit Care Nurs*. 2010;29:65–68.
6. Di Sabatino A, Carsetti R, Corazza GR. Post-splenectomy and hyposplenic states. *Lancet*. 2011;378:86–97.
7. Morgan TL, Tomich EB. Overwhelming post-splenectomy infection (OPSI): A case report and review of the literature. *J Emerg Med*. 2012; 43:758–763.
8. Davies JM, Lewis MP, Wimperis J, Rafi I, Ladhani S, Bolton-Maggs PH. Review of guidelines for the prevention and treatment of infection in patients with an absent or dysfunctional spleen, prepared on behalf of the British Committee for Standards in Haematology by a working party of the Haemato-Oncology task force. *Br J Haematol*. 2011;155:308–317.
9. Evans DI. Postsplenectomy sepsis 10 years or more after operation. *J Clin Pathol*. 1985;38:309–311.
10. Torres A, Bonanni P, Hryniewicz W, Moutschen M, Reinert RR, Welte T. Pneumococcal vaccination: What have we learnt so far and what can we expect in the future? *Eur J Clin Microbiol Infect Dis*. 2015;34:19–31.
11. Centers for Disease Control and Prevention (CDC). Recommended Adult Immunization Schedule – United States, 2016. www.cdc.gov/vaccines/schedules/downloads/adult/adult-schedule.pdf. Accessed February 25, 2016.
12. Zandvoort A, Timens W. The dual function of the splenic marginal zone: Essential for initiation of anti-TI-2 responses but also vital in the general first-line defense against blood-borne antigens. *Clin Exp Immunol*. 2002;130:4–11.
13. Adeegbe D, Matsutani T, Yang J, Altman NH, Malek TR. CD4(+) CD25(+) Foxp3(+) T regulatory cells with limited TCR diversity in control of autoimmunity. *J Immunol*. 2010;184:56–66.
14. Bonelli M, Savitskaya A, von Dalwigk K, et al. Quantitative and qualitative deficiencies of regulatory T cells in patients with systemic lupus erythematosus (SLE). *Int Immunol*. 2008;20:861–868.
15. Sempere-Ortells JM, Perez-Garcia V, Marin-Alberca G, et al. Quantification and phenotype of regulatory T cells in rheumatoid arthritis according to disease activity score-28. *Autoimmunity*. 2009;42:636–645.
16. Annunziato F, Cosmi L, Santarlasci V, et al. Phenotypic and functional features of human Th17 cells. *J Exp Med*. 2007;204:1849–1861.
17. Wilson NJ, Boniface K, Chan JR, et al. Development, cytokine profile and function of human interleukin 17-producing helper T cells. *Nat Immunol*. 2007;8:950–957.
18. Afzali B, Lombardi G, Lechler RI, et al. The role of T helper 17 (Th17) and regulatory T cells (Treg) in human organ transplantation and autoimmune disease. *Clin Exp Immunol*. 2007;148:32–46.
19. Yang J, Chu Y, Yang X, et al. Th17 and natural Treg cell population dynamics in systemic lupus erythematosus. *Arthritis Rheum*. 2009;60: 1472–1483.
20. Shao XS, Yang XQ, Zhao XD, et al. The prevalence of Th17 cells and FOXP3 regulate T cells (Treg) in children with primary nephrotic syndrome. *Ped Nephrol*. 2009;24:1683–1690.
21. Yu S, Liu C, Li L, et al. Inactivation of Notch signaling reverses the Th17/Treg imbalance in cells from patients with immune thrombocytopenia. *Lab Invest*. 2015;95:157–167.
22. Klatka M, Grywalska E, Partyka M, Charytanowicz M, Kiszczak-Bochynska E, Rolinski J. Th17 and Treg cells in adolescents with Graves' disease: Impact of treatment with methimazole on these cell subsets. *Autoimmunity*. 2014;47:201–211.
23. Grywalska E, Surdacka A, Miturski A, et al. Characterisation of lymphocyte subsets in asplenic patients: Preliminary report. *Centr Eur J Immunol*. 2010;35:239–244.
24. Pasiarski M, Rolinski J, Grywalska E, et al. Antibody and plasmablast response to 13-valent pneumococcal conjugate vaccine in chronic lymphocytic leukemia patients: Preliminary report. *PLoS One*. 2014;9: e114966.
25. Josefowicz SZ, Lu LF, Rudensky AY. Regulatory T cells: Mechanisms of differentiation and function. *Annu Rev Immunol*. 2012;30:531–564.
26. Bettelli E, Carrier Y, Gao W, et al. Reciprocal developmental pathways for the generation of pathogenic effector TH17 and regulatory T cells. *Nature*. 2006;441:235–238.
27. Noack M, Miossec P. Th17 and regulatory T cell balance in autoimmune and inflammatory diseases. *Autoimmun Rev*. 2014;13:668–677.
28. Sakaguchi S. Naturally arising CD4+ regulatory T cells for immunologic self-tolerance and negative control of immune responses. *Annu Rev Immunol*. 2004;22:531–562.

Relationship between the expression of CD25 and CD69 on the surface of lymphocytes T and B from peripheral blood and bone marrow of patients with chronic lymphocytic leukemia and established prognostic factors of this disease

Ewelina Grywalska[1,A–D,F], Małgorzata Bartkowiak-Emeryk[1,C], Marcin Pasiarski[2,3,B], Karolina Olszewska-Bożek[1,B], Michał Mielnik[1,B], Martyna Podgajna[1,B], Monika Pieczykolan[1,C], Anna Hymos[4,B], Elżbieta Fitas[1,B], Agata Surdacka[1,C], Stanisław Góźdź[3,5,E,F], Jacek Roliński[1,E,F]

[1] Department of Clinical Immunology and Immunotherapy, Medical University of Lublin, Poland
[2] Department of Hematology, Holycross Cancer Center, Kielce, Poland
[3] Faculty of Health Sciences, Jan Kochanowski University, Kielce, Poland
[4] Department of Otolaryngology and Laryngeal Oncology, Medical University of Lublin, Poland
[5] Department of Oncology, Holycross Cancer Center, Kielce, Poland

A – research concept and design; B – collection and/or assembly of data; C – data analysis and interpretation; D – writing the article; E – critical revision of the article; F – final approval of the article

Advances in Clinical and Experimental Medicine, ISSN 1899-5276 (print), ISSN 2451-2680 (online) *Adv Clin Exp Med*. 2018;27(7):987–999

Address for correspondence
Ewelina Grywalska
E-mail: ewelina.grywalska@gmail.com

Funding sources
This work was supported by research grants No. UMO-2011/01/N/NZ6/1762, UMO-2012/05/B/NZ6/00792 and UMO-2016/21/B/NZ6/02279 from the National Science Center (Poland), and No. DS460 from the Medical University of Lublin (Poland).

Conflict of interest
None declared

Received on January 6, 2017
Reviewed on March 21, 2017
Accepted on June 6, 2017

DOI
10.17219/acem/74437

Abstract

Background. Chronic lymphocytic leukemia (CLL) is a condition characterized by the accumulation of morphologically mature monoclonal lymphocytes B with the CD19+/CD5+/CD23+ phenotype in lymphoid tissue, peripheral blood and bone marrow. The clinical course of patients with CLL is heterogeneous, ranging from indolent to aggressive. The role of lymphocyte activation in the natural history of CLL is still a matter of discussion.

Objectives. The aim of this study was to determine the percentages and absolute numbers of lymphocytes B and T in peripheral blood and bone marrow of CLL patients. Moreover, we analyzed the relationship between the number of CD25-positive and CD69-positive lymphocytes and the established prognostic factors in CLL.

Material and methods. The study included 80 untreated patients with CLL and 20 healthy subjects. The immunophenotype of peripheral blood mononuclear cells (in both groups) and bone marrow cells (solely in the CLL group) was determined by means of flow cytometry.

Results. Patients with CLL showed a higher absolute number of activated lymphocytes B with phenotypes CD19+CD25+ and CD19+CD69+, as well as a higher absolute number of CD3+CD25+ lymphocytes T than the controls. The enhanced activation of peripheral blood and bone marrow lymphocytes was associated with higher Rai stages, an increased concentration of lactate dehydrogenase and beta-2 microglobulin and the progression of the disease. The number of lymphocytes B CD19+ZAP-70+ correlated positively with the number of CD19+CD25+ B cells and CD3+CD69+ T cells.

Conclusions. The study confirmed the association between an unfavorable prognosis and a high expression of activation markers in CLL patients. The determination of CD25+ and CD69+ lymphocytes T and B constitutes a valuable diagnostic tool, completing the cytometric evaluation of CLL.

Key words: flow cytometry, chronic lymphocytic leukemia, prognostic marker, lymphocyte count

Introduction

Chronic lymphocytic leukemia (CLL) is a condition characterized by the accumulation of morphologically mature monoclonal lymphocytes B with the CD19+/CD5+/CD23+ phenotype in lymphoid tissue, peripheral blood and bone marrow. It is estimated that CLL constitutes 25–30% of all diagnosed leukemia cases, making it the most frequent malignancy of this type amongst adults from North America and Europe.[1]

The course of CLL is chronic by default. Of note, however, is its heterogeneity. Only 30% of the patients survive 10–20 years following the diagnosis. The remaining patients enter the terminal phase within the initial 5–10 years, despite an indolent onset of the condition. Individuals with the aggressive form of CLL survive only 2–3 years upon establishing the diagnosis. Spontaneous regression of CLL is of rare evidence.[2] Treatment with various combinations of cytostatics and biological agents can induce remission, but a relapse occurs in most of the patients, making CLL an incurable condition.

Criteria allowing for distinguishing between low and high risk groups of CLL patients did not exist prior to the mid-1970s; subsequently, Rai et al., followed by Binet et al., proposed independent classification systems that are used to the present.[3,4] According to Rai et al., patients are classified into 1 of 4 clinical stages[3]; in contrast, the classification by Binet et al. is comprised of 3 stages.[4]

The survival time of CLL patients differs across age categories. The younger the age at diagnosis, the more aggressive is the course of the leukemia. The proportion of CLL patients with Rai stage 2 or higher is larger in patients younger than 65 years and the loss of life expectancy in younger patients is more than twice as high as in older individuals.[5]

Amongst other prognostic factors, lymphocyte doubling time (LDT) in untreated patients deserves special attention. Lymphocyte doubling time longer than 12 months is usually associated with a mild course of CLL; however, the shorter the LDT, the more aggressive is the phenotype of the disease.[6–9] The concentration of beta-2 microglobulin is another established prognostic factor: the higher the value of this parameter, the worse is the prognosis.[10]

Chronic lymphocytic leukemia cells differ in terms of the mutational status of genes encoding immunoglobulin heavy chain variable (IgVH), which is correlated with the intracellular expression of ζ-associated protein-70 (ZAP-70), the presence of the CD38 antigen and the degree of activation and susceptibility to apoptosis.[11] Some of these cellular markers are the established prognostic factors in CLL. The prognosis is better in patients with mutated IgVH genes than in those without the mutation.[12,13] A high expression of CD38 and ZAP-70 constitute a negative prognostic factor.[14,15] Disorders of apoptosis are also postulated to play an important role in CLL, and the induction of programmed cell death by some medications is a determinant of successful therapy.[16–18] However, the role of lymphocyte activation in the natural history of CLL is still a matter of discussion.

Most CLL patients develop hypogammaglobulinemia along with the disease progression.[19,20] The detectable deficit can refer to both immunoglobulin G class, and to M and A classes. The deficiency develops irrespectively of the status of the established prognostic factors, such as the mutational status of IgVH.[21]

The role of chronic immunological stimulation and the resultant activation of lymphocytes B in the pathogenesis of CLL has not been explained thus far. The in vivo activation of the lymphocytes is known to result from the presence of various antigens, including pathogens.

In a study of more than 77,000 initially healthy individuals, 129 participants developed CLL during an average period of 9.8 years. The authors studied the presence of monoclonal protein and immunoglobulin light chains in the blood samples of these patients, obtained prior to establishing the diagnosis.[20] Amongst 61 individuals with a normal ratio of free light chains (FLC) κ/λ and without monoclonal protein, 17 individuals showed elevated levels of FLC κ/λ, which suggests a polyclonal activation of lymphocytes B. These findings support the hypothesis involving chronic immunological stimulation in the pathogenesis of CLL.

De Fanis et al. analyzed the expression of CD95, the best-described cell surface antigen associated with apoptotic pathways, on lymphocyte B before and after the in vitro induction of leukemia with phorbol-12-myristate 13-acetate (PMA), ionomycin, phytohemagglutinin, or myogen.[22] The degree of activation was monitored on the basis of the early activation marker (CD69) expression. Chronic lymphocytic leukemia cells were revealed to be characterized by a markedly lower expression of CD95 than normal lymphocytes. Additionally, the leukemia cells were incapable of enhancing the expression of this molecule upon activation; although, it must be mentioned that such phenomenon was documented in the case of normal lymphocytes. Both CLL cells and normal lymphocytes showed a higher expression of CD69 after stimulation. Consequently, these findings suggest that CLL cells express the early activation marker to a similar extent as normal cells, but their activation-induced apoptosis is impaired.[22]

Compared to CD25-negative cells, lymphocytes B CD25+ release larger amounts of interleukin (IL)-6, IL-10 and interferon gamma (IFNγ) in response to the agonists of Toll-like receptors, are superior at presenting antigens to CD4+ cells, and are capable of a spontaneous synthesis of immunoglobulin classes A, G and M. Therefore, this subpopulation of lymphocytes B is postulated to correspond to mature, activated memory cells.[6] Furthermore, Hassanein et al. revealed that the proportion of CLL cells expressing CD25, a marker of lymphocyte activation, was significantly higher in the ZAP70+ group compared with the ZAP70– group.[23]

The activation of lymphocytes B results from the synthesis of cytokines by activated T cells. Rossmann et al. analyzed the lymphocyte synthesis of cytokines, both spontaneous and induced by polyclonal activation.[24] They observed that patients with the progressive form of CLL had significantly higher counts of T cells that spontaneously released IL-2, IL-4 and granulocyte-macrophage colony-stimulating factor (GM-CSF) as compared to healthy subjects and individuals with mild-course CLL. Also, an in vitro polyclonal activation of peripheral blood T lymphocytes was reflected by an increased fraction of the cells releasing the aforementioned cytokines, as well as tumor necrosis factor (TNF) and IFN-γ, both in patients with any form of CLL and in the controls. These findings suggest that lymphocytes T of individuals with CLL show relatively high functional efficiency. Therefore, the enhanced synthesis of cytokines in vivo is likely to result from the stimulation of lymphocytes T, especially in the progressive form of the disease. In turn, the abovementioned cytokines are involved in processes of maintaining the growth of leukemic lymphocytes B.[24]

The aim of this study was to determine the percentages and absolute numbers of lymphocytes B and T in the peripheral blood and bone marrow of untreated CLL patients. We analyzed the relationship between the number of CD25- and CD69-positive lymphocytes and the established prognostic factors in CLL.

Material and methods

Participants

The study included 80 untreated patients with CLL diagnosed on the basis of clinical examination, morphological evaluation and immunophenotyping of peripheral blood and bone marrow lymphocytes. The control group comprised 20 healthy subjects (13 women and 7 men) in whom the immunophenotype of lymphocytes was determined in 10 mL samples of peripheral blood. The characteristics of the study participants are summarized in Table 1.

None of the participants used immunomodulating agents, showed signs of infection within 1 month prior to the study, underwent blood transfusion, or was diagnosed with an autoimmune condition or allergy.

Table 1. Characteristics of the study participants

Parameter		Study group (n = 80)	Controls (n = 20)	p-value
Gender	women, n (%) men, n (%)	38 (47.5%) 42 (52.5%)	13 (65%) 7 (35%)	–
Rai stage, n (%)	0 I II III IV	29 (36.25%) 20 (25%) 20 (25%) 7 (8.75%) 4 (5%)	–	–
Early stage	Rai stage 0–I, n (%)	49 (61.25%)	–	–
Late stage	Rai stage II–IV, n (%)	31 (38.75%)	–	–
Age [years]	median (range)	65 (32–85)	62.5 (34–73)	NS*
Leukocytes [1 × 10^9/L]	median (range)	32.2 (12–110)	7.02 (4.23–9.63)	0.0000000001
Lymphocytes [1 × 10^9/L]	median (range)	26.13 (6.71–98.49)	2.62 (1.39–4.96)	0.0000000001
Doubled lymphocyte count on follow-up	yes, n (%) no, n (%)	19 (23.75%) 61 (76.25%)	– –	– –
Lymphocyte doubling time [months]	median (range)	10 (1–20)	–	–
Lymphocyte doubling time <12 months	yes, n (% of those with doubling) no, n (% of those without doubling)	15 (78.95%) 4 (21.05%)	– –	– –
Hemoglobin concentration [g/dL]	median (range)	12.90 (7.80–15.40)	14.35 (12.5–16.9)	0.00064
Thrombocytes [1 × 10^9/L]	median (range)	188 (62.67–447)	281.5 (186–403)	0.00051
Beta-2-microglobulin [mg/dL]	median (range)	2.72 (0.19–11.60)	1.58 (0.13–2.12)	0.00037
Lactate dehydrogenase [IU/L]	median (range)	368 (228–938)	147 (83–198)	0.000026
Implementation of treatment on follow-up	yes, n (%) no, n (%)	33 (41.25%) 47 (58.75%)	– –	– –
Time between diagnosis and treatment [months]	median (range)	3 (0–73)	–	–
Response, n (% of the treated patients)	complete/partial remission progression/death ongoing treatment	12 (36.36%) 15 (45.45%) 6 (18.18%)	– – –	– – –

* not statistically significant (NS).

The protocol of the study was approved by the Local Bioethics Committee of the Medical University in Lublin. All participants gave their written informed consent prior to the start of any procedures.

Blood and bone marrow samples

Samples of peripheral blood (20 mL) were obtained from the basilic vein of all the CLL patients. Moreover, a bone marrow aspirate (5 mL) was obtained from the iliac crest during routine diagnostic procedures. Additionally, peripheral blood samples (10 mL) of the controls were examined. The material was collected into ethylenediaminetetraacetic acid (EDTA) tubes (aspiration and vacuum systems, Sarstedt AG & Co. KG, Nümbrecht, Germany) and analyzed shortly thereafter.

Isolation of mononuclear cells

Peripheral blood and a bone marrow aspirate were diluted with 0.9% phosphate-buffered saline (PBS) without calcium (Ca^{2+}) or magnesium (Mg^{2+}) (Biochrom AG, Berlin, Germany) at a 1:1 and 1:2 ratio, respectively. The diluted material was built up with 3 mL of Gradisol L (specific gravity 1.077 g/mL; Aqua Medica, Białystok, Poland) and centrifuged in a density gradient at 700 × g for 20 min. The obtained fraction of mononuclear cells of peripheral blood and bone marrow was collected with Pasteur pipettes and washed twice in PBS without Ca^{2+} or Mg^{2+} for 5 min. Subsequently, the cells were suspended in 1 mL of PBS without calcium or magnesium, and counted in the Neubauer chamber or tested for viability in trypan blue solution (0.4% Trypan Blue Solution, Sigma Pharmaceuticals, Croydon, UK).

Flow cytometry

FACSCalibur flow cytometer (Becton Dickinson, Franklin Lakes, USA) equipped with an argon laser emitting at 488 nm was used to determine the immunophenotype of the mononuclear cells of peripheral blood and bone marrow. The results were analyzed with CellQuest software (Becton Dickinson) and a CaliBRITE calibration set (Becton Dickinson) was used to optimize the flow cytometer settings. A total of 10,000 cells were acquired from each sample based on the lymphocytic gate forward-scattered light (FSC)/side-scattered light (SSC). "Purity" of the lymphocytic gate was verified on the basis of the cellular distribution in a CD45/CD14 coordinate system.

Preparation of cells for cytometry

Peripheral blood mononuclear cells were suspended in PBS at a concentration equal to 2×10^7 cells per mL, and 50 µL of the solution were placed in 5 mL Falcon tubes (Becton Dickinson). Subsequently, the cells were subjected to 2- or 3-chrome labeling with monoclonal antibodies, according to the manufacturer's protocols (Table 2).

Table 2. Characteristics of fluorochrome-conjugated monoclonal antibodies used in the study

Specificity	Fluorochrome	Manufacturer
anti-CD3	FITC/PE/PE-Cy5	BD Biosciences, San Jose, USA
anti-CD19	FITC/PE/PE-Cy5	BD Biosciences, USA
anti-CD25	PE/PE-Cy5	BD Biosciences, USA
anti-CD38	FITC	BD Biosciences, USA
anti-CD69	PE/PE-Cy5	BD Biosciences, USA
anti-CD5/CD19	FITC/PE	BD Biosciences, USA
anti-CD45/CD14	FITC/PE	BD Biosciences, USA
anti-CD3/CD19	FITC/PE	BD Biosciences, USA

Following 30-min incubation with monoclonal antibodies at 4°C, the cells were washed with PBS containing 0.1% sodium azide and 1% fetal bovine serum, centrifuged at 700 × g for 5 min, and fixed in 0.5 mL of 1% paraformaldehyde solution (Sigma Pharmaceuticals).

The results of the cytometric analysis were presented as a fraction of cells labeled with fluorochrome-conjugated monoclonal antibodies or as a mean fluorescence intensity (MFI), corresponding to the expression of a given antigen on a cellular surface.

Intracellular ZAP-70 kinase detection

The BD Perm/Wash buffer (Becton-Dickinson) and anti-ZAP-70 PE (Becton Dickinson) were added to the appropriate tubes and incubated for 15 min at room temperature in darkness. Finally, the cells were washed and analyzed by flow cytometry. For each analysis, 20,000 events were acquired and analyzed using CellQuest software (Becton Dickinson).

Statistical analysis

Normal distribution of continuous variables was tested using the Shapiro-Wilk test, and the homogeneity of their variances was verified with Levene's test and the F-test. Depending on their distribution, the statistical characteristics of continuous variables were presented as arithmetic means and standard deviations (SD), or as medians and ranges (min-max). The Mann-Whitney U-test or the Kruskal-Wallis test were used for intergroup comparisons of continuous variables. The power and direction of relationships between 2 continuous variables was determined using Pearson's coefficient of linear correlation (r). All calculations were carried out with STATISTICA v. 9 (StatSoft, Tulsa, USA) package, with the level of significance set at $p < 0.05$. To present the survival function, the Kaplan-Meier estimator (survival curve) was used.

Results

Number of activated lymphocytes T and B

The immunophenotypes of basic subpopulations of peripheral blood lymphocytes in patients and healthy controls are presented in Table 3. Compared to healthy individuals, patients with CLL showed a higher absolute number of lymphocytes B with phenotypes CD19+CD25+ (p = 0.000016) and CD19+CD69+ (p = 0.0003). Moreover, they had a higher absolute number of CD3+CD25+ (p = 0.00047) as well as CD3+CD69+ lymphocytes T (p = 0.07), although this latter difference lacked statistical significance.

Relationship between the fraction of activated cells in peripheral blood and bone marrow and the established prognostic factors in CLL

We revealed that higher Rai stages of CLL were associated with the enhanced activation of B cells in peripheral blood (p = 0.018). Specifically, patients with stage 0 CLL showed a significantly lower percentage of CD19+CD25+ lymphocytes B in peripheral blood than those in Rai stage 3 (31.24% vs 78.67%, p = 0.003), and patients with stage 2 CLL showed a significantly lower percentage of CD19+CD25+ lymphocytes B in peripheral blood than those in Rai stage 3 (50.24% vs 78.67%, p = 0.021) (Fig. 1A). Moreover, there was a significant association between the percentage of CD19+ B cells in peripheral blood and the expression of the early marker of activation, CD69 (p = 0.005). Specifically, patients with Rai stage 3 showed a significantly higher percentage of CD19+CD69+ B cells (47.16%) than those with CLL stages 0 (18.13%, p = 0.009) and 2 (19.09%, p = 0.019) (Fig. 1B).

Furthermore, the number of CD19+CD69+ lymphocytes B in bone marrow was significantly associated with the CLL stage (p = 0.023). Specifically, patients with Rai stage 3 showed a higher fraction of activated lymphocytes in bone marrow than those with Rai stage 0 (51.07% vs 19.34%, p = 0.018) and 2 (51.07% vs 19.74%, p = 0.006) (Fig. 1C). Finally, there was a significant association between the fraction of CD3+CD25+ T cells and the stage of the disease (p = 0.029). The difference was particularly evident in the case of Rai stages 3 and 1 (36.78% vs 13.01%, p = 0.003) (Fig. 1D).

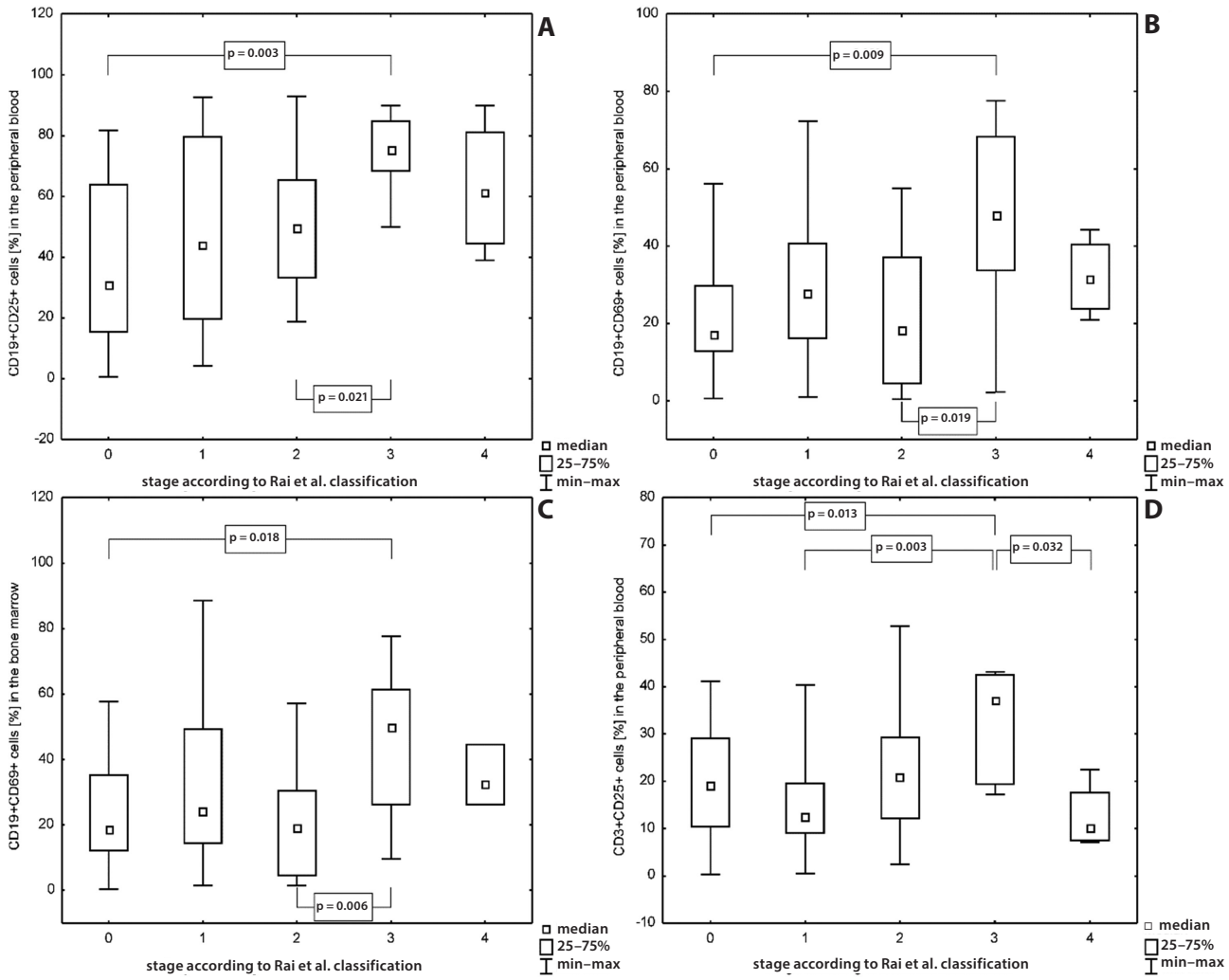

Fig. 1. Assessment of the frequencies of CD19+CD25+ cells in the peripheral blood of CLL patients with stage 0–4 according to Rai et al.'s classification (A); assessment of the frequencies of CD19+CD69+ cells in the peripheral blood of CLL patients with stage 0–4 according to Rai et al.'s classification (B); assessment of the frequencies of CD19+CD69+ cells in the bone marrow of CLL patients with stage 0–4 according to Rai et al.'s classification (C); assessment of the frequencies of CD3+CD25+ cells in the peripheral blood of CLL patients with stage 0–4 according to Rai et al.'s classification (D)

Table 3. The immunophenotype of peripheral blood lymphocytes in the CLL patients and the controls; data presented as an absolute number of cells ($10^3/mm^3$)

Parameter		CLL patients	Controls	p-value
CD19+/ZAP-70+ [$10^3/mm^3$]	median (min–max)	12.28 (0.91–64.19)	–	–
ZAP-70+ (patients with >20% or <20% of ZAP-70+ B cells)	>20% of B cells <20% of B cells	22 (27.5%) 58 (72.5%)		
CD19+/CD38+ [$10^3/mm^3$]	median (min–max)	4.61 (0.06–91.00)		
CD38+ (patients with >20% or <20% of CD38+ B cells)	>20% of B cells <20% of B cells	27 (33.75%) 53 (66.25%)		
CD3+ [$10^3/mm^3$]	median (min–max)	2.25 (0.16–17.31)	1.69 (0.96–3.27)	NS*
CD19+ [$10^3/mm^3$]	median (min–max)	21.84 (4.90–90.68)	0.33 (0.11–0.50)	0.000000003
CD5+/CD19+ [$10^3/mm^3$]	median (min–max)	20.80 (1.67–89.56)	0.10 (0.03–0.25)	0.0000000001
CD19+/CD25+ [$10^3/mm^3$]	median (min–max)	11.50 (0.05–63.84)	0.08 (0.01–0.20)	0.000016
CD19+/CD69+ [$10^3/mm^3$]	median (min–max)	6.09 (0.04–64.81)	0.02 (0.01–0.08)	0.0003
CD3+/CD25+ [$10^3/mm^3$]	median (min–max)	5.12 (0.10–45.53)	0.18 (0.04–0.48)	0.00047
CD3+/CD69+ [$10^3/mm^3$]	median (min–max)	0.70 (0.03–25.28)	0.05 (0.01–0.10)	NS*

* not statistically significant (NS).

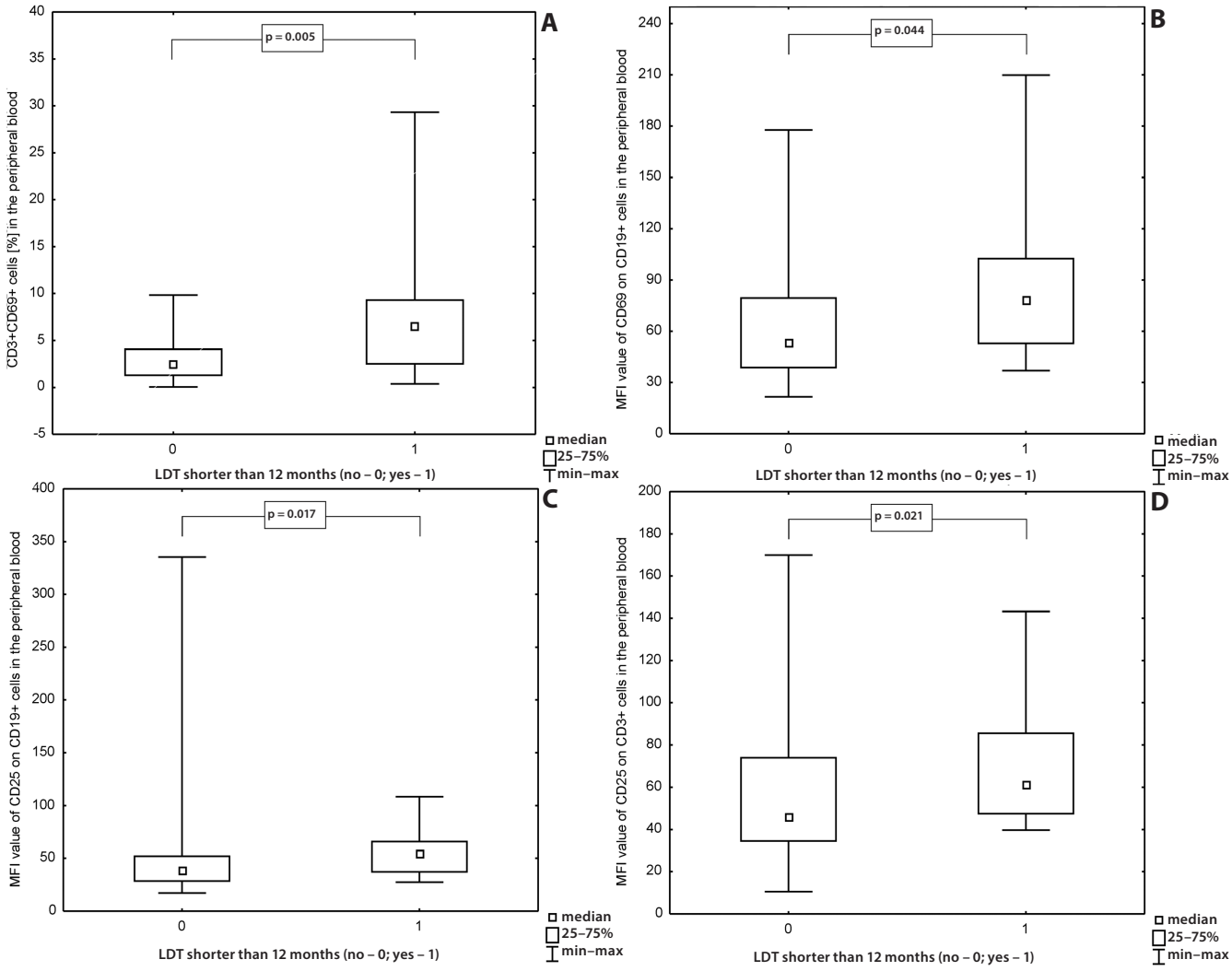

Fig. 2. Assessment of the frequencies of CD3+CD69+ cells in the peripheral blood of CLL patients in correlation with LDT (A); assessment of the CD69 MFI values on CD19+ cells in the peripheral blood of CLL patients in correlation with LDT (B); assessment of the CD25 MFI values on CD19+ cells in the peripheral blood of CLL patients in correlation with LDT (C); assessment of the CD25 MFI values on CD3+ cells in the peripheral blood of CLL patients in correlation with LDT (D)

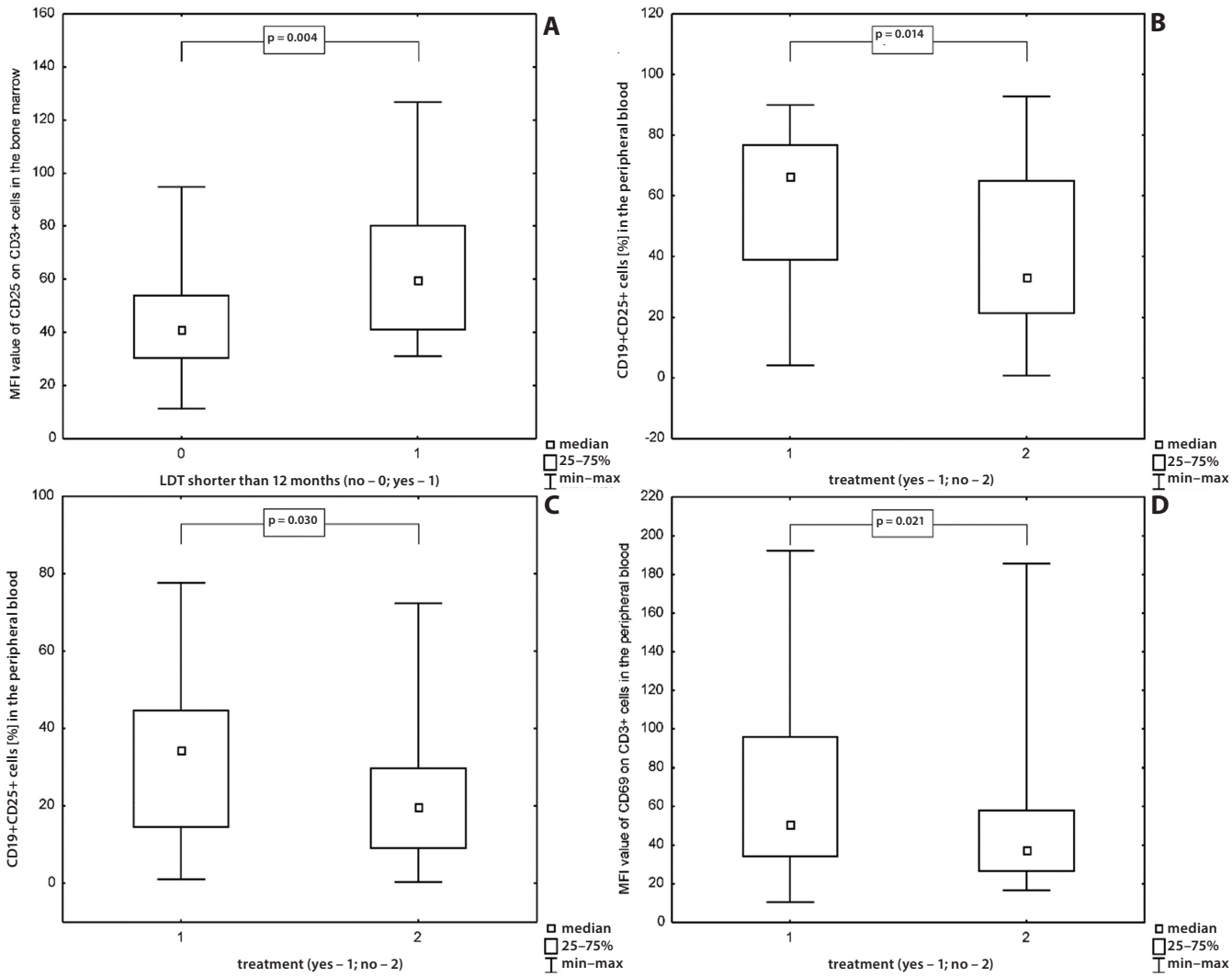

Fig. 3. Assessment of the CD25 MFI values on CD3+ cells in the bone marrow of CLL patients in correlation with LDT (A); assessment of the frequencies of CD19+CD25+ cells in the peripheral blood among 2 groups of CLL patients: those who received a treatment or the untreated individuals (B); assessment of the frequencies of CD19+CD69+ cells in the peripheral blood among 2 groups of CLL patients: those who received a treatment or the untreated individuals (C); assessment of the CD69 MFI values on CD3+ cells in the peripheral blood among the 2 groups of CLL patients: those who received a treatment or the untreated individuals (D)

The concentration of lactate dehydrogenase (LDH) correlated positively with the percentage of lymphocyte B CD19+CD25+ (r = 0.248; p = 0.035) and CD19+CD69+ (r = 0.243; p = 0.033), and lymphocyte T CD3+CD69+ (r = 0.308; p = 0.008) of peripheral blood, as well as with lymphocyte B CD19+CD69+ of bone marrow (r=0.298; p = 0.011). Moreover, the concentration of LDH was correlated positively with MFI of CD69 on lymphocyte B (r = 0.391; p = 0.0004), and MFI of CD25 (r = 0.537; p = 0.0001) and CD69 (r = 0.349; p = 0.002) on lymphocyte T in peripheral blood, as well as with MIF of CD25 on lymphocyte T in bone marrow (r = 0.382; p = 0.001).

The concentration of beta-2 microglobulin showed a positive correlation with MFI of CD25 and CD69 on lymphocyte T in peripheral blood (r = 0.289; p = 0.014 and r = 0.286; p = 0.015, respectively), as well as with MFI of CD25 on lymphocyte T in bone marrow (r = 0.393; p = 0.001).

We observed a significant negative correlation between the fraction of CD3+CD69+ lymphocyte T in peripheral blood and LDT (r = –0.558; p = 0.016). The mean fluorescence intensity of CD69 on CD19+ cells of peripheral blood was inversely correlated with LDT (r = –0.494; p = 0.032). Additionally, LDT correlated inversely with MFI of CD25 on lymphocytes B (r = –0.654; p = 0.002) and T (r = –0.680; p = 0.002) in peripheral blood, as well as on lymphocyte T in bone marrow (r = –0.636; p = 0.005). Patients who experienced lymphocyte doubling in less than 12 months had a higher percentage of CD3+CD69+ lymphocyte T than those who did not (7.31% vs 2.49%, p = 0.005) (Fig. 2A), a higher MFI value of CD69 on the surface of B CD19+ lymphocytes (79.35 vs 54.17, p = 0.044) (Fig. 2B), a higher MFI value of CD25 on the surface of B CD19+ lymphocytes (52.02 vs 39.91, p = 0.017) (Fig. 2C), and a higher MFI value of CD25 on the surface of T CD3+ lymphocytes (61.47 vs 43.16, p = 0.021) (Fig. 2D) in peripheral blood.

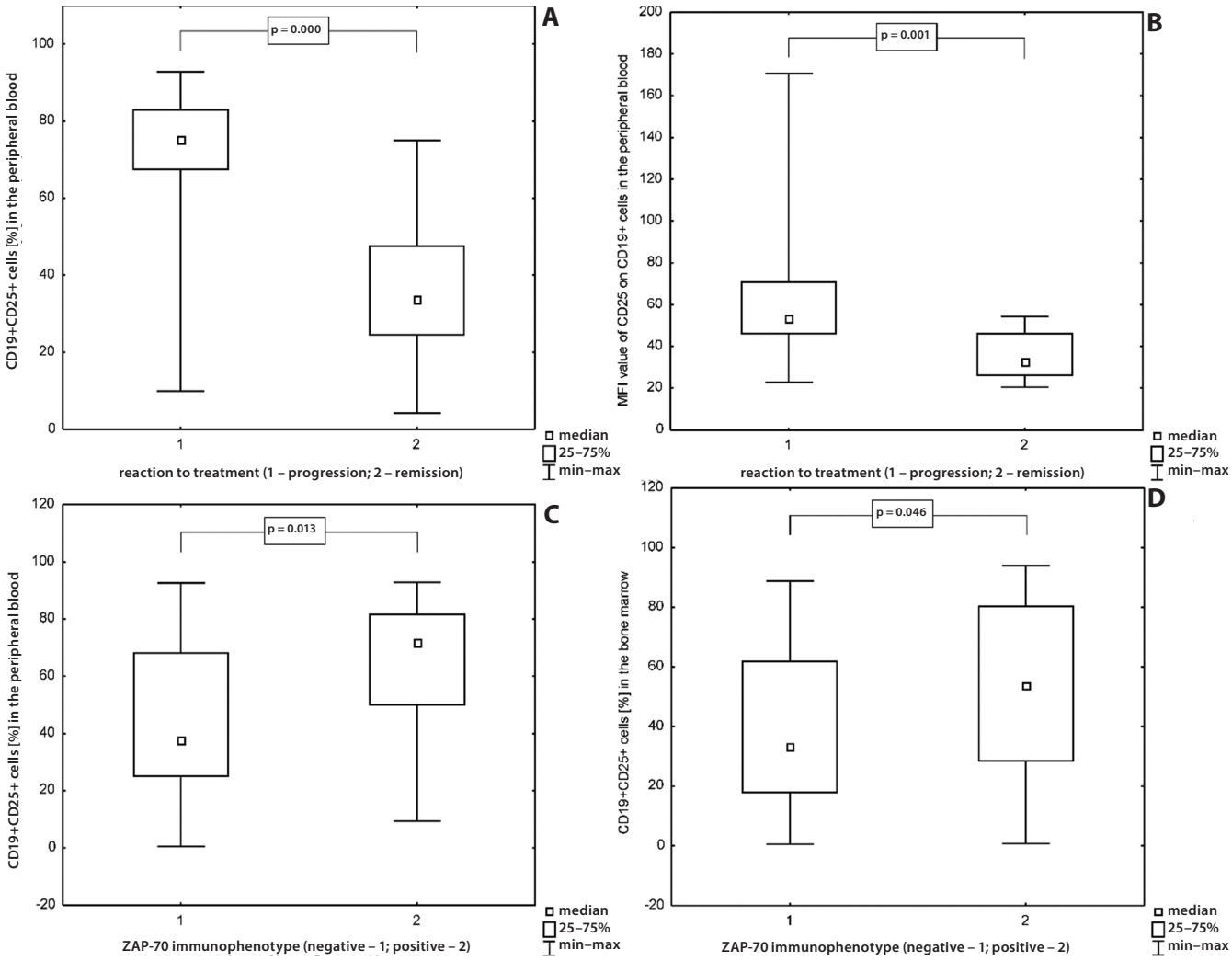

Fig. 4. Assessment of the frequencies of CD19+CD25+ cells in the peripheral blood of CLL patients with disease progression or remission reflected by the treatment (A); assessment of the CD25 MFI values on CD19+ cells in the peripheral blood of CLL patients with disease progression or remission reflected by the treatment (B); assessment of the frequencies of CD19+CD25+ cells in the peripheral blood of CLL patients with ZAP-70 positive or negative immunophenotype (C); assessment of the frequencies of CD19+CD25+ cells in the bone marrow of CLL patients with ZAP-70 positive or negative immunophenotype (D)

Patients who experienced lymphocyte doubling in less than 12 months had a higher MFI value of CD25 on the surface of T CD3+ lymphocytes in bone marrow than those who did not (60.04 vs 41.83, p = 0.004) (Fig. 3A).

We observed that patients who started therapy due to rapid progression of the disease had a significantly higher percentage of CD19+CD25+ B cells in peripheral blood compared to untreated individuals (67.46% vs 33.91%, p = 0.014) (Fig. 3B). Moreover, these patients showed a higher percentage of lymphocyte B CD19+CD69+ (34.03% vs 20.15%, p = 0.03) (Fig. 3C) and a higher MFI of CD25 on lymphocyte T (51.46 vs 38.97, p = 0.021) in peripheral blood (Fig. 3D).

Individuals in whom treatment was reflected by remission were characterized by a lower percentage of lymphocyte B CD19+CD25+ in peripheral blood than those who experienced progression and/or died (34.18% vs 75.03%, p = 0.00013) (Fig. 4A). The mean fluorescence intensity of CD25 on the surface of lymphocyte B of peripheral blood was significantly higher in patients in whom treatment was reflected by progression and/or death than in those who showed remission (52.19 vs 32.07, p = 0.001) (Fig. 4B). The individuals whose lymphocyte B showed the expression of ZAP-70+ had higher frequencies of CD19+CD25+ B cells in peripheral blood (71.12% vs 36.98%, p = 0.013) (Fig. 4C) and bone marrow (53.24% vs 32.16%, p = 0.046) compared to ZAP-70– individuals (Fig. 4D).

The number of lymphocytes B CD19+ZAP-70+ correlated positively with the number of CD19+CD25+ B cells (r = 0.386; p = 0.001) and CD3+CD69+ T cells (r = 0.323; p = 0.005) in peripheral blood, as well as with the number of CD19+CD25+ B cells in bone marrow (r = 0.307; p = 0.007).

The mean fluorescence intensity of CD25 on lymphocyte T of peripheral blood (r = 0.314; p = 0.006) and bone marrow (r = 0.298; p = 0.012), and MFI of CD25 on the surface of lymphocyte B of bone marrow (r = 0.244; p = 0.036) increased proportionally to the fraction of CD19+ZAP-70+

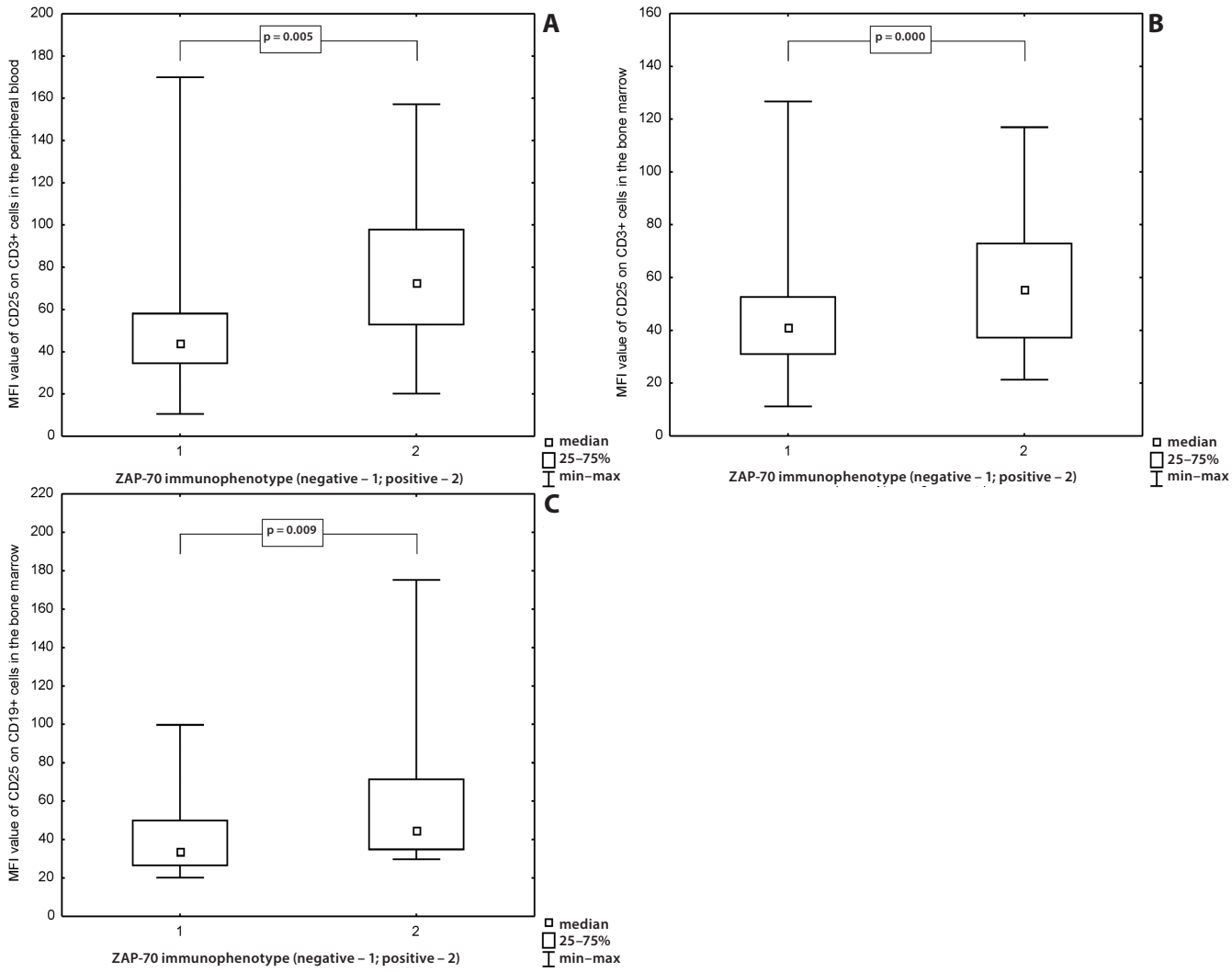

Fig. 5. Assessment of the CD25 MFI values on CD3+ cells in the peripheral blood of CLL patients with ZAP-70 positive or negative immunophenotype (A); assessment of the CD25 MFI values on CD3+ cells in the bone marrow of CLL patients with ZAP-70 positive or negative immunophenotype (B); assessment of the CD25 MFI values on CD19+ cells in the bone marrow of CLL patients with ZAP-70 positive or negative immunophenotype (C)

B cells. The mean fluorescence intensity of CD25 on the surface of lymphocyte T in peripheral blood (71.01 vs 42.14, p = 0.005) (Fig. 5A) and lymphocyte T in bone marrow (56.11 vs 41.63, p = 0.00012) (Fig. 5B), and on the surface of B cells in bone marrow (44.17 vs 32.81, p = 0.009) was higher in patients with ZAP-70+ lymphocyte B (Fig. 5C).

Relationship between the fraction of activated cells in peripheral blood and the probability of survival after the diagnosis of CLL

We revealed factors that significantly increase the probability of survival after the diagnosis of the disease in the study group. The patients with the percentage of CD19+/CD25+ lymphocytes <56% (p = 0.0002) (Fig. 6A) and the absolute number of CD19+/CD25+ lymphocytes <12.5 × 10^3 cells/μL (p = 0.0295) (Fig. 6B), as well as the absolute number of CD19+/CD69+ lymphocytes <7.7 × 10^3 cells/μL (p = 0.0047) (Fig. 6C) and the percentage of CD19+/CD69+ lymphocytes <29.65% (p = 0.0001) (Fig. 6D) demonstrated increased survival.

Additionally, an absolute count of CD3+/CD69+ lymphocytes <0.65 × 10^3 cells/μL (p = 0.0205) constituted a positive survival factor (Fig. 7A).

A major factor that increased the probability of doubling the lymphocyte count was a percentage of CD19+/CD25+ cells >29.65% (p = 0.0191) (Fig. 7B). An absolute count of CD19+/CD25+ lymphocytes >12.5 × 10^3 cells/μL was also a factor that increased the likelihood of doubling of the lymphocytosis (p = 0.0246) (Fig. 7C).

Discussion

Chronic lymphocytic leukemia results from the expansion of mature lymphocytes B CD5+. Probably, these cells proliferate in bone marrow and in the lymph nodes, while

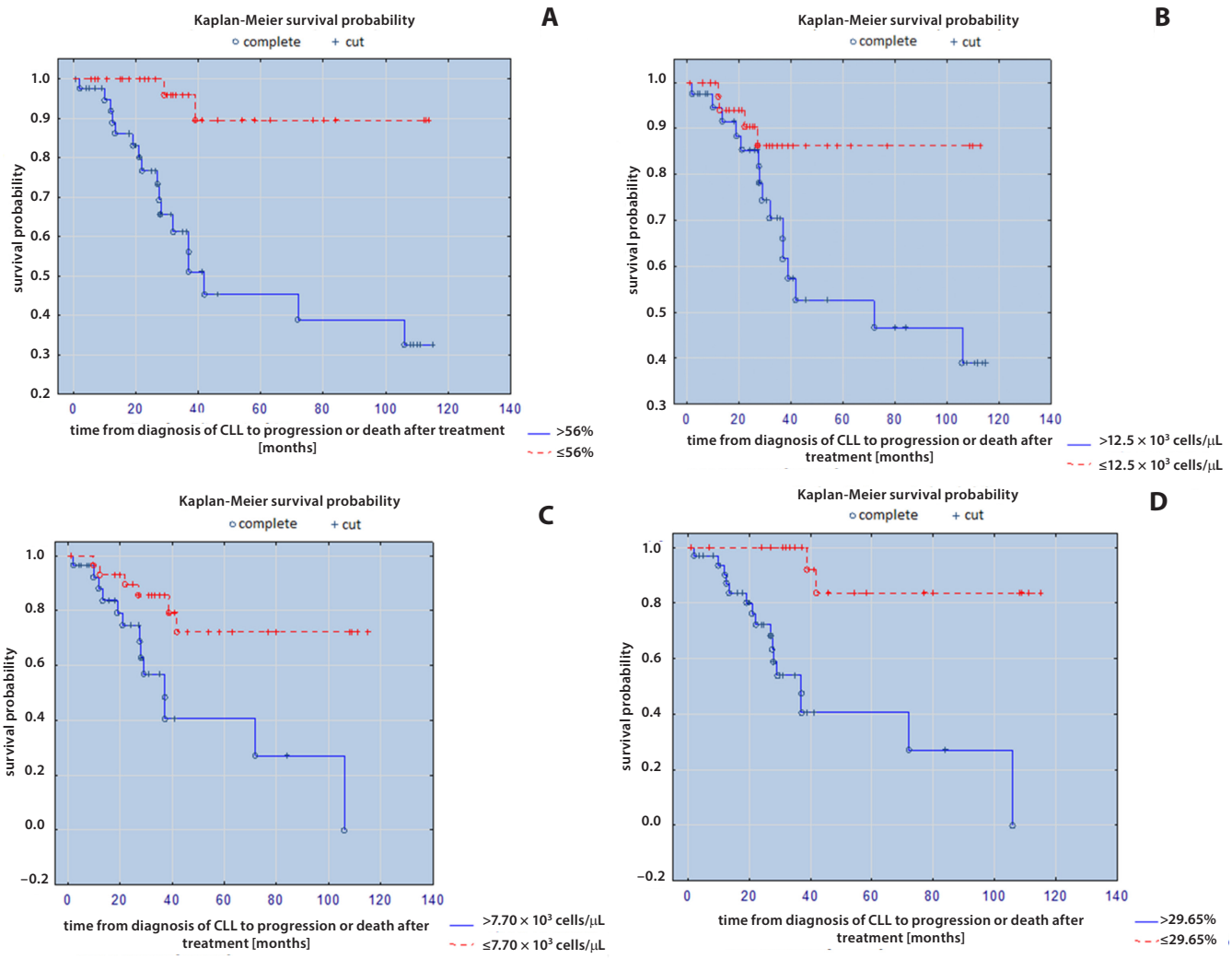

Fig. 6. Assessment of the survival probability with the time from diagnosis of CLL to progression or death after treatment in correlation with the percentage of CD19+/CD25+ cells (A); assessment of the survival probability with the time from diagnosis of CLL to progression or death after treatment in correlation with the absolute number of CD19+/CD25+ cells (B); assessment of the survival probability with the time from diagnosis of CLL to progression or death after treatment in correlation with the percentage of CD19+/CD69+ cells (C); assessment of the survival probability with the time from diagnosis of CLL to progression or death after treatment in correlation with the absolute number of CD19+/CD69+ cells (D)

the leukemic lymphocytes of peripheral blood remain at the G0/G1 phase. The expression of genes in leukemic cells resembles that of memory B lymphocytes; moreover, they express cell surface antigens specific to lymphocyte B which had contact with an antigen (CD23, CD27, IgM, and IgD).[25–27] The aim of the research, which has already continued for a significant number of years, is to identify subgroups of CLL patients with a similar clinical course of the disease.[28] A high expression of ZAP-70 and CD38 was revealed to be associated with a more aggressive course of CLL.[29]

CD25, i.e., the alpha chain of the IL-2 receptor, is present on the surface of leukemic cells in 30–50% of CLL patients. The density of the expression of this molecule on leukemic cells is higher than on normal lymphocyte B, as well as on lymphocyte B during the so-called monoclonal B-cell lymphocytosis of undetermined significance (B-MLUS).[30–34] CD25 is postulated to be associated with the activation status of cells expressing this antigen. Probably, it also serves as a growth factor receptor and regulates the proliferation of lymphocyte B.[35,36] Aside from CLL, a high expression of this molecule was also detected on the surface of B cells in promyelocytic and hair-cell leukemia.[37,38] The expression of CD25 on the surface of lymphocytes and an elevated serum concentration of soluble CD25 are associated with a negative prognosis in acute lymphoblastic leukemia and diffuse large B-cell lymphoma.[39,40] The data on the role of CD25 as a prognostic factor in CLL is inconclusive. Although according to some authors, the prognosis is worse in patients showing a high expression of CD25, other researchers observed that the CD25+ phenotype is associated with a milder course of CLL.[31,33] The most recently published data from a retrospective study of 281 individuals with CLL followed-up for 8 years did not confirm a relationship between the expression of CD25 and the survival time or the time elapsed between diagnosis and the implementation of treatment.[28] This study revealed that the expression

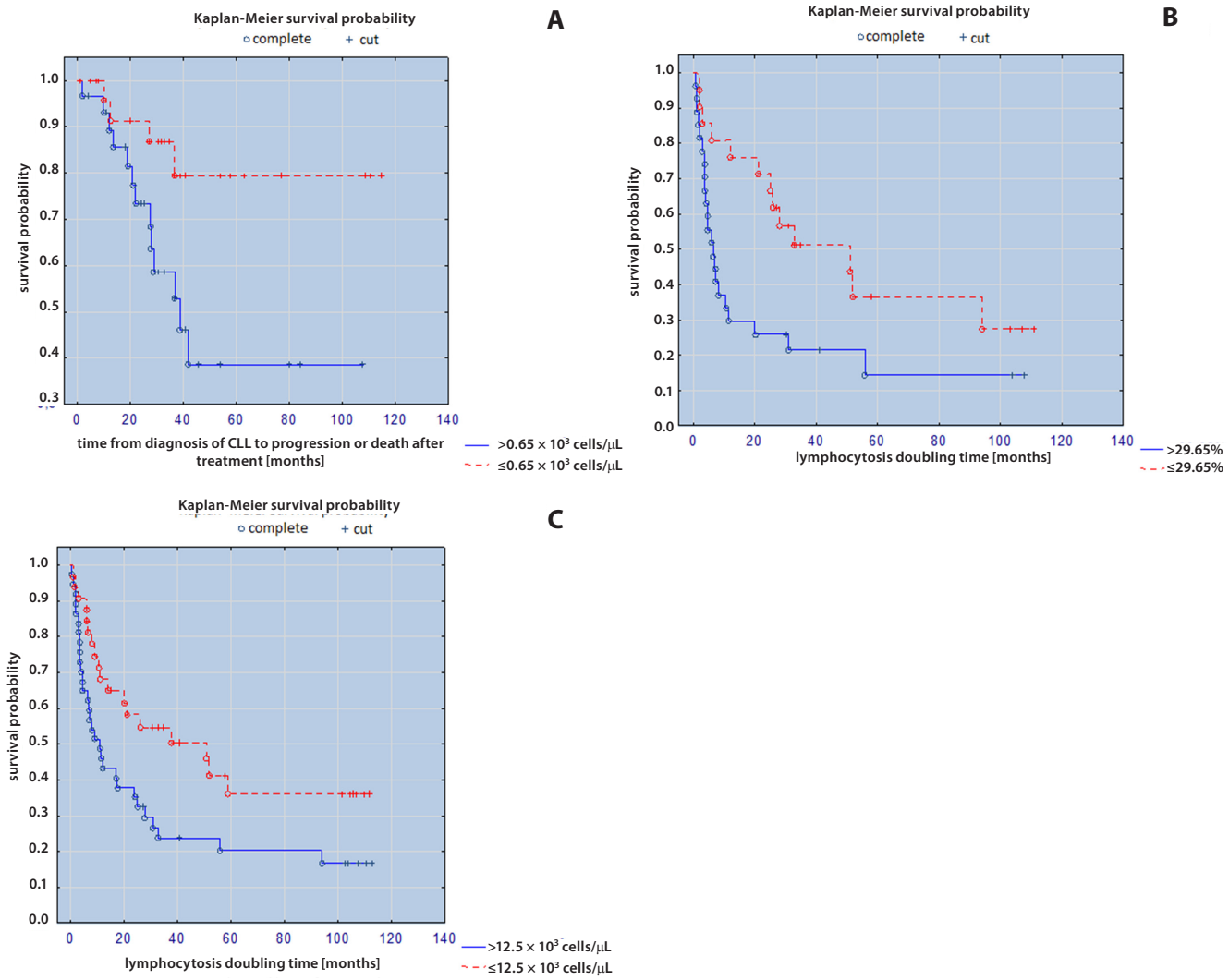

Fig. 7. Assessment of the survival probability with the time from diagnosis of CLL to progression or death after treatment in correlation with the absolute number of CD3+/CD69+ cells (A); assessment of the survival probability with LDT in correlation with the percentage of CD19+/CD25+ cells (B); assessment of the survival probability with LDT in correlation with the absolute number of CD19+/CD25+ cells (C)

of CD-25 on lymphocyte B of leukemia patients is many times higher than in the controls. Moreover, an association between the established prognostic factors in CLL and the CD25 expression was analyzed. The previously mentioned studies revealed a relationship between the number of lymphocytes B with the CD19+CD25+ phenotype and Rai clinical stage. The percentage of lymphocyte B CD19+CD25+ was higher in more advanced stages. Moreover, there was an inverse correlation between LDT and MFI of CD25 on lymphocyte B in peripheral blood, and a positive correlation between the concentration of LDH and the percentage of lymphocyte B CD19+CD25+ in peripheral blood. We revealed that the number CD19+CD25+ B cells in the peripheral blood of individuals who required treatment due to rapid progression of the disease was significantly higher than in untreated patients, which is contradictory to findings reported by Shvidel et al.[28] Moreover, the patients who showed remission after the treatment were characterized by a higher percentage of lymphocyte B CD19+CD25+ in peripheral blood than individuals who experienced progression and/or died. The mean fluorescence intensity of CD25 on the surface of lymphocyte B of peripheral blood was higher in individuals who showed progression and/or died after the treatment than in those with remission. Our analysis of the relationship between documented prognostic factors and the markers of activation revealed that the number of lymphocytes B CD19+ZAP-70+ correlated positively with the number of CD19+CD25+ B cells in peripheral blood and bone marrow. Moreover, MFI of CD25 on the surface of lymphocyte B in bone marrow also increased proportionally to the number of CD19+ZAP-70+ cells. Individuals in whom the phenotype of lymphocytes B was determined as ZAP-70+ had more CD19+CD25+ B cells in peripheral blood and bone marrow than patients whose lymphocytes did not show the expression of this marker. Also, MFI of CD25 on the surface of lymphocyte B in bone marrow was higher in individuals whose lymphocytes were

classified as ZAP-70+. Similarly to Shvidel et al., our study did not reveal significant differences in the prevalence of anemia, thrombocytopenia and an elevated concentration of beta-2 microglobulin between patients with a high and low number of CD25+ lymphocytes.[28] Although our studied group was smaller than that analyzed by previously mentioned authors, the number of studied parameters was markedly higher. Plausibly, further extensive studies are needed to eventually verify the significance of the CD25 expression on leukemic lymphocytes in CLL.

Furthermore, our study also revealed that the expression of CD25 on lymphocyte T is higher in patients with CLL than in healthy individuals. Activated lymphocytes T of patients with CLL are known to stimulate the proliferation and promote the survival of leukemic cell clones, despite qualitative and quantitative disorders of their population.[21] However, we did not find any literature evidence of the relationship between the lymphocyte T expression of CD25 and the prognostic factors in CLL. We revealed that a higher prevalence of CD3+CD25+ T cells was associated with higher Rai stages of CLL. Moreover, we observed an inverse correlation between LDT and MFI of CD25 on lymphocyte T of peripheral blood and bone marrow. Furthermore, the concentration of LDH and beta-2 microglobulin also correlated positively with MFI of CD25 on lymphocyte T of peripheral blood and bone marrow. The mean fluorescence intensity of CD25 on lymphocyte T of peripheral blood and bone marrow increased proportionally to the percentage of CD19+ZAP-70+ B cells. We revealed that ZAP-70+ patients showed a significantly higher MFI of CD25 on lymphocyte T of peripheral blood and bone marrow. Moreover, MFI of CD25 was also significantly higher in individuals who required the implementation of treatment than in those who did not.

The expression of CD69 on activated cells can be observed early; namely, within 4 h of stimulation. As early as in 2002, Damle et al. revealed a significantly higher fraction of CD19+CD69+ lymphocytes in individuals without a mutation in IgVH genes and with the CD38+ phenotype of B cells.[25] Similarly to normal lymphocytes, CLL cells can undergo activation, which can be determined on the basis of the CD69 expression.[22] Our study of the expression of CD69 on leukemic cells revealed that higher Rai stages are associated with a higher prevalence of CD19+CD69+ lymphocyte B, both in peripheral blood and in bone marrow. The mean intensity of fluorescence of CD69 on lymphocyte B of peripheral blood was inversely correlated with LDT. Moreover, we observed a positive correlation between the concentration of LDH and the percentage of CD19+CD69+ lymphocyte B of peripheral blood and bone marrow. Additionally, the concentration of LDH correlated positively with MFI of CD69 on lymphocyte B. Individuals in whom rapid progression of the disease required the implementation of treatment had a higher fraction of CD19+CD69+ lymphocyte B than untreated individuals. Aside from the expression of CD69 on B cells, we analyzed the relationship between the expression of this molecule on lymphocyte T and the established prognostic factors in CLL. We revealed an inverse correlation between the fraction of CD3+CD69+ lymphocyte T in peripheral blood and LDT. The density of the CD69 expression on lymphocyte T of peripheral blood was also inversely correlated with LDT. Moreover, we observed a positive correlation between the serum concentration of LDH and the percentage of CD3+CD69+ lymphocyte T in peripheral blood. A higher fraction of CD3+CD69+ lymphocytes was documented in patients with lymphocyte doubling. Also, the serum concentration of LDH and beta-2 microglobulin correlated positively with MFI of CD69 on lymphocyte T of peripheral blood. The number of CD19+ZAP-70+ lymphocytes B was associated with the number of CD3+CD69+ T cells in peripheral blood.

In conclusion, this study confirmed earlier findings on the association between a negative prognosis and a high expression of activation markers in CLL patients. The determination of CD25+ and CD69+ lymphocytes T and B constitutes a valuable diagnostic tool, completing the cytometric evaluation of CLL. Perhaps, aside from the established markers, such as CD38 and ZAP-70, the number of activated lymphocytes should also be determined in CLL patients, as this parameter supplements their prognosis. Further research is required in order to identify antigen(s) causing the activation of leukemic cells and normal lymphocytes T.

References

1. Linet M, Schubauer-Berigan M, Weisenburger D, et al. Chronic lymphocytic leukaemia: An overview of aetiology in light of recent developments in classification and pathogenesis. *Br J Haematol*. 2007; 139(5):672–686. doi:10.1111/j.1365-2141.2007.06847.x
2. Thomas R, Ribeiro I, Shepherd P, et al. Spontaneous clinical regression in chronic lymphocytic leukaemia. *Br J Haematol*. 2002;116(2): 341–345. doi:10.1046/j.0007-1048.2001.03286.x
3. Rai KR, Sawitsky A, Cronkite EP, Chanana AD, Levy RN, Pasternack BS. Clinical staging of chronic lymphocytic leukemia. *Blood*. 1975;46(2): 219–234.
4. Binet J, Auquier A, Dighiero G, et al. A new prognostic classification of chronic lymphocytic leukemia derived from a multivariate survival analysis. *Cancer*. 1981;48(1):198–206.
5. Klepfish A, Rachmilewitz E, Sarid M, Schattner A. Evaluating the impact of age and disease on survival of chronic lymphocytic leukaemia patients by a new method. *Int J Clin Pract*. 2009;63(11):1601–1603. doi:10.1111/j.1742-1241.2009.02008.x
6. Amu S, Gjertsson I, Brisslert M. Functional characterization of murine CD25 expressing B cells. *Scand J Immunol*. 2010;71(4):275–282. doi:10.1111/j.1365-3083.2010.02380.x
7. Karp M, Kosior K, Karczmarczyk A, et al. Cytotoxic activity of valproic acid on primary chronic lymphocytic leukemia cells. *Adv Clin Exp Med*. 2015;24(1):55–62. doi:10.17219/acem/29264
8. Pepper C, Majid A, Lin T, et al. Defining the prognosis of early stage chronic lymphocytic leukaemia patients. *Br J Haematol*. 2012;156(4): 499–507. doi:10.1111/j.1365-2141.2011.08974.x
9. Bazargan A, Tam C, Keating M. Predicting survival in chronic lymphocytic leukemia. *Expert Rev Anticancer Ther*. 2012;12(3):393–403. doi:10.1586/era.12.2
10. Wierda W, O'Brien S, Wang X, et al. Characteristics associated with important clinical end points in patients with chronic lymphocytic leukemia at initial treatment. *J Clin Oncol*. 2009;27(10):1637–1643. doi:10.1200/jco.2008.18.1701

11. Rassenti L, Kipps T. Clinical utility of assessing ZAP-70 and CD38 in chronic lymphocytic leukemia. *Cytometry B Clin Cytom*. 2006;70(4): 209–213. doi:10.1002/cyto.b.20129
12. Martinelli S, Cuneo A, Formigaro L, et al. Identifying high-risk chronic lymphocytic leukemia: A pathogenesis-oriented appraisal of prognostic and predictive factors in patients treated with chemotherapy with or without immunotherapy. *Mediterr J Hematol Infect Dis*. 2016; 8(1):e2016047. doi:10.4084/MJHID.2016.047
13. Molica S, Shanafelt T, Giannarelli D, et al. The chronic lymphocytic leukemia international prognostic index predicts time to first treatment in early CLL: Independent validation in a prospective cohort of early stage patients. *Am J Hematol*. 2016;91(11):1090–1095. doi:10.1002/ajh.24493
14. Karabon L, Partyka A, Jasek M, et al. Intragenic variations in *BTLA* gene influence mRNA expression of *BTLA* gene in chronic lymphocytic leukemia patients and confer susceptibility to chronic lymphocytic leukemia. *Arch Immunol Ther Exp.* 2016;64(S1):137–145. doi:10.1007/s00005-016-0430-x
15. Kubeczko M, Nowara E, Spychałowicz W, et al. Efficacy and safety of vitamin D supplementation in patients with chronic lymphocytic leukemia. *Postepy Hig Med Dosw (Online)*. 2016;70:534–541. doi:10.5604/17322693.1202482
16. Grywalska E, Hymos A, Korona-Głowniak I, et al. Assessment of the influence of peripheral blood mononuclear cell stimulation with *Streptococcus pneumoniae* polysaccharides on expression of selected Toll-like receptors, activation markers and Fas antigen in patients with chronic lymphocytic leukemia. *Postepy Hig Med Dosw (Online)*. 2016;70:959–967. doi:10.5604/17322693.1219399
17. Chiorazzi N, Rai K, Ferrarini M. Chronic lymphocytic leukemia. *N Engl J Med*. 2005;352(8):804–815. doi:10.1056/nejmra041720
18. Ziolkowska E, Wolowiec D, Cebula-Obrzut B, et al. Cytotoxic and apoptosis-inducing effects of bendamustine used alone and in combination with rituximab on chronic lymphocytic leukemia cells in vitro. *Postepy Hig Med Dosw (Online)*. 2014;68:1433–1443. doi:10.5604/17322693.1130704
19. Andersen M, Vojdeman F, Andersen M, et al. Hypogammaglobulinemia in newly diagnosed chronic lymphocytic leukemia is a predictor of early death. *Leuk Lymphoma*. 2016;57(7):1592–1599. doi:10.3109/10428194.2016.1142082
20. Tsai H, Caporaso N, Kyle R, et al. Evidence of serum immunoglobulin abnormalities up to 9.8 years before diagnosis of chronic lymphocytic leukemia: A prospective study. *Blood*. 2009;114(24):4928–4932. doi:10.1182/blood-2009-08-237651
21. Scrivener S, Goddard R, Kaminski E, Prentice A. Abnormal T-cell function in B-cell chronic lymphocytic leukaemia. *Leuk Lymphoma*. 2003;44(3): 383–389. doi:10.1080/1042819021000029993
22. De Fanis U, Romano C, Dalla Mora L, et al. Differences in constitutive and activation-induced expression of CD69 and CD95 between normal and chronic lymphocytic leukemia B cells. *Oncol Rep*. 2003;10(3): 653–658.
23. Hassanein N, Perkinson K, Alcancia F, Goodman B, Weinberg J, Lagoo A. A single tube, four-color flow cytometry assay for evaluation of ZAP-70 and CD38 expression in chronic lymphocytic leukemia. *Am J Clin Pathol*. 2010;133(5):708–717. doi:10.1309/ajcpqs4oxjjsz5kn
24. Rossmann E, Lewin N, Jeddi-Tehrani M, Osterborg A, Mellstedt H. Intracellular T cell cytokines in patients with B cell chronic lymphocytic leukaemia (B-CLL). *Eur J Haematol*. 2002;68(5):299–306. doi:10.1034/j.1600-0609.2002.01612.x
25. Damle R, Ghiotto F, Valetto A, et al. B-cell chronic lymphocytic leukemia cells express a surface membrane phenotype of activated, antigen-experienced B lymphocytes. *Blood*. 2002;99(11):4087–4093. doi:10.1182/blood.v99.11.4087
26. Seifert M, Küppers R. Human memory B cells. *Leukemia*. 2016;30(12): 2283–2292. doi:10.1038/leu.2016.226
27. Rosenwald A, Alizadeh A, Widhopf G, et al. Relation of gene expression phenotype to immunoglobulin mutation genotype in B cell chronic lymphocytic leukemia. *J Exp Med*. 2001;194(11):1639–1648. doi:10.1084/jem.194.11.1639
28. Shvidel L, Braester A, Bairey O, et al. Cell surface expression of CD25 antigen (surface IL-2 receptor alpha-chain) is not a prognostic marker in chronic lymphocytic leukemia: Results of a retrospective study of 281 patients. *Ann Hematol*. 2012;91(10):1597–1602. doi:10.1007/s00277-012-1492-4
29. Moreno C, Montserrat E. New prognostic markers in chronic lymphocytic leukemia. *Blood Rev*. 2008;22(4):211–219. doi:10.1016/j.blre.2008.03.003
30. Rivkina A, Holodnuka-Kholodyuk I, Murovska M, Soloveichika M, Lejniece S. Peripheral blood lymphocyte phenotype of ZAP-70(+) and ZAP-70(–) patients with B-cell chronic lymphocytic leukaemia. *Exp Oncol*. 2015;37(1):73–76.
31. Hjalmar V, Hast R, Kimby E. Cell surface expression of CD25, CD54, and CD95 on B- and T-cells in chronic lymphocytic leukaemia in relation to trisomy 12, atypical morphology and clinical course. *Eur J Haematol*. 2002;68(3):127–134. doi:10.1034/j.1600-0609.2002.01515.x
32. Ma ES. Recurrent cytogenetic abnormalities in non-Hodgkin's lymphoma and chronic lymphocytic leukemia. *Methods Mol Biol*. 2017; 1541:279–293. doi:10.1007/978-1-4939-6703-2_22
33. Amaya-Chanaga C, Rassenti L. Biomarkers in chronic lymphocytic leukemia: Clinical applications and prognostic markers. *Best Pract Res Clin Haematol*. 2016;29(1):79–89. doi:10.1016/j.beha.2016.08.005
34. Rawstron A, Shingles J, de Tute R, Bennett F, Jack A, Hillmen P. Chronic lymphocytic leukaemia (CLL) and CLL-type monoclonal B-cell lymphocytosis (MBL) show differential expression of molecules involved in lymphoid tissue homing. *Cytometry B Clin Cytom*. 2010;78(S1):S42–S46. doi:10.1002/cyto.b.20534
35. Martkamchan S, Onlamoon N, Wang S, Pattanapanyasat K, Ammaranond P. The effects of anti-CD3/CD28 coated beads and IL-2 on expanded T cell for immunotherapy. *Adv Clin Exp Med*. 2016;25(5): 821–828. doi:10.17219/acem/35771
36. Zuśka-Prot M, Jaroszewski J, Maślanka T. Involvement of regulatory T cells and selected cytokines in the pathogenesis of bronchial asthma. *Postepy Hig Med Dosw (Online)*. 2016;70:668–677. doi:10.5604/17322693.1207511
37. Wotherspoon A, Attygalle A, Mendes LS. Bone marrow and splenic histology in hairy cell leukaemia. *Best Pract Res Clin Haematol*. 2015; 28(4):200–207. doi:10.1016/j.beha.2015.10.019
38. Janik J. Tumor markers in hairy cell leukemia. *Leuk Lymphoma*. 2011; 52(Suppl 2):69–71. doi:10.3109/10428194.2011.568651
39. Nakase K, Kita K, Miwa H, et al. Clinical and prognostic significance of cytokine receptor expression in adult acute lymphoblastic leukemia: Interleukin-2 receptor α-chain predicts a poor prognosis. *Leukemia*. 2007;21(2):326–332. doi:10.1038/sj.leu.2404497
40. Oki Y, Kato H, Matsuo K, et al. Prognostic value of serum soluble interleukin-2 receptor level in patients with diffuse large B cell lymphoma, treated with CHOP- or RCHOP-based therapy. *Leuk Lymphoma*. 2008;49(7):1345–1351. doi:10.1080/10428190802108888

Validation of a windowing protocol for accurate in vivo tooth segmentation using i-CAT cone beam computed tomography

Babak Rastegar[1,2,A–F], Brice Thumilaire[3,B–F], Guillaume A. Odri[4,C–F], Sergio Siciliano[5,D–F], Jan Zapała[6,D–F], Pierre Mahy[7,D–F], Raphael Olszewski[7,8,A–F]

[1] Service de Parodontologie, Université libre de Bruxelles, Belgium
[2] PhD student, Jagiellonian University Medical College, Kraków, Poland
[3] Private practice, Libramont, Belgium
[4] Service de Chirurgie Orthopédique et Traumatologique, CHU Lariboisière, Paris, France
[5] Service de Stomatologie et de Chirurgie Maxillo-faciale, Clinique St-Elisabeth, Brussels, Belgium
[6] Department of Cranio-Maxillofacial Surgery, Jagiellonian University Medical College, Rydygier Hospital, Kraków, Poland
[7] Service de Stomatologie et de Chirurgie Maxillo-faciale, Cliniques Universitaires Saint Luc, Université Catholique de Louvain, Brussels, Belgium
[8] Visiting professor, Department of Cranio-Maxillofacial Surgery, Jagiellonian University Medical College, Rydygier Hospital, Kraków, Poland

A – research concept and design; B – collection and/or assembly of data; C – data analysis and interpretation;
D – writing the article; E – critical revision of the article; F – final approval of the article

Advances in Clinical and Experimental Medicine, ISSN 1899-5276 (print), ISSN 2451-2680 (online) *Adv Clin Exp Med*. 2018;27(7):1001–1008

Address for correspondence
Raphael Olszewski
E-mail: raphael.olszewski@uclouvain.be

Funding sources
We would like to thank the Fondation St-Luc, Cliniques Universitaires Saint-Luc, for awarding a post-doctoral scholarship to Prof. Raphael Olszewski in 2008 to study 3D Slicer software at the Surgical Planning Lab, Harvard Medical School, Boston, USA.

Conflict of interest
None declared

Acknowledgements
We would like to thank Mr. B. Konieczny and Prof. J. Sokołowski from the Department of Dental Materials at the Medical University of Lodz, Poland, for their help with tooth laser scanning.

Received on September 29, 2016
Reviewed on December 30, 2016
Accepted on December 28, 2016

DOI
10.17219/acem/68117

Abstract

Background. Validation of three-dimensional (3D) reconstructions of full dental arches with crowns and roots based on cone beam computed tomography (CBCT) imaging represents a key issue in 3D digital dentistry.

Objectives. The aim of the study was to search for the most accurate in vivo windowing-based manual tooth segmentation using CBCT. The null hypothesis was that all applied windowing protocols were equivalent in terms of in vivo tooth volume measurement using CBCT.

Material and methods. This retrospective study was based on preoperative CBCT images from patients who underwent further tooth extractions for reasons independent of this study. Written informed consent was obtained from all the participants, and the study was approved by the Ethics Committee of Cliniques Universitaires Saint-Luc (Brussels, Belgium). The radiological protocol was I-CAT CBCT, 0.3 mm slice thickness, 8 cm × 16 cm field of view, 120 kVp, and 18 mAs. A total of 36 teeth were extracted from 14 patients between the ages of 18 and 68 years. Using 3D Slicer software, segmentations were performed twice by 2 independent observers, with a 1-month time period between the 2 segmentations to study intra- and inter-observer repeatability and reproducibility. Four windowing protocols (level/window) were applied: 1. 1131/1858, 2. 2224/4095, 3. 1131/4095, and 4. AUTO, an automatic protocol provided by default by the software. A total of 576 segmentations were performed. Tooth volumes were automatically calculated using the software. To compare the volumes obtained from CBCT segmentations with a gold-standard method, we laser-scanned the extracted teeth.

Results. Excellent intra- and inter-observer intraclass correlations were found for all of the protocols used. The best windowing protocol was 1131/1858 for both observers. Tooth volumes were obtained by manual segmentation of the CBCT images and using windowing protocol 1131/1858. No significantly different tooth volumes were found by laser scanning.

Conclusions. Our null hypothesis was rejected. Only windowing protocol 1131/1858 allowed for significantly closer 3D in vivo segmentation of a tooth compared to I-CAT CBCT, with excellent intra-observer repeatability and inter-observer reproducibility.

Key words: cone-beam computed tomography, grey levels, segmentation, 3-dimensional

Validation of 3-dimensional (3D) reconstruction of full dental arches with crowns and roots based on cone beam computed tomography (CBCT) imaging represents a key issue for 3D digital dentistry. Accurate 3D tooth reconstruction allows the construction of individual virtual orthodontic set-ups, roots resorption analysis, virtual planning for mini-implants, and mini-screw insertion.[1–4] Accurate 3D tooth reconstruction is important when using 3D printed tooth replicas during autotransplantation procedures, and in custom-made anatomic implantology.[5–8] Moreover, in forensic odontology accurate tooth volume measurements are important for calculating the tooth/pulp volume ratio, which is strongly correlated with age estimation.[9] A few studies have already tried to determine and validate in vivo tooth volumes from available 3D CBCT using manual segmentation, which still represents the gold standard for obtaining volume measurements from medical images.[10,11,13–16] The first was a 2010 article by Liu et al., who described a feasibility study of in vivo tooth volume determination from CBCT imaging. However, that article had various methodological issues. The authors compared the volume of teeth before extraction (on CBCT), and after extraction (with water displacement as the reference method) on 24 premolars (which represented limited complexity of root anatomy) from 9 patients, using 2 different CBCT devices and 4 different radiological protocols.[10] Two independent observers manually segmented the 24 premolars twice with Amira 3D software (FEI Visualization Sciences Group, Hillsboro, USA), applying subjective modifications of the windowing of CBCT images during the segmentation process. The reference method was based on water displacement: A subjective visual assessment of the lower level of meniscus (0.1 mL gradation) was performed when the tooth was placed in a graduated cylinder.[10] Liu et al. concluded that there was a significant difference between the physical volume measurements of the extracted teeth and the CBCT measurements (–4% to +7%; $p < 0.05$). The authors also stated that surface smoothing reduced the volume by 3–12%, and that no specifications could be given at that time regarding how to accurately segment teeth from CBCT.[10] In a 2011 study by Wang et al., 27 premolars from 15 patients were CBCT-scanned before extraction and micro-CT-scanned after extraction as a comparative reference system.[11] A unique threshold (1673 to 2000 HU) was employed using Mimics software (Materialise NV, Leuven, Belgium) for tooth segmentation. Intra-observer repeatability was high for both observers (intraclass correlation coefficient [ICC] = 0.999 and 0.998), while inter-observer reproducibility was less impressive (ICC = 0.740).[11] The ICC is used for quantitative measurements of units organized into groups. It describes how strongly units in the same group resemble each other.[12] The effect of the threshold on segmentation was not the purpose of that study.[11] Forst et al. proposed to test the intra-and inter-observer reproducibility of 3 types of in vivo segmentation on 10 maxillary upper molars from CBCT: 1. manual human segmentation on a repeated 2-dimensional (2D) basis, 2. automated segmentation without human refinement, and 3. automated segmentation with manual human refinement on a repeated 2D basis.[13] The results of automated segmentation with human refinement corresponded to the results of manual segmentation by Liu et al.[10] However, because the teeth were not extracted after CBCT in that study, it was impossible to determine the true tooth volume using any of the existing reference methods (micro-CT scan, laser scanning, water displacement method, etc.).[13] The segmentation method proposed by Forst et al. still needs to be validated. The windowing protocol for manual segmentation was not described or tested in that article.[13] Moreover, some windowing protocols (center level/band width) have been cited in the literature as providing the best tooth visualization in CBCT. Spin-Neto et al. suggested a 1131/1858 protocol for the best tooth visualization.[17] Lee et al. used a 2224/4095 protocol to generate 3D virtual surface models of the maxillary and mandibular dental arches that include whole with the roots.[18] However, the protocols by Spin-Neto et al. and Lee et al. have not been validated. Therefore, we proposed to search for the potentially most accurate in vivo windowing-based tooth segmentation protocol from CBCT. We wanted to compare the 2 protocols found in the literature with 2 proposed by our research team: 1. automatic adjustment of the windowing by the 3D Slicer software AUTO protocol, and 2. a mixed approach based on the protocols found in the literature: 1131/4095.[17,18] The null hypothesis was that all 4 windowing protocols were equivalent for in vivo tooth volume measurement from CBCT.

Material and methods

This retrospective study was conducted between 2010 and 2014, on the basis of preoperative CBCT examinations of patients who underwent further tooth extractions for reasons independent of the present study. Preoperative CBCTs were also performed independently of this study. Written informed consent was obtained from all the participants in the study, which was approved by the Ethics Committee of Cliniques Universitaires Saint-Luc (Brussels, Belgium; no. B40320096961). The radiological protocol was I-CAT (Imaging Sciences International Inc., Hatfield, USA), with 0.3 mm slice thickness, field of view 8 cm in height × 16 cm in diameter, 120 kVp and 18 mAs. The main reasons for performing CBCT were: 1. to evaluate the distance between the roots of the wisdom teeth and the inferior alveolar nerve when a close relationship was seen on previously obtained panoramic X-rays; 2. to evaluate the positioning of supranumerary teeth when 2D X-rays failed to provide a final diagnosis; and 3. to evaluate cystic involvement in the maxillary sinus region associated with maxillary tooth extraction. For the purpose of our study, we used all the extracted teeth that were fully present in the CBCT field of view. For example,

if CBCT was performed to evaluate the distance between the lower wisdom teeth roots and the inferior alveolar nerve, and simultaneously, the upper wisdom teeth were present in the same CBCT field of view, and were extracted at the same time as the lower wisdom teeth, then the upper wisdom teeth were also used in our study. The inclusion criteria were: adult patients, teeth without demineralization (without decay and without immature roots), teeth without metallic fillings or crowns, and teeth that were not sectioned or damaged during oral surgery. The 36 teeth included were extracted from 14 patients, aged between 18–68 years old. Ten females and 4 males participated in this study. Out of the 36 teeth, 23 were wisdom teeth. Each extracted tooth was first cleaned of blood, soft tissue and bone fragments, and brushed under running water. Next, each tooth was separately conserved in a closed storage box, fully immersed in 0.1% chloramine.

To study intra- and inter-observer reproducibility, manual segmentations were performed twice for each of the 36 teeth from CBCT imaging by 2 independent observers, with a 1-month time period between the 2 segmentations. Both observers were dentists, and a calibration session was provided by the senior researcher prior to the start of the study to explain how the software worked, how to save the data, how to use different segmentation tools and how to modify the windowing protocols. Prior to the start of the study, the two observers had trained with manual segmentation on 10 other teeth that were then excluded from the main study. The segmentations were performed using 3D Slicer 3.6.1 open source software (SPL, Harvard Medical School, Boston, USA).[19] Each segmentation consisted of a contour of the tooth image (enamel, dentin, crown and roots), slice-by-slice, by looking at the slices on the computer screen, using a mouse, and using the Editor module of the 3D Slicer software tools, with such functions as: 1. "paint", 2. "level tracing" and 3. "draw". The segmentations were mainly performed on axial slices, and some adjustments were then performed on sagittal and coronal views (Fig. 1). Four different windowing protocols (level/window) were applied: 1. 1131/1858,[16] 2. 2224/4095,[18] 3. a mixed protocol based on protocols 1 and 2: 1131/4095, and 4. AUTO, an automatic protocol provided by default by the software (Fig. 2). In total, 576 segmentations were performed. Three-dimensional reconstruction of each tooth was automatically performed using 3D Slicer software, and the tooth volume was automatically calculated by the software. No smoothing function was used, as smoothing may modify the entire volume of the tooth.[10] The volume was also automatically measured in mm^3 using the Statistics module of the 3D Slicer software. To compare the volumes obtained from CBCT segmentations with a gold-standard method, we used the laser scanning method (Ceramill Map300, Amann Girrbach AG, Koblach, Austria), which is based on structural light. The 36 teeth were laser-scanned according to the manufacturer's instructions, within an error of 20 μm (Tables 1–4). Prior to the start of the measurements with the laser scanner, the device was calibrated using a 3D model provided by the manufacturer. A plaster custom-made support was created for each tooth. The tooth was attached to the support using dental wax. All the surfaces of the tooth were covered with a very thin layer of talc used in the spray for laser scanning purposes (Lava™, 3M ESPE AG, Seefeld, Germany). The volume was automatically measured by the software included with the laser scanner, and was rechecked with Netfabb basic software (Netfabb GmbH, Parsburg, Germany). Laser scanning one tooth took approx. 40–80 min.

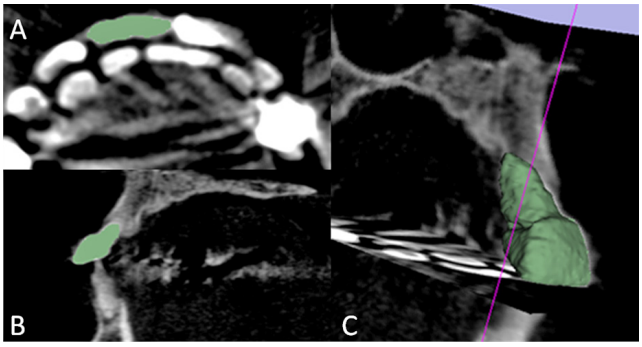

Fig. 1. Manual segmentation of tooth number 11 with 3D Slicer software

A – segmentation on axial slice; B – segmentation on sagittal slice; C – three-dimensional reconstruction and automatic volume measurement.

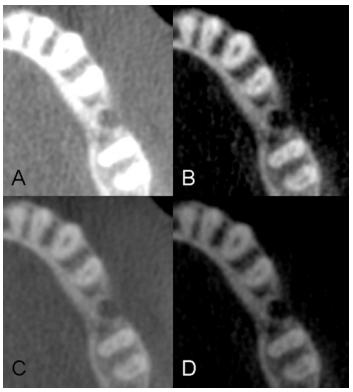

Fig. 2. Four windowing protocols applied to the same single axial slice from I-CAT cone beam computed tomography

A – AUTO; B – 1131/1858; C – 1131/4095; D – 2224/4095.

Statistical analysis

To compare the 1st and 2nd measurements for each windowing protocol, we used multiple paired Student's t-tests with the Bonferroni correction; the level of significance was set at $p < 0.00625$ for intra-observer correlations ($p < 0.05/8$, because there were 8 tests) and $p < 0.0125$ for inter-observer correlations ($p < 0.05/4$, because there were 4 tests). To determine the reproducibility of measurements, we used the intraclass correlation coefficient ICC2.1 (single measurement, absolute agreement, 2-way random effect analysis of variance model). To compare manually segmented volumes from CBCT and the true volume obtained by laser scanner, we again used multiple paired Student's t-tests with the Bonferroni correction; the level of significance was again set at $p < 0.00625$. The correlation

Table 1. Comparisons between the true volumes of teeth measured by laser scanner and the volumes obtained by 2 observers using the AUTO windowing protocol twice. The measurements are in mm^3

Tooth	Type of tooth	True volume	AUTO			
			Obs 1 1st	Obs 1 2nd	Obs 2 1st	Obs 2 2nd
1	18	830	876.71	888.20	964.83	767.43
2	18	490	520.83	539.17	524.61	513.65
3	28	770	806.37	798.06	858.10	850.21
4	18	630	639.32	645.30	659.11	638.40
5	28	580	591.07	621.53	638.05	649.50
6	18	590	612.21	618.81	643.48	647.39
7	28	710	767.08	751.30	803.21	807.74
8	28	910	908.09	915.27	910.61	920.92
9	18	820	744.22	914.88	839.74	846.57
10	18	560	579.78	599.07	610.78	612.10
11	46	860	872.49	875.36	986.75	1024.74
12	28	850	960.04	932.26	973.20	980.92
13	18	1150	1207.30	1187.00	1214.36	1194.70
14	18	510	549.26	532.61	548.65	536.72
15	12	320	346.91	372.51	395.03	412.20
16	13	590	600.49	714.89	642.42	719.89
17	14	420	444.81	501.92	453.21	497.62
18	34	350	380.96	401.26	411.98	413.44
19	44	350	372.94	396.94	395.59	374.23
20	45	300	297.59	293.46	303.31	320.64
21	18	590	662.71	623.04	695.10	685.76
22	28	680	762.59	756.48	803.96	765.38
23	11	490	655.84	606.86	659.07	654.99
24	12	350	458.88	374.92	452.74	430.08
25	13	460	596.74	528.92	656.59	626.83
26	21	530	625.24	580.27	629.51	623.97
27	22	270	306.21	297.36	310.53	293.84
28	23	630	750.39	703.54	747.25	744.55
29	28	790	835.56	762.92	838.76	797.07
30	38	900	1045.50	839.63	997.55	975.00
31	38	930	1014.50	1050.50	1032.22	1013.61
32	28	750	826.42	847.08	895.81	872.49
33	28	710	799.70	812.23	830.33	842.54
34	38	830	878.43	903.59	901.48	890.90
35	48	720	779.17	784.13	790.02	805.71
36	18	560	579.01	584.98	583.19	570.20

Table 2. Comparisons between the true volumes of teeth measured by laser scanner and the volumes obtained by 2 observers using the 1131/1858 windowing protocol twice. The measurements are in mm^3

Tooth	Type of tooth	True volume	1131/1858			
			Obs 1 1st	Obs 1 2nd	Obs 2 1st	Obs 2 2nd
1	18	830	812.84	821.35	781.71	861.07
2	18	490	495.80	492.39	440.75	474.01
3	28	770	703.14	756.56	726.61	863.06
4	18	630	639.32	645.30	659.11	638.40
5	28	580	565.07	596.51	459.57	577.92
6	18	590	574.13	567.44	526.16	591.53
7	28	710	668.17	698.85	654.44	742.38
8	28	910	912.44	868.10	828.26	926.59
9	18	820	788.81	808.79	774.18	837.33
10	18	560	519.74	524.69	558.18	550.14
11	46	860	729.98	773.71	740.40	812.46
12	28	850	875.04	886.71	865.41	848.32
13	18	1150	1103.30	1132.06	1130.68	1162.84
14	18	510	514.96	521.46	487.55	539.37
15	12	320	325.27	323.59	350.67	288.00
16	13	590	579.35	558.31	561.12	487.28
17	14	420	419.70	405.73	389.47	331.41
18	34	350	356.47	356.85	379.64	304.25
19	44	350	358.53	342.88	359.34	294.78
20	45	300	279.74	267.46	296.36	203.36
21	18	590	590.67	587.95	582.84	603.57
22	28	680	702.10	673.09	668.94	669.21
23	11	490	560.34	546.17	485.59	559.95
24	12	350	381.72	345.23	313.66	378.75
25	13	460	440.54	476.65	447.71	529.20
26	21	530	532.49	556.71	503.87	574.48
27	22	270	263.44	267.86	236.06	289.49
28	23	630	671.54	642.07	568.92	689.99
29	28	790	670.78	663.75	748.17	675.41
30	38	900	933.11	781.05	764.45	787.67
31	38	930	977.14	1048.90	948.00	963.12
32	28	750	774.10	741.15	684.84	756.60
33	28	710	622.50	647.84	609.42	784.92
34	38	830	774.91	783.32	753.76	819.21
35	48	720	681.24	704.02	644.25	763.08
36	18	560	545.97	502.08	519.41	593.07

was calculated between the volume obtained by manual segmentation according to the type of windowing protocol and the true volume measured by the laser scan. A correlation was described as strong if the ICC was greater than 0.8. All the tests were performed using SPSS® for Windows, v. 16.0 (SPSS Inc., Chicago, USA).

Results

Table 5 shows the intra-observer correlations for the 2 observers in relation to the 4 different windowing protocols. There were no significant differences between the 1st and 2nd measurements. There was a good intraclass correlation for all of the protocols used. The means of the 1st and 2nd measurements were then used for further tests.

Table 3. Comparisons between the true volumes of teeth measured by laser scanner and the volumes obtained by 2 observers using the 2224/4095 windowing protocol twice. The measurements are in mm^3

Tooth	Type of tooth	True volume	2224/4095			
			Obs 1 1st	Obs 1 2nd	Obs 2 1st	Obs 2 2nd
1	18	830	781.02	815.64	767.43	821.67
2	18	490	477.70	460.26	396.60	430.57
3	28	770	701.50	716.47	703.66	752.53
4	18	630	596.34	580.47	579.27	595.71
5	28	580	559.58	529.92	545.74	565.42
6	18	590	556.45	543.12	523.17	544.47
7	28	710	662.02	661.58	681.73	679.55
8	28	910	846.81	787.04	788.13	828.42
9	18	820	778.60	776.70	766.54	745.18
10	18	560	507.03	519.70	521.79	519.17
11	46	860	786.28	776.82	768.61	720.64
12	28	850	876.79	835.67	859.63	794.40
13	18	1150	1087.80	1096.10	1125.50	1071.26
14	18	510	478.58	494.05	479.80	467.87
15	12	320	314.44	302.51	285.49	258.89
16	13	590	582.47	545.13	501.67	464.14
17	14	420	406.77	388.00	354.66	336.11
18	34	350	313.70	329.41	315.64	253.12
19	44	350	336.86	331.32	335.49	263.86
20	45	300	260.19	254.73	239.49	190.75
21	18	590	580.50	570.66	565.77	564.80
22	28	680	648.11	652.61	652.68	632.51
23	11	490	582.23	493.28	470.77	502.55
24	12	350	354.87	322.98	309.80	331.83
25	13	460	436.18	488.34	461.86	464.29
26	21	530	500.24	527.38	499.61	526.88
27	22	270	236.80	262.04	231.31	262.33
28	23	630	595.12	593.16	544.73	600.99
29	28	790	690.23	700.29	676.49	675.87
30	38	900	851.05	730.93	793.53	754.25
31	38	930	991.08	974.34	917.73	838.27
32	28	750	750.85	747.15	672.99	742.86
33	28	710	612.83	633.57	605.29	661.20
34	38	830	745.58	748.93	736.21	751.47
35	48	720	652.53	674.17	654.16	674.65
36	18	560	513.32	461.85	501.89	531.43

Table 4. Comparisons between the true volumes of teeth measured by laser scanner and the volumes obtained by 2 observers using the 1131/4095 windowing protocol twice. The measurements are in mm^3

Tooth	Type of tooth	True volume	1131/4095			
			Obs 1 1st	Obs 1 2nd	Obs 2 1st	Obs 2 2nd
1	18	830	769.40	824.60	753.72	868.49
2	18	490	485.01	473.10	441.56	435.35
3	28	770	709.14	751.61	705.44	835.79
4	18	630	592.90	596.51	570.28	581.40
5	28	580	563.01	545.85	538.99	559.99
6	18	590	551.58	553.29	518.93	600.36
7	28	710	683.46	686.94	642.86	762.87
8	28	910	877.42	820.92	816.70	889.79
9	18	820	770.56	788.76	742.89	815.90
10	18	560	484.13	516.45	528.86	529.86
11	46	860	748.23	743.90	665.04	823.15
12	28	850	867.41	846.44	865.12	855.07
13	18	1150	1124.70	1116.50	1102.98	1122.48
14	18	510	497.86	512.51	463.71	553.51
15	12	320	315.35	332.07	345.39	253.85
16	13	590	535.99	530.88	536.24	444.62
17	14	420	404.35	387.22	374.14	332.12
18	34	350	336.04	377.02	341.26	275.77
19	44	350	337.06	232.99	356.47	256.38
20	45	300	253.50	267.99	269.34	183.59
21	18	590	585.79	566.60	565.69	564.61
22	28	680	671.81	658.48	642.02	703.36
23	11	490	571.48	519.61	467.67	537.27
24	12	350	375.25	327.25	291.17	348.11
25	13	460	431.31	472.40	439.37	499.80
26	21	530	541.04	541.26	467.75	546.89
27	22	270	249.97	256.29	246.75	295.24
28	23	630	642.55	615.97	624.48	642.79
29	28	790	644.69	690.69	667.52	612.60
30	38	900	894.85	761.80	778.49	771.69
31	38	930	964.89	997.30	951.00	953.70
32	28	750	786.99	747.79	677.68	738.14
33	28	710	587.19	672.03	589.65	745.66
34	38	830	761.49	762.65	719.17	786.27
35	48	720	670.95	689.62	649.22	693.04
36	18	560	533.38	517.29	497.46	571.17

Table 6 shows the inter-observer correlations for the 2 observers in relation to the 4 different windowing protocols. The inter-observer correlation was excellent for all 4 windowing protocols. There was a significant difference between the 2 observers for the AUTO and 2224/4095 protocols. However, this error is small compared to the measured volume (excellent ICC).

Table 7 shows the measurements of the correlation coefficient between the measurement of volume obtained from the different windowing protocols and the true volume. The best windowing protocol was 1131/1858 for both observers. Tooth volumes obtained with manual segmentation of CBCT images and using the 1131/1858 windowing protocol were not significantly different from tooth volumes obtained by laser scan.

Table 5. Intra-observer correlations for the 2 observers, in relation to the 4 different types of windowing protocols

Observer	Windowing protocol (level/width)	ICC	p-value (paired Student's t-test between first and second measurements)
Observer 1	AUTO	0.964	0.56
	1131/1858	0.983	0.53
	2224/4095	0.985	0.15
	1131/4095	0.979	0.37
Observer 2	AUTO	0.983	0.23
	1131/1858	0.934	0.0073
	2224/4095	0.981	0.82
	1131/4095	0.936	0.015

ICC – two-way random, absolute agreement; p-value is significant if $p < 0.05/8$ (because there were 8 tests) = $p < 0.00625$.

Table 6. Inter-observer correlations for the 2 observers, in relation to the 4 different types of windowing protocols

Windowing protocol	ICC	p-value (paired Student's t-test between measurements by observers 1 and 2)
AUTO	0.986	<0.0001*
1131/1858	0.986	0.24
2224/4095	0.986	0.0004*
1131/4095	0.991	0.04

* p-value is significant if $p < 0.05/4$ (because there were 4 tests) = $p < 0.0125$.

Table 7. Measurements of correlation coefficients between the measurements of volume obtained using different windowing protocols and the true volume from the laser scanner

Observer	Windowing protocol	Mean difference	p-value	Correlation of coefficient r
Observer 1	AUTO	–50.7	<0.0001	0.988
	1131/1858	13.3	0.048	0.983
	2224/4095	35.85	<0.0001	0.986
	1131/4095	28.29	<0.0001	0.983
Observer 2	AUTO	–74.491	<0.001	0.979
	1131/1858	19.95	0.0012	0.987
	2224/4095	54.23	<0.0001	0.989
	1131/4095	37.694	<0.0001	0.982

Discussion

Pauwels et al. stated in 2015 that the quantitative use of grey values should be avoided in CBCT imaging, as grey values are unreliable.[20] Grey values measured on CBCT are dependent on the type of CBCT device, the exposure parameters, the position of the measurement inside the field of view, and the amount of mass inside and outside the field of view.[20] The lack of consistent grey values means that a threshold value for bone and other tissues cannot be established for CBCT images.[20] However, a modified grey-value approach has also been investigated, with positive results in vitro and in vivo in terms of bone quality measurements and implant planning.[21–24] In this study we did not measure grey values in CBCT; we only tested different windowing protocols for CBCT images to find the best contrast between teeth and the surrounding structures. We found that a protocol proposed (but not validated) by Spin-Neto for I-CAT (1131/1858) was significantly the best for obtaining accurate tooth volumes from in vivo I-CAT CBCT images (Fig. 2).[17] Moreover, during manual segmentation, we encountered various parameters that may directly affect the qualitative and quantitative aspects of manual segmentation. These parameters may explain why the measurements were different between the 2 observers, and why the measurements were different when using different windowing protocols. These parameters could be categorized as: 1. parameters specific to the volume to be segmented, 2. parameters specific to the observer, and 3. parameters associated with the segmentation software. Parameters that were specific to the volume to be segmented were 1. the anatomy of the tooth and of adjacent periodontal structures, 2. the position of the tooth in the surrounding bone, 3. the level of mineralization of the tooth, 4. the presence of metallic artifacts, and 5. contact between adjacent teeth. The anatomy and density of a tooth is heterogeneous from the crown to the apex. A tooth crown is easier to segment due to its mineralized enamel and because the enamel presents a clear contrast with the adjacent air. The root and especially the apex are areas that are more complex to delineate by segmentation, due to the less clear difference between root tissue and the surrounding alveolar bone. Moreover, a disease-free periodontal ligament (lamina dura) cannot be distinguished on CBCT images with the field of view we used in our study, and may be mistaken for the tooth, in which case the final volume would be overestimated (Fig. 3). When we consider the position of the tooth in relation to the surrounding bone, segmentation between the tooth and bone becomes more difficult when the roots are closer to the cortical bone. This occurs more often on the mandible, where the teeth are positioned between the thin internal and external cortical bone, compared to the maxilla (Fig. 4).

Problems inherent to the mineralization of the tooth, such as the presence of decay and immature roots, may also complicate segmentation. For this reason, one of the initial exclusion criteria was the presence of major decay

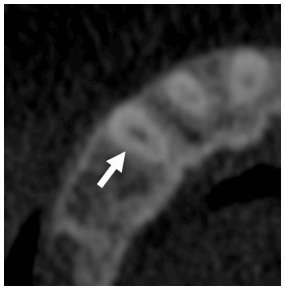

Fig. 3. The impossibility of discerning between the periodontal ligament and tooth (arrow). Windowing protocol 2224/4095

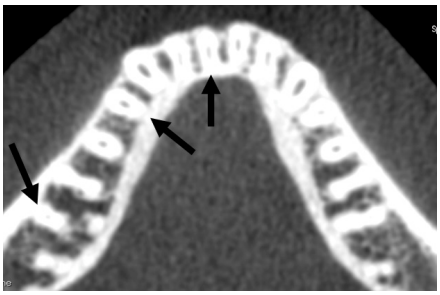

Fig. 4. AUTO windowing protocol. Fusion of the image of the tooth with the adjacent cortical bone (arrows)

Fig. 5. Manual segmentation (green) of tooth number 18. Level tracing tool errors in selecting surrounding bony structures independent of the tooth (arrows)

that was clinically diagnosed prior the tooth removal. Immature roots present with low density in the apex region, and the limits of the apex in relation to the surrounding bone become difficult to determine.[25] Metallic crowns and dental fillings create major artifacts in 3D tooth reconstruction and prevent accurate segmentation of crowns (Fig. 1). For this reason, we also excluded all teeth with crowns and metallic fillings from our study. Inter-dental contact makes segmentation and the interpretation of the external limits of dental crowns difficult. The teeth appear to be merged together on 2D slices.

Parameters specific to the observer that may affect the results of segmentation include: 1. the observer's experience using segmentation software; 2. his/her knowledge of dental anatomy, which is important when the observer needs to contour the apex region with complex root anatomy; and 3. any tiredness on the observer's part during the manual segmentation process, which may decrease the accuracy of segmentation, particularly with complex root anatomy, and when the time spent on one segmentation is excessively long.

Parameters specific to the software used (3D Slicer) are 1. the tools used for manual segmentation, and 2. the contrast/windowing control. We mainly used the "paint", "draw" and "level tracing" tools in the 3D Slicer software. The "level tracing" tool is well suited for tooth segmentation with clear limits, but if the limits are not precise or if there is a structure with a density close to that of the tooth, the "level tracing" tool is not the best option (Fig. 5).

Other parameters that may modify the results of manual segmentation are related to the CBCT radiological protocol, such as mAs, kVp, slice thickness, field of view and voxel size, and also due to movement artifacts in the CBCT device.[26,27]

The limitations of this study are related to the CBCT radiological protocol. We tested the windowing protocols in only one type of radiological protocol, without modification of the type of CBCT device, mAs, kVp, slice thickness, field of view or voxel size. We also did not compare windowing protocol results between different types of CBCT devices. Therefore, our findings are strictly limited to the use of 3D Slicer software and to I-CAT CBCT, with a 0.3 mm slice thickness, 8 cm × 16 cm field of view, 120 kVp and 18 mAs. Also, we used only manual segmentation, as this technique still represents a gold standard. However, other in vitro teeth segmentation methods that have already been tested, provide much faster segmentation and are useful in clinical practice.[28–30]

In conclusion, the null hypothesis was rejected. Compared with the other windowing protocols we investigated, the 1131/1858 windowing protocol allows for significantly closer 3D in vivo segmentation of a tooth from I-CAT CBCT, with excellent intra-observer repeatability and inter-observer reproducibility.

References

1. Yezdani AA. Transparent aligners: An invisible approach to correct mild skeletal class III malocclusion. *J Pharm Bioallied Sci*. 2015;7: S301–S306.
2. Li W, Chen F, Zhang F, et al. Volumetric measurement of root resorption following molar mini-screw implant intrusion using cone beam computed tomography. *PLoS One*. 2013;8:e60962. doi:10.1371/journal.pone.0060962
3. Kalra S, Tripathi T, Rai P, Kanase A. Evaluation of orthodontic mini-implant placement: A CBCT study. *Prog Orthod*. 2014;15:61. doi:10.1186/s40510-014-0061-x
4. Morea C, Hayek JE, Oleskovicz C, Dominguez GC, Chilvarquer I. Precise insertion of orthodontic miniscrews with a stereolithographic surgical guide based on cone beam computed tomography data: A pilot study. *Int J Oral Maxillofac Implants*. 2011;26:860–865.
5. Shahbazian M, Jacobs R, Wyatt J, et al. Validation of the cone beam computed tomography-based stereolithographic surgical guide aiding autotransplantation of teeth: Clinical case-control study. *Oral Surg Oral Med Oral Pathol Oral Radiol*. 2013;115:667–675.
6. Khalil W, EzEldeen M, Van De Casteele E, et al. Validation of cone beam computed tomography-based tooth printing using different three-dimensional printing technologies. *Oral Surg Oral Med Oral Pathol Oral Radiol*. 2016;121:307–315.
7. Anssari Moin D, Hassan B, Wismeijer D. A novel approach for custom three-dimensional printing of a zirconia root analogue implant by digital light processing. *Clin Oral Implants Res*. 2016;25. doi:10.1111/clr.12859
8. Pirker W, Kocher A. Root analog zirconia implants: True anatomical design for molar replacement – a case report. *Int J Periodontics Restorative Dent*. 2011;31:663–668.
9. Vandevoort FM, Bergmans L, Van Cleynenbreugel J, et al. Age calculation using X-ray microfocus computed tomographical scanning of teeth: A pilot study. *J Forensic Sci*. 2004;49:787–790.
10. Liu Y, Olszewski R, Alexandroni ES, Enciso R, Xu T, Mah JK. The validity of in vivo tooth volume determinations from cone-beam computed tomography. *Angle Orthod*. 2010;80:160–166.
11. Wang Y, He S, Yu L, Li J, Chen S. Accuracy of volumetric measurement of teeth in vivo based on cone beam computer tomography. *Orthod Craniofac Res*. 2011;14:206–212.

12. Koch GG. Intraclass correlation coefficient. In: Kotz S, and Johnson NL, ed. *Encyclopedia of Statistical Sciences*. 4th ed. New York , NY: John Wiley & Sons; 1982:213–217.
13. Forst D, Nijjar S, Flores-Mir C, Carey J, Secanell M, Lagravere M. Comparison of in vivo 3D cone-beam computed tomography tooth volume measurement protocols. *Prog Orthod*. 2014;15:69. doi:10.1186/s40510-014-0069-2
14. Aizawa M, Nishikawa K, Sasaki K, et al. Automatic segmentation of teeth from dentomaxillofacial 3D-CT images. *Nihon Hoshasen Gijutsu Gakkai Zasshi*. 2010;66:343–352.
15. Le BH, Deng Z, Xia J, Chang YB, Zhou X. An interactive geometric technique for upper and lower teeth segmentation. *Med Image Comput Assist Interv*. 2009;12:968–975.
16. Zhao M, Ma L, Tan W, Nie D. Interactive tooth segmentation of dental models. Conf Proc IEEE *Eng Med Biol Soc*. 2005;1:654–657.
17. Spin-Neto R, Marcantonio E Jr, Gotfredsen E, Wenzel A. Exploring CBCT-based DICOM files. A systematic review on the properties of images used to evaluate maxillofacial bone grafts. *J Digit Imaging*. 2011;24:959–966.
18. Lee RJ, Pham J, Choy M, el al. Monitoring of typodont root movement via crown superimposition of single cone-beam computed tomography and consecutive intraoral scans. *Am J Orthod Dentofacial Orthop*. 2014;145:399–409.
19. Fedorov A, Beichel R, Kalpathy-Cramer J, et al. 3D Slicer as an Image Computing Platform for the Quantitative Imaging Network. *Magn Reson Imaging*. 2012;30:1323–1341.
20. Pauwels R, Jacobs R, Singer SR, Mupparapu M. CBCT-based bone quality assessment: Are Hounsfield units applicable? *Dentomaxillofac Radiol*. 2015;44:20140238. doi:10.1259/dmfr.20140238
21. Bujtár P, Simonovics J, Zombori G, et al. Internal or in-scan validation: A method to assess CBCT and MSCT gray scales using a human cadaver. *Oral Surg Oral Med Oral Pathol Oral Radiol*. 2014;117:768–779.
22. Andruch K, Płachta A. Evaluating maxilla bone quality through clinical investigation of voxel grey scale values from cone-beam computed tomography for dental use. *Adv Clin Exp Med*. 2015;24:1071–1077.
23. Valiyaparambil JV, Yamany I, Ortiz D, et al. Bone quality evaluation: Comparison of cone beam computed tomography and subjective surgical assessment. *Int J Oral Maxillofac Implants*. 2012;27:1271–1277.
24. Parsa A, Ibrahim N, Hassan B, Motroni A, van der Stelt P, Wismeijer D. Reliability of voxel gray values in cone beam computed tomography for preoperative implant planning assessment. *Int J Oral Maxillofac Implants*. 2012;27:1438–1442
25. Maret D, Molinier F, Braga J, et al. Accuracy of 3D reconstructions based on cone beam computed tomography. *J Dent Res*. 2010;89:1465–1469.
26. Al-Rawi B, Hassan B, Vandenberge B, Jacobs R. Accuracy assessment of three-dimensional surface reconstructions of teeth from cone beam computed tomography scans. *J Oral Rehabil*. 2010;37:352–358.
27. Ye N, Jian F, Xue J, et al. Accuracy of in-vitro tooth volumetric measurements from cone-beam computed tomography. *Am J Orthod Dentofacial Orthop*. 2012;142:879–887.
28. Na SD, Lee G, Lee JH, Kim MN. Individual tooth region segmentation using modified watershed algorithm with morphological characteristic. *Biomed Mater Eng*. 2014;24:3303–3309.
29. Ji DX, Ong SH, Foong KW. A level-set based approach for anterior teeth segmentation in cone beam computed tomography images. *Comput Biol Med*. 2014;50:116–128.
30. Gan Y, Xia Z, Xiong J, Zhao Q, Hu Y, Zhang J. Toward accurate tooth segmentation from computed tomography images using a hybrid level set model. *Med Phys*. 2015;42:14–27.

Evidence-based strategies for the minimally invasive treatment of carious lesions: Review of the literature

Rodrigo A. Giacaman[1,A,C,D,F], Cecilia Muñoz-Sandoval[1,B,D,F], Klaus W. Neuhaus[2,E,F], Margherita Fontana[3,E,F], Renata Chałas[4,C,E,F]

[1] Cariology Unit, Department of Oral Rehabilitation and Interdisciplinary Excellence Research Program on Healthy Aging (PIEI-ES), University of Talca, Chile
[2] Department of Preventive, Restorative and Pediatric Dentistry, School of Dental Medicine, University of Bern, Switzerland
[3] Department of Cariology, Restorative Sciences and Endodontics, School of Dentistry, University of Michigan, Ann Arbor, USA
[4] Department of Conservative Dentistry and Endodontics, Medical University of Lublin, Poland

A – research concept and design; B – collection and/or assembly of data; C – data analysis and interpretation;
D – writing the article; E – critical revision of the article; F – final approval of the article

Advances in Clinical and Experimental Medicine, ISSN 1899-5276 (print), ISSN 2451-2680 (online) *Adv Clin Exp Med*. 2018;27(7):1009–1016

Address for correspondence
Renata Chałas
E-mail: renata.chalas@umlub.pl

Funding sources
These investigations have been funded by the Chilean Government Grant Fondecyt No.: 1140623 to Rodrigo A. Giacaman. This manuscript was submitted in partial fullfillment of the requirements for the Graduate Program in Pediatric Dentistry by Cecilia Muñoz-Sandoval at the University of Talca, Chile.

Conflict of interest
None declared

Received on April 11, 2017
Reviewed on June 18, 2017
Accepted on September 15, 2017

Abstract

Resulting in a high economic and biological cost, the traditional therapeutic approach to carious lesion management is still largely restorative. Minimally invasive (MI) treatment offers an attractive alternative to managing carious lesions in a more conservative and effective manner, resulting in enhanced preservation of tooth structure. The aim of this review was to summarize the evidence behind several MI alternatives for carious lesion management, including the use of sealants, infiltration, atraumatic restorative treatment (ART), and selective carious tissue removal (e.g., indirect pulp capping, stepwise removal, or selective removal to soft dentine). Relevant literature was screened, and articles reporting randomized controlled trials or systematic reviews of strategies to manage non-cavitated or cavitated carious lesions in adults and children were included. Fifty six articles met the inclusion criteria. For non-cavitated lesions, the use of sealants is supported by strong evidence, while the evidence for infiltration of proximal lesions is moderate. For deep cavitated lesions, selective removal to soft dentin and/or stepwise excavation is supported by strong evidence. The use of the ART technique to restore cavitated lesions is also supported by strong evidence as a suitable strategy that has been used extensively in the literature concerning non-dental settings. Preservation of tooth structure through the use of MI treatment for both non-cavitated and cavitated lesions is supported by moderate-strong evidence, which supports the paradigm shift towards routine use of more conservative strategies in the treatment of carious lesions.

Key words: dental caries, minimally invasive treatment, partial caries removal, stepwise technique, atraumatic restorative treatment

DOI
10.17219/acem/77022

Introduction

Dental caries is a sugar and biofilm dependent disease, where frequent sugars exposure leads to an ecologic imbalance in the environment of the dental biofilm. The ecological shift turns the otherwise commensal bacteria to a cariogenic condition with increased production of demineralizing acids and the subsequent carious lesion formation on the dental hard tissues. Minimally invasive (MI) treatment of dental caries is an approach that considers handling carious lesions with conservative techniques to preserve maximum tooth structure.[1] The MI treatment is also a conceptual framework that ranges from primary prevention and management of the caries disease process, to the management of carious lesions by surgical and non-surgical means. Besides considering the type of lesion, the selection of a treatment technique based on the MI philosophy must be the result of a personalized risk analysis of each patient.[2] Personalized medicine is being increasingly used in medicine and is expected to be included within the dental field, as well. In fact, caries risk-based care is an essential component of targeted health care delivery and is of paramount importance within the context of high healthcare costs and resource constraints.[3]

Successful caries management for an individual patient must include strategies to manage the caries disease process at the patient level, as well as strategies to manage the existing lesions at the tooth level.[4,5] Yet, there is a tendency in many places, either private practice or public oral care services, to prioritize caries treatment primarily by means of traditional operative dentistry. In many countries, financial and/or reimbursement models for caries management, either in the private or public domain, are built primarily around traditional "restorative" procedures for the management of cavitated caries lesions. Reimbursement for more conservative strategies, either at the patient or tooth level, is much more difficult and varied, which hinders implementation. New studies show that when appropriately trained in MI techniques, dentists and patients have a favorable opinion, and in many instances they prefer more conservative therapies for caries management.[6]

Many strategies for the MI management of caries lesions have been developed and evaluated in the literature throughout the last 50 years. For example, in the early 1970s silver diamine fluoride was developed in Japan as a conservative alternative for the management of cavitated lesions without the need of tissue removal or subsequent restoration.[7] This topic is not reviewed here, as this is a non-invasive approach, but the reader is referred to an updated review.[8] The development of dental sealants opened the door to prevention and conservative management of non-cavitated lesions.[9] Over time, other techniques have been developed having the same MI-based philosophy. For example, the idea of a "Preventive Resin Restoration" was first reported in 1977 as a way to call attention to a shift in philosophy, away from the traditional GV Black's "extension for prevention", to a more conservative approach, made possible with the use of resin-composite materials for the management of cavitated carious lesions.[4,5] Atraumatic restorative treatment (ART) was developed as an alternative treatment for the management of cavitated lesions, in which demineralized tissue is removed with hand instruments only, and thus pain is kept to a minimum. Originally, ART was developed for use in rural developing countries, because it does not require local anesthesia or electricity, but more recently, ART has become increasingly accepted in developed countries because of its "atraumatic" approach in relation to stress and pain, and because it conserves tooth structure.[10] More recently, infiltration was developed as an alternative to the management of interproximal non-cavitated carious lesions.[11] Furthermore, regarding caries removal prior to restorative procedures, current recommendations focus on preserving the tooth structure, and guidelines have evolved to currently include, for example, that in deep cavitated carious lesions, selective removal to soft dentine and/or stepwise removal should be performed to maintain the health of the pulp.[5]

The aim of this review is to examine the scientific evidence behind some of the most commonly MI alternatives for caries lesion management used today, including sealants, infiltration, ART and selective and/or stepwise removal for the management of deep carious lesions.

Methods

Relevant literature was retrieved by searching several databases, including MEDLINE (EBSCO), ProQuest, Cochrane Library (Wiley), and PubMed. The following search terms were used either alone or in combination: "minimally invasive treatment", "caries management", "partial caries removal", "stepwise technique", "incomplete caries removal", "atraumatic restorative treatment", "indirect pulp treatment", "resin infiltration", "proximal sealing" and "caries arrest". Only studies published between 1966 and 2016 in English language were considered.

To be included, studies must be conducted in human subjects, including randomized controlled trials (RCT), systematic reviews, and meta-analyses. References used in the cited systematic reviews were included by means of a manual search. Studies that considered surrogate outcomes, such as bacterial counts or marginal staining, were not included, leaving only those that reported carious lesion progression, restoration survival, pulp exposure, or symptoms derived from caries activity. A total of 297 articles dealing with the subject were found, but only 56 articles fulfilled the inclusion criteria and were finally included in this revision of the literature. All the articles were searched by one of the authors (CMS) and then revised by a second researcher to confirm the pertinence of the selection criteria (RAG). When there were discrepancies in article selection, discussions were undertaken until an agreement was reached.

Results and discussion

Despite a reported decrease in prevalence, dental caries remains a major public health problem worldwide, as it remains the leading cause of tooth loss and the most common human condition, affecting 35% of the world population at all ages.[12] Unfortunately, the disease is not being treated in most developing countries due to the high economic and social costs associated with its treatment by conventional restorative-focused methods.[13] New cost-effective strategies to treat the disease and its resulting caries lesions are, therefore, required. In this context, MI treatment allows increased access with reduced cost and complexity. By using targeted disease prevention and management, based on the best available evidence, and using simpler techniques in the management of carious lesions, a better distribution of resources may be implemented directing them to the population groups with the highest caries needs.

Carious lesion diagnosis and minimally invasive therapies

Before discussing the use of MI strategies for caries management, a brief mention about lesion detection and monitoring is needed. Despite the undeniable usefulness of WHO criteria in portraying the epidemiological burden of the disease worldwide for many years, more inclusive methods for caries detection and diagnosis have been established during the last few decades.[14] The WHO criteria count caries only when there is a cavitation in dentine, but they disregard less extensive lesions. Thus, treatment decisions based primarily on WHO criteria are mostly restorative. Hence, the need for improved diagnostic accuracy has resulted in the development of further refined caries detection systems. Currently, perhaps the most internationally recognized and used visual caries detection system, including clinical research, is the International Caries Detection and Assessment System (ICDAS).[15] The main aim of the ICDAS methodology is to detect and classify the small variations in visual signs that occur at the tooth level throughout the progression of caries disease. Besides the extent of the disease, the activity status of the lesions must also be taken into account, as different clinical behavior is expected for 2 lesions of the same ICDAS code, but different activity status. Nyvad's activity criteria are a reasonable way to assess lesion activity, which permits the implementation of MI therapies.[16]

Non-invasive management of non-cavitated lesions

The treatment of choice for non-cavitated lesions should be based on the diagnosis of the lesions, both its extension and the status of active or inactive, the caries risk at the patient level, and the best evidence available to support the treatment decision. In the case of active non-cavitated lesions (ICDAS codes 1 and 2), it is essential to ensure that any selected treatment arrests progression, thus preventing cavitation. Since these lesions maintain tooth surface integrity, at least at the clinical level, it is possible to induce remineralization to revert the process.[2] Although this review focuses on sealants and infiltration, this approach must be taken in the context of proper exposure to fluoride and dietary counselling. The effect of non-invasive treatment relies on an ecological change in the oral environment that will favor remineralization.[17] With vast evidence available, fluoride is the most effective caries preventive measure.[18] Topical fluorides in the form of toothpastes, mouthwashes, gels, and varnishes are effective interventions in preventing dental caries in children and adolescents.[19] Although most of the available evidence derives from fluoride-based products, other substances have also been proposed as remineralizing agents, such as casein phosphopeptide-amorphous calcium phosphate (CPP-ACP), but clinical evidence is still limited and prevents us from drawing definitive conclusions.[20]

Sealing and infiltration; minimally invasive treatment of non-cavitated carious lesions

Along with the strong evidence on the use of sealants to prevent dental caries in children at different risk levels, this simple dental procedure is also effective in halting lesion progression.[10,21] Sealant-treated teeth show a mean annual progression of non-cavitated lesions of 2.6% compared to 12.6% for unsealed lesions.[22] Robust evidence indicates that caries lesions do not progress under well retained sealants.[23] In a further step, a recent study in a high-caries population in the US showed that even caries lesions without frank cavitation (ICDAS codes 1–4) showed very small progression rate at a follow-up of 44 months.[24] Sealants impair nutrient acquisition from the oral environment by invading bacteria, which results in a reduction in the number and viability of microorganisms under the material over time, thus arresting the lesion.[25] In the case of non-cavitated proximal lesions, the use of resin sealants has shown to be more effective in reducing progression than the use of dental floss.[26] Recently, a new system of lesion infiltration has been developed to seal proximal lesions in a tri-dimensional fashion using a low-viscosity light-curing resin.[11] A clinical study of non-cavitated interproximal lesions radiographically extending into the inner half of the enamel (E2) or in the outer third of the dentine (D1) showed a progression rate of 7% in the infiltrated lesions compared to 37% in untreated lesions.[27] Another randomized controlled clinical trial showed a progression rate of 4% in infiltrated lesions

compared to 42% in untreated lesions at a 3-year follow-up.[11] Unlike occlusal lesions, it is not possible to conclude that sealing or infiltrating proximal lesions is superior to controlling lesions by stabilizing the oral ecosystem with good hygiene, dietary control and appropriate fluoride use.[28]

Caries lesions may be treated using resin or glass ionomer (GI) sealants. It is uncertain whether one type of sealant performs better than the other. It has been suggested that conventional GI sealants used as therapy for non-cavitated occlusal lesions may be not effective enough to prevent lesion progression.[29] In contrast, one clinical trial showed that non-cavitated occlusal carious lesions sealed with a high-viscosity GI sealant in a non-clinical setting was effective in avoiding lesion progression over a period of 6 years.[30] It has been claimed that resin-based sealants are highly sensitive technique, requiring strict moisture control during placement with the use of rubber dam. This technical requirement is not always easy to achieve in children. Under those conditions, the hydrophilic properties of GI make them an attractive alternative material, but still with limited evidence.

In summary, there is consistent and strong good quality evidence to support non-invasive or MI treatment of non-cavitated lesions using sealants. Infiltration of proximal lesions shows consistent positive results for management of non-cavitated caries lesions, but the amount of good quality studies is still limited (moderate evidence). Individual risk assessment and a comprehensive clinical judgment should be considered when choosing the most appropriate therapeutic procedure for these caries lesions.

Minimally invasive therapy for cavitated carious lesions

The management of deep dentine carious lesions imposes several challenges for the clinician. Besides the technical complexity in removing compromised tissues in more extensive lesions, these procedures may result in pulp exposure and loss of vitality, which implies the need for even more complex restorative treatments. In an effort to preserve tooth structure as much as possible and prevent irreversible pulp damage, conservative techniques have been proposed for carious dentine removal.[4–5,31] Unlike the traditional and, unfortunately, still more popular complete excavation method or non-selective removal to hard dentine, techniques for carious dentine removal based on the MI philosophy are similar in that they are conservative and aimed at removing only a portion of the compromised tissues.[4,32] There are several techniques for the MI approach to deep dentine caries treatment (selective removal of carious tissue, stepwise removal or nonselective removal to hard dentine),[4,5] but only techniques with broader support of external evidence will be discussed; atraumatic restorative treatment (ART), stepwise removal (SW), and selective removal to soft dentine (also known as partial caries removal) (Table 1).

Atraumatic restorative treatment

Atraumatic restorative treatment (ART) is the MI treatment technique aimed at arresting caries progression of extensive cavitated lesions through the partial removal of the involved tissues with hand instruments and their subsequent restoration with high viscosity GI.[10] Several studies with ART suggest that this therapy has a comparable success rate than traditional complete removal technique and the subsequent restoration with composite resin or amalgam.[33,34] A meta-analysis on the survival of ART restorations found survival rates on one surface and multiple surfaces in primary teeth for more than 2 years of 93% and 62%, respectively.[35] In permanent teeth, ART restorations on one surface exhibited survival at 3 and 5 years of 85% and 80%, respectively. Similarly, another systematic review showed a survival of ART restorations on one surface of 95% and 86% at 1 and 3 years, respectively and of 72% at 6 years after placement.[36] The available evidence suggests that ART is a scientifically-supported MI treatment. Since this technique allows treatment in non-clinical settings at low cost, it may enhance access to care for the community, especially in developing countries. Importantly, ART restorations on multiple surfaces appear to be less successful and would require more complex restorations to ensure greater longevity.[37]

Stepwise removal

Besides ART, other MI therapies have been devised for deep dentine caries, such as indirect pulp capping (IPC), excavation in 2 stages, or SW excavation or removal, and more recently, the partial caries removal technique, or selective removal to soft or to firm dentine (Table 1).[38,39,40,4] IPC is a form of selective caries removal which involves leaving a thin layer of demineralized tissue over the pulp which is covered by a protective liner. Final restoration is made in the same session. The material used for pulp protection does not appear to influence treatment success, according to a Cochrane review.[41] Lesion arrest was reported in primary teeth with a success rate of 78% at 4 years, with no difference between an adhesive system and calcium hydroxide used as liners.[42]

The main disadvantage of IPC is that it involves procedures that are quite close to the pulp, thereby increasing the chances of pulp exposure. A less invasive approach for lesion removal without reaching the proximity of the pulp, is the SW technique, which involves lesion removal in 2 stages.[43,44] Stepwise removal technique consists of a first step involving partial carious tissue removal, leaving soft carious tissue on the pulpal cavity floor of a deep carious lesion, in a vital tooth. Teeth are temporarily restored for a period of up to 12 months. A re-entry is then necessary to remove the carious tissue to firm dentine, followed by a permanent final restoration.[31] During the temporary sealing, the soft carious dentine, which was intentionally

Table 1. Evaluation of the effectiveness of the removal of cavitated carious lesions with minimally invasive techniques; stepwise (SW) and selective removal to soft dentine (SRSD) or partial caries removal

Source	Technique	Control	Number of evaluated teeth	Age [years]	Follow-up [years]	Main results
(Magnusson and Sundell, 1977)[39]	stepwise	nonselective to hard dentine (complete removal)	110 primary teeth (55 SW and 55 complete removal)	5–10	no follow-up	pulp exposure: stepwise 11% vs complete removal 53%
(Heinric, Kneist, and Künzel, 1991)[46]	stepwise	nonselective to hard dentine (complete removal)	125 primary teeth (52 SW and 52 complete removal)	6–7	1.3	pulp exposure: stepwise 15% vs complete removal 31%; pulp symptoms: stepwise 8% vs complete removal 18%
(Leksell et al., 1996)[45]	stepwise	nonselective to hard dentine (complete removal)	134 permanent teeth	6–16	3	pulp exposure: stepwise: 17.5% vs complete removal 40%
(Maltz et al., 2007)[54]	SRSD	----	32 permanent teeth	12–23	3.75	6–7 months: 31 of 32 without symptoms: 97%; 14–18 months: 22 of 22 without symptoms: 100%; 36–45 months: 24 of 24 without symptoms: 100%; between 14–18 36–45 months: 2 patients restoration and endodontics
(Bjørndal et al., 2010)[44]	stepwise	nonselective to hard dentine (complete removal)	314 permanent teeth (156 SW and 158 control)	>18	1	pulp exposure: stepwise 17.5% vs complete removal 28.9%
(Alves et al., 2010)[55]	SRSD	----	32 permanent teeth	12–13	10	92.3% no change or decrease in depth; 76.9% tertiary dentin formation
(Orhan, Oz, and Orhan, 2010)[49]	indirect pulp capping, SRSD	nonselective to hard dentine (complete removal)	154 (94 primary and 60 permanent)	4–15	1	pulp exposure: indirect pulp capping: 8%; SRSD: 6%; complete removal: 22%
(Maltz et al., 2012)[58]	SRSD	stepwise	299 permanent teeth (152 partial caries removal and 147 SW)	6–53	3	pulp vitality: SRSD 91% vs SW 69%
(Maltz et al., 2012)[52]	SRSD	stepwise	299 permanent teeth (153 partial caries removal and 146 SW)	6–53	1.5	pulp vitality: SRSD 99% vs 89% SW
(Franzon et al., 2014)[50]	SRSD	nonselective to hard dentine (complete removal)	120 primary teeth (66 partial caries removal and 54 complete removal)	3–8	2	pulp exposure: 2% partial caries removal vs 27.5% complete removal; pulp vitality: 92% partial caries removal vs 96% complete removal
(Oliveira et al., 2006)[56]	partial caries removal	----	32 permanent teeth	12–23	1.5	100% no clinical symptoms and positive cold test

left remaining, becomes harder and drier, both characteristics of inactive lesions, exhibiting a low level of bacterial infection.[31] The objective of this procedure is to facilitate the physiological reaction of the pulp-dentine complex, including dentinal sclerosis and tertiary dentine formation. Thus, a 2-step process ensures pulp protection by minimizing the risk of exposure. Several studies have indicated that SW is a highly successful procedure.[45,46] A recent meta-analysis has revealed a 56% reduction in the incidence of pulp exposure in SW excavation compared to complete caries removal or non-selective to hard dentine, as it is the most recently agreed term.[4,47] The main problems of the SW technique are the risk of pulp exposure during re-entry, the failure of the temporary restoration, and increased costs resulting from the 2 sessions that are required to complete treatment. Furthermore, it has been observed that one of the causes of failure is that some patients do not return for the final restoration due to the absence of symptoms.[48]

Selective removal to soft dentine or partial caries removal

As a way to improve the effectiveness of the SW and IPC techniques, it has been proposed that selective removal of the carious tissue to soft dentine in deep cavitated lesions, with vital teeth, be performed.[49,50] A recently published consensus paper has named this procedure as selective removal to soft dentine, formerly known as partial caries removal.[4] In this strategy the final restoration should be performed during the same session, completing

the procedure in a single appointment.[51,52] In fact, it has been suggested that re-entering the cavity after partial or selective removal in the SW technique is unnecessary.[53] In the selective removal of soft dentine technique, selective removal to firm dentine from the lateral walls of the lesion is necessary, removing gently and without pressure only the most outer layer of softened dentine from the pulp wall with manual or rotary instrumentation, and placing the final restoration in the same session.[54] A study that followed a cohort of patients treated with selective removal to soft dentine showed that 12 of 13 teeth with lesions remained unchanged for 10 years.[55] Radiographic analysis showed tertiary dentine in 77% of cases. Likewise, another study checked the arrest of selective removal to soft dentine-treated lesions by radiographic follow-up with subtraction imaging techniques.[56] The number of microorganisms was also reduced after sealing the cavity, reaching similar recovery levels to those found in nonselective to hard dentine or complete removal.[57] Considering that selective removal to soft dentine is even more MI and conservative than IPC or SW, the risk of pulp exposure was expected to be even lower. Recently, a multicenter clinical study has evaluated the efficacy of selective removal to soft dentine and restoration in a single session compared to SW for the treatment of deep caries lesions.[58] The results showed a success rate of 91% with selective removal to soft dentine compared with 69% for the SW technique. The accumulated evidence from clinical trials confirms that this is an appropriate and helpful MI approach to treat lesions in close proximity to the pulp (strong evidence), reducing the risk of exposure and postoperative symptoms compared with non-selective to hard dentine or complete removal.[4] Additionally, this technique has a lower economic cost and lower long-term risk of pulp complications.[46] The evidence supporting these MI procedures is still limited. Thus, further research is needed before more definitive conclusions can be drawn.[59] In fact, a recently published meta-analysis states that the evidence remains insufficient to determine which technique is most effective for the management of deep dentine lesions and emphasizes the need for more studies to generate evidence.[60]

Conclusions

Minimally invasive techniques for carious lesion treatment reviewed here offer an attractive alternative for improving dental care coverage at the individual and the community level. It is important to remark that before making decisions on the therapies for the lesions, clinicians must evaluate caries risk at the patient level and also assess the lesions. Preventive measures must always be considered and implemented to control the onset of new lesions on unaffected tissues. After treating current lesions, a permanent follow-up regime must be implemented to reinforce prevention and to monitor lesions over time (Fig. 1).

The use of sealants as MI treatment for active non-cavitated lesions is supported by strong evidence and it is, therefore, a reasonable strategy for the management of non-cavitated lesions at a very low cost. Sealants and infiltration appear to be effective alternatives for management on interproximal active carious lesions. The ability to treat non-cavitated lesions with even less expensive methods, such as tooth brushing with fluorides, remains

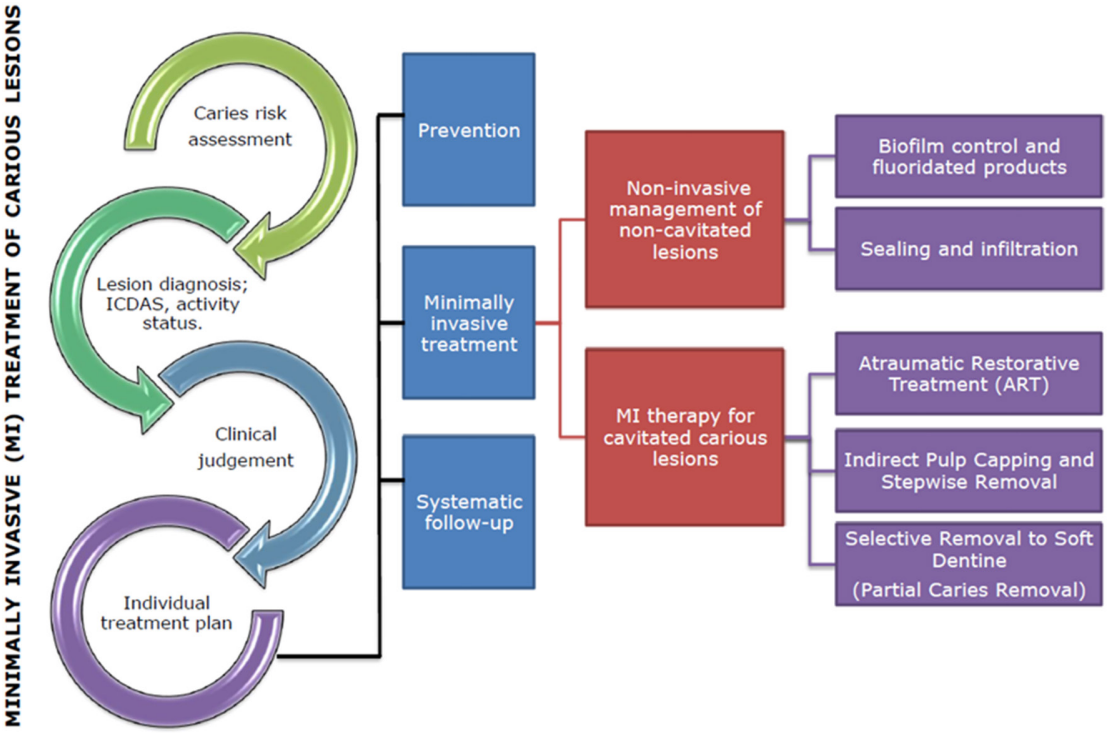

Fig. 1. Article content overview. Minimally invasive approach for caries lesion treatment requires different steps before making a therapeutic decision. Preventive strategies must be included in order to control the disease and to avoid the onset of new lesions. Depending on whether lesions are categorized as non- or cavitated, clinicians must choose among the different MI techniques. As important as the treatment itself, patients must be incorporated into a systematic follow-up plan, with a preventive focus and lesions monitored over time

a potential solution, but the studies in occlusal surfaces are still insufficient for their recommendation compared to sealants. Selective removal to soft dentine in cavitated deep dentine lesions allows fast and inexpensive procedures that generate very little discomfort to the patient, greatly reducing the possibility of pulp exposure and, consequently, the need for complex treatments. Evidence appears to support the idea that selective removal to soft dentine is a safe technique, although the need for further studies is suggested. Similarly, ART is a good alternative in situations where there is a need to provide care in communities lacking a traditional dental clinic. Minimally invasive treatment of both cavitated and non-cavitated carious lesions constitutes a rational strategy for the management of dental caries and should be encouraged at the public, private, and educational level in universities. Despite the obvious advantages of these techniques compared with the more traditional approaches, there is a natural resistance to change in many professionals. It is, therefore, necessary to confront the clinicians with the available evidence to engage them into a more MI treatment philosophy.

References

1. Tyas MJ, Anusavice KJ, Frencken JE, Mount GJ. Minimal intervention dentistry – a review. FDI Commission Project 1–97. *Int Dent J*. 2000;50(1):1–12.
2. Walsh LJ, Brostek AM. Minimum intervention dentistry principles and objectives. *Aust Dent J*. 2013;58(Suppl 1):3–16.
3. Fontana M. The clinical, environmental, and behavioral factors that foster early childhood caries: Evidence for caries risk assessment. *Pediatr Dent*. 2015;37(3):217–225.
4. Innes NP, Frencken JE, Bjorndal L, et al. Managing carious lesions: Consensus recommendations on terminology. *Adv Dent Res*. 2016; 28(2):49–57.
5. Schwendicke F, Frencken JE, Bjorndal L, et al. Managing carious lesions: Consensus recommendations on carious tissue removal. *Adv Dent Res*. 2016;28(2):58–67.
6. Santamaria RM, Innes NP, Machiulskiene V, Evans DJ, Alkilzy M, Splieth CH. Acceptability of different caries management methods for primary molars in a RCT. *Int J Paediatr Dent*. 2015;25(1):9–17.
7. Yamaga R, Nishino M, Yoshida S, Yokomizo I. Diammine silver fluoride and its clinical application. *J Osaka Univ Dent Sch*. 1972;12:1–20.
8. Gao SS, Zhang S, Mei ML, Lo EC, Chu CH. Caries remineralisation and arresting effect in children by professionally applied fluoride treatment – a systematic review. *BMC Oral Health*. 2016;16(1):12. doi: 10.1186/s12903-016-0171-6
9. Ahovuo-Saloranta A, Forss H, Walsh T, et al. Sealants for preventing dental decay in the permanent teeth. *Cochrane Database Syst Rev*. 2013;(3):CD001830. doi: 10.1002/14651858.CD001830.pub4
10. Frencken JE, Leal SC, Navarro MF. Twenty-five-year atraumatic restorative treatment (ART) approach: A comprehensive overview. *Clin Oral Investig*. 2012;16(5):1337–1346.
11. Meyer-Lueckel H, Bitter K, Paris S. Randomized controlled clinical trial on proximal caries infiltration: Three-year follow-up. *Caries Res*. 2012;46(6):544–548.
12. Kassebaum NJ, Bernabé E, Dahiya M, Bhandari B, Murray CJ, Marcenes W. Global burden of untreated caries: A systematic review and metaregression. *J Dent Res*. 2015;94(5):650–658.
13. Yee R, Sheiham A. The burden of restorative dental treatment for children in Third World countries. *Int Dent J*. 2002;52(1):1–9.
14. Petersen PE. The World Oral Health Report 2003: Continuous improvement of oral health in the 21st century – the approach of the WHO Global Oral Health Programme. *Comm Dent Oral Epidemiol*. 2003;31(Suppl 1):3–23.
15. Ismail AI, Sohn W, Tellez M, et al. The International Caries Detection and Assessment System (ICDAS): An integrated system for measuring dental caries. *Comm Dent Oral Epidemiol*. 2007;35(3):170–178.
16. Nyvad B, Machiulskiene V, Baelum V. Reliability of a new caries diagnostic system differentiating between active and inactive caries lesions. *Caries Res*. 1999;33(4):252–260.
17. Marsh PD. Dental plaque as a microbial biofilm. *Caries Res*. 2004;38(3): 204–211.
18. Jones S, Burt BA, Petersen PE, Lennon MA. The effective use of fluorides in public health. *Bull World Health Organ*. 2005;83:670–676.
19. Marinho VC, Higgins JP, Logan S, Sheiham A. Fluoride varnishes for preventing dental caries in children and adolescents. *Cochrane Database Syst Rev*. 2002;(3):CD002279.
20. Fontana M. Enhancing Fluoride: Clinical Human Studies of Alternatives or Boosters for Caries Management. *Caries Res*. 2016;50,Suppl 1:22–37.
21. Ahovuo-Saloranta A, Hiiri A, Nordblad A, Worthington H, Mäkelä M. Pit and fissure sealants for preventing dental decay in the permanent teeth of children and adolescents. *Cochrane Database Syst Rev*. 2004;(3):CD001830. doi: 10.1002/14651858.CD002279
22. Griffin SO, Oong E, Kohn W, Vidakovic B, Gooch BF, Bader J; Group C.D.S.S. R.W. The effectiveness of sealants in managing caries lesions. *J Dent Res*. 2008;87(2):169–174.
23. Borges BC, de Souza Borges J, Braz R, Montes MA, de Assunção Pinheiro IV. Arrest of non-cavitated dentinal occlusal caries by sealing pits and fissures: A 36-month, randomised controlled clinical trial. *Int Dent J*. 2012;62(5):251–255.
24. Fontana M, Platt JA, Eckert GJ, et al. Monitoring of sound and carious surfaces under sealants over 44 months. *J Dent Res*. 2014;93(11): 1070–1075.
25. Oong EM, Griffin SO, Kohn WG, Gooch BF, Caufield PW. The effect of dental sealants on bacteria levels in caries lesions: A review of the evidence. *J Am Dent Assoc*. 2008;139(3):271–278.
26. Martignon S, Ekstrand KR, Ellwood R. Efficacy of sealing proximal early active lesions: An 18-month clinical study evaluated by conventional and subtraction radiography. *Caries Res*. 2006;40(5): 382–388.
27. Paris S, Hopfenmuller W, Meyer-Lueckel H. Resin infiltration of caries lesions: An efficacy randomized trial. *J Dent Res*. 2010;89(8):823–826.
28. Abuchaim C, Rotta M, Grande RH, Loguercio AD, Reis A. Effectiveness of sealing active proximal caries lesions with an adhesive system: 1-year clinical evaluation. *Braz Oral Res*. 2010;24(3):361–367.
29. da Silveira AD, Borges BC, de Almeida Varela H, de Lima KC, Pinheiro IV. Progression of non-cavitated lesions in dentin through a nonsurgical approach: A preliminary 12-month clinical observation. *Eur J Dent*. 2012;6(1):34–42.
30. Bishara SE, Oonsombat C, Ajlouni R, Denehy G. The effect of saliva contamination on shear bond strength of orthodontic brackets when using a self-etch primer. *Angle Orthod*. 2002;72(6):554–557.
31. Bjørndal L, Larsen T, Thylstrup A. A clinical and microbiological study of deep carious lesions during stepwise excavation using long treatment intervals. *Caries Res*. 1997;31(6):411–417.
32. Mount GJ, Ngo H. Minimal intervention: Advanced lesions. *Quintessence Int*. 2000;31(9):621–629.
33. Kikwilu EN, Mandari GJ, Honkala E. Survival of Fuji IX ART fillings in permanent teeth of primary school children in Tanzania. *East Afr Med J*. 2001;78(8):411–413.
34. Mickenautsch S, Kopsala J, Rudolph MJ, Ogunbodede EO. Clinical evaluation of the ART approach and materials in peri-urban farm schools of the Johannesburg area. *SADJ*. 2000;55(7):364–368.
35. de Amorim RG, Leal SC, Frencken JE. Survival of atraumatic restorative treatment (ART) sealants and restorations: A meta-analysis. *Clin Oral Investig*. 2012;16(2):429–441.
36. van 't Hof MA, Frencken JE, van Palenstein Helderman WH, Holmgren CJ. The atraumatic restorative treatment (ART) approach for managing dental caries: A meta-analysis. *Int Dent J*. 2006;56(6):345–351.
37. Arrow P. Restorative outcomes of a minimally invasive restorative approach based on atraumatic restorative treatment to manage early childhood caries: A randomised controlled trial. *Caries Res*. 2016;50(1):1–8.
38. Kerkhove BC, Herman SC, Klein AI, McDonald RE. A clinical and television densitometric evaluation of the indirect pulp capping technique. *J Dent Child*. 1967;34(3):192–201.

39. Magnusson BO, Sundell SO. Stepwise excavation of deep carious lesions in primary molars. *J Int Assoc Dent Child*. 1977;8(2):36–40.
40. Ricketts DN, Kidd EA, Innes N, Clarkson J. Complete or ultraconservative removal of decayed tissue in unfilled teeth. *Cochrane Database Syst Rev*. 2006;(3):CD003808. doi: 10.1002/14651858.CD003808.pub2
41. Miyashita H, Worthington HV, Qualtrough A, Plasschaert A. Pulp management for caries in adults: Maintaining pulp vitality. *Cochrane Database Syst Rev*. 2007;(2):CD004484. doi: 10.1002/14651858.CD004484.pub2
42. Casagrande L, Bento LW, Dalpian DM, García-Godoy F, de Araujo FB. Indirect pulp treatment in primary teeth: 4-year results. *Am J Dent*. 2010;23(1):34–38.
43. Bjørndal L. Indirect pulp therapy and stepwise excavation. *Pediatr Dent*. 2008;30(3):225–229.
44. Bjørndal L, Reit C, Bruun G, et al. Treatment of deep caries lesions in adults: Randomized clinical trials comparing stepwise vs direct complete excavation, and direct pulp capping vs partial pulpotomy. *Eur J Oral Sci*. 2010;118(3): 290–297.
45. Leksell E, Ridell K, Cvek M, Mejàre I. Pulp exposure after stepwise versus direct complete excavation of deep carious lesions in young posterior permanent teeth. *Endod Dent Traumatol*. 1996;12(4), 192–196.
46. Heinrich R, Kneist S, Künzel W. Clinical controlled study on the treatment of deep carious lesions in deciduous molars. *Dtsch Zahnarztl Z*. 1991;46(9):581–584.
47. Ricketts D, Lamont T, Innes NP, Kidd E, Clarkson JE. Operative caries management in adults and children. *Cochrane Database Syst Rev*. 2013;3:CD003808. doi: 10.1002/14651858.CD003808.pub3
48. Schwendicke F, Stolpe M, Meyer-Lueckel H, Paris S, Dörfer CE. Cost-effectiveness of one- and two-step incomplete and complete excavations. *J Dent Res*. 2013;92(10):880–887.
49. Orhan AI, Oz FT, Orhan K. Pulp exposure occurrence and outcomes after 1- or 2-visit indirect pulp therapy vs complete caries removal in primary and permanent molars. *Pediatr Dent*. 2010;32(4):347–355.
50. Franzon R, Guimarães LF, Magalhães CE, Haas AN, Araujo FB. Outcomes of one-step incomplete and complete excavation in primary teeth: A 24-month randomized controlled trial. *Caries Res*. 2014;48(5): 376–383.
51. Maltz M, Alves LS, Jardim JJ, Moura MoS, de Oliveira EF. Incomplete caries removal in deep lesions: A 10-year prospective study. *Am J Dent*. 2011;24(4):211–214.
52. Maltz M, Jardim JJ, Mestrinho HD, et al. Partial removal of carious dentine: A multicenter randomized controlled trial and 18-month follow-up results. *Caries Res*. 2013;47(2):103–109.
53. Bjørndal L. Reentry may not be needed after partial caries removal in mainly young permanent molars with caries involving half or more of the dentin thickness. *J Evid Based Dent Pract*. 2013;13(2):62–63.
54. Maltz M, Oliveira EF, Fontanella V, Carminatti G. Deep caries lesions after incomplete dentine caries removal: 40-month follow-up study. *Caries Res.* 2007;41(6):493–496.
55. Alves LS, Fontanella V, Damo AC, Ferreira de Oliveira E, Maltz M. Qualitative and quantitative radiographic assessment of sealed carious dentin: A 10-year prospective study. *Oral Surg Oral Med Oral Pathol Oral Radiol Endod*. 2010;109(1):135–141.
56. Oliveira EF, Carminatti G, Fontanella V, Maltz M. The monitoring of deep caries lesions after incomplete dentine caries removal: Results after 14–18 months. *Clin Oral Investig*. 2006;10(2):134–139.
57. Lula E, Monteiro-Neto V, Alves CM, Ribeiro CC. Microbiological analysis after complete or partial removal of carious dentin in primary teeth: A randomized clinical trial. *Caries Res*. 2009;43(5):354–358.
58. Maltz M, Garcia R, Jardim JJ, et al. Randomized trial of partial vs stepwise caries removal: 3-year follow-up. *J Dent Res*. 2012;91(11):1026–1031.
59. Schwendicke F, Dörfer CE, Paris S. Incomplete caries removal: A systematic review and meta-analysis. *J Dent Res*. 2013;92(4):306–314.
60. Bergenholtz G, Axelsson S, Davidson T, et al. Treatment of pulps in teeth affected by deep caries – A systematic review of the literature. *Singapore Dent J*. 2013;34(1):1–12.

Review

Ovarian cancer stem cells: A target for oncological therapy

Anna Markowska[1,A,D], Stefan Sajdak[2,E], Adam Huczyński[3,D,E], Sandra Rehlis[4,B], Janina Markowska[5,D–F]

[1] Department of Perinatology and Women's Diseases, Poznan University of Medical Sciences, Poland
[2] Department of Gynecological Surgery, Poznan University of Medical Sciences, Poland
[3] Faculty of Chemistry, Adam Mickiewicz University in Poznań, Poland
[4] Klinikum Fulda, Universitätsmedizin, Marburg, Germany
[5] Department of Oncology, Poznan University of Medical Sciences, Poland

A – research concept and design; B – collection and/or assembly of data; C – data analysis and interpretation;
D – writing the article; E – critical revision of the article; F – final approval of the article

Advances in Clinical and Experimental Medicine, ISSN 1899-5276 (print), ISSN 2451-2680 (online) *Adv Clin Exp Med*. 2018;27(7):1017–1020

Address for correspondence
Anna Markowska
E-mail: annamarkowska@vp.pl

Funding sources
None declared

Conflict of interest
None declared

Received on January 11, 2017
Reviewed on April 2, 2017
Accepted on May 23, 2017

Abstract

According to numerous studies, failures in treatment of ovarian cancer, i.e., a relapse and metastases, result from a small population of cancer stem cells (CSCs). They may also be responsible for tumor initiation. Cancer stem cells are resistant to chemo- and radiotherapy. Eradication of CSCs may involve the application of salinomycin, metformin and *Clostridium perfringens*; the effect of anti-angiogenic factors remains controversial. Salinomycin is an antibiotic isolated from *Streptomyces albus* bacteria. Its CSC-eradicating effect has been demonstrated both in ovarian cancer cell lines and in women with breast cancer. *Clostridium perfringens* enterotoxin (CPE) has been demonstrated to destroy CSCs in ovarian cancer both in vivo and in vitro. Metformin, apart from its hypoglycemic effect, reduces the CSC population and inhibits the proliferation of neoplastic cells and angiogenesis. Cancer stem cells with expression of VEGFR1+ have been described as affecting circulating cancer cells and influencing the formation of metastases. Both positive and negative effects of anti-angiogenic therapy on the CSC population have been documented.

Key words: angiogenesis, metformin, salinomycin, ovarian cancer stem cells, *Clostridium perfringens* enterotoxin

DOI
10.17219/acem/73999

Among all malignant gynecological tumors, ovarian cancer represents the leading cause of death. The majority of patients are diagnosed with advanced stages. Standard treatment for ovarian cancer is primary maximum cytoreductive surgery followed by chemotherapy with carboplatin and paclitaxel. After initial debulking and first line chemotherapy, around 50–70% of patients reach full clinical response. However, in 80% of patients this is followed by a relapse of the disease, the cause of therapeutic failure.[1,2]

According to numerous studies, the principal cause of the cancer relapse and metastases stems from a small cell population resistant to chemo- and radiotherapy, comprising less than 2–5% of tumor mass and involving cancer stem cells (CSCs). Most probably, this specific cell subpopulation is also linked to the initiation of the tumor (cancer initiating cells – CICs).[1,3–6]

Cancer stem cells manifest the capacity of self-renewal, DNA repair, persisting in the G1 or G0 cell cycle phases as inactive dormant cells and asymmetric cell division. They do not undergo apoptosis and they manifest overexpression of *ABC* genes, which is linked to their resistance to cytostatic drugs. Control of their self-replacement is associated in principle with numerous signaling pathways, including Notch, Sonic hedgehog (Shh) and Wnt.[2,7,8]

Cancer stem cells can be identified and isolated due to their specific markers, such as CD44, CD133 (prominin-1), CD117 (c-Kit), ALDH1 (aldehyde dehydrogenase), and OCT3/4 (POU5F1), the transcription factor of the POU family.[9–11]

In 2010, CSCs were isolated and identified in ovarian cancer.[10] In 2014, in in vivo and in vitro conditions, cisplatin was demonstrated to inhibit both the formation of metastases and the invasion of CICs manifesting the marker of $CD/44^+/CD117^+$, but only those with overexpression of CXCR4. Thus, cisplatin inhibited the activity of the SDF-1/CXCR4 axis (the factor originating from stromal cells and its ligand).[12]

Using an animal model, Abubaker et al. demonstrated that short-term application of chemotherapy (cisplatin and paclitaxel) enriched the cell population with high expression of Oct-4 and CD117.[13] Similar experiments were performed by Zhou et al.[14] Following the administration of cisplatin, the dormant cells of human ovarian cancer manifested an augmented expression of cells with Oct-4, nestin, CD-117, and CD44 markers, proving the resistance of this stem cell fraction to cisplatin.

Both the CSC population with its typical markers and the signaling pathways that CSCs take advantage of are thought to provide potential targets for therapy.[7,8,13]

According to Massard et al., there are 2 options for eradicating CSCs: one involves the induction of their differentiation, upon which they lose their capacity of self-replacement (retinoic acid demonstrated such an ability); the other one involves the elimination of CSCs by targeted inhibitors of signaling pathways.[3]

Below, we outline the manners of CSC eradication using salinomycin, metformin and enterotoxin of *Clostridium perfringens*, and we discuss the controversial effects of anti-angiogenic factors.

Salinomycin

Isolated in Japan in 1974 from *Streptomyces albus*, salinomycin represents a carboxylic polyether ionophore antibiotic, leading to disturbances in Na^+/K^+ ion equilibrium in biological membranes and, due to reduced K^+ concentration, in mitochondria and cytoplasm, resulting in cell apoptosis.[15,16] Salinomycin is also active through several other mechanisms in tumors of various locations. It inhibits the conserved Wnt pathway, providing CSCs with the ability to self-replace and resist radiotherapy. Salinomycin also reduces the resistance of CSCs to chemotherapy as it affects the activity of ABC transporters. It seems that several mechanisms of salinomycin action are currently discussed.[5,17–19]

Studies by Zhang et al. in in vivo and in vitro conditions demonstrated that salinomycin induces apoptosis in the cells of ovarian cancer resistant to cisplatin, apoptosis linked to the pathway of mitogen-activated protein kinase (MAPK).[20] Studies by Kaplan and Teksen on the stable ovarian cancer cell line (OVCAR-3) demonstrated the activity of salinomycin: 40% of cells underwent apoptosis within 24 h of exposure.[21] A decrease was noted in the expression of the anti-apoptotic gene *Bcl2*.

Chung et al., using the OVCAR-3 ovarian cancer cell line, isolated stem cells of markers $CD44^+$ and $CD117^+$, linked to chemoresistance.[22] They used paclitaxel + salinomycin. Supplementation with salinomycin significantly inhibited the growth of the cells. Another mechanism of salinomycin activity is linked to the activity of death receptor 5 (DR5) and the activation of apoptosis-initiating caspase 8.

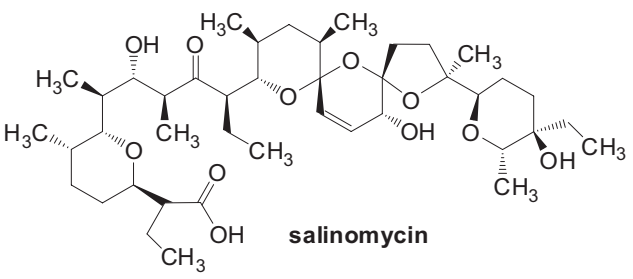

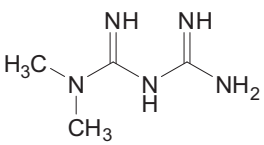

Fig. 1. The structure of salinomycin and metformin

Binding of DR5 to its ligand leads to alterations in death domain (DD, part of the caspase), mobilizing the enzymatic cascade which results in the death of the cell.[23]

Another mechanism of apoptosis in the ovarian cancer cells resistant to cisplatin involves the inhibitory effect of salinomycin on the nuclear transcription factor NF-kB, which affects the control of several other genes.[24]

In practice, salinomycin is also being used by prof. Cord Naujokat in Heidelberg, Germany, obtaining good results among invasive carcinoma in screening studies. The administration of salinomycin has resulted in the inhibition of disease progress over an extended period of time. It is worth noting that acute side effects were rare and serious long-term adverse side effects were not observed.[17]

It has also been demonstrated that salinomycin is able to kill CSCs, regular tumor cells and highly indolent tumor cells displaying resistance to cytotoxic drugs, radiation and the induction of apoptosis.[16]

Up to now, the results obtained from in vivo studies on human xenograft mice and also clinical studies have revealed that salinomycin is able to effectively eliminate CSCs and to induce partial clinical regression in therapy-resistant cancers.[17]

Metformin

Metformin represents a drug of the biguanide group, used orally in patients with diabetes type II, particularly in overweight/obese patients. Population studies have proved that metformin-treated patients manifested a lowered risk of malignant tumors in several locations, including the preventive effect of the drug in ovarian cancer. In comparison to patients not using metformin, women who develop ovarian cancer and being treated with this drug are older and diagnosed more frequently at earlier International Federation of Gynecology and Obstetrics (FIGO) clinical stages. In the course of the disease, these women manifest longer duration to progression and display a higher 5-year survival percentage.[25–28]

Numerous studies have shown that the favorable effect of metformin in the development and course of malignant tumors, including ovarian cancer, may be linked to its inhibitory effect on CSCs.[29–31]

Studies on the SKOV3 and A2780 cell lines of ovarian cancers conducted by Zhang et al. demonstrated that low doses of metformin selectively inhibit CSCs with markers CD44+ and CD117+, and inhibit epithelial mesenchymal transition (EMT).[32] Epithelial mesenchymal transition is linked to the activity of transcription factors and the activation of several genes, resulting in the inhibition of apoptosis and an increased mobility of cells, linked to metastases.

Shank et al. confirmed better prognosis in ovarian cancer patients treated with metformin.[29] The authors expressed the opinion that the mechanism of its action involved a reduction in the CSC population with ALDH1+ marker, reduced cell proliferation and inhibited angiogenesis. They argued that the results provided rationale for the application of metformin in patients treated due to ovarian cancer.

Clostridium perfringens enterotoxin

Natural receptors for *Clostridium perfringens* enterotoxin (CPE) involve claudins 3 and 4. Claudins 3 and 4 represent the family of tight junction proteins responsible for the integrity of the cell membrane and for its functions. In ovarian cancer, overexpression of claudins 3 and 4 is noted; they play a critical role in invasion and metastases as well as in resistance to chemotherapy. They may provide an attractive target in the treatment of cancer resistant to platins.[33]

Casagrande et al. described the mechanism through which CPE becomes activated in ovarian cancer.[34] They examined a small number of ovarian CSCs in vitro and in vivo, carrying the marker of CD44+. They exhibited a high expression of claudin 4. Following the exposure to CPE, the cells underwent apoptosis. Following a sublethal dose of CPE, ovarian cancer xenografts to mice regressed, resulting in a long survival of the animals. Similar results were described by other authors conducting research on ovarian CSCs, CD44+, resistant to paclitaxel and carboplatin. *Clostridium perfringens* enterotoxin may represent an unconventional therapy eradicating ovarian cancer CSCs.[35]

How about an anti-angiogenic therapy?

Bevacizumab, an anti-angiogenic humanized monoclonal antibody, is used in first line therapy in advanced ovarian cancer. According to Rauh-Hain et al., relapses of ovarian cancer in patients treated with bevacizumab were located in other body parts than in patients not treated with the antibody.[36] Those receiving bevacizumab more frequently developed relapses in the pleura, lungs, brain, liver, and lymph nodes than patients on the anti-angiogenic treatment.

Since relapses, as presented above, were linked to CSC metastases, one can speculate on a link between anti-angiogenic therapy and CSC activity. Kaplan et al. found that CSCs with expression of VEGFR1+ promote chemotaxis and adherence of circulating tumor cells.[37] VEGFR1+ cells establish specific "premetastatic" niches, forming cellular clusters there before the inflow of tumor cells. The application of the antibody specific to VEGFR1+ or the removal of the cells prevents metastases. In addition, VEGFR1+ cells manifest expression of VLA4 (known as integrin $\alpha_{4\beta1}$), the ligand of which involves fibronectin taking part in cell

interaction with the matrix. According to Chau et al., the identification of factors targeted at CSCs and associating them with angiogenesis inhibitors might warrant their better clinical efficacy.[38] The authors also suggest that anti-angiogenic therapy leads to tumor hypoxia, resulting in the growth of the CSC population. In their study, Conley et al. presented a similar hypothesis.[39] The problem of anti-angiogenic therapy in ovarian cancer and, in particular, its relationship with CSCs, is extremely intriguing. Anti-angiogenic action based on immunotherapy (vaccine) might uncover another relationship with CSCs.[40] Regarding future directions in the treatment of ovarian cancer, it would seem that combined therapy – cytostatics, anti-angiogenics and anti-CSCs – is a very promising option.

References

1. Chen J, Wang J, Zhang Y, et al. Observation of ovarian cancer stem cell behavior and investigation of potential mechanisms of drug resistance in three-dimensional cell culture. *J Biosci Bioeng*. 2014; 118(2):214–222.
2. Shah MM, Landen CHN. Ovarian cancer stem cells: Are they real and why are they important? Review. *Gynecol Oncol*. 2014;132(2):483–489.
3. Massard C, Deutsch E, Soria JC. Tumor stem cell-targeted treatment: Elimination or differentiation. *Ann Oncol*. 2006;17(11):1620–1624.
4. Rich JN. Cancer stem cells in radiation resistance. *Cancer Res*. 2007; 67(19):8980–8984.
5. Shukla G, Srivastava AK, Patidar R, Khara P, Saxen R. Therapeutic potential, challenges and future perspective of cancer stem cells in translational oncology: A critical review. *Curr Stem Cell Res Ther*. 2017;12(3):207-224.
6. Garcia-Rubino ME, Lozano-Lopez C, Campos JM. Inhibitors of cancer stem cells. *Anticancer Agents Med Chem*. 2016;16(10):1230–1239.
7. Tomao F, Papa A, Rossi L, et al. Emerging role of cancer stem cells in the biology and treatment of ovarian cancer: Basic knowledge and therapeutic possibilities for an innovative approach. *J Exp Clin Cancer Res*. 2013;32:48.
8. Eyler CE, Rich JN. Survival of the fittest: Cancer stem cells in therapeutic resistance and angiogenesis. *J Clin Oncol*. 2008;26(17): 2839–2845.
9. Zeng J, Ruan J, Luo L, et al. Molecular portraits of heterogeneity related to cancer stem cells in human ovarian cancer. *Int J Gynecol Cancer*. 2014;24(1):29–35.
10. Bapat SA. Human ovarian cancer stem cells. *Reproduction*. 2010;140(1): 33–41.
11. Shi YY, Jiang H. Prognostic role of the cancer stem cell marker CD44 in ovarian cancer: A meta-analysis. *Genet Mol Res*. 2016;15(3). doi: 10.4238/gmr.15038325
12. Yu Z, Liu T, Zhao Y, et al. Cisplatin targets the stromal cell-derived factor-1-CXC chemokine receptor type 4 axis to suppress metastasis and invasion of ovarian cancer-initiating cells. *Tumor Biol*. 2014; 35:4637–4644.
13. Abubaker K, Latifi A, Luwor R, et al. Short-term single treatment of chemotherapy results in the enrichment of ovarian cancer stem cell-like cells leading to an increased tumor burden. *Mol Cancer*. 2013;12:24. doi:10.1186/1476-4598-12-24
14. Zhou N, Wu X, Yang B, Zhang D, Qing G. Stem cell characteristics of dormant cells and cisplatininduced effects on the stemness of epithelial ovarian cancer cells. *Mol Med Rep*. 2014;10(5):2495–2504.
15. Miyazaki Y, Shibuya M, Sugawara H, Kawaquchi O, Hirsoe C. Salinomycin, a new polyether antibiotic. *J Antibiot* (*Tokyo*). 1974;27(11): 814–821.
16. Antoszczak M, Huczyński A. Anticancer activity of polyether ionophore-salinomycin. *Anticancer Agents Med Chem*. 2015;15(5):575–591.
17. Naujokat C, Steinhart R. Salinomycin as a drug for targeting human cancer stem cells. *J Biomed Biotechnol*. 2012;950658. doi:10.1155/2012/950658
18. Fuchs D, Heinold A, Opelz G, Daniel V, Naujokot C. Salinomycin induces apoptosis and overcomes apoptosis resistance in human cancer cells. *Biochem Biophys Res Commun*. 2009;390(3):743–749.
19. Kim JH, Yoo HI, Kang HS, Ro J, Yoon S. Salinomycin sensitizes antimitotic drugs-treated cancer cells by increasing apoptosis via the prevention of G2 arrest. *Biochem Biophys Res Commun*. 2012;418(1): 98–103.
20. Zhang B, Wang X, Cai F, Chen W, Loesch U, Zhong XY. Antitumor properties of salinomycin on cisplatin-resistant human ovarian cancer cells in vitro and in vivo: Involvement of p38 MAPK activation. *Oncol Rep*. 2013;29(4):1371–1378.
21. Kaplan F, Teksen F. Apoptotic effects of salinomycin on human ovarian cancer cell line (OVCAR-3). *Tumour Biol*. 2016;37(3):3897–3903.
22. Chung H, Kim YH, Kwon M, et al. The effect of salinomycin on ovarian cancer stem-like cells. *Obstet Gynecol Sci*. 2016;59(4):261–268.
23. Parajuli B, Shin SJ, Kwon SH, et al. Salinomycin induces apoptosis via death receptor-5 up-regulation in cisplatin-resistant ovarian cancer cells. *Anticancer Res*. 2013;33(4):1457–1462.
24. Parajuli B, Lee HG, Kwon SH, et al. Salinomycin inhibits Akt/NF-κB and induces apoptosis in cisplatin resistant ovarian cancer cells. *Cancer Epidemiol*. 2013;37(4):512–517.
25. Libby G, Donnelly LA, Donnan PT, Alessi DR, Morris AD, Evans JM. New users of metformin are at low risk of incident cancer: A cohort study among people with type 2 diabetes. *Diabetes Care*. 2009;32(9): 1620–1625.
26. Dilokthornsakul P, Chaiyakunapruk N, Termrungruanglert W, Pratoomsoot C, Saokaew S, Sruamsiri R. The effects of metformin on ovarian cancer: A systematic review. *Int J Gynecol Cancer*. 2013;23(9): 1544–1551.
27. Kumar S, Meuter A, Thapa P, et al. Metformin intake is associated with better survival in ovarian cancer: A case-control study. *Cancer*. 2013;119(3):555–562.
28. Romero IL, McCormick A, McEwen KA, et al. Relationship of type II diabetes and metformin use to ovarian cancer progression, survival, and chemosensitivity. *Obstet Gynecol*. 2012;119(1):61–67.
29. Shank JJ, Yang K, Ghannam J, et al. Metformin targets ovarian cancer stem cells in vitro and in vivo. *Gynecol Oncol*. 2012;127(2):390–397.
30. Del Barco S, Vazquez-Martin A, Cufí S, et al. Metformin: Multi-faceted protection against cancer. *Oncotarget*. 2011;2(12):896–917.
31. Charafe-Jauffret E, Monville F, Ginestier C, Dontu G, Birnbaum D, Wicha MS. Cancer stem cells in breast: Current opinion and future challenges. *Pathobiology*. 2008;75(2):75–84.
32. Zhang R, Zhang P, Wang H, et al. Inhibitory effects of metformin at low concentration on epithelial-mesenchymal transition of CD44(+) CD117(+) ovarian cancer stem cells. *Stem Cell Res Ther*. 2015;6:262.
33. English DP, Santin AD. Claudins overexpression in ovarian cancer: Potential targets for Clostridium perfringens enterotoxin (CPE) based diagnosis and therapy. *Int J Mol Sci*. 2013;14(5):10412–10437.
34. Casagrande F, Cocco E, Bellone S, et al. Eradication of chemotherapy-resistant CD44+ human ovarian cancer stem cells in mice by intraperitoneal administration of Clostridium perfringens enterotoxin. *Cancer*. 2011;117(24):5519–5528.
35. Hashimoto Y, Yagi K, Kondoh M. Roles of the first-generation claudin binder, Clostridium perfringens enterotoxin, in the diagnosis and claudin-targeted treatment of epithelium-derived cancers. *Pflugers Arch*. 2016. doi:10.1007/s00424-016-1878-6
36. Rauh-Hain JA, Guseh SH, Esselen KM, et al. Patterns of recurrence in patients treated with bevacizumab in the primary treatment of advanced epithelial ovarian cancer. *Int J Gynecol Cancer*. 2013;23(7): 1219–1225.
37. Kaplan RN, Riba RD, Zacharoulis S, et al. VEGFR1-positive haematopoietic bone marrow progenitors initiate the pre-metastatic niche. *Nature*. 2005;438(7069):820–827.
38. Chau CH, Figg WD. Angiogenesis inhibitors increase tumor stem cells. *Cancer Biol Ther*. 2012;13(8):586–587.
39. Conley SJ, Gheordunescu E, Kakarala P, et al. Antiangiogenic agents increase breast cancer stem cells via the generation of tumor hypoxia. *Proc Natl Acad Sci USA*. 2012;109(8):2784–2789.
40. Wagner SC, Ichim TE, Ma H, et al. Cancer anti-angiogenesis vaccines: Is the tumor vasculature antigenically unique? *J Transl Med*. 2015;13:340. doi:10.1186/s12967-015-0688-5

Advances
in Clinical and Experimental
Medicine